January 2019

The Balance Between Prostaglandin E2 Ep3 And Ep4 Receptors Determines Severity Of Cardiac Damage In Myocardial Infarction And An Angiotensin Ii-Induced Model Of Hypertension

Timothy Dean Bryson
Wayne State University, Brysont1990@gmail.com

THE BALANCE BETWEEN PROSTAGLANDIN E2 EP3 AND EP4 RECEPTORS DETERMINES SEVERITY OF CARDIAC DAMAGE IN MYOCARDIAL INFARCTION AND AN ANGIOTENSIN II-INDUCED MODEL OF HYPERTENSION

by

TIMOTHY DEAN BRYSON

DISSERTATION

Submitted to the Graduate School

of Wayne State University,

Detroit, Michigan

in partial fulfillment of the requirements

for the degree of

DOCTOR OF PHILOSOPHY

2019

MAJOR: PHYSIOLOGY

Approved By:

_____

Advisor Date

_____

_____

_____

_____

DEDICATION

Dedicated to my family

For their continuous love and support

To my parents and sister Ashley

To my wife and best friend Brittany

For Liam James

ACKNOWLEDGEMENTS

First and foremost, I would like to thank my advisor and mentor, Dr. Pamela Harding. Dr. Harding accepted me into her lab as a rotational student and was daring enough to allow me to stay in her lab to pursue my doctoral degree. She was always instructive, supportive, and most of all patient. Dr. Harding's lab and the Hypertension & Vascular Research Division at Henry Ford Hospital in general, demand excellence and productivity of their trainees. I am now very appreciative for that experience. Dr. Harding provided me with many laboratory and life skills necessary for a career in science. Dr. Harding was always a strong advocate for her lab and her students and allowed me the privilege of traveling and presenting at several national meetings. I am honored to say I was her first PhD graduate student.

My appreciation also extends to the various members of the lab throughout my PhD studies. Dave Taube helped to train me in several different lab techniques and was always a source of entertaining and insightful discussions about both science and life. To all the other students that have worked with me in the lab; Jacob Ross, Teja Pandrangi, Emily Matthews, Maggie Clevenger, Karan Kataria, Remonda Khalil, and Safa Khan; I extend my most sincere gratitude for your help in making this dissertation a possibility. Additionally, I would like to thank Drs. Jiang Xu and Xiao-Ping Yang for teaching me how to perform echocardiography and assisting/teaching me in surgical procedures. I also thank the members of the histology core at One Ford Place for their assistance in cutting and processing our frozen sections.

I sincerely thank my graduate committee members, Drs. Robert Lasley, Raymond Mattingly, and Robert Wessells for their extremely valuable time and support. The entire

committee has made very important suggestions along the way to help shape this project into what it has become.

Lastly, I would like to extend my gratitude to the Physiology department. I started in the department as an undergraduate doing research for course credit and thanks to the dedicated faculty and staff of the department, I will become a graduate of the PhD program. I need to especially thank Christine Cupps, whom is absolutely essential for the success of the students in the physiology department.

TABLE OF CONTENTS

LIST OF TABLES

LIST OF FIGURES

LIST OF ABBREVIATIONS

AAV9 – Adeno-associated virus serotype 9

ACE – Angiotensin converting enzyme

AKT/PKB – Protein kinase B

αMHC – Alpha myosin heavy chain

Ang II – Angiotensin II

AP-1 - Activator protein 1

ARBs – Angiotensin receptor blockers

AVF – Adult ventricular fibroblasts

AVM – Adult ventricular cardiomyocytes

βMHC – Beta myosin heavy chain

BMI – Body mass index

BNP – Brain natriuretic peptide

BSA – Bovine serum albumin

BW – Body weight

CAMKII/MEF2 - Calcium/calmodulin-dependent protein kinase II

CCL12 – Monocyte chemoattractant protein 5 (see MCP-5)

CCR2 – CC motif chemokine receptor 2

CD4 – Cluster of differentiation 4

CD8 – Cluster of differentiation 8

CD11b – Cluster of differentiation 11b

CD31 – Cluster of differentiation 31

CD45 – Cluster of differentiation 45

CD68 – Cluster of differentiation 68

CD163 – Cluster of differentiation 163

CM-EP4 KO – Cardiomyocyte specific EP4 knockout

CO – Cardiac output

COX – cyclooxygenase

cPGES – Cytosolic prostaglandin E synthase

CREB - cAMP response element-binding protein

DAMPS - Damage associated molecular patterns

db cAMP – Dibutyryl cAMP

Dnase - deoxyribonuclease

DOCA – deoxycorticosterone acetate

DP – Prostaglandin D_2 receptor

dPBS – Dulbecco's phosphate buffered saline

DRB – Benzimidazole, 5,6-dichloro-1-(5-chloro-5-deoxy-beta-D-ribofuranosyl)

EAM – Experimental autoimmune myocarditis

EF – Ejection fraction

ELISA - Enzyme-linked immunosorbent assay

eNOS – Endothelial nitric oxide synthase

EP3 Tg – EP3 Transgenic

EP4RAG – EP4 receptor agonist

ER – Estrogen receptor

ERK - Extracellular signal–regulated kinases

F4/80 - EGF-like module-containing mucin-like hormone receptor-like 1

FITC - Fluorescein isothiocyanate

FP – Prostaglandin F_2 receptor

GAPDH - Glyceraldehyde 3-phosphate dehydrogenase

GPCRs – G-protein coupled receptors

HA - hemagglutinin

HBSS – Hanks balanced salt solution

HFrEF – Heart failure with reduced ejection fraction

HR – Heart rate

HTN - Hypertension

IFN-γ – Interferon gamma

IgG - Immunoglobulin G

IHC - Immunohistochemistry

IKK - IκB kinase

IL - Interleukin

iNOS – inducible nitric oxide synthase

IP – Prostacyclin receptor

I.P. - Intraperitoneal

I/R – Ischemia/reperfusion

ISO - Isoproterenol

LAD – Left anterior descending coronary artery

LPS - Lipopolysaccharide

LV – Left ventricle

LVDs – Left ventricle dimension at systole

LVDd – Left ventricle dimension at diastole

LVH – Left ventricle hypertrophy

Ly6C/Gr-1 - Lymphocyte antigen 6 complex, locus C1

MAPKs - Mitogen-activated protein kinases

MCP-1 – Monocyte chemoattractant protein 1

MCP-5 – Monocyte chemoattractant protein 5 (a.k.a CCL12)

MCSA – Myocyte cross sectional area

MHC – Major histocompatibility complex

MI – Myocardial infarction

MMHg – Millimeters mercury

MMPs – Matrix metalloproteinase enzymes

mPGES – Microsomal prostaglandin E synthase

NADPH - nicotinamide adenine dinucleotide phosphate

NFAT - Nuclear factor of activated T-cells

NF-κB – Nuclear factor kappa B

Nox - nicotinamide adenine dinucleotide phosphate oxidase

NS – Not a significant difference

NSAIDs – Nonsteroidal anti-inflammatory drugs

OCT – Optimal cutting temperature

PBS – Phosphate buffered saline

PE - Phycoerythrin

PerCP - Peridinin-Chlorophyll-Protein

PG – Prostaglandin

PGD_2 - Prostaglandin D_2

PGE_2 – Prostaglandin E_2

$PGF_{2\alpha}$ – Prostaglandin $F_{2\alpha}$

PGHS – Prostaglandin endoperoxide H synthase

PGI_2 – Prostacyclin

PI3K - Phosphatidylinositol 3-kinases

PKA - Protein kinase A

PLA_2 – Phospholipase A_2

PLN - Phospholamban

PRRs – Pattern recognition receptors

PSR – Picrosirius red staining

PWT – Posterior wall thickness

RANTES - Chemokine (C-C motif) ligand 5

RAS – Renin angiotensin system

ROS – Reactive oxygen species

RT-PCR – Reverse transcription polymerase chain reaction

SAPK/JNK - Stress-activated protein kinase/c-Jun N-terminal kinases

SBP – Systolic blood pressure

S.C. – Subcutaneous

SERCA - Sarco/endoplasmic reticulum calcium adenosine triphosphatase

SF – Shortening fraction

SPARC - secreted protein acidic and rich in cysteine (a.k.a Osteonectin)

STEMI – ST segment elevated myocardial infarction

TBS – Tris buffered saline

TGF – β – Transforming growth factor beta 1

Th1 - T helper cells 1

Th2 - T helper cells 2

Th17 - T helper cells 17

TIMP – Tissue inhibitor of metalloproteinases

TLR-2 – Toll like receptor 2

TLR-4 – Toll like receptor 4

TNF-α – Tumor necrosis factor alpha

Treg – Regulatory T cells

TxA_2 – Thromboxane

VEGF - Vascular endothelial growth factor

WT – Wild type

CHAPTER 1- GENERAL INTRODUCTION AND GENERAL HYPOTHESIS

Prostanoid Discovery and Biosynthesis

In 1935, the initial discovery of prostaglandins was made by Swedish physiologist Ulf Von Euler [2]. Additionally, prostaglandins were independently described by Goldblatt around the same time [3]. Prostanoids is the name given to a bioactive lipid subset of eicosanoids that contains the prostaglandins and thromboxanes; prostaglandin (PG) E_2 (PGE_2), prostaglandin D_2 (PGD_2), prostaglandin $F_{2\alpha}$ ($PGF_{2\alpha}$), prostacyclin (PGI_2), and thromboxane (TxA_2) [4]. Prostaglandin production is based on the activity of prostaglandin endoperoxide H synthases 1 and 2 (PGHS-1 and PGHS-2) also known as cyclooxygenase 1 (COX-1) and 2 (COX-2) [5]. In general, prostaglandin production occurs step-wise; membrane-bound phospholipids release the major prostanoid precursor Arachidonic acid (20:4 ω-6) by the actions of an enzyme termed phospholipase A_2. Phospholipase A_2 can be either secretory ($sPLA_2$) or cytoplasmic ($cPLA_2$) [6]. Arachidonate is then oxygenated by the prostaglandin synthases (COX-1 or COX-2) yielding PGG_2, an unstable intermediate that is quickly converted to PGH_2. Lastly, this intermediate is converted to the biologically active end prostanoid end products via tissue specific synthases [4, 5].

Different cell types possess different downstream synthases producing the various prostanoid products. Furthermore, some cells can express multiple isomerases at once. It has been shown that COX-1 typically couples with thromboxane synthase and $PGF_{2\alpha}$ synthase. COX-2 is associated with prostacyclin synthase and microsomal PGE_2 synthase-1 [7-9]. Thromboxane synthase is constitutively expressed in platelets and causes platelet aggregation [10]. PGI_2 classically antagonizes thromboxane and is largely produced by cells of the vasculature and acts to reduce platelet aggregation [11]. In

addition, PGD_2 is synthesized in mast cells, basophils, and in T helper cells by the actions of PGD synthases [12]. $PGF_{2\alpha}$ is produced by the cells of the uterus in response to oxytocin [13]. PGE_2 is ubiquitously distributed throughout the mammalian body. Its actions are the most diverse out of all the prostanoids with actions in the reproductive system, vasculature, kidney, brain, and cardiovascular system.

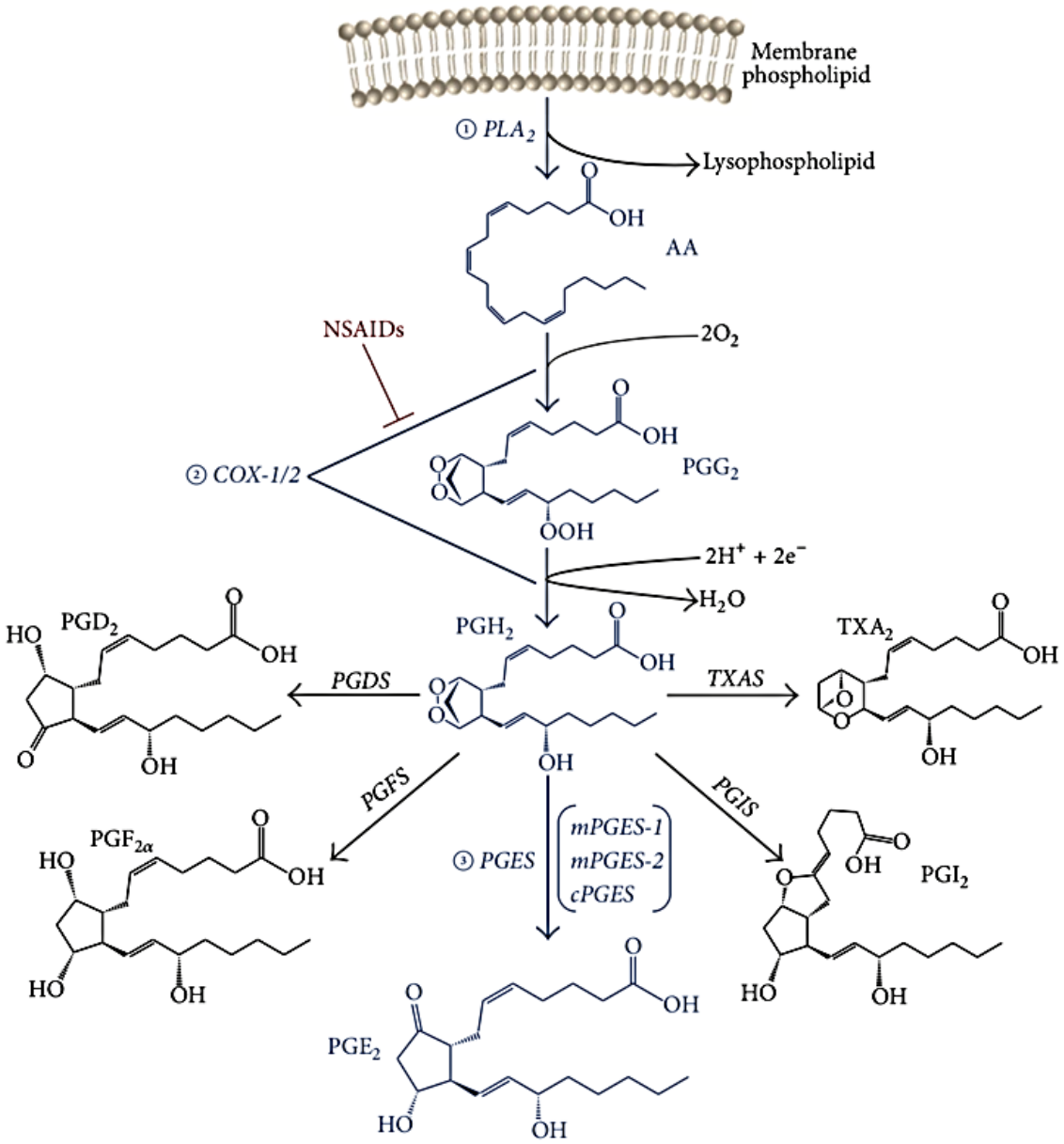

Figure 1: Scheme Depicting the Biosynthesis Pathway of the Prostaglandins and Thromboxane [14].

The cyclooxygenase enzymes have been important in medical drug discovery. COX-1 is constitutively expressed, while COX-2 is the inducible isozyme [4]. COX-1 and COX-2 are very similar in regard to active site structure, products, kinetics, etc. However, there are two major differences. First of all, the active site of COX-2 is larger which has allowed for the production of drugs (selective COX-2 inhibitors; rofecoxib, valdecoxib, celecoxib, etc.) that are selective for COX-2. Secondly, differences in allosteric regulation allows COX-2 to compete more efficiently for newly released arachidonic acid [5].

Nonsteroidal anti-inflammatory drugs (NSAIDs) are a class of drugs that reduce inflammatory pain. NSAIDs such as ibuprofen or aspirin inhibit both COX-1 and COX-2 enzymes. In contrast to ibuprofen, aspirin irreversibly inhibits cyclooxygenase. It has been shown that low dose aspirin preferentially and irreversibly inhibits thromboxane synthesis in platelets while only having a minor inhibition of PGI2 production [15]. Platelets only express the COX-1 isoform and constitutively produce thromboxane, thus promoting platelet aggregation. Furthermore, platelets do not contain a nucleus and therefore cannot synthesize new cyclooxygenase until there is platelet turnover after 8-12 days [16]. In the vascular endothelium, prostacyclin is constitutively produced and counteracts the pro-thrombotic actions of thromboxane. In contrast to platelets, endothelial cells have nuclei and normal rates of protein synthesis; therefore low-dose aspirin selectively inhibits thromboxane synthesis as opposed to prostacyclin. In contrast to NSAIDs, selective COX-2 inhibitors target the COX-2 isoform and therefore affect prostacyclin production rather than thromboxane synthesis [17]. NSAIDs have been used for decades to treat pain and inflammation. In addition to treatment of pain, daily low dose aspirin has become a popular regiment for reducing cardiovascular events. There are side effects, however, to chronic NSAID use. By inhibiting prostaglandin synthesis, NSAIDs have

gastrointestinal, cardiovascular, and renal side effects [18]. In the kidneys, adverse effects of NSAID use include reductions in sodium excretion, potassium excretion, and renal perfusion [19, 20]. Among the cardiovascular side effects, increased risk for MI has been studied in depth. The reduction in prostacyclin synthesis as a result of selective COX-2 inhibition has been linked to increased myocardial infarction by tipping the balance of prostacyclin/thromboxane in favor of pro-thrombotic thromboxane production [21, 22].

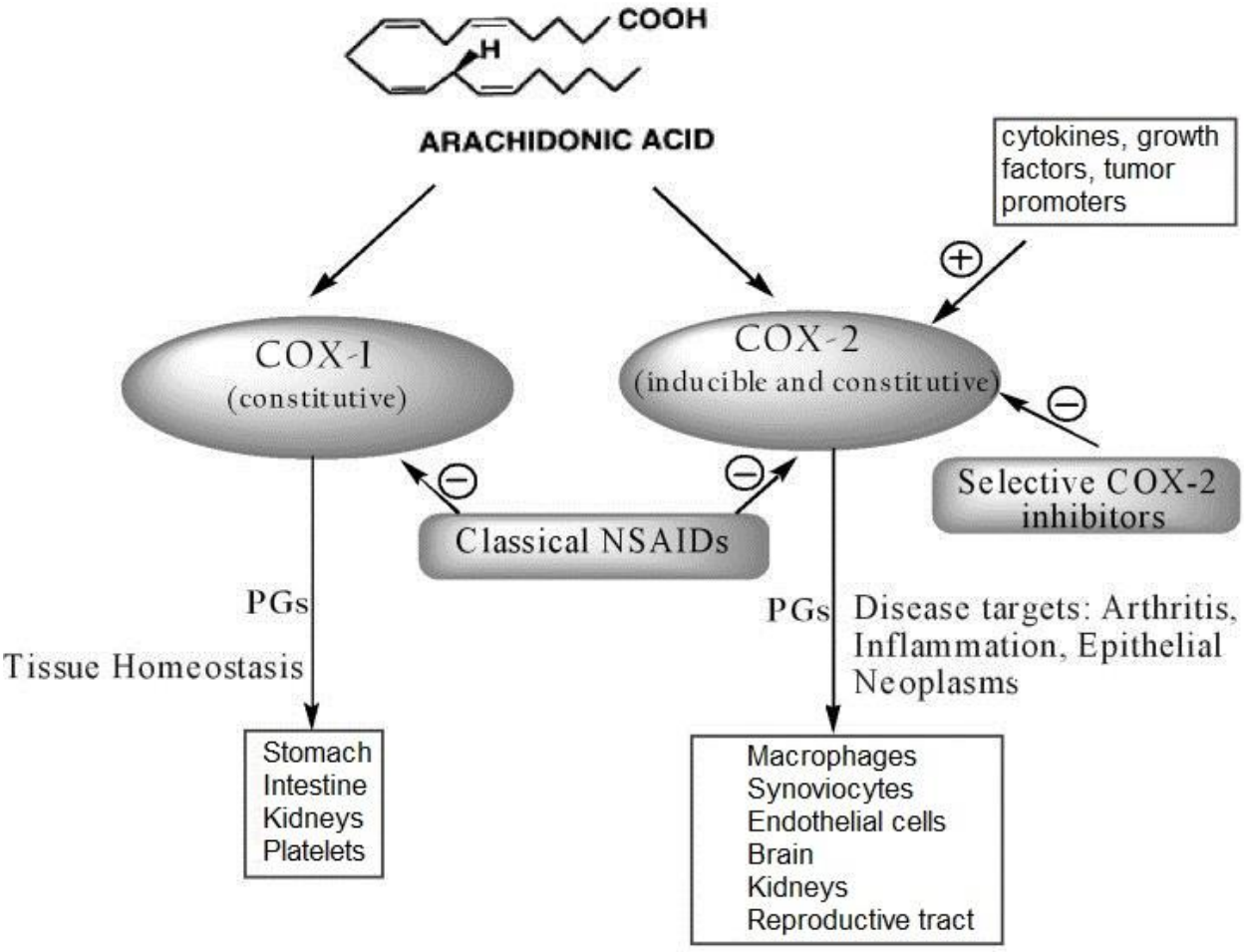

Figure 2: Scheme Depicting the Action of NSAIDs vs. Selective COX-2 Inhibitors [17]

Prostanoid Function

Prostanoids play an important role in sustaining homeostatic function, like blood

pressure, while also mediating pathogenic mechanisms (i.e. inflammatory response). For example, TXA_2 is a potent vasoconstrictor and causes platelet aggregation, while PGI_2 has important vasodilator effects and promotes sodium excretion by the kidneys [23]. Furthermore, the ability of prostanoids to exert both pro-and-anti- inflammatory effects relies upon which receptor is activated and which cell type it is activated in. The prostanoid receptor family consists of eight G-protein coupled receptors (GPCRs); the PGD receptor (DP), the $PGF_{2\alpha}$ receptor (FP), the PGI receptor (IP), the thromboxane receptor (TP), and the four known subtypes of the PGE receptor (EP1, EP2, EP3, and EP4) [24]. The IP, DP, EP2 and EP4 receptors all signal through G_s to stimulate cAMP production in the cell (relaxant response). On the other hand, TP, FP, and EP1 induce a calcium increase in the cell (contractile response). The EP3 receptor signals through G_i to reduce cAMP levels (inhibitory), however, the function and signaling of these receptors can change depending on ligand concentration as well as alternative splicing of certain receptors. For the purpose of this dissertation, only the role of PGE_2 will be discussed as this is the most relevant prostanoid to the project.

The four signs of acute inflammation *rubor* (red)*, calor* (heat)*, tumor* (swelling)*, and dolor* (pain) are characteristics of an inflammatory response. COX-2 derived PGE_2 is known to play a major role in inflammation. COX-2 has been shown in numerous studies to be increased in the site of inflammation [25]. It has also been shown in rodent models of inflammation, such as lambda carrageenan injection, COX-2 levels were increased substantially in the spinal cord [26-30], while the levels of COX-1 remained relatively unchanged [26]. In fact, inhibition of COX-2 is the mechanism by which non-steroidal anti-inflammatory drugs reduce PGE_2 and the above symptoms of inflammation. Early in inflammation, the vasodilation and increased vascular permeability are thought to be

attributed to COX-2 mediated PGE_2 [31]. At the site of inflammation, PGE_2 via its EP2 and EP4 receptors has been shown to increase local vasodilation and subsequent vascular permeability [32-35]. In contrast, PGE_2 acting via its EP3 receptor suppresses vascular leakage [35]. PGE_2 has also been implicated in promoting the pain associated with inflammation and it was reported that mice lacking mPGES-1 $^{-/-}$ had reduced pain and inflammation in a mouse model of collagen induced arthritis [36, 37].

Angiotensin II

Angiotensin II (Ang II) is a vasoconstrictor peptide produced from the renin angiotensin system (Figure 3). In the classical renin-angiotensin system pathway, renin

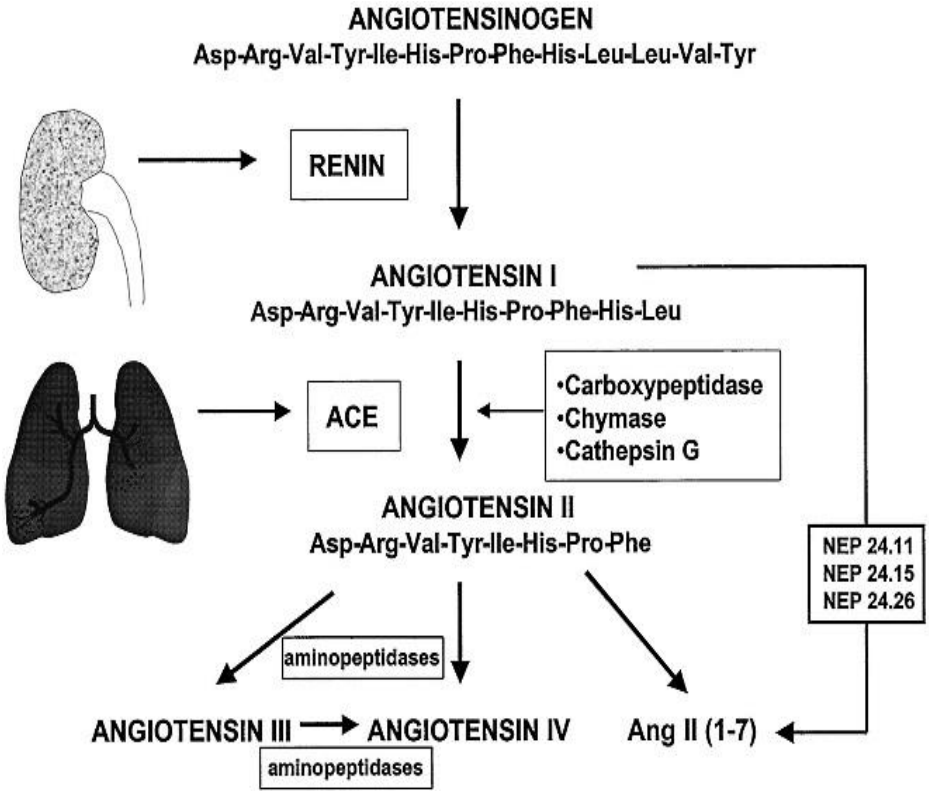

Figure 3: Scheme Depicting the Classical Renin-angiotensin System and Production of Angiotensin II. Angiotensin II can be further metabolized to Angiotensin III, Angiotensin IV, and Ang II (1-7) [1]. *ACE*-Angiotensin converting enzyme, *NEP*- Neutral endopeptidase.

produced from the kidney juxtaglomerular cells cleaves angiotensinogen (liver derived)

into angiotensin I. This is then converted by angiotensin-converting enzyme (ACE) in the lungs to form the active Ang II peptide [38-40]. Ang II is further processed by aminopeptidases to form Ang III, Ang IV, and Ang (1-7) [1]. Ang III promotes similar physiological responses as Ang II [41]. Ang IV is produced from cleavage of Ang III and has effects on blood flow, learning, and neuronal development [42]. Ang (1-7) is formed via the actions of the enzyme ACE2 on Ang II and is shown to be antagonistic to the actions of Ang II via its AT_1 receptor [43, 44].

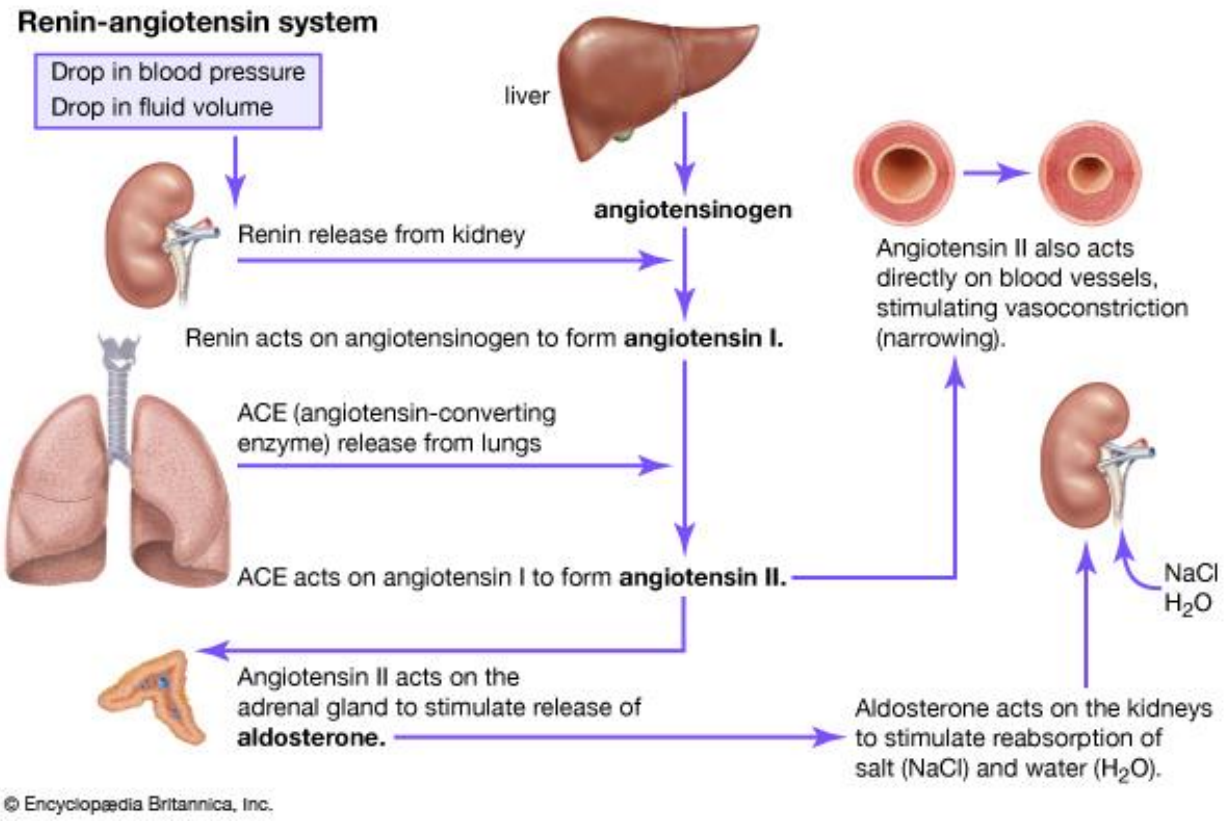

Figure 4: Scheme Depicting the Physiological Actions of Angiotensin II.

In addition to the classical renin-angiotensin pathway, local generation of Ang II has been well documented [45-47]. Aside from vasoconstriction and blood pressure regulation, Ang II also plays an important role in myocardial remodeling after MI and in vascular remodeling during chronic hypertension [1, 48-56]. Ang II mediates its effects

through two plasma membrane receptors AT_1 and AT_2. The AT_1 receptor is a G protein-coupled receptor that signals through G_q to activate phospholipase C [57, 58]. Literature suggests that most of the functions mediated by Ang II appear to be through the AT_1 receptor, especially in the vasculature [59]. AT_1 is expressed abundantly in the smooth muscle cells, with much lower levels in the adventitia and is virtually undetectable in the media [60, 61]. The AT_2 receptor is also a G protein-coupled receptor, although the exact signaling mechanism is still unknown. It is thought however, to antagonize the actions of AT_1. The AT_2 receptor is expressed at high levels in fetal tissue and then decreases after birth. Also, AT_2 expression in adults is detectable in the pancreas, kidney, adrenals, brain, vasculature (adventitia and media only), and the heart [62, 63]. The expression of both receptor subtypes can change with injury. For example, hypertension has been shown to cause overexpression of AT_1 in the kidney and brain, while overexpression of AT_2 has been shown in the mesenteric arteries and endothelium [64].

Chemokines and Cytokines in Cardiac Repair and Remodeling

One significant end point of chronic inflammation, chronic hypertension, or myocardial infarction (MI), is myocardial repair. After myocardial injury, chemokines such as CCL2 and cytokines including IL-6 and TNF-α are released and regulate myocyte survival by recruiting inflammatory cells (i.e., neutrophils and macrophages) to the site of injury to clear up debris and dead cells [65-67]. Chemokines are small 8-12 kDa proteins that activate and mediate the immune cell responses during an inflammatory event. There are four classes of chemokines, C, CC, CXC, and CX_3C. They are so named for the location of the first two cysteines. For example, in the CC family the two cysteines are adjacent, while in the CXC family, they are separated by any amino acid. Both the CC and CXC chemokines are significantly increased in the infarcted heart [65]. In general,

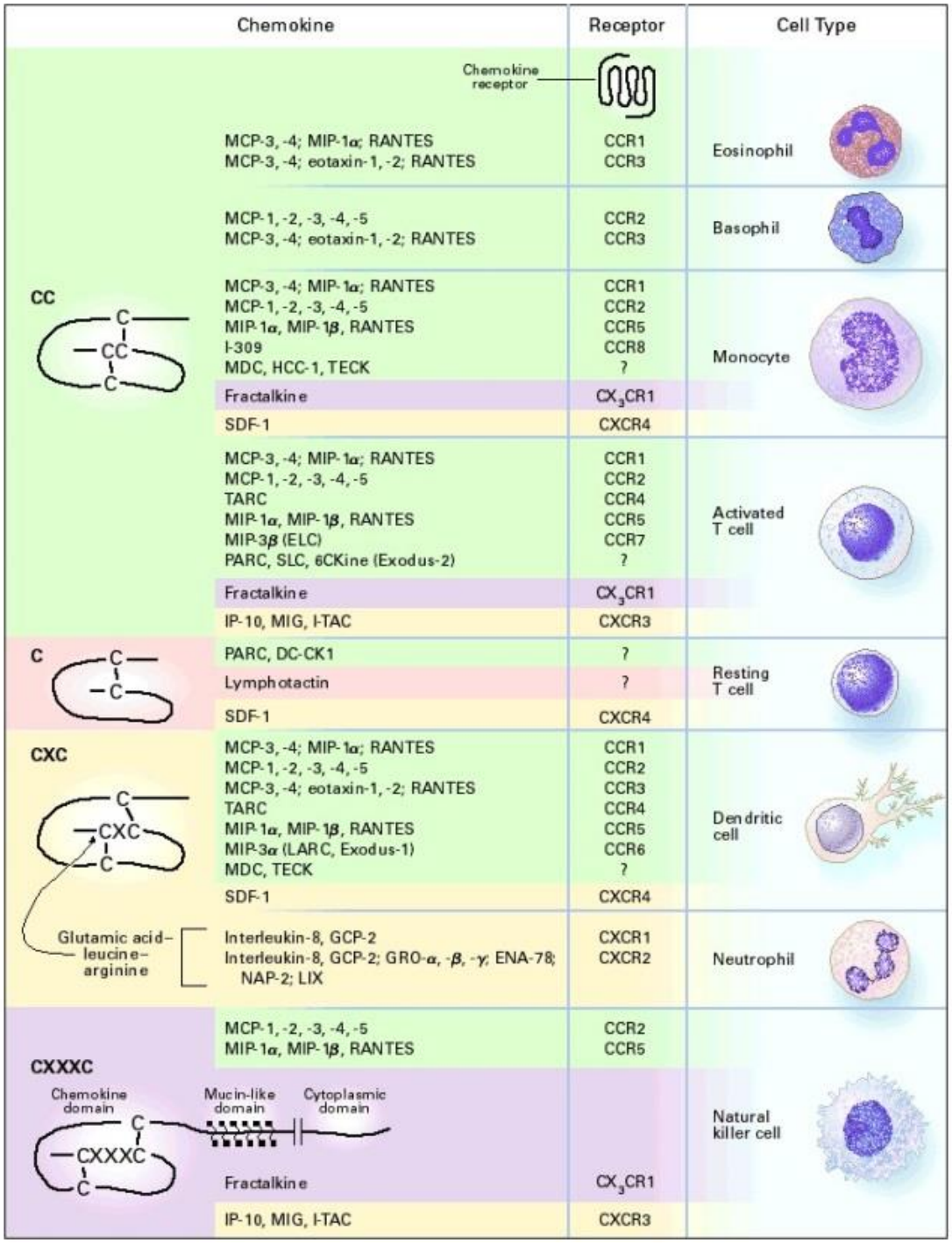

Figure 5: Scheme Depicting the Four Families of Chemokines, their Receptors, and the Cell Type that they Recruit [74].

the chemokines bind their respective receptors on the surface of the leukocytes. The chemokine contact with its receptor induces integrin activation and promotes a closer

interaction between the rolling leukocyte and the endothelium wall. This leads to infiltration of the leukocyte into the inflamed tissue [68, 69]. CCL2, or monocyte chemoattractant protein (MCP)-1, is rapidly increased in the infarcted heart and mediates monocyte recruitment to clear the myocardium of debris from apoptotic/necrotic cells [70]. Additionally, activated by the CC family of chemokines, CCR1, CCR2, and CCR5 receptors have been shown to be most important for leukocyte recruitment during an inflammatory cascade [71]. One particular chemokine, CCL12 (MCP-5), is the mouse analogue to human MCP-1. MCP-5 is a potent chemoattractant for monocytes via the CCR2 receptor subtype. Additionally, MCP-5 was shown to be produced by activated macrophages [72]. Thus MCP-5 is important in inflammatory processes such as cardiac remodeling and a previous study from our laboratory showed that MCP-5 was upregulated in the hearts of adult EP4 KO mice that are in heart failure [73].

Expression of pro-inflammatory cytokines IL-6, TNF-α, and IL-1β is increased in MI [75, 76]. Evidence suggests that initially, cytokine gene expression is increased by myocardial cells in response to the ischemic insult. By 24 hours, cytokine gene expression was shown to return to normal baseline levels. However, by 7 days there was a second wave of cytokine expression, largely produced by infiltrating macrophages [76]. These cytokines are not typically expressed in the normal heart and only released during an innate stress response [77]. This biphasic response in ischemic conditions is typically regulated by the size of the infarct. For example, if the infarct is small, cytokines can be upregulated in the infarct zone up to 50-fold but will quickly return to baseline levels [78, 79]. If the infarct is large, however, this cytokine upregulation can be prolonged and promote a second wave of remodeling (the chronic phase) extending into the remote zone and eventually, the entire myocardium [79, 80]. The release of cytokines during injury is

actually favorable, leading to cardiac healing and improved cardiac function. However, persistent inflammation can lead to heart failure through chronic remodeling [81]. Acutely, the increase in cytokines has 4 major effects on cardiomyocytes that contribute to cardiac remodeling; myocyte apoptosis [82, 83], hypertrophy [84], reduced contractility [85], and inflammatory signaling [67]. Chronically, cytokines such as TNF-a, IL-1β, and IL-6, have effects on integrins, vasculature, and the extracellular matrix [79, 86]. Mechanistically, myocardial stress is potentially sensed by mechanosensors (integrins, sarcolemmal proteins, and cytoskeleton) and leads to activation of MAPK, STAT, and calcineurin-dependent signaling. These pathways ultimately lead to downstream activation of pro-inflammatory transcription factors such as NF-κB and AP-1 [87].

Cardiac Inflammation and Remodeling

Myocardial Infarction

The pathological process of heart failure following myocardial infarction consists of a cardiac remodeling process. The adult heart has essentially no capacity to regenerate its tissue and therefore the process of remodeling the infarcted myocardium consists of an inflammatory response and repair of the heart via collagen deposition and formation of a scar [67, 88]. The normal heart contains a small population of immune cells, although the majority of resident immune cells have been shown to be macrophages [89-91]. This small population expands in the event of an infarct to start the repair process. The reparative response following an ischemic event is typically divided into three phases: the inflammatory phase, the proliferative phase, and the resolution/maturation phase [92].

During the inflammatory phase, ischemic cardiomyocytes release danger signals (DAMPs) that activate the Toll-Like receptor signaling in various cell types present in the heart (macrophages, cardiomyocytes, vascular cells, fibroblasts, infiltrating leukocytes,

etc.) [93]. Some examples of DAMPs include extracellular RNA [94], mitochondrial DNA [95, 96], Hyaluronan [97-99], HSP60 [100, 101], and IL-1β [102]. The signaling induced by these DAMPs promotes production of chemokines and cytokines and the subsequent recruitment of neutrophils (early), monocytes, and lymphocytes into the infarcted myocardium. The activated phagocytes clear the infarcted region of dead cells and debris. This clearance of debris is a transitionary event and is the beginning of the proliferative phase [88].

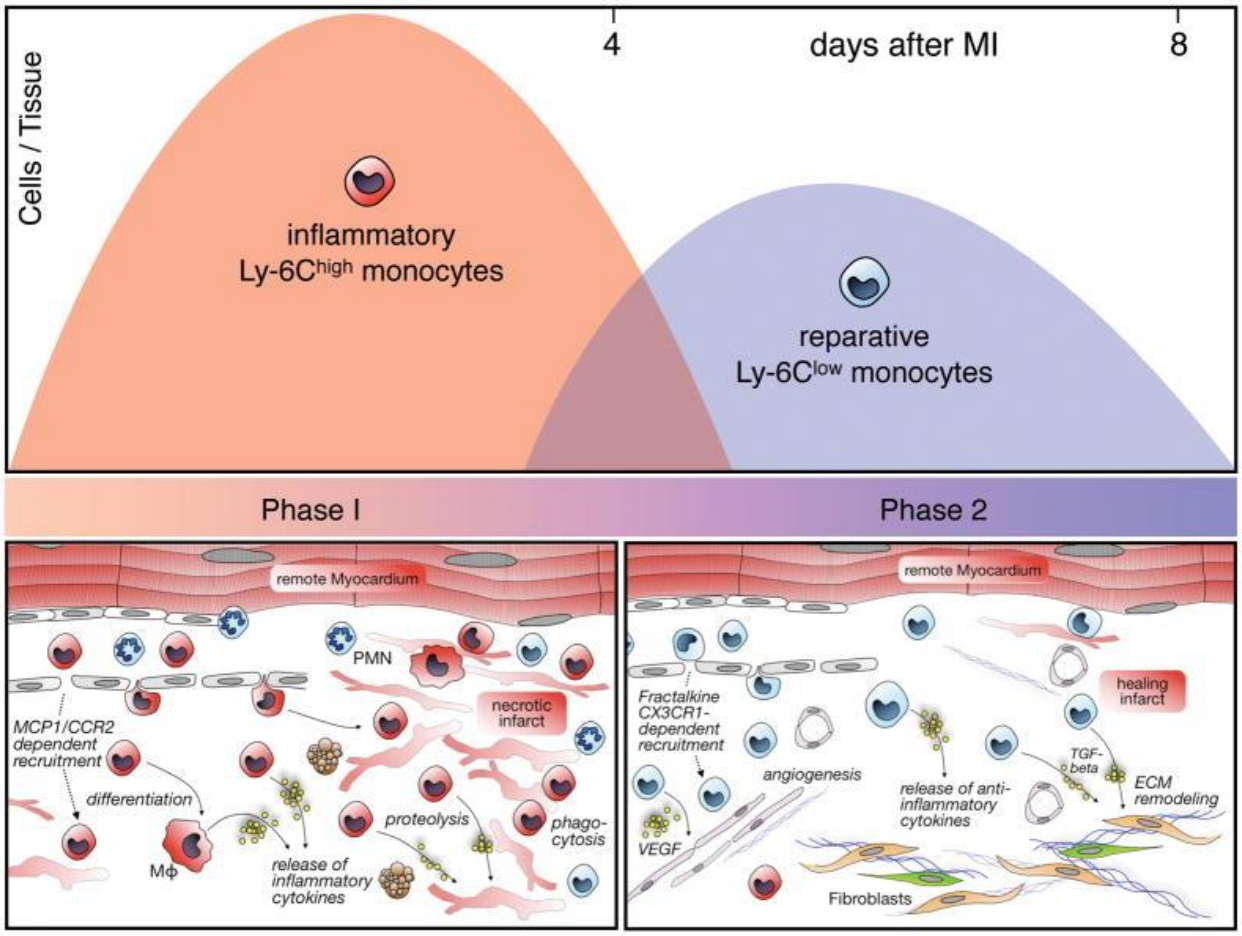

Figure 6: Scheme of the Monocyte Response in the Post-MI Mouse Heart. PMN: neutrophil, MΦ: macrophage, ECM: extracellular matrix [116].

During the proliferative phase, there is substantial expansion and activation of the cardiac fibroblasts and induction of angiogenesis [103, 104]. Fibroblasts within the infarct zone acquire an activated phenotype (myofibroblast) and are responsible for production

of extracellular matrix proteins and collagen within the infarct [105]. Fibroblasts are suited for this role because they are less susceptible to ischemic injury, are widely distributed throughout the heart, and have a close anatomical relationship with the myocytes [106]. The potential of the fibroblasts to initiate an inflammatory response has also been well documented [107-109]. Unfortunately, the role of cardiac fibroblasts as inflammatory cells is still not fully understood for multiple reasons. First, there are other cell types in the heart like endothelial cells and resident cardiac mast cells, both of which have been implicated in triggering inflammation post-MI [110, 111]. Secondly, there are no commercially available markers for cardiac fibroblasts that are reliable so investigating the fibroblast-specific inflammatory response has been challenging [112]. However, data from our lab suggests that in response to stimuli such as Lipopolysaccharide (LPS), isolated adult mouse cardiac fibroblasts produce a substantial amount of chemokines, including MCP-5.

Lastly, during the maturation phase, the newly synthesized extracellular matrix undergoes cross-linking and the collagen scar is reinforced. Without reinforcement of the scar, cardiac rupture can occur, although incidence in humans is low. Furthermore, the proliferation of the fibroblasts is inhibited to prevent further extracellular matrix deposition [113]. The cellular effectors important in the maturation of the scar are still unknown, however macrophages have been implicated in this process [88]. A normal, properly healed infarct contains extracellular matrix that matrix that can make up to 80% of the infarct area [114], presumably with little fibrosis in the remote area of the heart. Thickness of the scar has been correlated with improved LV function [115].

If the collagen deposition process becomes dysregulated, deposition can also occur in the interstitium promoting ventricular stiffness and cardiac dysfunction. Over time

this interstitial fibrosis leads to adverse remodeling of the ventricle and reduction of function [117]. Further contributing to fibrosis is the local production of Angiotensin II (discussed in greater detail in later sections). Ang II is produced in the heart by activated macrophages, cardiomyocytes, and the myofibroblasts and stimulates production of TGF-β1, and subsequently increased production of collagen by the myofibroblasts [118]. The persistent expression of Ang II, its AT_1 receptor (discussed later), and TGF-β1 have all been observed months following MI in rodents [118].

Excessive extracellular matrix turnover contributes to high morbidity and mortality in human patients [119]. This is in part due to the activity of matrix metalloproteinase enzymes (MMPs). There are 25 known MMPs, of which about half have been measured in the left ventricle post MI [120]. After MI, MMPs degrade the extracellular matrix and promote further recruitment of immune cells to phagocytize dead cells/debris. Long term stimulation of MMPs results in activation of the tissue inhibitor of metalloproteinases (TIMPs). This leads to long-term remodeling by reducing the MMP/TIMP ratio [121, 122]. The use of MMP inhibitors post MI is still being investigated [123]. However, several current therapies for MI and heart failure act as indirect inhibitors for MMPs (ACE inhibitors, Angiotensin receptor blockers (ARBs), beta-blockers) [119]. The indirect inhibition of MMPs by ACE inhibitors has been well documented and shown to improve cardiac outcomes post MI in human patients [124]. In addition, there is strong evidence for the use of ARBs post MI [125]. Rats that were treated with an ARB, losartan, had reduced expression of MMP-8, -13, TIMP-1, -2, and collagen in the heart post MI [125]. Moreover, deletion of the AT_1 receptor in mice reduced LV remodeling and improved survival of rats after MI [126].

A major complication of adverse cardiac remodeling is the development of heart

failure [127]. Infarct size is a major predictor of future heart failure [128]. Furthermore, the combination of the loss of ventricular muscle with the adverse cardiac remodeling that occurs during and after MI contributes to the development of heart failure. In addition, there are several geometric changes that occur in the heart that can lead to systolic and diastolic function such as ventricular wall thinning, chamber dilatation, and expansion of the infarct [129, 130]. At first, left ventricular enlargement is a compensatory mechanism in response to loss of ventricular muscle, to maintain stroke volume. However, this is a balance between chamber dilatation and increased heart volume. Over time, this can lead to further cardiac dysfunction and failure.

Chronic Hypertension

Chronic hypertension is the single most significant risk factor for developing heart failure globally [131]. A major consequence of chronic hypertension is the development of left ventricular hypertrophy (LVH) [132]. One of the major differences between hypertensive heart disease and other forms of heart failure is in the way the LV remodels. Hypertensive heart disease is a chronic disorder thus patients with hypertensive heart disease frequently present with LVH, but preserved systolic function, depending upon the stage of the disease. Patients with heart failure caused by ischemia, however, present with dilated LV chambers and frequently right ventricle enlargement as well, along with systolic dysfunction [133-135]. Hypertrophy of the left ventricle in the presence of hypertension is a powerful predictor of negative cardiovascular outcomes such as coronary heart disease, stroke, sudden cardiac death, and heart failure [136-140]. LVH is an adaptation to the increased workload in the heart in order to normalize wall tension and preserve cardiac function. However, persistent LVH leads to cardiac dysfunction in the form of ischemia, arrhythmias, heart failure, and/or sudden death [141]. In humans,

the occurrence of LVH is directly associated with the level of systolic blood pressure [142-146]. Blood pressure itself is not the only contributing factor in the development of LVH [147]. Other factors include sex, age, race, and body mass index (BMI). For example, the left ventricle mass of hypertensive women was reportedly higher than that of hypertensive men (57 % vs. 31 %, respectively) [136]. The frequency of LVH also increases with age and this effect is greater in women compared to men. African Americans have a 2-3 fold higher risk of LVH than whites with the same elevation of systolic blood pressure [148]. Obesity is also a major risk factor for LVH. It was reported that a 2 Kg/m^2 increase in BMI correlated with a 50 % risk of increased left ventricle mass in elderly men and women [149].

Mechanical stress inducing myocyte hypertrophy is one component contributing to LVH. However, hypertrophy of the myocytes without fibrosis does not appear to have negative implications. Samples taken from patients with LVH and hypertensive heart disease have increased collagen and fibrosis compared to normal hearts [150]. The pro-fibrotic process is controlled by a variety of hormones and cytokines such as Ang II, aldosterone, TGF-β. In contrast, breakdown of collagen is regulated by substances such as bradykinin, nitric oxide, and glucocorticoids [151]. Fibrosis in hypertensive heart disease is typically more widespread than in other causes of heart failure. It is found in the anterior, posterior, lateral walls of the left ventricle, interventricular septum, and right ventricle [135]. Changes in the collagen content in the hypertensive heart can impair systolic and diastolic function [152]. Normal collagen turnover by the fibroblasts is slow (80-120 days) [153]. In pathological conditions, the collagen turnover is determined by myofibroblasts and regulated by autocrine and paracrine factors. Animal models have provided insight into three potential mechanisms for the transition from LVH to heart

failure by degradation of the collagen network [152]. The first mechanism involves an interrupted collagen network, resulting in loss of support, geometric alignment, and coordination of cardiomyocyte contraction. The second mechanism involves loss of interaction between laminin and collagen with their receptors. The third mechanism involves loss of the number of muscular layers in the ventricular wall and LV dilation [135].

The MMPs and TIMPs also play a role in hypertensive heart disease, although the role of these molecules is not fully elucidated. In hypertensive Dahl salt-sensitive rats, MMP2, TIMP1, and TIMP2 expression increased in parallel with LVH [154]. Likewise, in spontaneously hypertensive rats, MMP2 activity is increased [155]. In patients with hypertension and LVH, there are increased TIMP1 levels, but reduced MMP1 and collagen type I telopeptide (a breakdown product of collagen) [156]. Patients with hypertension and LVH were also shown to have reduced levels of MMP2 and MMP13, but increased levels of MMP9 [157].

Cytokines are suggested to play a major role in the pathogenesis of hypertension. For example, TGF-β was suggested to play a role in hypertensive disease by regulating cell growth/differentiation and extracellular matrix/repair [158, 159]. Furthermore, polymorphisms within the TGF-β1 gene have been associated with increased risk of hypertension [160]. The role of inflammation in hypertensive end organ damage has become evident in the past several years. There is little data on immune cell infiltration in human organs but this has been investigated in several animal models. For example, mice lacking RAG1 lack all lymphocytes and had a blunted hypertensive response to Ang II, deoxycorticosterone acetate (DOCA)-salt, and norepinephrine challenges [161-163]. Likewise, deletion of this gene in Dahl salt-sensitive rats attenuates their hypertensive response after salt feeding [164] .

Polarization of Macrophages in Cardiac Inflammation and Remodeling

Macrophages exist in all tissues of the body, even in steady-state conditions [165]. These tissue resident macrophages contribute to homeostatic functions by removing dead or senescent cells and preventing infection [166]. Interestingly, macrophages can have tissue-specific functions. For example, macrophages in adipose tissue can produce catecholamines to maintain thermogenesis and promote insulin resistance [167]. Also, peritoneal macrophages promote migration of B cells to the intestines, thereby orchestrating their early response to pathogens and production of antibodies [168]. After an injury or during inflammation, circulating monocytes are recruited to the site of inflammation where they differentiate into macrophages. Furthermore, during the inflammatory phase of cardiac remodeling, the majority of the macrophages present are derived from these circulating monocytes [169].

The macrophages play a key role in response to MI [170, 171]. After MI, circulating monocytes infiltrate the infarct and border regions and differentiate into macrophages [116]. Within 7 days of MI, these cells have become the majority of the macrophages in the infarct [172]. Macrophages can phagocytize dead/dying cells, secrete pro-inflammatory or anti-inflammatory factors, and can interact with other cell types to assist in the reparative response [173, 174]. The ability of macrophages to have such diverse functions could be attributed to the different phenotypes and their polarization status. Macrophages can express different genes and possess different functions in response to environmental signals. Early after MI, macrophages have a proinflammatory M1 phenotype, while displaying an anti-inflammatory M2 phenotype in the later phase [175, 176].

Cardiac macrophages have been shown to be of the M2 phenotype in steady-state

conditions [169, 177]. Various markers for identification of monocytes and macrophages currently exist, such as CD68, CCR2, CD11b, CD163, F4/80, and MHCII [166, 178-186]. Additionally, the Ly6C/Gr-1 marker is used extensively and is unique to rodent models as it is not expressed in human macrophages. Cardiac macrophages have been shown to be heterogeneous in their origins and four populations have been identified in the mouse heart [187].

One population, $Ly6C^{-}CCR2^{-}$, comprises the vast majority of cardiac macrophages and are derived from the yolk sac. This population contains both $MHCII^{high}$ and $MHCII^{low}$ subsets and is further subdivided into the second population based on $Ly6C^{-}CCR2^{+}$ (second population). The third population $Ly6C^{+}CCR2^{-}$ and the fourth population $Ly6C^{+}CCR2^{+}$, originate from hematopoiesis [179, 187, 188]. The roles for these different macrophage populations within the heart are not fully understood. It has been shown that $MHCII^{high}$ macrophages present antigens to T cells more efficiently, while the $MHCII^{low}$ macrophages have more phagocytic capabilities [179]. Within the circulating pool of monocytes in mice, there are 2 subsets of Ly6C expression. $Ly6C^{hi}$ are proinflammatory and express high amounts of CCR2. In contrast, the second subset, $Ly6C^{low}$, express low levels of CCR2 [175].

Macrophages demonstrate high adaptability and heterogeneity, making an exact classification of their phenotype difficult. However, early after MI (days 1-3), the M1 macrophage phenotype dominates, whereas the predominant macrophage phenotype at days 5-7 is the M2 [189]. In the heart, the pro-inflammatory M1 macrophages secrete chemokines, cytokines, and other growth factors to cause phagocytosis of debris and extracellular matrix [176]. In contrast, the M2 macrophages are reparative and produce anti-inflammatory factors such as IL-10, and TGF-β1 [176]. The transition from the M1 to

M2 phenotype post MI has been shown to be crucial in promoting repair following MI in mice [190-193]. Furthermore it was shown in rodents that MMP-28, IL-10, and deletion of MMP-9 affect cardiac remodeling post MI by shifting the M1/M2 balance to the M2 phenotype [194-196].

The M1 and M2 macrophage phenotypes were originally based on data showing that treatment of macrophages with lipopolysaccharide and IFN-γ causes macrophages to produce pro-inflammatory molecules, such as IL-1β, IL-6, and TNF-α and was named M1. On the other hand, IL-4 promotes macrophage production of anti-inflammatory molecules, such as Arginase1, Fizz1, and Ym1 and was named M2 [194]. Unfortunately, *in vivo*, there is complex diversity in the macrophage population and trying to define macrophages as M1/M2 based on only one or a few markers is difficult. Additionally, the mechanism of macrophage polarization remains poorly understood. One hypothesis, presented by Nahrendof et al. states that early recruitment of $Ly6C^{high}$ cells relies on CCR2 signaling and that these cells can differentiate into $Ly6C^{low}$ during the reparative phase [197]. In contrast, they show that later $Ly6C^{low}$ recruitment depends on CX_3CR1. Furthermore, the same authors showed that the $Ly6C^{high}$ cells were proinflammatory and phagocytic, while the $Ly6C^{low}$ cells were anti-inflammatory and pro-reparative. This hypothesis agrees with others [189, 198, 199], although it fails to recognize the role of the local infarct environment on macrophage polarization. Further studies are necessary to identify distinct pathways that are involved in coordinating macrophage polarization.

PGE_2 has been shown to play a role in macrophage polarization by inducing the M2 phenotype through up-regulation of the CREB pathway. Furthermore, PGE_2 attenuates pro-inflammatory M1 macrophage gene expression by inducing IL-10 expression via cAMP-PKA-CREB signaling [200-202]. The EP receptor responsible for

these effects was not examined in the aforementioned studies; however, one can presume it is via the EP2/EP4 receptor axis due to increases in cAMP-PKA signaling.

The Role of T Cells in Cardiac Inflammation and Remodeling

T Cells in Myocardial Infarction

Several studies have implicated T cells in the cardiac remodeling process following MI, however their role is not fully understood and is controversial [203]. One major question in the field is whether or not the T cells are responding to tissue specific damage signals or systemic auto-antigens [204]. In contrast to the rapid response by cells of the innate immunity (i.e., monocytes/macrophages), cells of the adaptive immune response (e.g., T cells) respond much more slowly in response to injury. In general, T cells reside in the lymph node until stimulated [205]. Differentiated T cells leave the lymph node and migrate to inflammatory sites where they employ their unique functions. At steady state, there are less than 10,000 lymphocytes per milligram of tissue in the heart. After MI, the levels increase 5-10 fold due to an influx of recruited cells, peaking around day 7 [189]. One subset of T cell, $CD4^+$, are further classified into Th1, Th2, Th17, and Treg. Tregs are unique specialized cells that act to suppress inflammation [206, 207]. After MI, $CD4^+$ cells in the infarcted area are mainly Th1 cells and produce mainly IFN-γ [189]. It has also been shown that T cells regulate the infiltration of proinflammatory monocytes. The absence of $CD4^+$ T cells resulted in an increase in $Ly6C^{high}$ monocytes and subsequently increased collagen deposition and impaired cardiac remodeling by reducing capillary density 7 days post MI [208]. This mechanism still remains to be elucidated. Furthermore, depletion of $CD4^+$ cells resulted in a predominantly M1 phenotype in myocardial macrophages suggesting cross talk or interactions between the two cell populations [193].

T Cells in Chronic Hypertension

In recent years there have been numerous studies examining the contribution of inflammation and immunity to the development of hypertension. One study by Itani et al. employed a unique bone/liver/thymus humanized mouse to address the role of T cell activation in hypertension. Two weeks of Ang II infusion resulted in an increase in T cell ($CD4^+$ and $CD8^+$) infiltration in the kidneys, aorta, and lymph nodes. When blood pressure was normalized with diuretics (hydralazine and hydrochlorothiazide) the infiltration of T cells in the various tissues was abrogated, suggesting that Ang II does not directly activate T cells. The authors confirmed this by treating cultured T cells with Ang II and analyzing a panel of cytokines [209]. Other studies have suggested that T cells can increase reactive oxygen species as a result of their natural host defense activity, thereby promoting hypertension in response to hypertensive stimuli, such as Ang II [161, 210, 211].

To date, the effects on blood pressure and end organ damage via T cell activation remains to be elucidated. It is complicated by the fact that different T cell populations, T cell localization, activity of other immune cells, and the model used are all important variables in the T cell response observed.

Prostaglandin E_2 and Its Signaling

PGE_2 is produced from PGH_2 by the tissue specific synthases cPGES-1 (cytosolic form), mPGES-1 and mPGES-2 (microsomal forms). PGE_2 is one of the most abundant prostaglandins produced in the body and exerts a variety of biological effects. Additionally, PGE_2 is the most abundant PG produced in left ventricle myocytes [212]. Prostaglandin E_2 plays an important role in the cardiovascular system such as regulating vascular tone [213-215] and cardiac remodeling [73, 212, 216-219].

PGE_2 has four known receptor subtypes, EP1-EP4. EP1 couples to G_q [220, 221] and increases intracellular Ca^{2+} via activation of PLC and has many functions throughout the body, depending on where it is expressed. The highest expression of EP1 is recorded in the collecting duct of the kidneys [222]. The literature also describes expression of EP1 in the glomerulus, podocytes, and in the proximal tubules [223-226]. Furthermore, EP1 knockout mice have a reduced pressor response to angiotensin II infusion [227]. EP1 in the heart has been shown to increase the beating rate of neonatal rat cardiomyocytes [228] and in neonatal ventricular fibroblasts, activation of EP1 and/or EP3 in this cell type promotes fibroblast cell growth and proliferation, perhaps implicating this mechanism in increased cardiac fibrosis [229]. In general, research around the EP1 receptor has mostly focused on cancer, pain, inflammation, and stress responses [230].

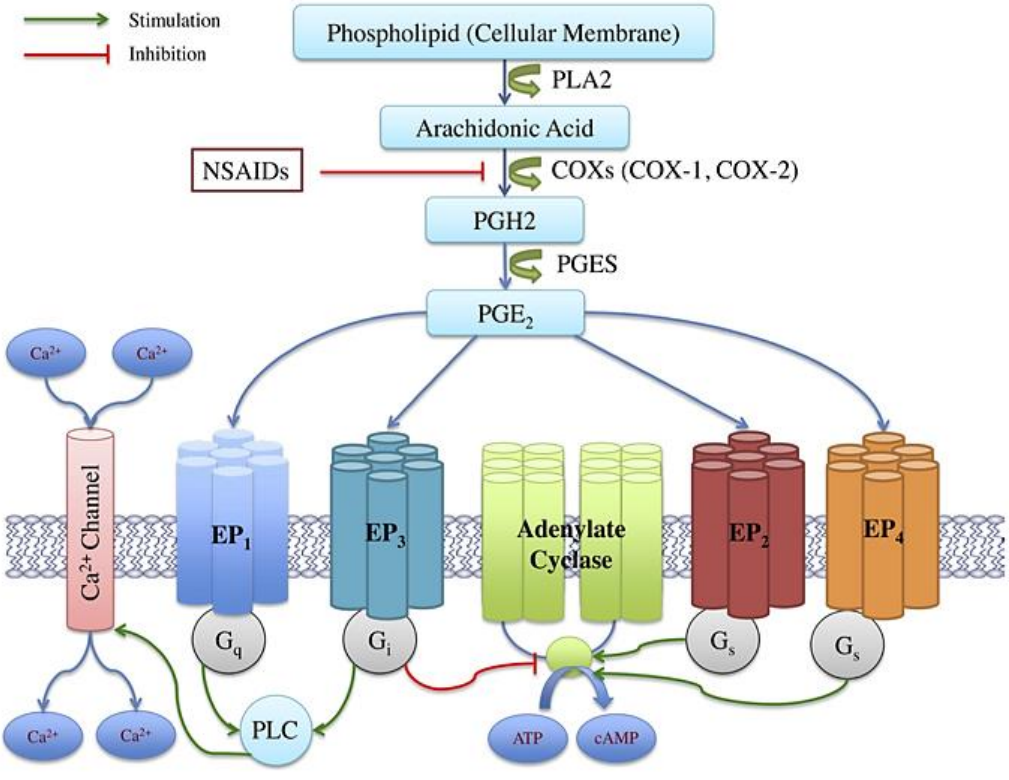

Figure 7: Scheme Depicting PGE_2 Biosynthesis, its Four Receptor Subtypes, and their Signaling Pathways [231].

The EP2 and EP4 receptors both couple to $G_{\alpha s}$, however EP4 has been shown to have additional signaling through the ERK and PI3K pathways. This has been implicated in cancer and inflammatory disorders [232]. Both receptors stimulate adenylate cyclase, increase cAMP production, and activate PKA. PKA activation has been shown to phosphorylate CREB and increase the activity of Tcf/lef-induced genes. EP2 and EP4 have various roles depending on where they are expressed although both typically induce smooth muscle relaxation [233]. The EP4 receptor has been heavily studied in the context of cancer research, but also has been shown to have cardioprotective effects in *in vitro* and *in vivo* models [234]. EP2 knockout mice have been shown to have an attenuated cardiac function after myocardial infarction, suggesting a protective role of this receptor in the heart.

In contrast to EP2/EP4 signaling, the EP3 receptor signals through Gi, to inhibit adenylate cyclase production. In the mouse, EP3 has 3 isoforms due to alternative splicing of the c-terminal tail [235]. It has been reported that these splice variants have differences in function, differences in signaling, different sensitivities to agonists, different trafficking patterns, and different internalization patterns [236-238]. Some EP3 isoforms can activate RhoA through $G_{\alpha 12}$ signaling [239]. Like the other receptor subtypes, EP3 has various functions throughout the body. In adult mouse cardiomyocytes and in a working Langendorff preparation, EP3 receptor activation was shown to directly reduce cardiac contractility, presumably via reductions in phosphorylated phospholamban [217].

The Role of Prostaglandin E_2 in Blood Pressure Regulation and Hypertension

In general, PGE_2 is a potent vasodilator, natriuretic [240], and diuretic. The vasodilatory effects of PGE_2 been demonstrated in several different tissues including hamster uterus, rabbit ductus arteriosus, human pulmonary vein, rabbit ear artery, and

rabbit saphenous vein [241-247]. Furthermore, a vasodilatory role for PGE_2 has been also been observed in resistance vessels; pig pial arterioles [248] and in canine renal juxtamedullary arterioles [249]. In contrast, vasoconstrictor actions of PGE_2 have been reported; in rings of human internal mammary arteries (via EP3 receptor) [250] and rat mesenteric arteries [251]. These different effects of PGE2 are most likely to the different receptors that are being activated in that tissue bed. Consistent with vasoconstriction, activation of the EP1 receptor is coupled with increases in intracellular calcium. In spontaneously hypertensive rats, EP1 antagonism reduced blood pressure as well as attenuated the pressor response of Sulprostone, an EP1/EP3 agonist [227]. It was shown in normal Sprague Dawley rats that the aorta and mesenteric arteries express EP3 and an EP3 agonist enhanced contraction of these vessels [215]. Another component of the variable response to PGE_2 is the genetic background of the rodent model being used. For example, studies using mPGES1 knockout (mPGES-1 $^{-/-}$) mice on a mixed genetic background had an accelerated hypertensive response to Ang II [252], whereas mice on a pure C57Bl/6 background achieved similar levels of systolic blood pressure after 8 weeks of Ang II infusion [218].

The Role of Prostaglandin E_2 in Inflammation

In contrast to the classical, pro-inflammatory notion of PGE_2, studies have shown an anti-inflammatory role for PGE_2 signaling via its EP4 receptor in a variety of different cell types [253-258]. Several studies also suggest that PGE_2 can modulate the inflammatory cell (i.e., monocytes, macrophages) response at the site of the injury/inflammation [256, 259-261]. EP4 activation reduces the production of chemokines, like MCP-1 and MIP-1α in human macrophages [256, 262] and reduced expression of adhesion molecules in human monocytes [263], however the exact mechanism is not fully

understood. A study by Ngoc and colleagues showed that PGE_2-EP4 signaling inhibits T-cell proliferation in a rat model of experimental autoimmune myocarditis. Furthermore, activation of the EP4 receptor lead to improvements in cardiac function, reduction of heart size, and reduced circulating MCP-1 levels [259].

Macrophages express the EP4 receptor more than any other of the EP receptor subtypes. It has been reported that PGE_2 can suppress the chemokines produced in LPS-stimulated human macrophages, presumably through EP4 receptor activation [256]. Also, it has been documented that PGE_2 can promote the anti-inflammatory M2 macrophage phenotype via activation of PKA and phosphorylation of CREB [200, 201]. In a study by Luan et al., bone marrow derived macrophages exposed to IL-4 and PGE_2 promoted induction of M2 macrophage markers, which was antagonized in CREB mutant cells [200]. Another study conducted by Sanin et al. confirmed these findings [264]. A separate study by Tang et al. examined the effect of the EP3 receptor on two separate populations of macrophages, $Ly6C^{high}$ (pro-inflammatory, M1 type) and $Ly6C^{low}$ (anti-inflammatory/reparative, M2 type). They found that deletion of the EP3 receptor impaired the expression of the chemokine receptor CX3CR1, suppressed TGFβ1 signaling, and therefore reduced infiltration of the $Ly6C^{low}$, M2 macrophage in mouse hearts after MI [265].

The Role of PGE_2 in Cardiac Remodeling

The role of PGE_2 has been well characterized in the context of ischemia/reperfusion (I/R) injury in the heart and in the MI model. Myocardial injury resulting from I/R is the cause of oxygen free radical production and the inflammatory response, leading to death of the cardiomyocytes and ventricular remodeling (i.e., interstitial fibrosis). It has been shown that EP4 receptor activation protects the heart from

I/R in a rat model, by reducing the number of inflammatory cells and suppressing the production of MCP-1 [266]. Moreover, our laboratory previously demonstrated that mice with cardiac specific knockout of the EP4 receptor have reduced cardiac function after MI, as well as a phenotype of dilated cardiomyopathy with age [73, 267]. In contrast to the EP4 receptor, Martin and colleagues report that in mice with cardiac overexpression of the EP3 receptor, I/R injury is attenuated by reducing ischemic contracture. However, these mice are also described as having moderately reduced ejection fractions and increased end systolic volume at baseline [268]. Other studies have shown that activation of the EP3 receptor confers cardio protection in I/R injury as well [269-271].

Angiotensin II and Hypertension

Ang II plays a critical role in the development of hypertension due to its direct effects on vascular cells leading to vasoconstriction, by promoting increased sodium reabsorption in the kidneys, and by increasing production of aldosterone, which further promotes sodium and water retention (Figure 4). When Ang II binds to its receptor(s) on the vascular cell surface it induces a variety of effects comprising immediate, early and late effects. Activation of phospholipase C and Src occur within seconds leading to increases in free [Ca^{2+}] and increased mobilization of Ca^{2+} [272-275]. Activation of phospholipase A_2, phospholipase D, and MAPKs occurs within minutes and leads to regulation of vascular smooth muscle function (i.e., growth, migration, and production of growth factors) [276].

Recently, Rho-kinase signaling has been recognized as an important mediator in inducing vasoconstriction by Ang II. One member of the Rho family, RhoA, is expressed in vascular smooth muscle cells and sensitizes contractile proteins to Ca^{2+} and promotes phosphorylation of myosin light chain, causing increased contraction in response to Ang

II [277-279]. In a rat model of hypertension induced by Ang II infusion, protein levels of RhoA were increased in the aorta [280]. It was also shown in cell culture that the activity of RhoA/Rho-kinase signaling pathway is increased after Ang II treatment [281, 282]. The role of other Rho family members such as RhoB in hypertension is still not understood. TNF-α was shown to induce RhoB expression in endothelial cells [283]. Another group was able to reproduce these findings and showed that stimulation with TNF-α for 16 hours upregulated RhoB expression and activation, whereas levels for RhoA remain unchanged [284]. Therefore in contrast to RhoA, RhoB appears to be inducible and may be an important, novel mediator in inflammatory signaling in response to cytokines like TNF-α.

Ang II can also stimulate phospholipase A_2 activity which leads to production of prostaglandins, like PGE_2 that can exert pro- or anti-hypertensive effects [285, 286]. Long term generation of oxidative stress and protein synthesis occurs in the order of hours or days and contributes to the late effects. Ang II has been shown to increase O_2^- and H_2O_2 production in cardiac, endothelial, vascular smooth muscle, and mesangial cells [287-291]. H_2O_2 dissociates into O_2^- and water and the production of these radical ions is important for the pathogenesis of hypertension. The literature suggests the underlying mechanism of Ang II-induced radical ion production is via p38 MAPK [291] and AKT/PKB [292] signaling. This evidence suggests that Ang II is critical in maintaining the vasculature integrity, thus playing a key role in cardiovascular disease and hypertension. Furthermore, clinical trials using ACE inhibitors and angiotensin receptor blockers (ARBs) improved morbidity and mortality in hypertension, congestive heart failure, and MI [293, 294]. Mainly this was by lowering blood pressure and improving cardiac remodeling [295-301].

Ang II also regulates blood pressure by its actions in the kidneys, primarily by

regulating salt and water balance. Dysregulation of this system can lead to hypertension and is believed to be a key player in the development and maintenance of essential hypertension [302]. Ang II has direct effects on renal vascular smooth muscle cells, causing vasoconstriction of both the efferent and afferent arterioles. This reduces renal blood flow, which favors sodium reabsorption [56]. Ang II can also act in the nephron directly, stimulating salt and water reabsorption [303]. Deletion of the AT1 receptor from the proximal tubule lowers blood pressure and reduces Ang II-dependent hypertension [304]. In this dissertation, however, the kidneys will not be studied.

Angiotensin II in Inflammation and Cardiac Remodeling

Early studies suggested that in hypertension, Ang II increased vascular permeability by indirect pressure-mediated injury to the endothelium [53, 305-307]. It was later shown, however, that Ang II could influence endothelial permeability independent of any changes in hemodynamics. Prostaglandins (e.g., PGE_2) and growth factors (e.g., VEGF) were considered potential players in this effect. In rats, AT_1 blockade with losartan prevented a prostanoid-dependent increase in vascular permeability [308]. Furthermore, in humans, ACE inhibitors increase vasodilation in the pulmonary circulation which can be blocked with cyclooxygenase inhibitors, suggesting an influential role of prostaglandins on Ang II signaling [309, 310].

A key characteristic of inflammation in cardiovascular disease is infiltration of monocytes/macrophages [51, 311]. In patients with cardiovascular disease, elevated levels of circulating MCP-1 were reduced with ACE inhibitor treatment as well as AT_1 antagonist treatment [312, 313]. Inflammatory cells themselves have been shown to be equipped with the RAS machinery and can produce Ang II locally [314-318] and Ang II can directly increase the phagocytic activity of macrophages [319, 320]. The expression

of several genes involved in inflammation can be regulated by nuclear transcription factors AP-1 and NF-κB [321, 322] and evidence suggests that NF-κB in particular may be a mediator of Ang II-induced inflammation [323, 324].

Studies have shown that Ang II has an important role in the processes involved in myocardial remodeling [49, 325, 326] and in left ventricular hypertrophy as a result of hypertension [327]. A chronic increase in blood pressure leads to left ventricular hypertrophy that can eventually lead to heart failure. Recent evidence suggests that Ang II can act both independently or synergistically with increased blood pressure to promote cardiac hypertrophy [49, 328].

Ang II can directly induce cardiac inflammation [52, 326, 329, 330] which in turn leads to cardiac remodeling. Furthermore, Ang II has been shown to have direct effects on cardiomyocytes, inducing hypertrophy, inflammation, and production of extracellular matrix [151, 331-333]. However, the direct effect of Ang II on cardiomyocytes *in vivo* is controversial [334]. The induction of cardiac hypertrophy via Ang II has been linked to ERK 1/2, NFAT, and CAMKII/MEF2 signaling cascades [335, 336]. It is thought that the action of Ang II in the cardiomyocytes *in vivo* is amplified by an activation of the immune system and inflammatory cascades [337-339]. This involves stimulation of pro-inflammatory factors, such as IL-18, IFN-γ, NF-κB, and reactive oxygen species (ROS) production via Nox2 and Nox4 [56]. Relevant molecules discussed in this dissertation are NF-κB and Nox2. Ang II promotes expression of an enhancer molecule, connection to IKK and SAPK/JNK (CIKS), leading to activation of NF-κB or AP-1 transcription factors and an upregulation of pro-inflammatory cytokines/chemokines [340]. Another study determined that Ang II infusion increases activated monocyte levels, enhances iNOS expression, and uncouples eNOS, promoting more oxidative stress [341]. Additionally,

ROS produced from NADPH oxidase stimulates MCP-1 expression through Toll-Like Receptor (TLR)-4 [56]. Moreover, TLR-4 is well characterized and associated with chronic inflammation and cardiovascular disease [342]. Recent evidence suggests that aside from its classical activation of AT_1, Ang II can also activate TLR-4 and its downstream signaling pathway [343], although this precise mechanism is unknown. Other evidence has shown that mice deficient in TLR-4 attenuated Ang II-induced cardiac hypertrophy, infiltration of macrophages/monocytes, and cardiac dysfunction. Importantly, this was in the absence of any difference in blood pressure [344].

Cardiac fibrosis induced by Ang II infusion has been shown to be dependent upon the infiltration of macrophages originating from the bone marrow [345]. The levels of macrophage infiltration into the myocardiumalso appears to be dose dependent [345, 346]. Furthermore, accumulation of the macrophages appears to be controlled by MCP-1 [347].

Animal Models Used in This Study/General Hypothesis

Myocardial Infarction Model

MI is induced by permanent ligation of the left anterior descending coronary artery (LAD), resulting in in ischemia [348, 349]. This model is applicable to the human conditions since MI can be caused by blockade of the coronary vessels due to a disrupted atherosclerotic plaque. This is typically accompanied by ST-segment elevation, determined by electrocardiogram (ST-elevated MI, STEMI) [350]. For many STEMI patients (15-25 %), there is no reperfusion therapy for various reasons. For example, current guidelines state that if the patient is hemodynamically stable for more than 12 hours after onset of symptoms, reperfusion is not recommended [351]. Thus, permanent LAD ligation in mice resembles this scenario. Following LAD ligation, the mice develop

heart failure characterized by left ventricular dilation, cardiac dysfunction, and infarct wall thinning. These heart failure characteristics are observed in human patients as well and are typically diagnosed as heart failure with reduced ejection fraction (HFrEF) [351, 352]. In mice, HFrEF is observed after 24 hours and worsens over time [353, 354]. In the mouse MI model, the left ventricle is often divided into three distinct regions following LAD ligation and ischemia: infarct, border, and remote zones. Generally, the inflammation and fibrosis are most abundant in the infarct zone [355]. This model allows us to examine the role of PGE_2 and its receptors on these inflammatory processes and on cardiac function 2 weeks after MI when the scar is fully formed and cardiac function is reduced.

Chronic Angiotensin II Infusion Model

Hypertension induced by chronic administration of Ang II in mice has been shown to mimic the chronic hypertension and neurohumoral effects observed in patients [350]. Ang II infusion causes cardiac injury and remodeling by both cardiac pressure overload and direct effects of Ang II and/or aldosterone on the heart [356]. Depending on the dose of Ang II used in the study, mice can display cardiac remodeling in the presence (pressor dose) [357] or absence (sub-pressor dose) [358] of hypertension. The degree of hypertension that is achieved is also dose dependent. Gomolak et al. reported that a low dose Ang II (0.1 $mg^{-1} \times kg^{-1} \times day^{-1}$) does not induce hypertension, whereas an intermediate dose (0.5 $mg^{-1} \times kg^{-1} \times day^{-1}$) increases blood pressure chronically, and a high dose (1.4 $mg^{-1} \times kg^{-1} \times day^{-1}$) causes a severe and immediate increase in blood pressure and hypertension after only 3 days [346]. Other studies implement a substantially high dose of Ang II such as 3 $mg^{-1} \times kg^{-1} \times day^{-1}$ [359]. This dose is used to cause increased end-organ damage, however it is not physiological or pathologically relevant. Our study implements the high pressor dose of Ang II (1.4 $mg^{-1}kg^{-1}day^{-1}$) to

achieve severe hypertension and subsequent cardiac end organ damage. In contrast to the ischemic MI model where the injury is localized and defined, the cardiac remodeling that takes place with Ang II infusion is less defined and more diffuse. For example, pressure overload induced by hypertension increases stretch of the cardiomyocytes and subsequent inflammatory cascades [360]. Pressure overload also may induce cell death and subsequent release of DAMPs promoting inflammation. Lastly, there are the concomitant effects of Ang II on blood pressure and direct effects of Ang II on the cardiac cells.

General Hypothesis

The purpose of this dissertation is to examine how the relative abundance of EP3 and EP4 receptors in the heart alters cardiac inflammation/remodeling after MI or Ang II infusion. We hypothesize that the EP3 receptor mediates the deleterious effects of PGE_2 in the heart, while the EP4 receptor is cardioprotective. To test our hypothesis, we will use two well-known models of heart failure: myocardial infarction and Ang II-induced hypertension.

CHAPTER 2 – OVEREXPRESSION OF PROSTAGLANDIN E2 EP4 RECEPTOR IMPROVES CARDIAC FUNCTION AFTER MYOCARDIAL INFARCTION

(This Chapter contains previously published material. See Appendix B)

Introduction

Prostaglandin E2 (PGE_2) signals through 4 separate G-protein coupled receptor sub-types (EP1, EP2, EP3 and EP4) to elicit a variety of physiological and pathophysiologic effects. EP2 and EP4 increase cAMP levels in the cell via adenylate cyclase activation, whereas EP3 inhibits cAMP production, and EP1 increases Ca^{2+} levels in the cell, although the cardiac effects of the receptors have not been studied in depth. Our laboratory has studied the role of PGE_2 via its EP4 receptor over the last decade and reported that the EP4 receptor causes hypertrophy of cardiomyocytes *in vitro*; that deletion of the EP4 receptor only in the cardiac myocyte worsens cardiac function after myocardial infarction (MI), and that male mice with cardiomyocyte deletion of the EP4 receptor develop a dilated cardiomyopathy with age that is characterized by reduced ejection fraction, left ventricle dilation, thinning of the posterior wall, and an increased interstitial cellular infiltrate [73, 218, 267]. Moreover, we recently reported that PGE_2 via its EP3 receptor could reduce contractility of preparations ranging from isolated myocytes to the whole heart by mechanisms that appeared to involve decreased phosphorylation of phospholamban (PLN) [217]. Presumably, this would lead to an inhibitory effect on SERCA, thereby decreasing contraction. Additionally, we reported that the EP3 receptor is upregulated after MI and although the EP4 receptor is also upregulated, it does not appear to be to a similar extent. We thus hypothesized that an imbalance in the EP3/EP4 ratio favoring expression of EP3 would explain some of the reduced contractility observed after MI and that over-expression of EP4 in the same model would improve cardiac

function. This was tested in the present study using a mouse model of MI with the use of AAV9-EP4 driven by the myosin heavy chain promoter to overexpress EP4 in the left ventricle.

Methods

Animal Use

10-12 week old male C57Bl/6 mice used for the MI studies and *in vitro* studies were from Jackson labs. The mouse model of MI using permanent ligation of the left anterior descending coronary artery was previously described by us [73] and is shown in Figure 8. All studies involving the use of animals were approved by the animal care and use committee (IACUC) at Henry Ford Hospital, in accordance with federal guidelines.

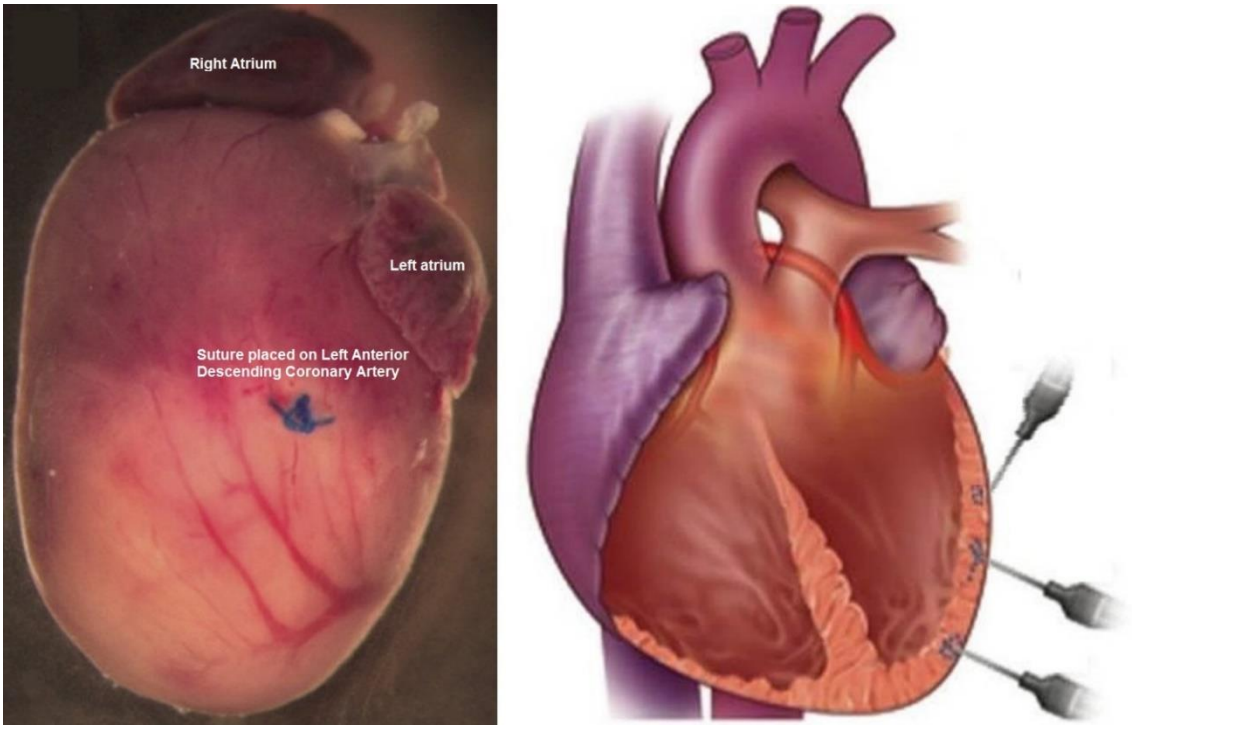

Figure 8: Demonstration of LAD Ligation and AAV9-EP4 Injection. *Left* Image adapted from Redgrave et al. [361] depicting a mouse heart 24 hours after permanent ligation of the left anterior descending branch of the coronary artery. Note the pale infarcted region. *Right* Cartoon depicting the 3 AAV9 injections into the left ventricle free wall. Importantly, the left ventricle cavity is not punctured.

AAV-9 EP4 Transduction of the Mouse Heart

Our viral constructs consisted of adeno-associated virus serotype 2/9 with EP4 (hereafter termed AAV9-EP4) and the control virus AAV2/9-CMV luciferase (hereafter termed AAV9-luc). AAV9-EP4 driven by the myosin heavy chain promoter and AAV9-CMV luciferase under control of the CMV promoter, were obtained from Vector BioLabs (Malvern, PA) and both were administered at the same viral load. To first determine the localization of AAV9-EP4, we performed intracardiac injections of AAV9-EP4 containing a hemagglutinin (HA) tag on the N-terminus (hereafter termed AAV9-EP4-HA; AAV9-aMHCp-HA-mPTGER4-WPRE; Vector BioLabs), with the same viral titer as AAV9-EP4/AAV9-luc. In the other experiments, we performed either sham operation or ligation of the coronary artery and just before the ligation we administered 30 µL (3 separate 10 µL injections) of either AAV9-EP4 or AAV9-luc for a total of 1×10^{12} viral particles. These injections were given into three different areas of the left ventricle free wall, but not in the predicted infarct zone (Figure 8). Two weeks after injection we performed immunohistochemistry with antibodies against the HA tag to visualize expression of the construct. We also performed confocal microscopy to examine localization of the construct in animals that received AAV9-luc or AAV9-EP4 virus.

Echocardiography

Echocardiography was performed on conscious animals at 2 weeks after sham or MI surgery. The cardiac function of all mice was assessed by echocardiography using an Acuson 256 system (Mountain View, CA) with a 15-MHz linear transducer, as reported previously [219]. Diastolic measurements were made at the maximum left ventricle cavity dimension, whereas systolic parameters were measured during maximum anterior motion of the posterior wall. All echocardiography was performed by the same investigator who

was blinded to the experimental groups.

Histology: Measurement of Myocyte Cross Sectional Area (MCSA), Picrosirius Red Staining, and Infarct Size

Histological assessment of myocyte cross sectional area (MCSA) was performed as previously described after 2 weeks of MI [362]. Briefly, mouse hearts were harvested and sectioned transversely into three slices from apex to base (sections A-C). The sections were frozen in Optimal cutting temperature (OCT) media pre-chilled in isopentane and stored at –80°C for determination of MCSA. All three sections of the heart were stained with fluorescein-labeled peanut agglutinin to delineate the myocytes. Four radially oriented microscope fields were selected from each section and photographed under the 20x objective. However, we did not analyze the scar itself as there are no visible cardiomyocytes in that region. MCSA was measured by computer-based planimetry (NIH Image J) and averaged across all 4 fields of the sections. The mean cardiomyocyte area was then calculated for each animal. All assessments were performed by blind observers. Infarct size was determined using the method described by Takagawa et al. for the mouse [363]. Briefly, using Metamorph software, infarct area was digitally traced and calculated as [(epicardial infarct ratio + endocardial infarct ratio) /2] ×100 for all sections and the average of the three sections was taken. To analyze collagen fraction, picrosirius red staining was performed using frozen sections of left ventricles and a method previously published [364]. Briefly, sections were postfixed in Bouin's fluid and they were then stained with 0.1% picrosirius red for 1 hour and washed twice with 0.5% acetic acid. Images of collagen staining were obtained under 2X objective and analyzed using Nikon Elements software.

Immunohistochemistry for Macrophages, T cells, and HA Tag-Ep4

The number of macrophages was assessed using $CD68^+$ staining (rat anti-$CD68^+$ antibody, BioRad) on frozen heart sections as we previously described [362]. T cells were visualized using $CD3^+$ staining (rabbit-anti $CD3^+$ antibody, Abcam). EP4 containing the HA tag was visualized using anti-HA Tag staining (mouse anti-HA, Cell Signaling). Briefly, frozen sections were fixed in acetone for 10 minutes, followed by incubation with fresh 0.3% hydrogen peroxide for 30 minutes. Sections were then blocked in 5% centrifuged milk in TBS (Tris- buffered saline) blocking buffer and incubated with either anti-$CD68^+$ (1:200 in blocking buffer), anti-$CD3^+$ (1:100 in blocking buffer), or anti-HA tag (1:100 in blocking buffer) overnight at 4^oC. Biotinylated secondary antibodies (1:200 dilution of anti-mouse IgG for CD68+ and HA Tag staining, 1:200 dilution of goat anti-rabbit IgG for CD3+ staining) were placed onto sections for 1 hour at room temperature. Sections were then incubated with horseradish peroxidase reagent for 40 minutes at room temperature and then visualized by AEC single solution (Vector laboratories; Burlingame, CA). After a rinse in water, slides were counterstained with Harris' hematoxylin solution for 1 min, then rinsed again in tap water and mounted onto slides using Aquamount (Lerner laboratories). Negative controls consisted of sections incubated in the absence of primary antibody. Photographs of five randomly-chosen fields per CD68+ stained section were taken under the 20X objective and the number of positively stained cells was counted by a blinded observer. For CD3+ staining, four randomly-chosen fields were taken under the 20X, 40X, and 100 X oil-immersion objectives. The number of cells per mm^2 was measured by a blinded observer using Image J software. For HA tag staining, photographs of the negative control were taken under 20X and positive slides were taken under the 20X, 40X, and 100X oil-immersion objective.

Co-localization of HA-EP4 Using Double Immunofluorescence

Frozen left ventricle sections were allowed to warm to room temperature followed by fixation with ice-cold acetone for 15 minutes. Slides were rinsed twice in ice-cold TBS followed by permeabilization with TritonX-100 (0.1 % in TBS; pH 7.6) for 5 minutes at room temperature. Slides were then blocked for 1 hr. at room temperature in a humidified chamber in 2% bovine serum albumin (BSA; pH 7.6). Slides were incubated with primary antibodies sequentially at room temperature in a humidified chamber. First, slides were incubated with biotinylated anti-HA tag (BAM0601; R&D Systems) for 2 hours, followed by three washes with TBS. These slides were then incubated with Streptavidin conjugated to Northern Lights^{TM} 557 (NL999; R&D Systems) for 1 hour in the dark. Slides were then washed 5 times with TBS, 5 minutes each, followed by incubation with either rat anti-CD31 (557355; BD BioSciences), the endothelial cell marker or rabbit anti-α-Sarcomeric Actinin (ab137346; Abcam), the cardiomyocyte marker, for 2 hours. Slides were washed as before followed by secondary antibody detection with either goat anti-rat FITC or goat anti-rabbit FITC for 1 hour in the dark. Slides were washed 5 times with TBS, followed by incubation with DAPI nuclear stain (1: 18,000 in TBS) for 10 minutes. Slides were then mounted using AquaMount (Lerner laboratories). Control sections were cryosections from animals that received AAV9-Luc virus and thus do not express HA-EP4. Slides were imaged using confocal microscopy.

Confocal Microscopy

Fixed and labeled left ventricle tissue slices were imaged by confocal microscopy using an Olympus FV1200 confocal microscope. Images were acquired using a 40X objective and an optical zoom function was used to acquire images at 200X. DAPI was excited with a 405 nm diode laser and fluorescence acquired between 420 and 490 nm.

FITC labeled CD31 or α sarcomeric actinin was excited at 489 nm and fluorescence acquired between 495 and 555 nm. Northern Lights ™ was excited at 557 nm and fluorescence acquired between 570 and 700 nm. No cross-bleed between channels was observed under these conditions. Images on the three channels were acquired simultaneously.

Western Blot

Phospholamban (PLN), phosphorylated PLN (p-PLN), and HA-EP4 expression were measured by Western Blot using homogenized left ventricles from sham and MI mice who received either AAV9-EP4 or AAV9-Luc, as we have previously described [217]. The p-PLN antibody is from Cell Signaling (Danvers, MA) and recognizes phosphorylation at Ser16/Thr17. After detection of p-PLN, the blot was stripped and a total phospholamban antibody (Cell signaling, Danvers, MA) was applied at a 1:1000 dilution. The p-PLN signal was corrected to total PLN. Expression of HA-EP4 was measured using antibodies raised against the HA tag (mouse anti-HA; Cell signaling, Cat No.2367) at a 1:1000 dilution. GAPDH was used to control for the amount of protein loaded.

In Situ Zymography

To assess MMP activity, we performed *in situ* zymography on frozen sections as previously described [365]. Fluorescein conjugated, dye-quenched gelatin from pig skin (DQ™-gelatin) was obtained from Molecular Probes (Invitrogen, Basel, Switzerland). A 1 mg/ml stock solution of DQ-gelatin was prepared in gelatinase reaction buffer (150 mM NaCl, 5 mM $CaCl_2$, 0.2 mM NaN_3, 50 mM Tris-HCl, pH 7.6) and stored at 4°C. The working solution for *in situ* zymography was made by directly diluting DQ-gelatin stock solution in reaction buffer to a final concentration of 20 µg/ml. Unfixed cryosections were thawed,

rounded with a wax pen, overlaid with 25 µl DQ-gelatin working solution and incubated at 37°C in a humidified dark chamber for 5 hours and pictures were immediately taken under the microscope. Control sections were incubated in the presence of 20 mM EDTA which inhibits gelatinase activity. Photographs of four randomly-selected fields were taken under the 20X objective and a threshold was set using Nikon elements that encompassed only the bright green fluorescence indicative of gelatinase activity. The percent area of gelatinase activity was calculated for each animal per field and the mean calculated for each group.

Real Time RT-PCR

Measurement of β-myosin heavy chain (β-MHC), brain natriuretic peptide (BNP), tumor necrosis factor α (TNFα), inducible nitric oxide synthase (iNOS), Secreted protein, acidic and rich in cysteines (SPARC), matrix metalloproteinase 2 (MMP2), EP1, EP2, EP3, and EP4 mRNA expression was performed by quantitative real-time RT-PCR using a SYBR green method. Real time RT-PCR was performed as follows: 1 µg of DNAse-treated total RNA sample was reverse transcribed using random primers and Omniscript reverse transcriptase (Qiagen, Valencia, CA) in a total volume of 20 µl for 1 hr. at 37 °C followed by an inactivation step of 95 °C for 5 min. 2 µl of the reverse transcription reaction was then amplified in a Roche version 2.0 lightcycler PCR instrument (Roche, Indianapolis, IN) using SYBR green dye (SA Biosciences, Frederick, MD) and specific primers. Reactions were set up in a final volume of 20 µl, which contained 2 µl of sample, 1 µM each of both the primers and 10 µl of 2x SYBR green PCR mix. After an initial “hot start” at 95^{o}C for 10 min, amplification occurred by denaturation at 95^{o}C for 15 s, then annealing at 58-60^{o}C for 40 s for a total of 30-40 cycles, followed by extension at 72^{o}C for 40 s. At the end of PCR cycling, melting curve analyses were performed. For all

Qiagen primers, extension and annealing were performed together in one step at 60°C for 1 minute. A relative quantitation method (ΔΔCt) [366] was used to evaluate expression of each gene relative to control. Real time RT-PCR of GAPDH was used for normalization of all data. Primer sequences are shown in Table 1.

Table 1: Primer Sequences.

Gene	Sense	Anti-Sense
β-MHC	5'-acaggaagaacctactgcgrc-3'	5'-agcttgttgacctgggact-3'
BNP	5'cccaaaaagagtccttcggt-3'	5'cctacaacaacttcagtgcgtt-3
iNOS	5'cccttcaatggttggtacatgg-3'	5'acattgatctccgtgacagcc-3'
MMP2	5'-ataccccaagccactgacca-3'	5'-ccaggagtctgcgatgagct-3'
GAPDH	5'-caaggtcatcccagagctg-3'	5'-tgtcatcatacttggcaggtt-3'
TNF-α	Qiagen, NM_013693.3	
EP1	Qiagen, NM_013641.2	
EP2	Qiagen, NM_008964	
EP3	Qiagen, NM_011196	
SPARC	Qiagen, NM_009242	

Primers from Qiagen are proprietary and only the RefSeq number for the mRNA sequence is provided.

Cytokine/Chemokine Multiplex ELISArray

To identify changes in expression of major cytokines/chemokines after MI with injection of either control AAV9-Luc virus or AAV9-EP4 virus, we performed a multiplex Enzyme-Linked ImmunoSorbent Assay (ELISA) using a commercially available kit from Qiagen (Cat No. MEM-005A). Following the manufacturer's instructions, we homogenized 20 mg of left ventricle tissue in sample buffer provided in the kit with the addition of a protease inhibitor (Cat No. 4693132001, Roche). The 96-well plate was analyzed at 450 nm and 570 nm using a plate reader. The absorbance at 570 was to account for auto-fluorescence of the plate and was subtracted from final readings per the manufacturer's instructions. After being corrected, absorbance values were corrected for amount of protein in each well of the assay plate.

Statistical Analysis

All statistical analysis was performed by a statistician in the Department of Public Health Sciences of Henry Ford Hospital using the statistical package SAS Version 9.4. All data are shown as mean ± standard error of the mean (SEM). Data were analyzed using multiple two-sample Wilcoxon tests for unequal variances along with a Hochberg's correction for multiple comparisons. This procedure provides a series of adjusted cutoff values for significance for 4 comparisons (cutoff p values are 0.05, 0.025, 0.017, and 0.013).

Results

Effect of AAV9-EP4 Injection on EP4 mRNA Expression

To determine the extent of EP4 expression after viral injection, we performed real time RT-PCR for EP4. After 14 days, sham-operated animals receiving AAV9-EP4 had a 2.86-fold increase in EP4 mRNA expression compared with control (1.08 ± 0.25 vs. 3.09 ± 0.73 in Sham + AAV9-EP4; p=0.05). The expression levels of EP1 (1.25 ± 0.10 vs. 1.11 ± 0.11 in Sham + AAV9-EP4), EP2 (1.02 ± 0.15 vs. 0.71 ± 0.16 in Sham + AAV9-EP4), and EP3 (1.13 ± 0.33 vs. 2.23 ± 1.01 in Sham + AAV9-EP4), were not significantly changed following administration of AAV9-EP4.

AAV9-EP4-HA Overexpression Level and Localization

To assess the level of AAV9-EP4 expression and localization after injection, we performed intracardiac injections as described in the methods in sham animals with an AAV9-EP4-HA construct. After two weeks, we performed immunohistochemistry with antibodies against the HA tag. Figure 9 A shows representative images of positive staining under different magnifications and of the negative control (bottom right panel). We observed intense positive staining throughout the left ventricle with staining around

cardiomyocyte nuclei and on the cell membrane. This expression was confirmed by western blot.

A

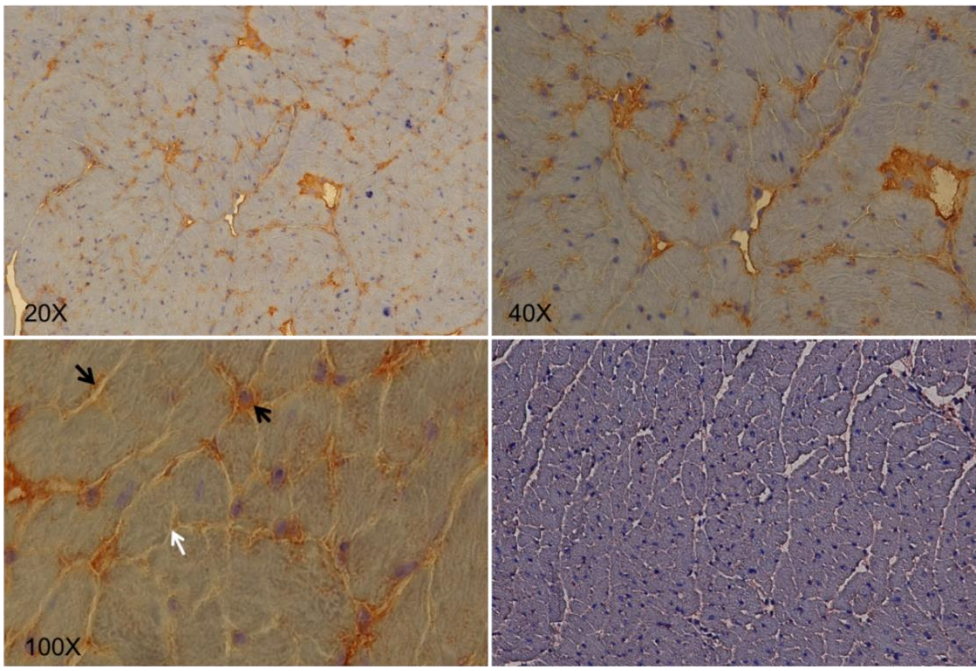

Figure 9 A: Representative EP4-HA Immunohistochemistry. Images showing anti-HA staining using the 20X objective (top left), a portion of this staining at 40X (top right), and 100X (bottom left). Bottom right panel shows a section incubated in the absence of primary antibody for a negative control. Positive staining is indicated by the black arrows. Also note that the interstitial region, indicated by the white arrow is devoid of staining.

Figure 9 B shows that HA-EP4 expression in the left ventricles of mice injected with AAV9-EP4 is highly abundant two weeks post MI, and is negative in animals that received AAV9-Luc**.**

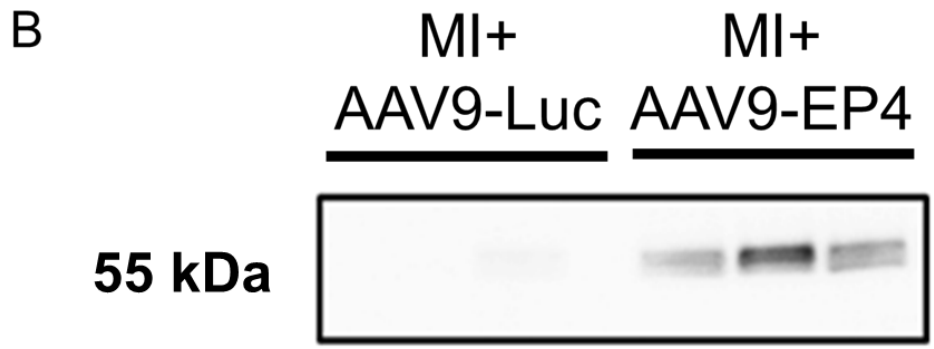

Figure 9 B: Representative EP4-HA Western Blot. Western blot for HA expression in homogenized left ventricles from MI animals that received injections of either CMV-Luciferase or AAV9-EP4.

Localization of HA-EP4 in the Left Ventricle

To determine localization of overexpressed EP4 within the heart, we performed double labeled immunofluorescence using the HA tag as a surrogate of EP4 expression. As a control we used cryosections from animals that received AAV9-Luc virus and therefore do not express the HA tag. Figure 9 C clearly shows that the HA tag is expressed only in those animals that received AAV9-EP4 virus, and not in animals that received the control virus AAV9-Luc. We next used confocal microscopy to determine whether the HA tag co-localized with either the endothelial cells (CD31) or within the myocytes (α-Sarcomeric Actinin) (Figure 9 D). The top panel clearly shows no association between the HA tag (red) and the endothelial cells (green). However, the HA-tag does co-localize with the α-Sarcomeric Actinin (green; bottom panel) within the cardiomyocytes.

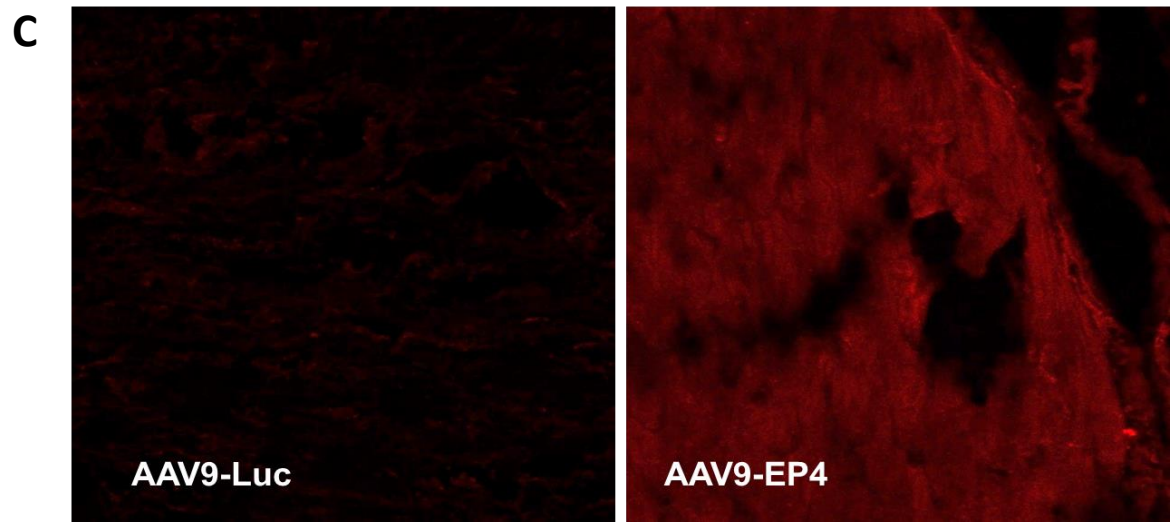

Figure 9 C: Representative EP4-HA Immunofluorescence. Images showing expression of the HA tag in the left ventricle of a mouse that received AAV9-Luc virus (left panel) vs. a mouse that received AAV9-EP4 (right panel). Images were taken under the same exposure.

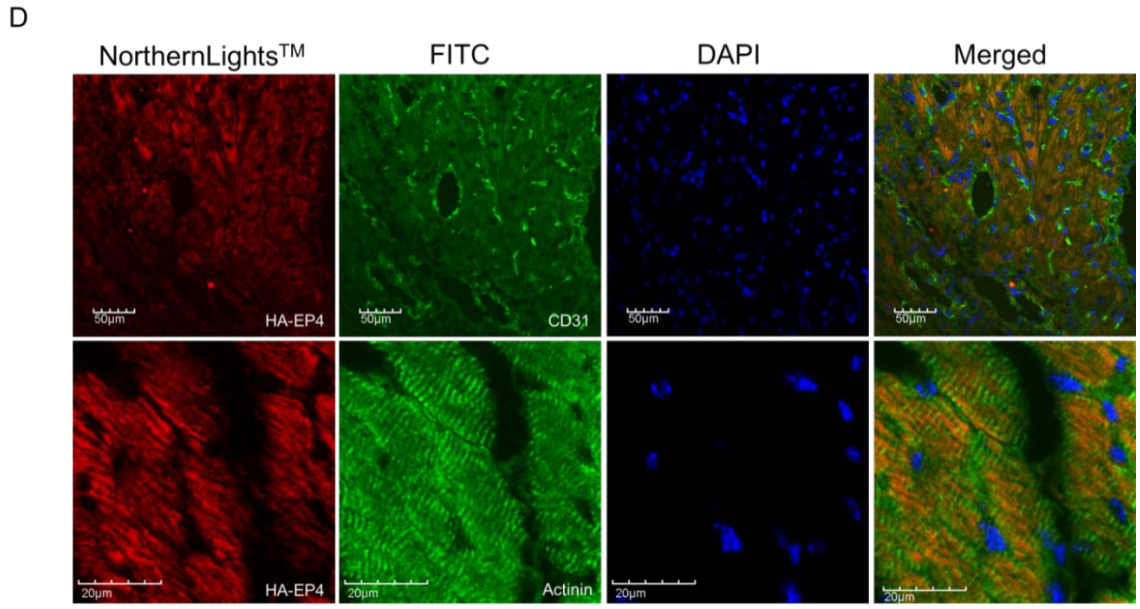

Figure 9 D: Confocal Microscopy of EP4-HA in the Cardiomyocytes. Images showing double immunofluorescence labeling of the HA tag with the endothelial cell marker CD31 (top right panel merged; 40X) and the cardiomyocyte marker α-Sarcomeric Actinin (bottom right panel merged; 200X). Note that the HA tag does not co-localize with the positive green CD31 signal outlining capillaries and vessels.

Effect of EP4 Overexpression on Cardiac Function

Representative echocardiography images (Figure 10 A) and data (Figure 10 B and Table 2) are presented. As expected, animals with MI exhibited a lower ejection fraction

(EF) than sham operated animals (37.8 ± 2.2 % for MI+AAV9-luc vs. 76.9 ± 2.1 % for sham + AAV9-luc, p =0.0001). The administration of AAV9-EP4 to MI animals resulted in a significant improvement in EF (to 47.7 ± 2.4 %, p=0.0025 compared to animals receiving AAV9-luc) whereas it had no effect in sham-operated mice. In addition to increased EF, our data show an improvement in shortening fraction (SF; p=0.0003) coupled with less ventricle dilatation at systole (LVDs; p=0.0013) and a tendency for reduced chamber dimension at diastole (LVD_d) also (p = 0.028 NS). Altogether, the data suggest that expression of EP4 improves cardiac function and alters ventricular remodeling. Furthermore, the effects on cardiac function appear to be independent of infarct size since there was no difference between MI + AAV9-luc vs. MI + AAV9-EP4 (33.53 ± 4.39% versus 31.29 ± 3.32%, respectively).

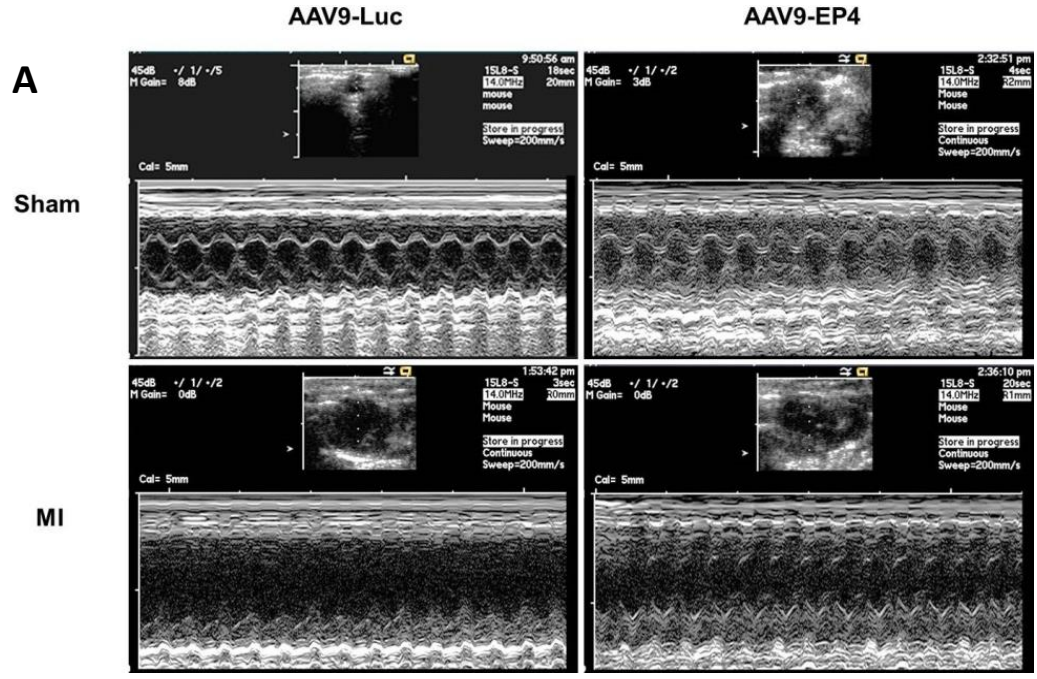

Figure 10 A: Representative M-mode of Echocardiography. Images from each of the four groups used for analysis.

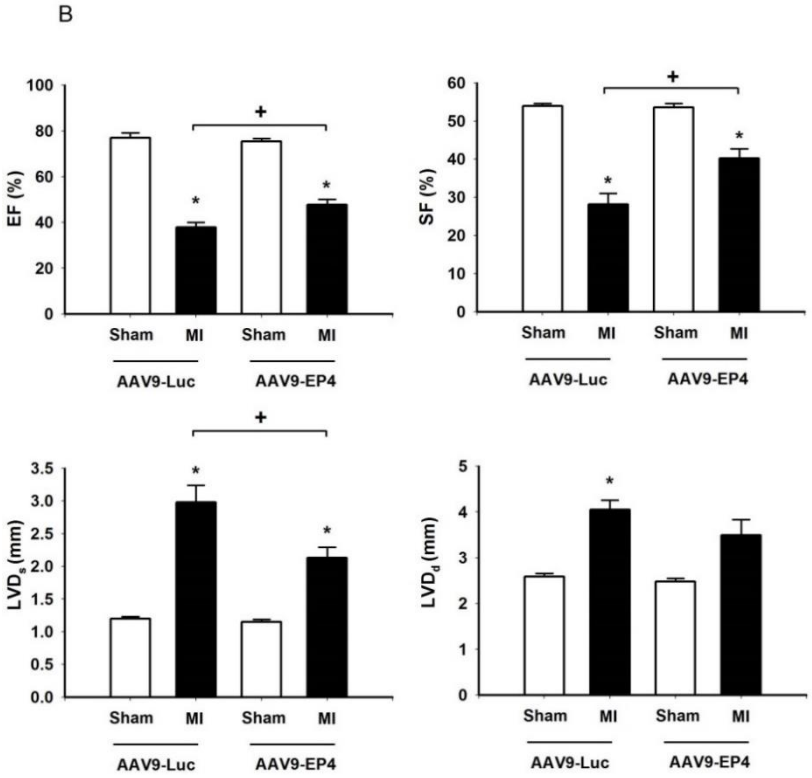

Figure 10 B: Quantitative Analysis of Echocardiography Data. EF-ejection fraction, SF-shortening fraction, LVD_s – left ventricle dimension at systole, LVD_d - left ventricle dimension at diastole. N = 9 for Sham + AAV9-luc, N=10 for Sham + AAV9-EP4, N=16 for MI + AAV9-luc, N=17 for MI + AAV9-EP4. * denotes statistical significance vs. respective sham group, + denotes statistical significance vs. MI+AAV9-Luc.

Table 2: Echocardiography Data of EP4 Overexpression Mice

Parameters	Sham + AAV9-Luc	Sham + AAV9-EP4	MI + AAV9-Luc	MI + AAV9 EP4
BW (g)	25.62 ± 0.62	26.73 ± 0.48	26.35 ± 0.38	27.46 ± 0.36
LV (mg)/10 g BW	32.88 ± 0.65	31.88 ± 0.54	37.55 ± 1.53 *	36.15 ± 1.02 ‡
HR (bpm)	670.22 ± 14.07	680.97 ± 11.27	648.03 ± 14.60	655.21 ± 78.03
CO (mL/min/10 g BW)	12.71 ± 0.67	10.75 ± 0.45	8.92 ± 0.63 *	9.65 ± 1.22
EF (%)	76.92 ± 2.14	75.47 ± 1.11	37.84 ± 2.21 *	47.69 ± 2.39 + ‡
SF (%)	53.90 ± 0.66	53.60 ± 0.97	28.20 ± 2.88 *	40.25 ± 2.46 + ‡
LVD_d (mm)	2.59 ± 0.07	2.48 ± 0.07	4.05 ± 0.21 *	3.49 ± 0.34 ‡
LVD_s (mm)	1.20 ± 0.03	1.15 ± 0.04	2.98 ± 0.26 *	2.13 ± 0.16 + ‡

Data presented as mean ± SEM. * represents a significant difference vs. Sham + AAV9-Luc, + BW- body weight, LV- left ventricle, HR- heart rate, CO- cardiac output, EF- ejection fraction, SF- shortening fraction, LVD – left ventricle dimension.* represents significant difference vs. MI + AAV9-Luc, and ‡ represents a significant difference vs. Sham + AAV9-EP4. N = 9 for Sham + AAV9-Luc, N=10 for Sham + AAV9-EP4, N=16 for MI + AAV9-Luc, N=17 for MI + AAV9-EP4.

With respect to survival, 20-30% of mice typically die of cardiac rupture in the first week following MI after ligation of the LAD. However, in our experiments, we did not observe any differences in mortality between mice receiving control virus (17.6%) and those receiving AAV9-EP4 (19.0%).

Effect of EP4 Overexpression on Collagen Fraction (Picrosirius Red Staining)

As expected, MI increased the collagen content in all three regions of the left ventricle examined (infarct, peri-infarct, and remote; Figure 11 B left, middle, and right panels respectively) by picrosirius red staining (PSR). In the infarcted region, animals that received MI and control AAV9-Luc virus showed an increase in collagen to 18.78 ± 2.58 % vs. 8.62 ± 1.13 % in sham operated animals. In animals that received MI and AAV9-EP4 virus, positive PSR staining was increased even further to 29.96 ± 2.94 %. In the peri-infarct region, animals given MI and AAV9-Luc virus had a similar significant increase in collagen content (25.10 ± 2.00 % vs. 7.13 ± 0.91 % in sham operated animals). In contrast to the infarcted region, collagen content in the peri-infarct was reduced after MI with injection of AAV9-EP4 to 17.12 ± 2.24 %. As anticipated, there was a small, but significant increase in collagen in the remote region of the heart (6.72 ± 1.14 % vs. 2.68

± 0.38 % in sham operated animals). This increase was also reduced to 3.62 ± 0.91 % in animals that received MI with AAV9-EP4 injection. Representative images of the staining from the peri-infarct zone are shown in Figure 11 A.

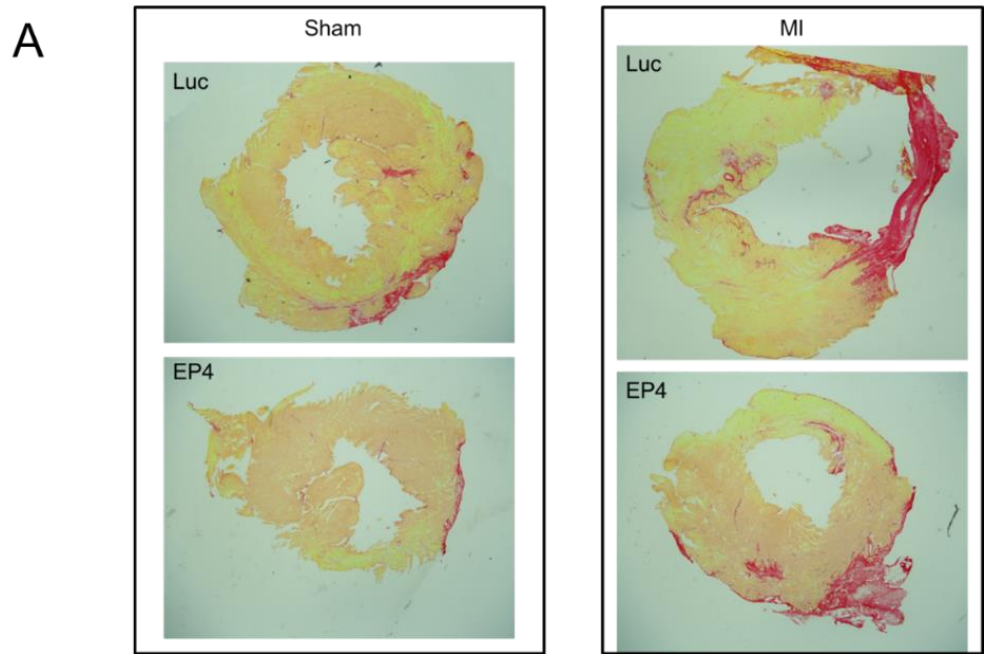

Figure 11 A: Representative Picrosirius Red Staining. Images captured under 2X objective from each treatment group taken from the peri-infarct zone.

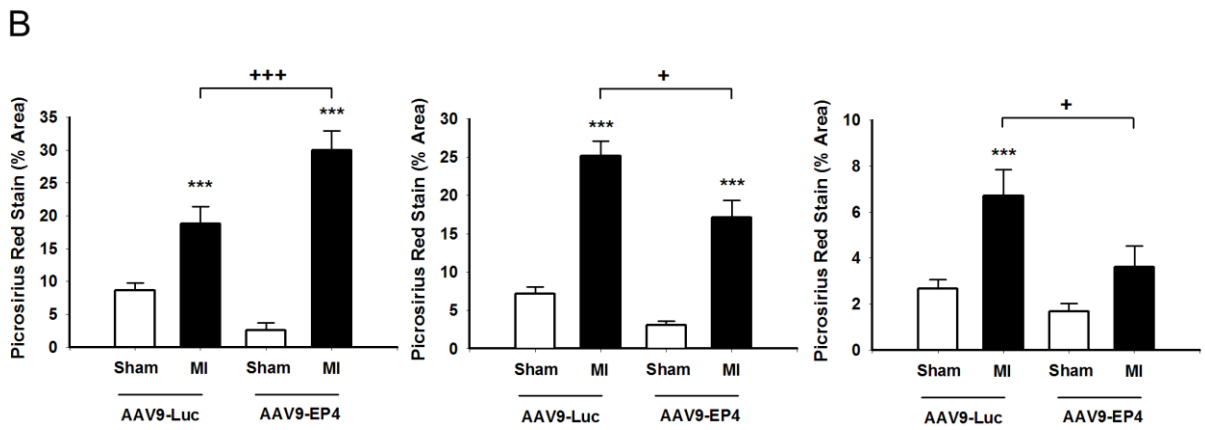

Figure 11 B: Quantification of Picrosirius Red Staining. Performed from the infarcted region (left panel), peri-infarct region (middle panel), and remote region (right panel) of frozen left ventricle sections. Data is presented as mean ± SEM. *** $p<0.001$ compared to respective sham group. + $p<0.05$, +++ $p<0.005$ compared to MI + AAV9-Luc. (Left panel) N=6 for Sham + AAV9-Luc, Sham + AAV9-EP4, and MI + AAV9-Luc, N=14 for MI + AAV9-EP4. For middle and right panels N=6/group.

Effect of EP4 Overexpression on Myocyte Cross-Sectional Area (MCSA)

As anticipated, MI increased MCSA but this increase was smaller in mice receiving AAV9-EP4 (Figure 11 C: 259.4 ± 4.0 μm^2 vs. 296.6 ± 6.0 μm^2, $p < 0.01$). The administration of AAV9-EP4 did not affect MCSA in sham-operated animals (202.3 ± 5.2 μm^2 for sham-operated receiving AAV9-luc vs. 231.4 ± 18.5 μm^2 for mice receiving AAV9-EP4, NS).

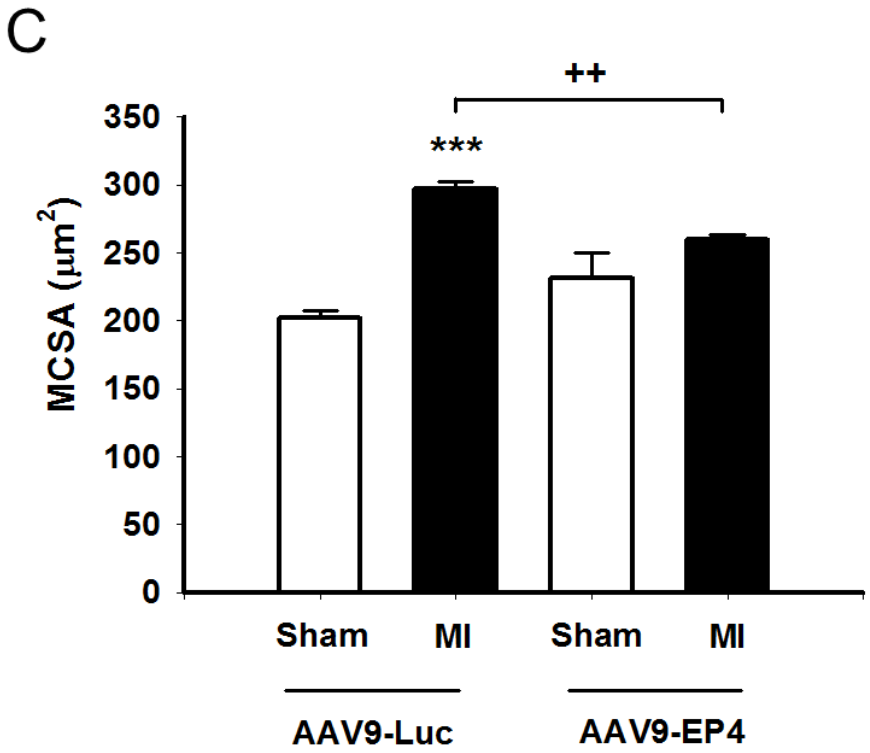

Figure 11 C: Myocyte Cross Sectional Area Analysis. Analyzed using NIH Image J software. MCSA is presented as mean ± SEM. *** $p< 0.005$ vs. Sham + AAV9-Luc, ++ $p<0.01$ vs. MI + AAV9-Luc. N=5 for Sham + AAV9-Luc, N=5 for Sham + AAV9-EP4, N=7 for MI + AAV9-Luc, N=11 for MI + AAV9-EP4.

Effect of EP4 Overexpression on Gene Markers of Cardiac Hypertrophy

Since treatment with AAV9-EP4 reduced MCSA in response to MI, we also measured expression of β-myosin heavy chain (β-MHC) and BNP, gene markers of hypertrophy, using real time RT-PCR, corrected to GAPDH. As shown in Figure 11 D,

both β-MHC and BNP were increased after MI and these increases were attenuated after treatment with AAV9-EP4; consistent with the MCSA data. After MI, β-MHC mRNA expression (Figure 11 D, left panel) was significantly increased 5-fold compared with sham animals (6.64 ± 1.9 vs. 1.31 ± 0.43, $p < 0.001$). Animals treated with AAV9-EP4 virus had a significant increase in β-MHC mRNA expression after MI, although this increase was only 2.2-fold that of sham animals (3.76 ± 1.2 vs. 1.75 ± 8.7, $p < 0.05$). Similarly, BNP mRNA expression (Figure 11 D, right panel) significantly increased after MI (3.46 ± 1.0 vs. 1.11 ± 0.17, $p < 0.001$). However, there was no difference in BNP mRNA expression after MI in animals who first received AAV9-EP4 treatment (1.65 ± 0.34 vs. 1.03 ± 0.11).

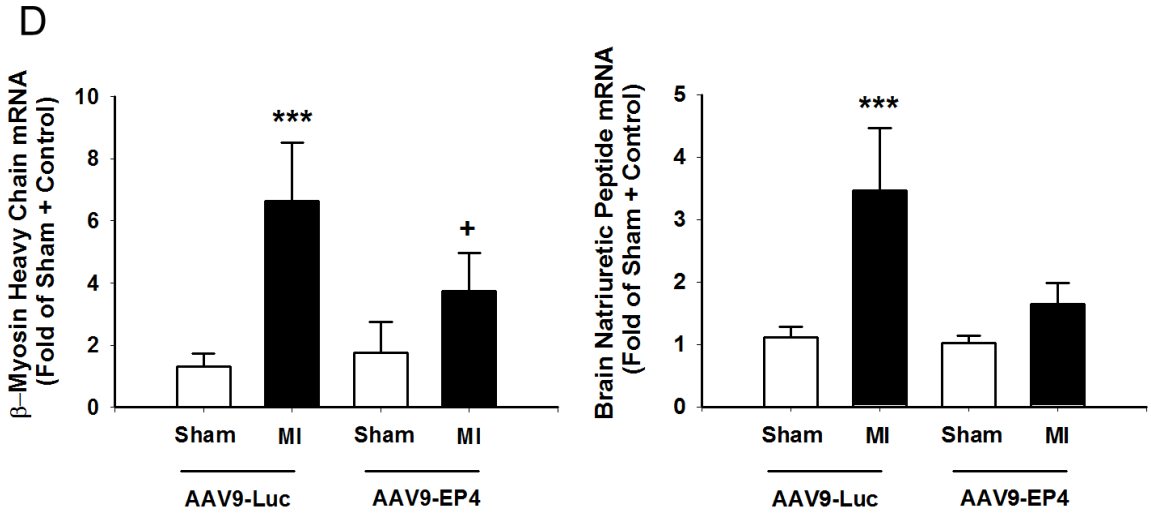

Figure 11 D: β-MHC and BNP mRNA Expression. β-myosin heavy chain (β-MHC) mRNA expression and Brain natriuretic peptide (BNP) mRNA expression. For both β-MHC and BNP data was corrected to GAPDH and presented as fold of Sham + AAV9-Luc control group. N = 10 for Sham + AAV9-Luc, N=9 for Sham + AAV9-EP4, N=14 for MI + AAV9-Luc, N=12 for MI + AAV9-EP4. ***$p<0.005$ vs. Sham + AAV9-Luc, + $p < 0.05$ vs. Sham + AAV9-EP4.

Effect of EP4 Overexpression on MMP-2 mRNA

Matrix metalloproteinases (MMPs) play an important role in extracellular matrix remodeling in various pathological conditions, including myocardial infarction [367-369].

Specifically, MMP-2 has been shown to play an important role in LV remodeling [368, 370]. For this reason, we determined the effect of EP4 overexpression on MMP-2 mRNA expression (Figure 12, left panel). There was a significant increase in MMP-2 expression in MI animals receiving control AAV9-Luc virus (2.91 ± 0.62 vs. 1.00 ± 0.06 in Sham + AAV9-Luc, $p<0.05$). However, in animals receiving AAV9-EP4, there was no change in expression of MMP-2 after MI (1.68 ± 0.65 vs. 1.47 ± 0.31 in Sham + AAV9- EP4, $p=0.85$). Since mRNA levels do not always reflect activity, we also performed *in situ* zymography to assess gelatinase activity (MMP-2 and MMP-9), shown in Figure 12,

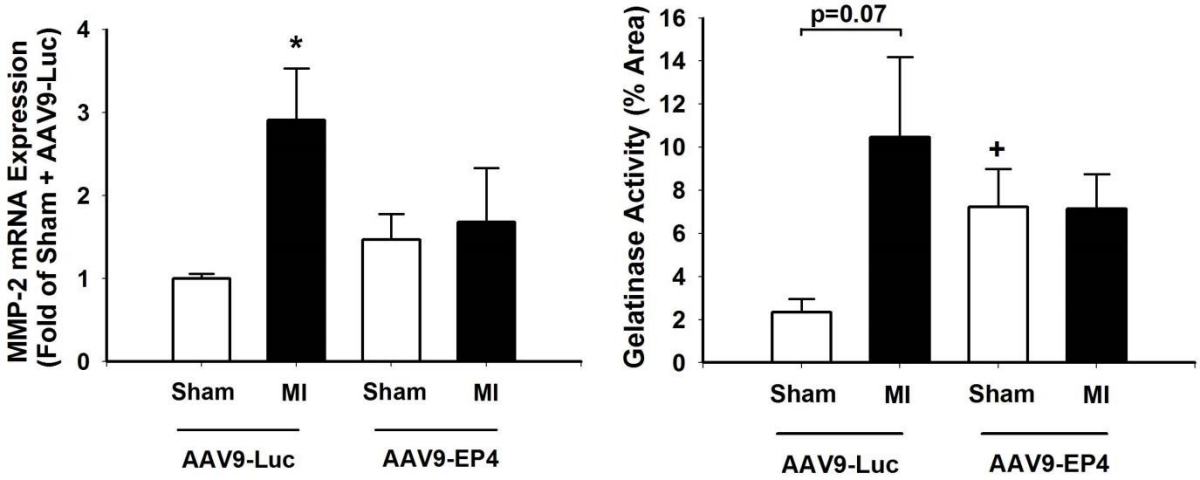

Figure 12: MMP-2 mRNA and Gelatinase Activity Assay. (Left panel): MMP-2 mRNA expression from left ventricles. Data is presented as mean ± SEM. N=3 for Sham + AAV9-Luc, N=4 for Sham + AAV9-EP4, N=8 for MI + AAV9-Luc, and N=6 for MI + AAV9-EP4. *$p < 0.05$ vs. Sham + AAV9-Luc. (Right panel): *In situ* zymography to assess gelatinase activity in infarct zone. Data is presented as mean % area positive. N=3/group, + $p< 0.05$ vs. Sham + AAV9-Luc.

right panel. As expected, gelatinase activity was increased in the infarct zone after MI in animals that received control virus (10.47 ± 3.71 RFU vs. 2.35 ± 0.60 RFU in sham animals that received the same virus; $p=0.07$). Surprisingly, treatment of sham-operated mice with AAV9-EP4 increased MMP activity (2.35 ± 0.60 RFU for sham-operated AAV9-luc vs. 7.23 ± 1.75 RFU, $p < 0.05$ for sham animals receiving AAV9-EP4). There was no

further increase in MMP activity after MI in animals that received AAV9-EP4 virus (7.15 ± 1.60 RFU vs. 7.23 ± 1.75 RFU in sham + AAV9-EP4 group).

In the remote region of the heart, a similar increase in MMP activity was noted after MI in mice receiving control virus (0.42 ± 0.16 RFU in sham + AAV9-Luc vs. 5.67 ± 1.59 RFU in MI + AAV9-Luc, $p < 0.05$). Similar to results noted in the infarct zone, administration of AAV9-EP4 to sham-operated animals tended to increase MMP activity although the change failed to achieve statistical significance (0.42 ± 0.16 RFU in sham + AAV9-Luc vs 2.75 ± 1.20 RFU in sham + AAV9-EP4, $p = 0.104$). After MI, there was no statistically significant change in MMP activity for animals that received AAV9-EP4 (2.75 ± 1.20 RFU for sham + AAV9-EP4 vs 5.31 ± 1.51 RFU for MI + AAV9-EP4). Secreted protein, acidic and rich in Cysteines (SPARC) is a glycoprotein that plays an important role in activation and production of MMPs. We measured the expression of SPARC mRNA by real time RT-PCR and we found that SPARC was significantly increased after MI in animals that received control virus, compared to sham animals (3.57 ± 0.69 vs. 1.02 ± 0.14 in sham animals; $p=0.001$). SPARC expression was not changed in sham-operated animals overexpressing EP4 (1.02 ± 0.14 for AAV9-luc vs 0.83 ± 0.25 for AAV9-EP4) and neither was it altered in mice subject to MI (3.37 ± 0.63 in MI+AAV9-EP4; $p=0.787$).

Effect of EP4 Overexpression on Macrophage Migration and Polarization

A representative image of macrophage migration in all four groups is presented in Figure 13 A. Figure 13 B shows a representative image of the $CD68^+$ staining

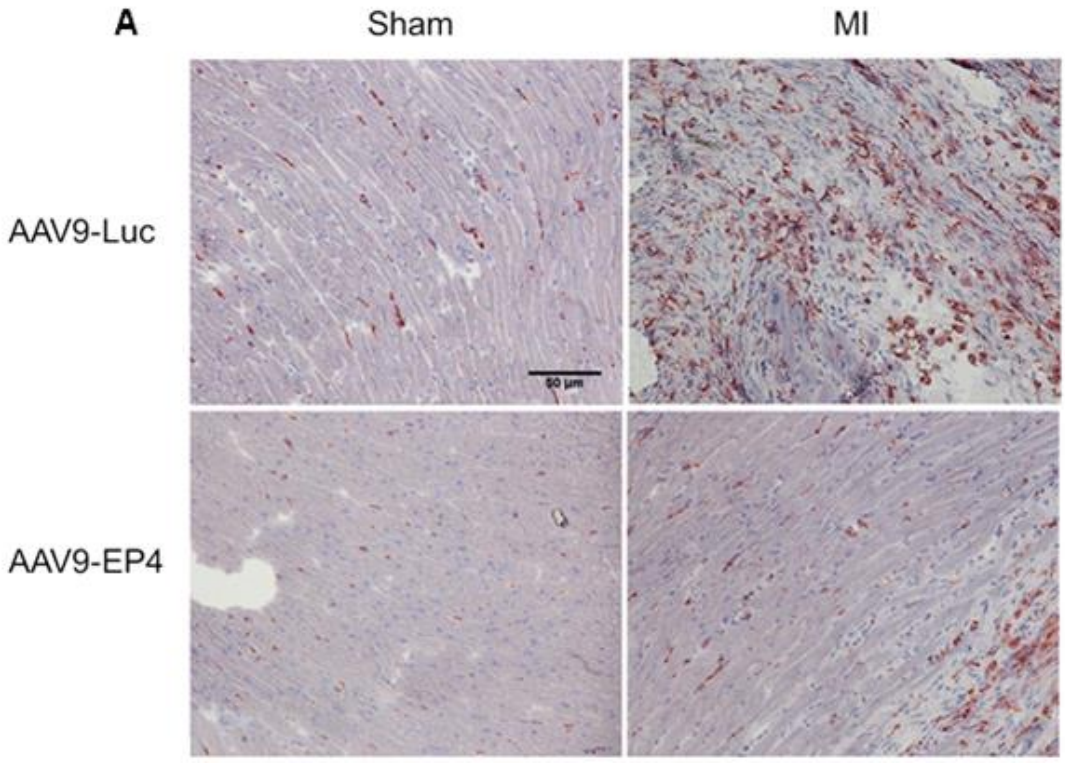

Figure 13 A: Representative $CD68^{+}$ Staining (20X). Images from all four groups showing CD68+ staining for macrophages in the infarct / peri-infarct region of frozen left ventricle sections.

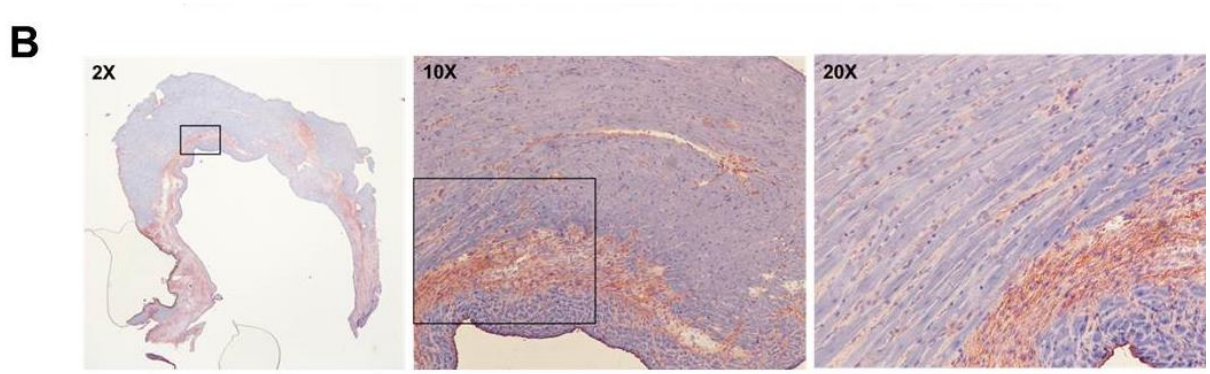

Figure 13 B: Representative CD68+ Staining (2, 10, and 20X). Images of CD68+ staining from the infarct zone under 2X (left panel), 10X (middle panel) and 20X (right).

observed in the infarct/peri-infarct zone after 2 weeks of MI under different magnifications. As expected, after 2 weeks of MI, the number of macrophages in the infarct/peri-infarct region was increased 2.2-fold (Figure 13 C, left panel), from a value of 181.79 ± 10.2 cells/mm^2 in sham-operated animals receiving AAV9-luc to 401.65 ± 58.6 cells/mm^2 in MI

+ AAV9-luc injected hearts ($p < 0.001$). Treatment with AAV9-EP4 substantially reduced the number of infiltrating macrophages in the MI heart to a value of 281.77 ± 28.2 cells/mm^2 ($p=0.09$). In the remote zone of the heart (Figure 13 C, right panel), the number of CD68$^+$ cells was unchanged after MI (102.02 ± 22.04 cells/mm^2 vs. 98.10 ± 15.51 cells/mm^2 in sham-operated animals), however, injection of AAV9-

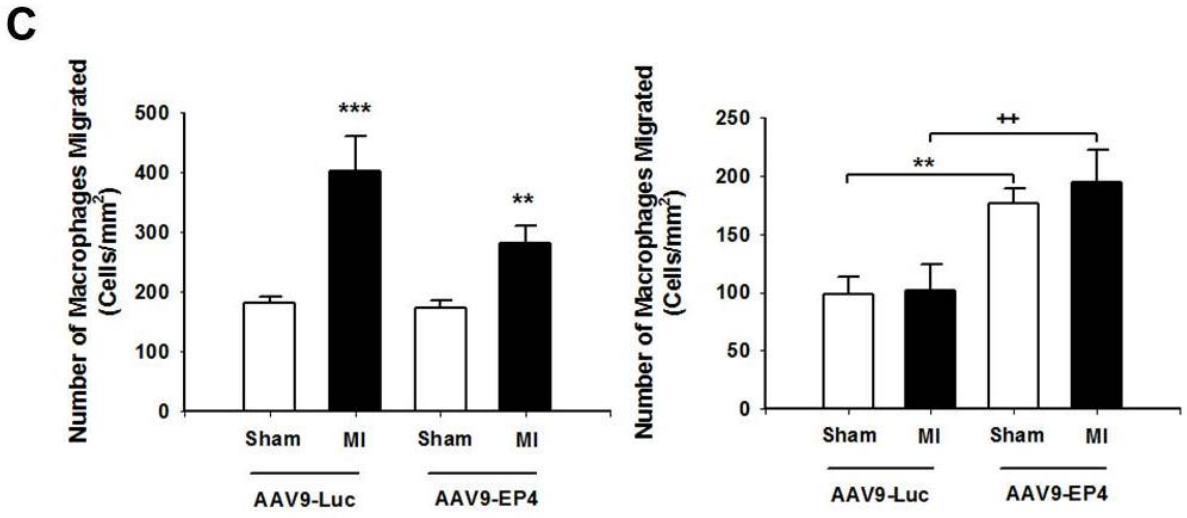

Figure 13 C: Quantification of CD68+ staining. In the infarct / peri-infarct region (left panel) and in the remote region (right panel) of the left ventricle. Data are presented as means ± SEM. N=12 per group. ** $p<0.01$, ***$p<0.005$ vs. respective sham group, ++$p<0.01$ vs. MI + AAV9-Luc

EP4 resulted in a significant increase in CD68$^+$ cells in sham animals (176.30 ± 13.41 cells/mm^2 vs. 98.10 ± 15.51 cells/mm^2) and this was further increased after MI to 194.80 ± 27.48 cells/mm^2. We also performed real time RT-PCR for inducible nitric oxide synthase (iNOS), one established marker of the M1 macrophage phenotype. As shown in Figure 13 D, the expression of iNOS (corrected to GAPDH) in the left ventricles was significantly increased in MI mice receiving control virus (2.04 ± 0.31; $p<0.01$). However, there was no increase in iNOS mRNA expression after MI in mice that received AAV9-EP4.

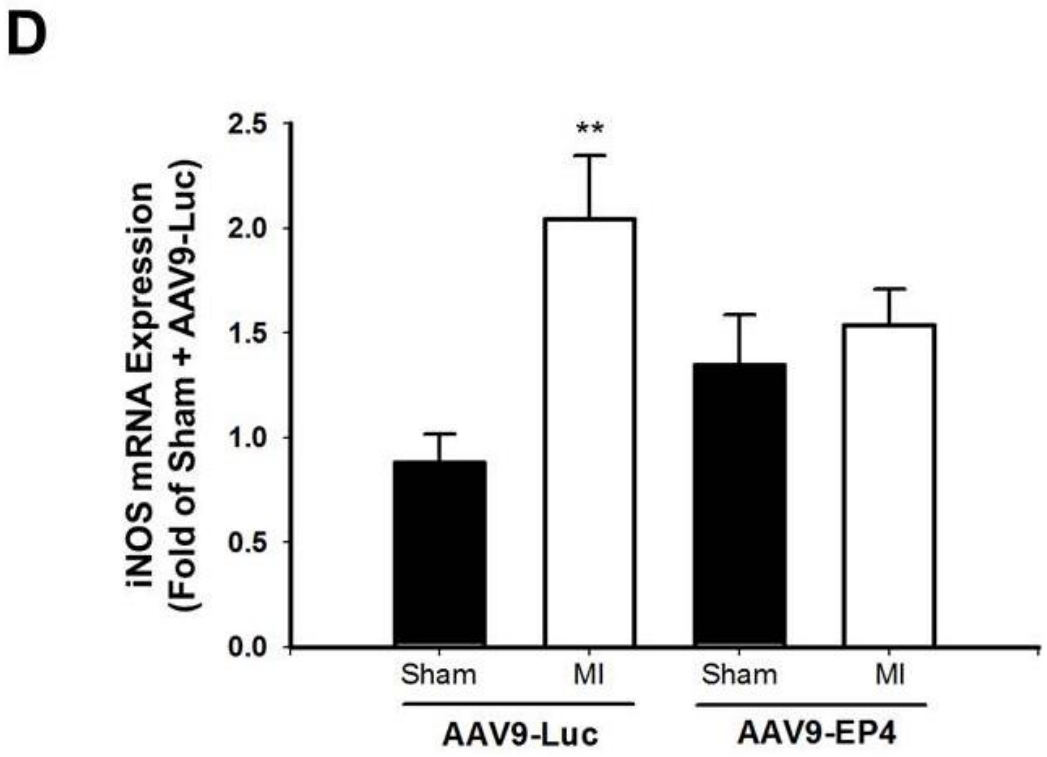

Figure 13 D: iNOS mRNA Expression. Inducible nitric oxide synthase (iNOS) mRNA expression; data are corrected to GAPDH control and are presented as mean ± SEM fold of Sham + AAV9-Luc. ** $p<0.05$ vs. Sham + AAV9-Luc. N = 3 for Sham + AAV9-Luc, N=4 for Sham + AAV9-EP4, N=8 for MI + AAV9-Luc, N=6 for MI + AAV9-EP4.

Effect of EP4 Overexpression on T cells

Figure 13 E displays representative images of CD3+ staining for each of the four groups and Figure 13 F shows a representative image of the $CD3^+$ staining observed in the infarct/peri-infarct zone after 2 weeks of MI under different magnifications. Figure 13 G (left panel) shows that two weeks post MI there was a 2.26-fold increase in positive T cell staining in the infarct region of mice that received AAV9-luc compared to sham-operated mice that received the same control virus (504.39 ± 46.80 cells/mm^2 vs. 222.61 ± 18.27 cells/mm^2 respectively, $p<0.001$). Furthermore, the increase in T cells was prevented when MI mice were treated with AAV9-EP4 (329.71 ± 33.53 cells/mm^2 vs. 504.39 ± 46.80 cells/mm^2 MI + AAV9-Luc mice). $CD3^+$ cell staining was not different

between groups when the remote zone was analyzed (Figure 13 G, right panel).

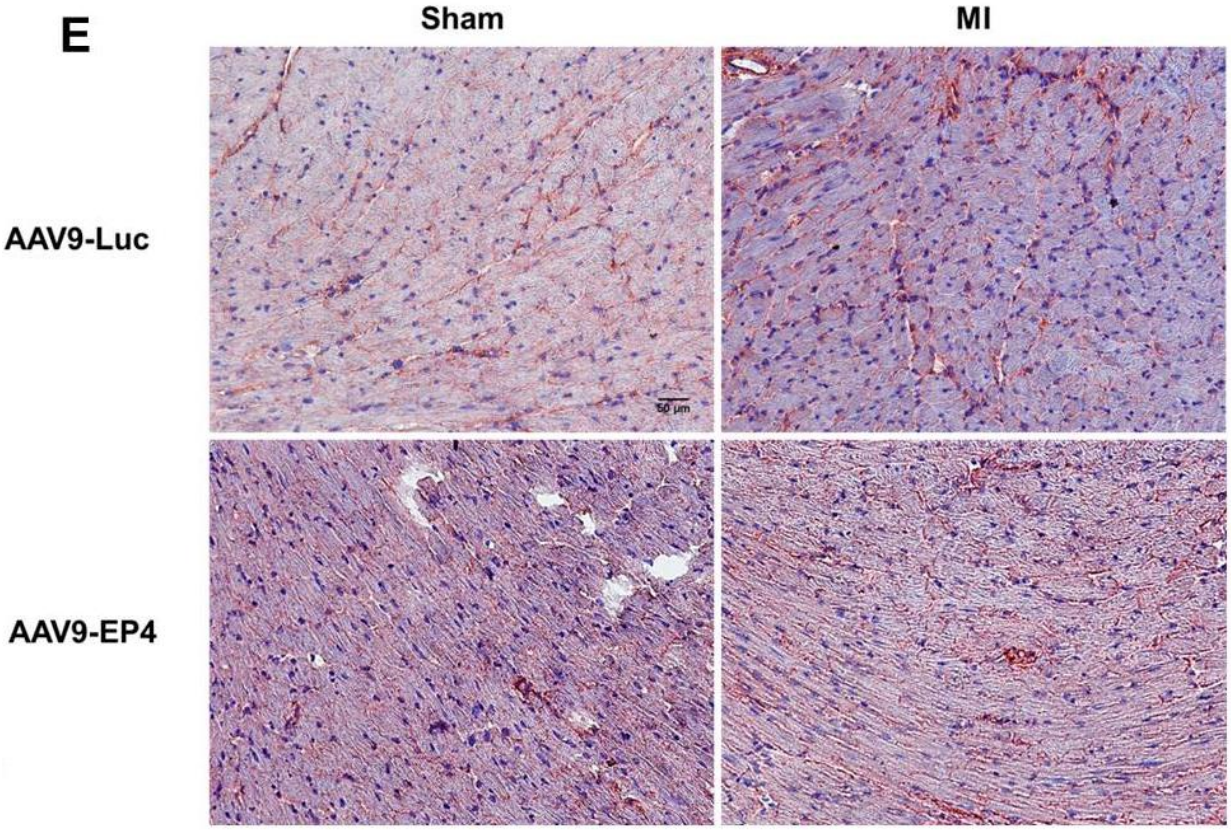

Figure 13 E: Representative of CD3+ Staining (20X). Images showing CD3+ staining for T lymphocytes in the peri-infarct zone in frozen left ventricle sections taken under 20X objective.

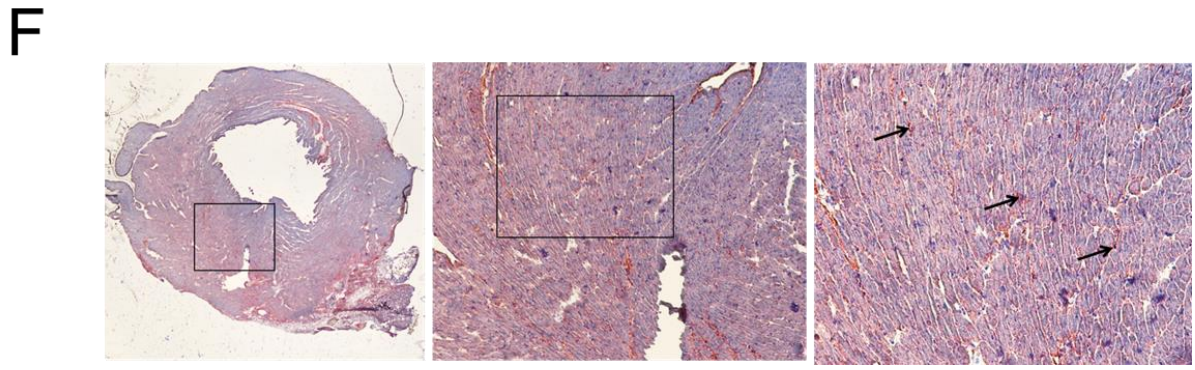

Figure 13 F: Representative CD3+ Staining (2, 10, and 20X). Images of CD3+ staining taken under 2X (left panel), 10X (middle panel) and 20X (right panel). Arrows depict regions of positive staining.

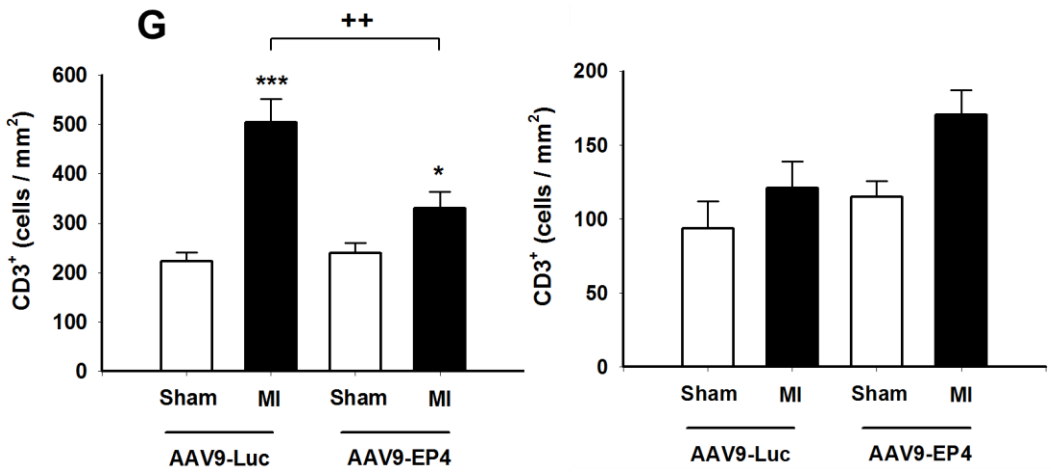

Figure 13 G: Quantification of CD3+ Staining. In the infarct + peri-infarct zones (left panel), and in the remote zone of the left ventricle (right panel); data are presented as means ± SEM. N = 12/group for Sham + AAV9-Luc, Sham + AAV9-EP4, and MI + AAV9-Luc. N=16 for MI + AAV9-EP4. * $p<0.05$, *** $p< 0.005$ vs. respective sham group. ++ $p<0.01$ vs. MI + AAV-Luc.

Effect of EP4 Overexpression on Cytokines

It is well known that cytokines like TNFα play an important role in the pathophysiology of heart failure. Since increased expression of TNFα has been correlated with an increased severity of heart failure, we determined if treatment with AAV9-EP4 would prevent its expression. Figure 14 A shows that TNFα mRNA expression (corrected to GAPDH) significantly increased after MI in mice receiving control virus (2.65 ± 0.63 vs. 1.05 ± 0.23 in sham animals, $p = 0.002$). However, TNFα mRNA did not increase after MI in mice receiving AAV9-EP4 (1.74 ± 0.24 vs. 1.17 ± 0.39; NS). We next performed a multiplex ELISA on left ventricle homogenates to identify key cytokines/chemokines that might be changing in MI with overexpression of EP4 (Figure 14 B). Using the array kit, we identified a significant reduction in MCP-1 expression (left panel) in mice receiving AAV9-EP4 (0.254 ± 0.0146 vs. 0.167 ± 0.0187 in MI + AAV9- EP4; $p< 0.01$) and an increase in IL-10 (0.025 ± 0.0061 vs. 0.044 ± 0.0121 in MI + AAV9-EP4; $p=0.172$), although this did not reach statistical significance (right panel). In isolated cardiomyocytes

from MI mice that received either control virus or AAV9-EP4, levels of these cytokines/chemokines were below the levels of detection. However, these data indicate that overexpression of EP4 may reduce the expression of pro-inflammatory chemokines/cytokines (MCP-1) while increasing expression of anti-inflammatory cytokines (IL-10).

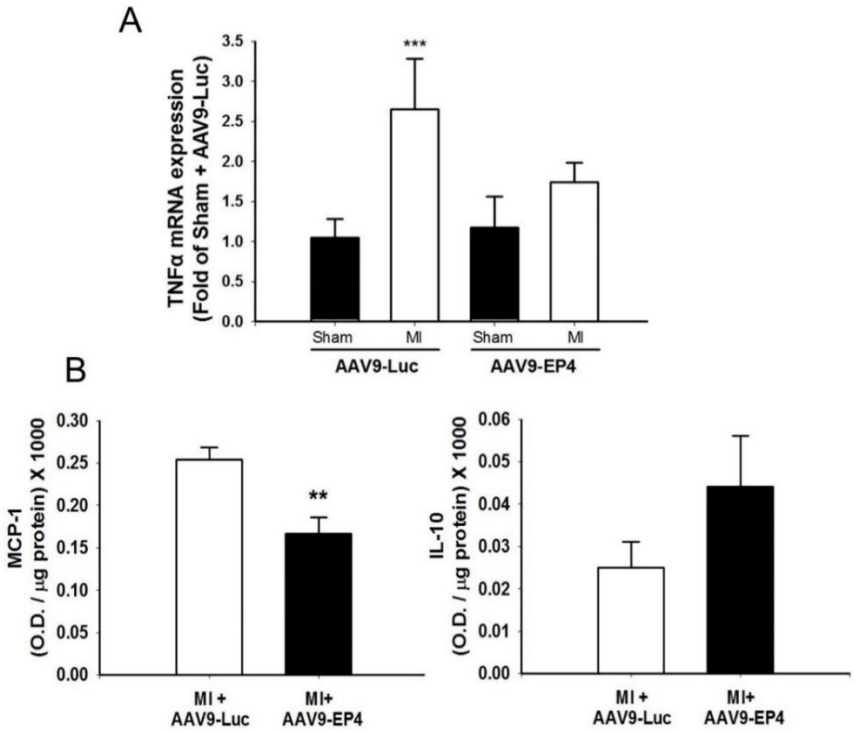

Figure 14. TNFα mRNA Expression and Cytokine ELISarray. Panel A: Tumor necrosis factor α (TNF α) mRNA expression. Data was corrected to GAPDH and all data are presented as mean ± SEM as fold of Sham + AAV9-Luc. N = 3 for Sham + AAV9-Luc, N=4 for Sham + AAV9-EP4, N=8 for MI + AAV9-Luc, N=6 for MI + AAV9-EP4. *** $p<0.001$ vs. Sham + AAV9-Luc. Panel B: Cytokine/chemokine multiplex ELISA data. Left panel shows protein expression of the chemokine MCP-1 and the right panel shows protein expression of the cytokine IL-10. Data presented is optical density (O.D.) corrected for µg of protein in each well x 1000. Data are presented as mean ± SEM. Panel A: N = 4 for MI + AAV9-Luc, N=5 for AAV9-EP4. Panel B: N = 6 for MI + AAV9-Luc, N=5 for AAV9-EP4. ** $p < 0.01$ vs. MI + AAV9-Luc.

Effect of EP4 Overexpression on Phosphorylation of Phospholamban

Since phosphorylation of phospholamban is important in regulating the sarco/endoplasmic reticulum Ca^{2+} ATPase (SERCA) and therefore contractility, we

performed western blot analysis of p-PLN and total PLN expression (Figure 15). There was a significant increase in expression of p-PLN, corrected to total PLN, in sham animals who received AAV9-EP4 compared with sham animals that received the control AAV9-Luc virus (1.01 ± 0.16 vs. 0.35 ± 0.09; $p<0.05$). In animals subject to MI with injection of AAV9-EP4, the expression of p-PLN was already elevated and thus there was no further increase.

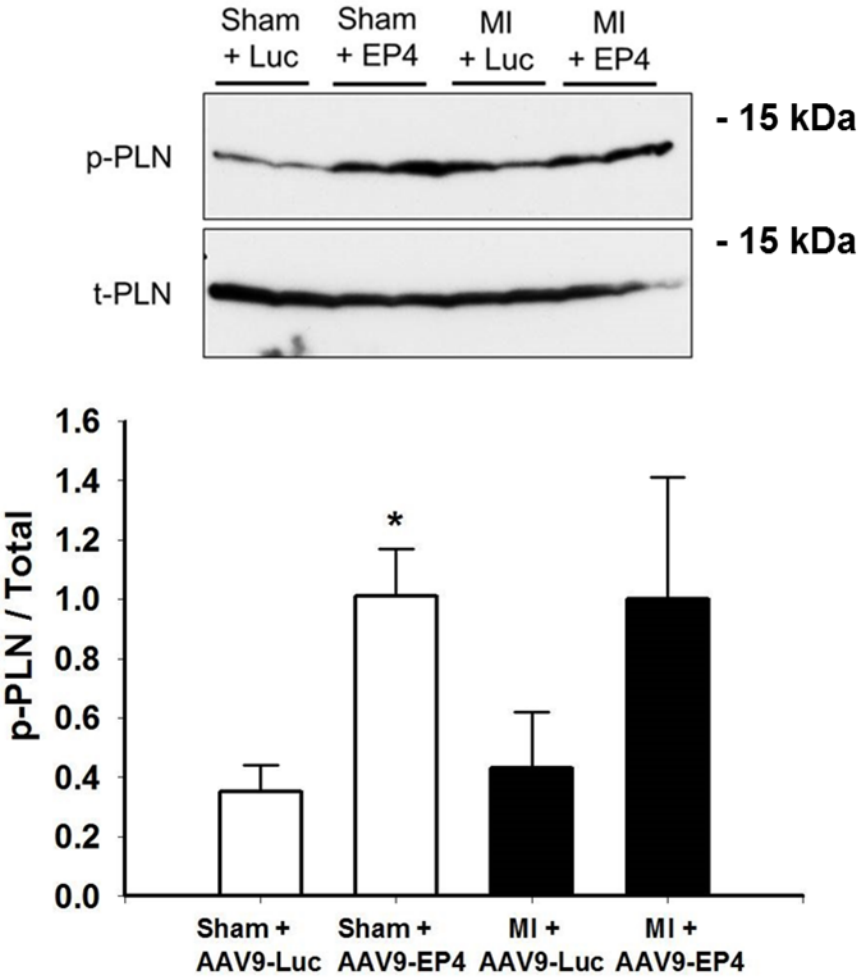

Figure 15. Western Blot for the Expression of Phosphorylated Phospholamban. p-PLN in left ventricles of mice that received either sham or MI operation with injection of either AAV9-Luc or AAV9-EP4. Total phospholamban (t-PLN) served as a loading control. Top panel shows a representative blot, while the bottom panel shows the quantification. Data is presented as mean ± SEM. *p< 0.05 compared to Sham+AAV9-Luc. N=5 per group

Discussion

The results of this study show, for the first time, that administration of AAV9-EP4 into the left ventricle of mice with MI is beneficial in improving cardiac function. We have previously reported that male mice lacking the EP4 receptor in cardiomyocytes (EP4-KO)

have worsened cardiac function after MI and develop dilated cardiomyopathy with age [73, 267]. More recently we also reported that PGE_2 via its EP3 receptor reduced contractility whereas stimulation of EP4 had the opposite effect. These effects appeared to involve changes in the phosphorylation of phospholamban. Moreover, we also reported that after MI, expression of the EP3 receptor subtype in the left ventricle was increased to a greater extent than EP4 [217]. We therefore hypothesized that overexpression of EP4 in the heart would improve cardiac function after MI. Thus, in our experiments described here, we used an adeno-associated viral vector driven by the alpha myosin heavy chain promoter to increase the expression of the EP4 receptor in the cardiomyocytes rather than increase the activation of receptors already present. The results support our hypothesis, with significant improvements in ejection fraction and shortening fraction noted, coupled with reductions in left ventricular dimension after MI without affecting infarct size.

Overexpression of EP4 also significantly reduced hypertrophy and fibrosis after MI as evidenced by a smaller MCSA and reduced picrosirius red staining in the peri-infarct and remote zone, and the former was confirmed by reductions in β-MHC and BNP mRNA expression. Previously, other studies have shown a protective role for the EP4 receptor in ischemia-reperfusion injury. Xiao et al [371] reported that global EP4 KO mice had larger infarcts after reperfusion injury while administration of an EP4 agonist had the opposite effect. A study by Hishikari et al [266], using a rat model described similar findings but also indicated that treatment with an EP4 agonist could reduce cytokine secretion stimulated by the ischemia/reperfusion. Our data using the permanent coronary ligation model with EP4 overexpression agrees with the aforementioned findings except that we did not observe a change in infarct size at the end of the study. Whether this

relates to the different models or different time points remains unknown. Since we also recently reported that PGE_2 via its EP3 receptor reduced contractility of the heart via mechanism(s) that appeared to involve decreased phospholamban phosphorylation; we examined phosphorylation of phospholamban in these studies. Sham-operated mice who received AAV9-EP4 exhibited a significant increase in phosphorylated phospholamban, consistent with our *in vitro* data using the EP4 agonist in isolated cardiomyocytes [217]. A similar trend was observed in animals with MI, although the data did not achieve statistical significance. We therefore speculate that the increased EP3 receptor abundance after MI could account, in part, for the decreased contractility observed. The role of the EP3 receptor in cardiac function is controversial. Martin et al [268] reported that cardiac overexpression of the EP3 receptor attenuated ischemia-induced myocardial injury. However, that paper used an isolated heart perfusion method and curiously, EP3 transgenic animals exhibited a reduced ejection fraction as measured *in vivo* using MRI. In subsequent studies, we think it will be necessary to identify the impact of EP3 receptor inhibition with simultaneous EP4 overexpression on cardiac function.

Treatment with AAV9-EP4 also improved aspects of adverse cardiac remodeling. The increased collagen deposition noted in the peri-infarct and remote zone after MI was substantially attenuated by use of AAV9-EP4 and there were significant reductions in the number of macrophages and T cells infiltrating the left ventricle. Although the beneficial role of the EP4 receptor in heart failure has not been fully explored, our data agree with several other studies suggesting an anti-inflammatory role for the PGE_2 EP4 receptor subtype. Our data agree with the beneficial role of the EP4 receptor reported in other cell types. In a rat model of autoimmune myocarditis, Ngoc et al. [259] reported that treatment with an EP4 agonist reduced immune cell infiltration, heart size, and area of fibrosis. More

recently, a publication by Wang et al. [372] demonstrated that an EP4 receptor agonist could prevent cardiac dysfunction and cardiac fibrosis in a pressure overload, transaortic constriction mouse model.

In human samples, Haywood et al. [373] showed that iNOS was undetectable in control heart samples but could be detected in 36 of 51 patients with heart failure. Our data show that iNOS expression in the left ventricle is increased after MI and can be attenuated by treatment with AAV9-EP4, consistent with a cardioprotective effect. iNOS is also one marker for the M1 macrophage phenotype but it is unclear from our data obtained from left ventricle samples whether the iNOS originates from resident/infiltrating macrophages or another cell type such as cardiomyocytes. If the former, then the reduction noted in iNOS may relate simply to a reduction in the number of infiltrating macrophages observed after AAV9-EP4 treatment. Alternatively, PGE_2 has been shown to have anti-inflammatory effects in macrophages by reducing TNFα expression and increasing Interleukin 10 expression via the EP4/cAMP/protein kinase A (PKA) pathway, which promotes macrophage M2 polarization [374-376]. It remains to be elucidated if overexpression of EP4 in the left ventricle mediates macrophage polarization towards an anti-inflammatory M2 phenotype and our data using a limited number of markers do not allow us to draw any complete conclusions.

Another aspect of cardiac remodeling involves the matrix metalloproteinases (MMPs) family of proteins and other molecules that play a role in collagen deposition. Specifically, MMP-2 has been implicated in LV remodeling and furthermore, MMP-2 KO mice are reported to have lower incidences of cardiac rupture after MI [377, 378], although the mechanism of how MMP-2 contributes to cardiac rupture is not well understood. Also, reports show that broad inhibition of MMPs contributes to attenuation of LV dilatation [379,

380]. Several MMPs are involved in this process, although MMP-2 may play a key role. Matsumura et al. [369] reported that deletion of MMP-2 in mice profoundly improved survival rates after MI. Moreover, they reported that deletion of MMP-2 completely reduced macrophage migration after MI. Our data using *in situ* zymography which measures gelatinase activity (MMP-2 and MMP-9) is interesting but rather perplexing in that we observe increased MMP activity in sham-operated animals treated with AAV9-EP4 that is not significantly increased further after MI. Overall, our data indicate that treatment with AAV9-EP4 alters the cardiac remodeling process after MI and changes in MMP activity may be an important player in the mechanism of reduced macrophage migration and the subsequent prevention of LV dilatation we observed with overexpression of EP4. The secreted protein, acidic and rich in cysteines (SPARC) was also shown to affect remodeling after MI. Schellings et al [381] reported that deletion of SPARC increased rupture following MI and a role for this molecule in macrophage clearance has also been postulated [382]. Our data show no effect of EP4 overexpression on this molecule, consistent with its high expression in fibroblasts and endothelial cells but low expression in myocytes [383].

Previously, we have described increased expression of both cytokine and chemokine mRNA (e.g. MCP-5 and fractalkine) in the left ventricle of male EP4-KO mice with dilated cardiomyopathy [73]. Takayama et al. [256] have shown that PGE_2 potently inhibits cytokine/chemokine secretion (MCP-1, interleukin 8, macrophage inflammatory protein, and CxCL10) in human macrophages. Thus, inhibition of chemokine or cytokine release may be a significant mechanism to explain how treatment with AAV9-EP4 reduces macrophage infiltration. Treatment with AAV9-EP4 also significantly prevented increases in TNFα mRNA after MI. TNFα is a major cytokine implicated in heart failure

and increases in TNFα have been correlated with the severity of cardiac disease although anti-TNFα therapies have met with little clinical success [384, 385]. In addition to alterations in TNFα, our results also show that overexpression of EP4 affects other chemokines/cytokines. Using a mouse cytokine/chemokine array we detected a significant reduction in MCP-1 protein levels in the left ventricle and increases in IL-10, an anti-inflammatory cytokine, after treatment of MI hearts with AAV9-EP4. Unfortunately, protein levels of these cytokines/chemokines were below the limits of detection in isolated mouse cardiomyocytes treated with AAV9-EP4 or control virus, even after stimulation with LPS. Thus, we cannot be certain if overexpression of EP4 affects production of these factors from cardiomyocytes or if it has paracrine effects. However, our data show that reduction of pro-inflammatory cytokines/chemokines may be one mechanism by which over-expression of the EP4 prevents the deleterious effects of MI.

One limitation of the study is that the viral package was administered at the same time as MI and would have better clinical relevance if it was administered post-MI. However, this would require multiple major open-chest surgeries. Furthermore, it would take at least 48 hours for the viral DNA to insert itself into the host genome and to transcribe the EP4. We believe this is key to the model's success. If EP4 is overexpressed too early, the reduced inflammation may result in poor scar formation and result in increased rates of cardiac rupture. Our timing is ideal in that we reduce persistent inflammation during the inflammatory phase of cardiac remodeling and promote a resolving, healing phase in the heart.

Conclusion

We have demonstrated for the first time that overexpression of the EP4 receptor is protective in a mouse MI model. We have also shown that overexpression of the EP4

receptor may prevent inflammation involved in cardiac remodeling post MI, thus contributing to the preserved cardiac function. If our results can be applied to the human condition, our data support therapeutic interventions that increase EP4 expression.

CHAPTER 3 - PROSTAGLANDIN E2 AND AN EP4 RECEPTOR AGONIST INHIBIT LPS-INDUCED MONOCYTE CHEMOTACTIC PROTEIN 5 PRODUCTION AND SECRETION IN MOUSE CARDIAC FIBROBLASTS VIA AKT AND NF-κB SIGNALING

(This Chapter contains previously published material. See Appendix B)

Introduction

Chemokines are a group of small (8-14 kDa) chemoattractant molecules that regulate the trafficking of various leukocytes, mainly neutrophils, monocytes, lymphocytes, and eosinophils to various tissues [386]. Chemokines bind to about 20 different receptors, all of which belong to the seven transmembrane G-protein-coupled class of receptors [387]. One particular chemokine, monocyte chemoattractant protein-5 (MCP-5), is the mouse analogue to human MCP-1, and is a potent chemoattractant for monocytes and macrophages [72]. Several studies have implicated MCP-1 in diseases characterized by infiltrating monocytes, especially myocardial ischemia [388-390]. Far less is known about the murine MCP-5, however.

Prostaglandin E_2 (PGE_2) signals through 4 distinct receptor subtypes (EP1, EP2, EP3, and EP4) to elicit a variety of effects. EP2 and EP4 both increase cAMP levels in the cell via adenylate cyclase activation, whereas EP3 inhibits cAMP production. EP1 increases Ca^{2+} levels in the cell [391, 392]. The differences in signaling of these receptors in cardiac tissue have still not been studied in depth. Previously, our lab developed a mouse line in which the EP4 receptor is deleted specifically in the cardiomyocytes. These mice develop a phenotype of dilated cardiomyopathy with reduced ejection fraction with age, as well as pockets of interstitial infiltrate within the left ventricle. Gene array data showed that these mice have increased production of chemokine/cytokines in their left ventricles, including CCL12 (MCP-5) [73]. Very recently, we reported that overexpression

of the EP4 receptor improves cardiac function in a myocardial infarction (MI) model (chapter 2). Moreover, we showed that overexpression of the EP4 receptor was associated with an anti-inflammatory effect shown by reduced levels of MCP-1 with increased IL-10 in the left ventricle [216]. Precisely how PGE_2 exerts its anti-inflammatory effects in the heart has not been elucidated. PGE_2 signaling through its EP4 receptor, however, has been shown to have anti-inflammatory effects in organ systems and cell types other than the heart [256, 259, 393-396]. Specifically, PGE_2-EP4 signaling has been shown to inhibit bacterial lipopolysaccharide (LPS) signaling [396], but this result has not been reported for isolated adult mouse cardiac fibroblasts.

Damage-associated molecular patterns (DAMPs), such as LPS, activate pattern recognition receptors (PRRs) of the toll-like receptor (TLR) family, particularly TLR-2 and 4 [397]. Activation of TLRs characteristically leads to the transcriptional activation of genes which encode pro-inflammatory cytokines and other mediators of inflammation by transcription factors such as nuclear factor κB (NF-κB). Both TLR-2 and TLR-4 have been shown to be expressed in cardiomyocytes and fibroblasts [398]. Cardiac fibroblasts play a particularly important role in cardiac injury due to their ability to maintain the integrity of the extracellular network. Furthermore, cardiac fibroblasts play an important role in secreting and responding to cytokines/chemokines in response to injury [399].

In this current study, we take an *in vitro* approach to examine whether treatment of cardiac fibroblasts with exogenous PGE_2 affects chemokine production. We hypothesized that PGE_2 inhibits LPS-induced MCP-5 secretion in adult mouse cardiac fibroblasts via its EP4 receptor.

Methods

Animal Use

Male 16-20 wks. old C57Bl/6 mice used for cardiac cell isolation were from Jackson labs. The isolation of adult ventricular fibroblasts (AVF) was previously described by us [73]. All studies involving the use of animals were approved by the institutional review committee at Henry Ford Hospital, in accordance with federal guidelines.

Chemicals

EP1 antagonist (SC-51089), EP2 agonist (Butaprost), EP2 antagonist (TG4-155), EP4 agonist (CAY10598), EP4 antagonist (GW627368X), and prostaglandin E_2 were from Cayman Chemical (Ann Arbor, MI). EP3 antagonist (L798, 106) and cardamonin were obtained from Tocris (Minneapolis, MN). IKK inhibitor III was from Millipore Sigma (Burlington, MA). Tri-reagent was obtained from Molecular Research Center (Cincinnati, OH). All other drugs were obtained from Sigma Aldrich.

Treatment of Isolated Cardiac Fibroblasts

For all AVF experiments, the cells were passaged to p3 followed by serum starvation for at least 16 hours. *Time Course Experiment;* cells were pre-treated with vehicle (ethanol), PGE_2 (1 μM), or the EP4 agonist (CAY10598; 1 μM) for 1 hour. After 1 hour, cells were treated with lipopolysaccharide (LPS; 10 μg/ml) for 1, 2, 4, and 24 hours. Media were collected and snap-frozen in liquid nitrogen for ELISA analysis. Cells were scraped in 1 ml of Tri-reagent and snap frozen for future RNA isolation and real time RT-PCR. *EP receptor antagonist experiment;* In another set of experiments, the cells were first pre-treated with the EP1 antagonist SC-51089 (1 μM), EP2 antagonist TG4-155 (0.5 μM), EP3 antagonist L798, 106 (1 μM), or an EP4 antagonist GW627368X (1 μM) prior to treatment as described above for 24 hrs. In separate experiments at shorter time points

(0, 5, 15, 30 mins), protein lysate was collected for Western blot analysis by scraping the cells on ice with lysis buffer containing protease and phosphatase inhibitors (Roche). *Dibutyryl cAMP (db cAMP)*; cells were pre-treated with vehicle (DMSO), Dibutyryl cAMP (100 μM), or the EP4 agonist (1 μM) for 1 hour. After 1 hour, cells were treated with LPS (10 μg/ml) for 24 hours. Media were collected and snap-frozen for ELISA analysis. *PI3K Inhibitor (*wortmannin and LY290042); cells were pre-treated with vehicle (DMSO and ethanol), PGE_2 (1 μM), or Wortmannin (1 μM) or LY290042 (10 μM) for 1 hour. After 1 hour, cells were treated with LPS (10 μg/ml) for 24 hours. Media were collected and snap-frozen for ELISA analysis. *NF-κB inhibition* (cardamonin and IKK inhibitor III)*;* cells were pre-treated with vehicle (ethanol), cardamonin (10 μM), or IKK inhibitor III (10 μM), for 1 hour. After 1 hour, LPS (10 μg/ml) was added to the appropriate wells for 24 hours. Media were collected and snap-frozen for ELISA analysis and protein lysates were collected for western blot analysis. *JNK inhibitor (SP600125);* cells were pre-treated with vehicle (ethanol), or SP600125 (10 μM) for 1 hour. After 1 hour, the cells were treated with vehicle (ethanol and DMSO), PGE_2 (1 μM), or the EP4 agonist (1 μM) for 1 hour. After 1 hour, cells were treated with LPS (10 μg/ml) for 24 hours. Media were collected and snap-frozen in liquid nitrogen for ELISA analysis. Protein lysates were collected for western blot analysis.

MCP-5 Secretion Analyses

MCP-5 ELISA analysis of media samples was performed according to the manufacturer's instructions (Ray BioTech; Catalog No. ELM-MCP5). For all ELISA experiments, data was collected as pg/ml, corrected for the amount of protein in each sample and then presented as fold of vehicle. This kit is specific for MCP-5 and shows no cross reactivity with a number of different cytokines/chemokines, including MCP-1. The

limit of detection for this kit is 0.5 pg/ml.

Polymerase Chain Reaction

Measurement of MCP-5 mRNA expression was performed by real-time RT-PCR using a SYBR green method as follows. 1 µg of DNase I-treated RNA sample was reverse transcribed using random primers and Omniscript reverse transcriptase kit (Qiagen; Valencia, CA). 2 µL of the reverse transcription reaction was amplified in a Roche version 2.0 lightcycler PCR machine (Roche; Indianapolis, IN) using SYBR green dye and specific primers against MCP-5, EP1, EP2, EP3, and EP4. Primers were purchased from TIB MolBiol (Adelphia, NJ) and Qiagen (Germantown, MD). It has been reported that stimulation with LPS in other cell types can affect GAPDH expression [400]. In our hands, the average GAPDH crossing points did not change with LPS stimulation, thus GAPDH was used as a control (17.00 ± 0.22 for vehicle treated mice vs. 17.37 ± 0.38 for LPS treated mice. p=0.796). To determine the mRNA expression of EP1, EP2, EP3, and EP4 in the fibroblasts, 2 µg of RNA was reverse transcribed in the same manner described above. 2 µl of the reverse transcription reaction was amplified in a Bio-Rad PTC-100 thermal cycler using Taq polymerase. PCR conditions were: 94°C for 30 s, 58–62°C for 30 s, 72°C for 90 s and a final extension at 72°C for 5 min. Sequences for all primers used are shown in Table 3.

Table 3: Primer Sequences

Gene	Sense	Anti-Sense
MCP5	5’-caagagratcaccagcagcagg-3’	5’- tgcttgaggtggttgtggaa-3’
GAPDH	5’-caaggtcatcccagagctg-3’	5’-tgtcatcatacttggcaggtt-3’
EP1	5’- atcatggtggtktcgtgcatct-3’	5’-catgggtccaggatctggtt-3’
EP2	5’-tatgctccytgcctttcac-3’	5’-ctcagtgaagtccgacaacag-3’
EP3	Qiagen, NM_011196.2	
EP4	5’-gtgcagagatccagatggtca-3’	5’-atcygggtttctgctgatgtc-3’

Primers from Qiagen are proprietary and only the RefSeq number for the mRNA sequence is provided.

MCP-5 mRNA Stability

Measurement of MCP-5 mRNA stability was determined using real time RT-PCR (see methods 2.5). AVF were pre-treated with PGE_2, EP4 agonist, or vehicle for 1 hour. After a 1-hour pre-treatment, cells were treated with LPS (10 μg/ml) for 2 hours. Previous experiments in our lab have determined that 2 hours is adequate to stimulate MCP-5 mRNA. After LPS treatment, AVF were treated with 5,6-Dichloro-1-β-D-ribofuranosylbenzimidazole (DRB) for 0 and 30 minutes to block transcription. The cells were harvested in Tri-reagent and stored at -80^{o}C for further PCR analysis.

Western Blot Analysis

Phosphorylated IκBα (p-IκBα; 1:1000), phosphorylated Akt (T308, p-Akt; 1:1000), phosphorylated JNK (p-JNK; 1:1000), phosphorylated p44/42 (p-p44/42; 1:1000) and phosphorylated p38 (p-p38; 1:1000) were measured by western blot using a method previously described by us [217]. Phosphorylated IκBα, p-Akt, p-JNK, p-p44/42, and p-p38 were corrected to total IκBα, Akt, JNK, p44/42 and p38 respectively. All antibodies were from Cell Signaling (Danvers, MA). Western blot was quantified using NIH Image J software (Bethesda, MD). Phosphorylated protein was corrected to total and then corrected to vehicle. LPS stimulation at 15 minutes was set to 100% and the effect of PGE_2 and the EP4 agonist are presented as the percentage of LPS stimulation.

Statistical Analysis

Statistical analysis was performed by a statistician in the Department of Public Health Sciences of Henry Ford Hospital using the statistical package SAS Version 9.4. For all tests, a two-sample Wilcoxon test with the Fligner-Policello correction for unequal variances was used. We also used a Hochberg's method for multiple testing. For the western blot analysis, a paired T-test was used. A p-value < 0.05 was considered as

evidence of a statistically significant difference for experimental data with the p values being two-sided.

Results

All EP Receptors are Expressed in Adult Mouse Cardiac Fibroblasts

Figure 16 shows the expression profile of the EP receptors in cultured adult mouse cardiac fibroblasts. The mRNAs for all four of the EP receptors are expressed and this experiment was repeated on two separate occasions using different preparations with the same result.

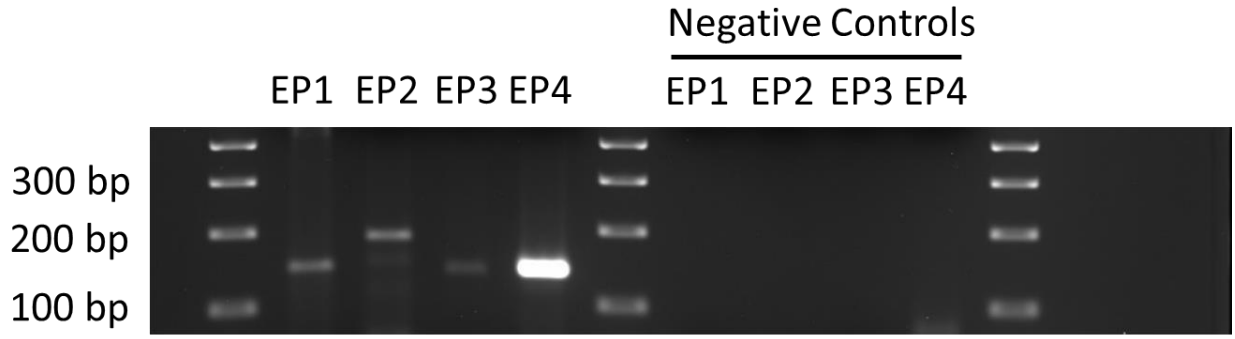

Figure 16. Representative EP Receptor mRNA Expression. 2 % Agarose gel of PCR products; product sizes (in bp) are as follows: EP1; 142, EP2; 186, EP3; 134, EP4; 139.

PGE_2 and an EP4 Receptor Agonist Inhibit MCP-5 Secretion after LPS-Stimulation

To first determine the effect of PGE_2 and the EP4 agonist on LPS-stimulation of MCP-5 secretion, we performed a time-course experiment, analyzing the concentration of MCP-5 in media at 1, 2, 4, and 24 hours after treatment with LPS (10 µg/ml). Cells were pre-treated with PGE_2 or the EP4 agonist for 1 hr prior to stimulation. On average, the baseline MCP-5 concentration in the media was 61.23 ± 19.51 pg/ml and this rose to 1470.51 ± 163.21 pg /ml after 24 hrs of LPS treatment. All data were corrected for total protein in the sample and presented as fold of vehicle control. After 1 or 2 hours of LPS stimulation, there was no detectable increase in MCP-5 in the media compared with

vehicle treated cells (0.95 ± 0.14 vs. 1.00 ± 0.0 in vehicle treated cells; p=0.423) and (1.38 ± 0.23 vs. 1.00 ± 0.0 in vehicle treated cells; p=0.240), respectively. After 4 hours of LPS treatment however, there was a significant increase in MCP-5 in the media (2.27 ± 0.42 fold vs. 1.00 ± 0.0 in vehicle treated cells; p=0.012). PGE_2 significantly reduced LPS-stimulated MCP-5 (1.23 ± 0.18 vs. 2.27 ± 0.42 in LPS treated cells; p=0.005). There was also a tendency for a decrease in LPS-stimulated MCP-5 when cells were pre-treated with the EP4 agonist, although this data did not reach statistical significance (1.77 ± 0.24 vs. 2.27 ± 0.42 in LPS treated cells; p=0.36). Figure 17 A shows that by 24 hours, LPS stimulation of MCP-5 remained significantly elevated (3.38 ± 0.36 vs. 1.00 ± 0.0 in vehicle treated cells; p=0.005). At this time point, both PGE_2 and the EP4 agonist significantly reduced MCP-5 production after LPS stimulation (1.18 ± 0.12 in PGE_2 pre-treated cells vs. 3.38 ± 0.36 in LPS treated cells; p=0.009 and 1.53 ± 0.20 in EP4 agonist pre-treated cells vs. 3.38 ± 0.36 in LPS treated cells; p=0.009). Since PGE_2 and the EP4 agonist both

A

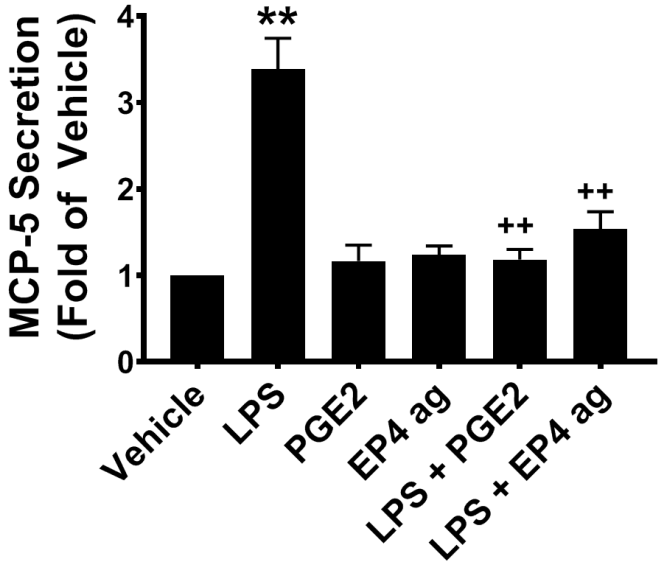

Figure 17 A: 24 Hour LPS Stimulation of MCP-5 ELISA. AVF were pre-treated for 1 hour with PGE_2 (1 µM) or the EP4 agonist (EP4 ag; 1 µM) followed by treatment with LPS (10 µg/ml) for 24 hours. All results were obtained as pg/ml and corrected for the amount of protein in each well. Data is presented as fold of vehicle treatment (set to 1.0) ± SEM. ** p<0.01 vs. vehicle, ++ p< 0.01 vs. LPS. N=5

reduce MCP-5 production after LPS stimulation, it suggests that the effect of PGE_2 is mediated via the EP4 receptor. To test this, we pre-treated the cells with an EP4 antagonist (GW627368X) prior to treatment with PGE_2 or the EP4 agonist and LPS for 24 hours (Figure 17 B).

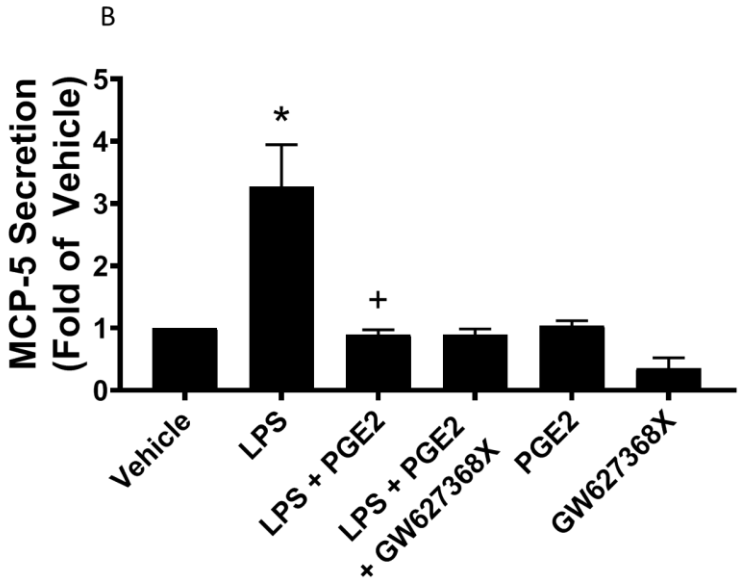

Figure 17 B: MCP-5 ELISA Analysis with GW627368X. AVF were pre-treated for 1 hour with the EP4 antagonist GW627368X (GW; 1 µM). Cells were then treated with or without PGE_2 (1 µM) for 1 hour, followed by treatment with LPS (10 µg/ml) for 24 hours. All results were obtained as pg/ml and corrected for the amount of protein in each well. Data are presented as fold of vehicle treatment (set to 1.0) ± SEM. *$p<0.05$ vs. vehicle, + $p<0.05$ vs. LPS. N=6-9

Surprisingly, GW627368X did not reverse the inhibitory effect of PGE_2 suggesting some of the effects of PGE_2 are through a mechanism other than the EP4 receptor signaling pathway. However, the inhibitory effect of the EP4 agonist was significantly attenuated with GW627368X (Figure 17 C), suggesting that the EP4 agonist is specific and its inhibitory effects are indeed through the EP4 receptor (3.80 ± 0.22 in LPS treated vs. 1.36 ± 0.15 in LPS + CAY10598 treated; $p<0.005$ and 2.97 ± 0.16 in LPS + CAY10598 + GW627368X treated vs. 1.36 ± 0.15 in LPS + CAY10598 treated; $p=0.000009$). Additionally, we pretreated the AVF with antagonists to either EP1, EP2, or EP3 receptors. Antagonism of these receptors had no effect on the ability of PGE_2 to reduce LPS-stimulated MCP-5 secretion suggesting they are not responsible for the inhibition of LPS-stimulated MCP-5 by PGE_2 (EP1: 0.89 ± 0.08 in LPS + PGE_2 vs. 0.73 ± 0.06 in LPS

+ SC-51089 + PGE2; EP2: 0.89 ± 0.08 in LPS + PGE2 vs. 1.04 ± 0.08 in LPS + TG4-155 + PGE_2; EP3: 0.89 ± 0.08 in LPS + PGE_2 vs. 0.55 ± 0.06 in LPS + L798, 106 + PGE_2). None of the EP receptor antagonists alone affected basal MCP-5 secretion.

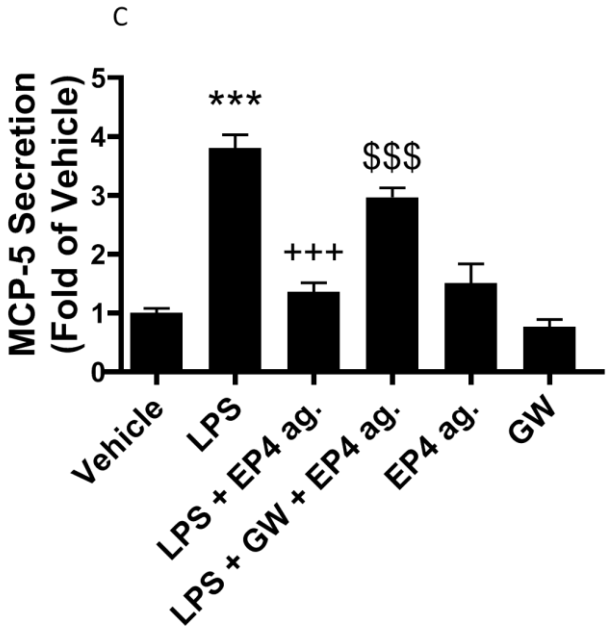

Figure 17 C: GW627368X Reverses EP4 Agonist. AVF were pre-treated for 1 hour with the EP4 antagonist GW627368X (GW; 1 µM). Cells were then treated with the EP4 agonist (1 µM) for 1 hour, followed by treatment with LPS (10 µg/ml) for 24 hours. All results were obtained as pg/ml and corrected for the amount of protein in each well. Data is presented as fold of vehicle treatment (set to 1.0) ± SEM. ***p<0.005 vs. vehicle, +++ p<0.005 vs. LPS, $$$ p<0.005 vs. LPS + EP4 agonist. N=6.

PGE_2 and an EP4 Agonist Reduce LPS-Stimulated MCP-5 mRNA

Both LPS-stimulation of MCP-5 secretion and its inhibition by PGE_2 and the EP4 agonist appears to take at least 4 hours to be detectable, suggesting that PGE_2 and EP4 signaling may regulate MCP-5 transcription as well as its secretion. To test this, we performed a time-course experiment examining MCP-5 mRNA levels after 1, 2, 4, and 24 hours post LPS stimulation. We also examined the effects of PGE_2 and its EP4 receptor agonist at these time points. Figure 17 D shows that after 1 hour of LPS stimulation, MCP-5 mRNA increased over 4-fold compared to vehicle (4.49 ± 0.71 vs. 1.00 in vehicle treated cells; p=0.005). Treatment with the EP4 agonist significantly blunted the response to LPS (2.09 ± 0.82 vs. 4.49 ± 0.71 in LPS-treated cells; p=0.004). Similarly, at the same time point, PGE_2 treatment attenuated MCP-5 levels after LPS stimulation, although this failed to reach statistical significance (2.68 ± 1.04 vs. 4.49 ± 0.71 in LPS-treated cells;

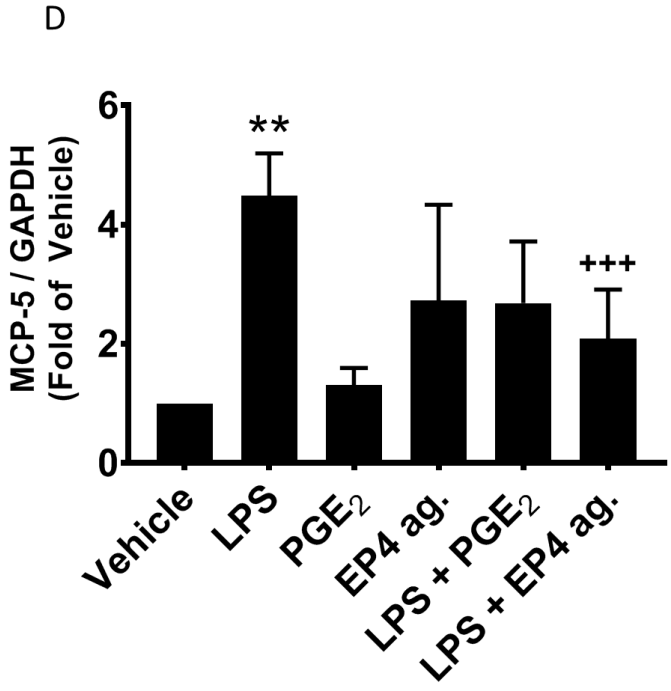

Figure 17 D: Real Time RT-PCR of MCP-5 mRNA after LPS Stimulation. AVF were pre-treated for 1 hour with PGE_2 (1 µM) or the EP4 agonist (1 µM) followed by treatment with LPS (10 µg/ml) for 1 hour. All results were obtained as fold induction and corrected to the housekeeping gene GAPDH. Data are presented as fold of vehicle treatment, means ± SEM. ** $p<0.01$ vs. vehicle. +++$p<0.005$ vs. LPS. N=5.

p=0.186). LPS stimulation resulted in a significant elevation in MCP-5 mRNA levels throughout all time points; however, there was no significant effect of either PGE_2 or the EP4 agonist at any other time points after 1 hr. These data suggest that EP4 receptor activation leads to downstream signaling that quickly downregulates MCP-5 mRNA. Since previous reports have suggested that LPS can directly affect the stability of pro-inflammatory chemokine/cytokine mRNA transcripts [401-403], we performed an

Figure 17 E: MCP-5 mRNA Stability. Real time RT-PCR analysis for MCP-5 mRNA stability. AVF were pre-treated with PGE_2 (1 µM) for 1 hour, followed by treatment with LPS (10 µg/ml) for 2 hours. After 2 hours, transcription was blocked using DRB (60 µM) and the decay of MCP-5 mRNA was assessed after 30 minutes. Data are presented as fold of LPS-stimulated MCP-5. N=6.

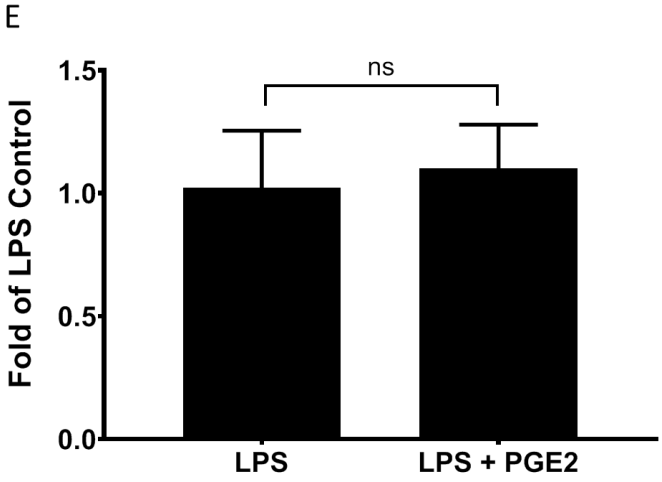

experiment using the transcriptional inhibitor DRB (60 μM). Figure 17 E shows that after 30 minutes of DRB treatment, there was no effect of PGE_2 on LPS-stimulated MCP-5 mRNA (1.10 ± 0.18 vs. 1.02 ± 0.23 in LPS-stimulated cells; ns). These data suggest that the inhibition of LPS-stimulated MCP-5 is not due to an effect on MCP-5 mRNA stability.

Inhibition of NF-κB Abolishes LPS-induced Secretion of MCP-5

It is well known that NF-κB is an important transcription factor in regulating cytokine production [404-406]. Typically, the IκB complex sequesters NF-κB in the cytoplasm. Upon phosphorylation by IκB Kinase (IKK), IκBα is targeted for degradation allowing NF-κB p65 subunit to translocate into the nucleus to regulate transcription [404]. Therefore, we used p-IκBα as a surrogate of NF-κB activation. To determine if NF-κB is involved in regulating transcription of MCP-5, we pre-treated AVF with the NF-κB inhibitor, cardamonin. Figure 18 A shows that, as expected, 24 hours of LPS stimulation significantly increased MCP-5 production compared with vehicle treatment (9.11 ± 3.09 vs. 1.00 ± 0.0 in vehicle treated cells; p=0.003). Pre-treatment with cardamonin greatly reduced the MCP-5 produced after LPS treatment (1.71 ± 0.41 vs. 9.11 ± 3.09 in LPS treated cells; p=0.001). Furthermore, we confirmed the specificity of this inhibitor by examining phosphorylation of IκBα. The western blot in Figure 18 B clearly shows that after 24 hours of LPS + cardamonin treatment, p-IκBα is reduced compared to LPS alone. To confirm our findings, we repeated these experiments using an IKK inhibitor (IKKi). Similar to cardamonin, pre-treatment with the IKK inhibitor significantly reduced LPS-stimulation of MCP-5, (3.49 ± 0.34 in LPS vs. 1.02 ± 0.16 in LPS + IKKi; p=0.00000001). Together, these data suggest that NF-κB plays a major role in regulating the production of MCP-5 in LPS-stimulated cardiac fibroblasts.

Figure 18 A: MCP-5 ELISA Analysis with Cardamonin. Mouse MCP-5 ELISA analysis: AVF were pre-treated with the NF-κB inhibitor, cardamonin (10 µM) for 1 hour, followed by treatment with LPS (10 µg/ml) for 24 hours. Data were obtained as pg/ml of MCP-5, corrected to the amount of protein in each well and presented as fold of vehicle ± SEM. *** p<0.005 vs. vehicle. +++ p< 0.005 vs. LPS. N=6.

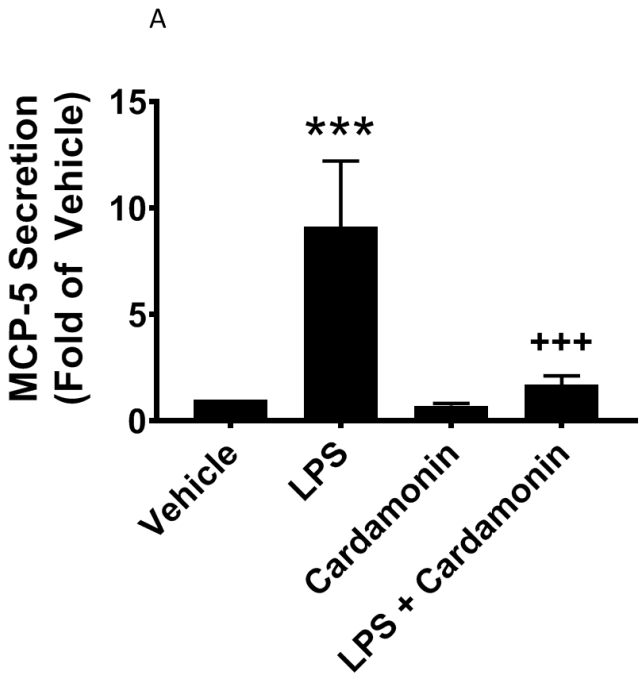

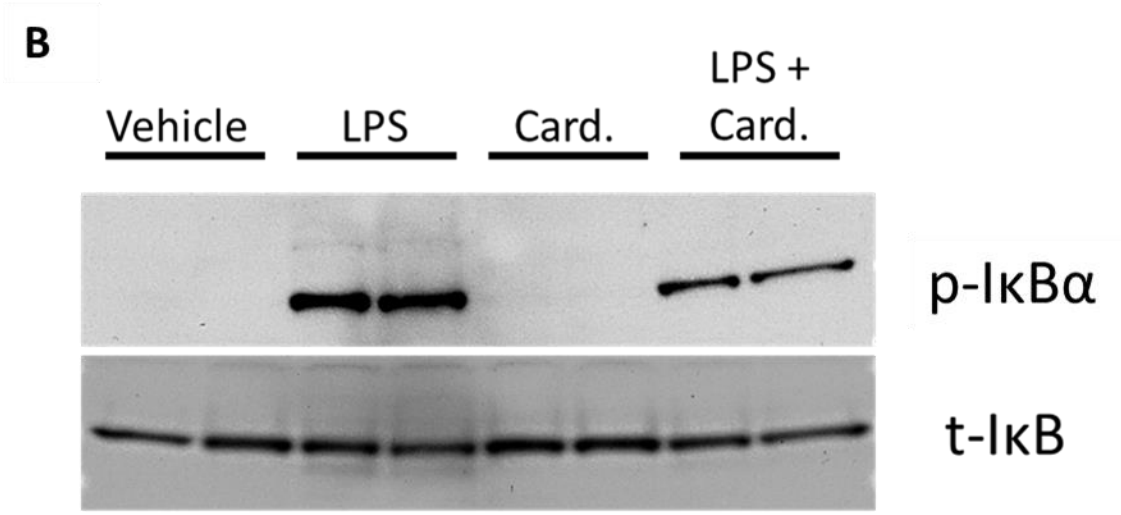

Figure 18 B: Western Blot Analysis for Phosphorylated IκB with Cardamonin. Phosphorylated IκBα and total IκBα used as a loading control.

PGE_2 and an EP4 Agonist Reduce LPS Stimulation of MCP-5 by Inhibiting NF-κB Signaling

NF-κB appears to be a major factor in regulating MCP-5 production after LPS challenge. Furthermore, the attenuation of MCP-5 production by PGE_2 and the EP4 receptor agonist only occur under LPS stimulation and not under basal conditions. Therefore, we sought to determine at which point in the inflammatory signaling cascade

PGE_2 and/or EP4 signaling is eliciting its effects. The western blot analysis in Figure 19 shows that after 15 minutes of LPS treatment, p-IκBα was reduced with PGE_2 and the

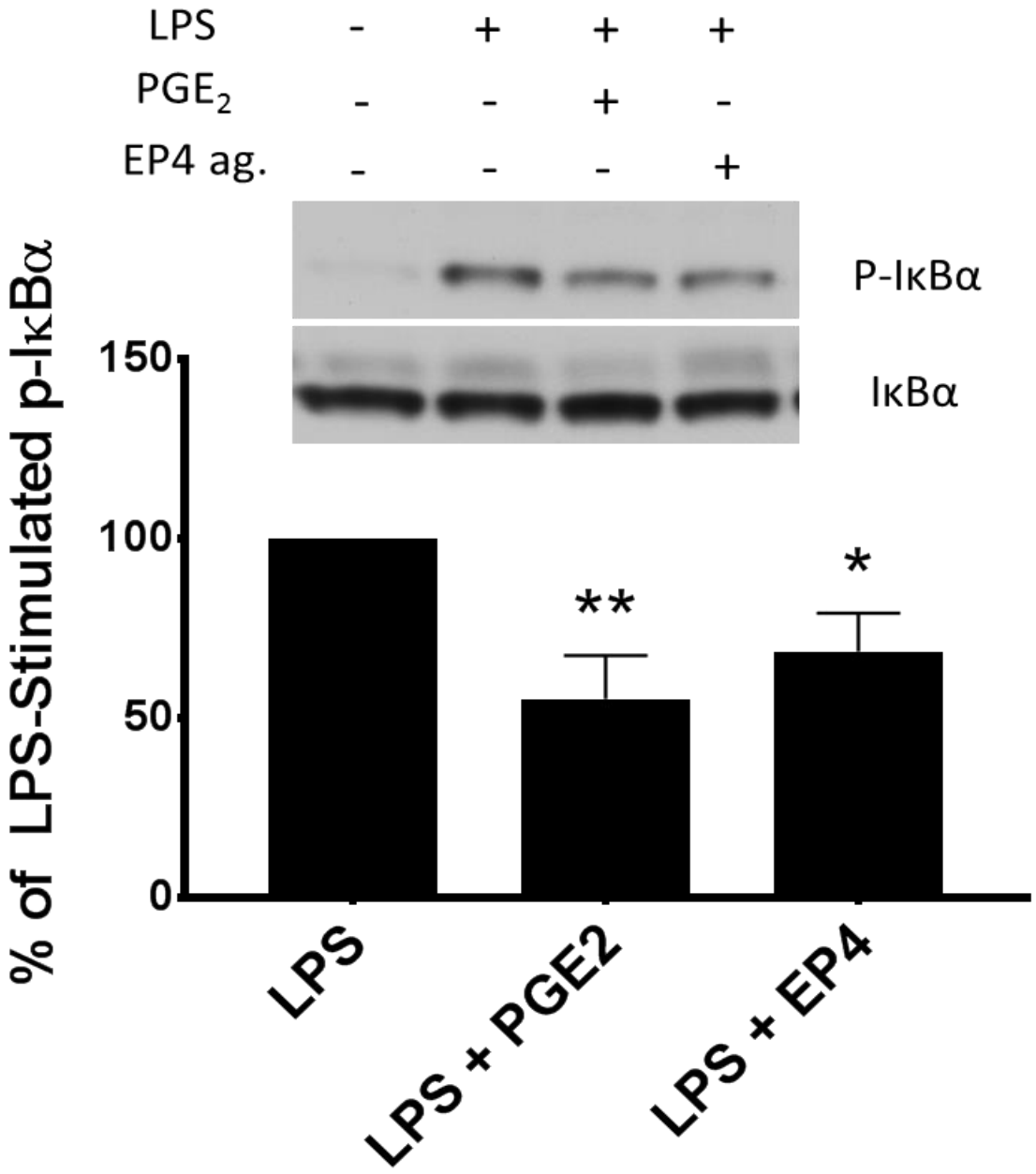

Figure 19: Western Blot Analysis of Phosphorylated IκB with PGE_2 and an EP4 Agonist. *Top panel*: Representative western blot analysis using antibodies against phosphorylated IκBα. AVF were pre-treated with PGE_2 (1 µM) and the EP4 agonist (1 µM) for 1 hour, followed by treatment with LPS (10 µg/ml) for 15 minutes. Data obtained were corrected to total IκBα. *Bottom panel*: LPS stimulation at 15 minutes was set to 100% and data was calculated as a percentage of the LPS stimulation. *p<0.05, ** p<0.01 vs. LPS. N=6.

EP4 agonist. Pretreatment of AVF with PGE_2 resulted in a 45% decrease in LPS-stimulated p-IκBα (55.2 ± 12.0 % vs. 100 ± 0.0 % in LPS treated cells; $p<0.005$). Likewise, when the cells were pretreated with the EP4 agonist, there was a 32% decrease in LPS-stimulated p-IκBα (68.5 ± 10.6 % vs. 100 ± 0.0 % in LPS treated cells; $p<0.05$). By 30 minutes p-IκBα remains greatly elevated with LPS treatment, however there was no significant reduction when cells were pretreated with PGE_2 or the EP4 agonist, suggesting that their inhibition on NF-κB signaling may be a rapid signaling event, climaxing at 15 minutes (415.91 % ± 157.5 vs. 100 % ± 0.0 at 15 minutes; $p=0.07$).

Inhibition of MCP-5 via PGE_2 and an EP4 Agonist is independent of the JNK, p38, and p44/42 Signaling Pathways

Since LPS treatment can stimulate c-Jun N-terminal kinase (JNK) signaling, p44/42 and p38 MAPK pathways in other cell types leading to cytokine production [407], we examined whether these pathways played a role in AVF. Figure 20 A shows that LPS treatment stimulates p-JNK. We observed an inhibitory effect of LPS-stimulated phosphorylation of JNK with PGE_2 and EP4 agonist treatment, although these data did not reach statistical significance (27.3 % reduction; 72.71 ± 17.9 % in PGE_2 treated vs. 100 ± 0.0 % in LPS treated cells and a 20 % reduction; 80.11 ± 22.7 % in EP4 agonist treated vs. 100 ± 0.0 % in LPS treated cells, respectively). The stimulation of p-JNK persisted for at least 30 minutes (141.2 ± 57.8 in LPS treated cells vs. 100 ± 0.0 % in LPS treated cells at 15 minutes). Similarly, PGE_2 and the EP4 agonist each had a 30 % reduction on the LPS-stimulation of p-JNK with values of 70.2 ± 11.2 % and 71.32 ± 12.3 %, respectively. To examine whether the reduction in p-JNK with PGE_2 and the EP4 agonist after LPS stimulation affects MCP-5 production/secretion, we treated AVF with the JNK inhibitor, SP600125. Treatment with PGE_2 and the EP4 agonist reduced LPS-

stimulated MCP-5 production as expected (1.4 ± 0.21 in PGE_2 treated vs. 4.7 ± 0.15 in LPS treated cells; $p<0.005$ and 2.2 ± 0.21 in EP4 agonist treated vs. 4.7 ± 0.15 in LPS; $p<0.005$).

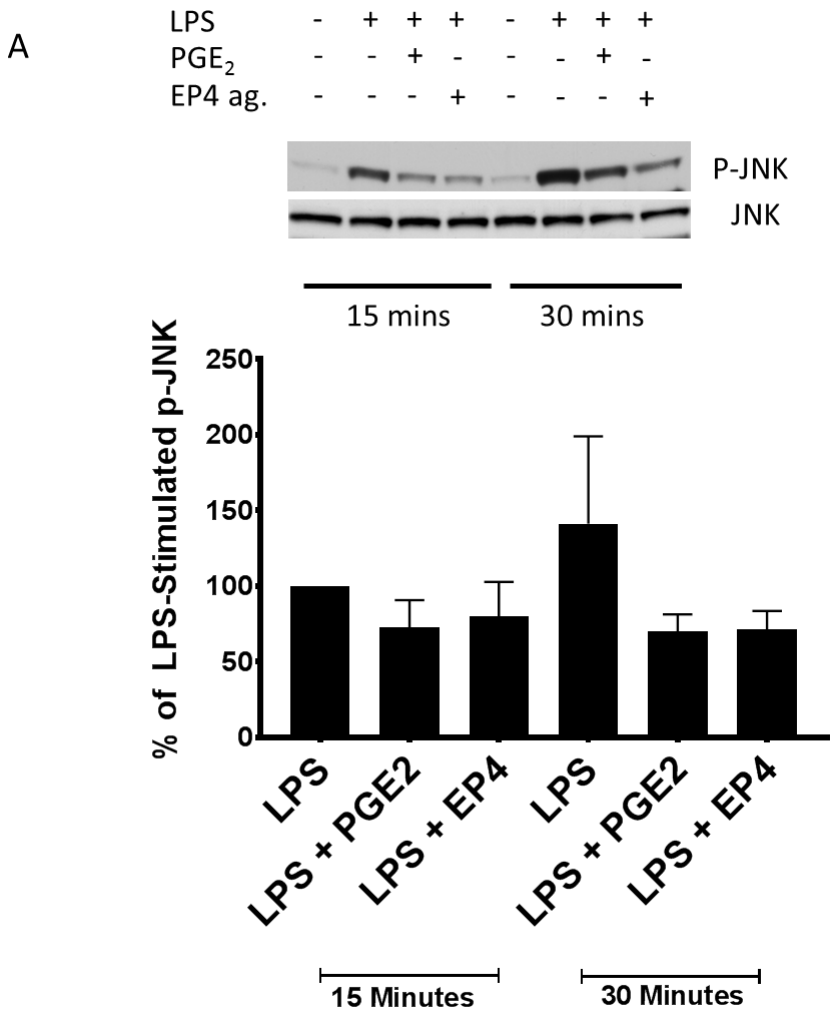

Figure 20 A: Representative JNK Western Blot Analysis. *Top panel.* Representative western blot for phosphorylated JNK. AVF were pre-treated with PGE_2 (1 µM) and the EP4 agonist (1 µM) for 1 hour, followed by treatment with LPS (10 µg/ml) for 15 and 30 minutes. *Bottom panel.* LPS stimulation at 15 mins was set to 100% and data were calculated as a percentage of the LPS stimulation at 15 mins. N=4.

However, as shown in Figure 20 B, when cells were pretreated with the JNK inhibitor (SP600125), there was an additional inhibitory effect, greater than the effect of PGE_2 or the EP4 agonist alone (0.6 ± 0.03 in LPS + PGE_2 + SP600125 vs. 1.4 ± 0.21 in

LPS + PGE_2; p<0.005 and 0.9 ± 0.04 in LPS + EP4 + SP600125 vs. 2.2 ± 0.21 in LPS + EP4; p<0.005). Furthermore, Figure 20 C shows that after LPS stimulation (3.6 ± 0.47 vs. 1.0 ± 0.03 in vehicle; p< 0.005), there was a slight reduction in MCP-5 production with the JNK inhibitor alone, however these data did not reach statistical significance (2.7 ± 0.32 vs. 3.6 ± 0.47 in LPS treated cells; p=0.12). Together these data suggest that JNK signaling may play a small role in LPS signaling. However, both PGE_2 and EP4 signaling appear to be acting through a pathway separate of JNK signaling to reduce MCP-5 production/secretion. Additionally, phosphorylation of p44/42 and p38 also increased after LPS treatment but neither PGE_2 nor the EP4 agonist had any effect (Figures 20 D and 20 E, respectively).

B

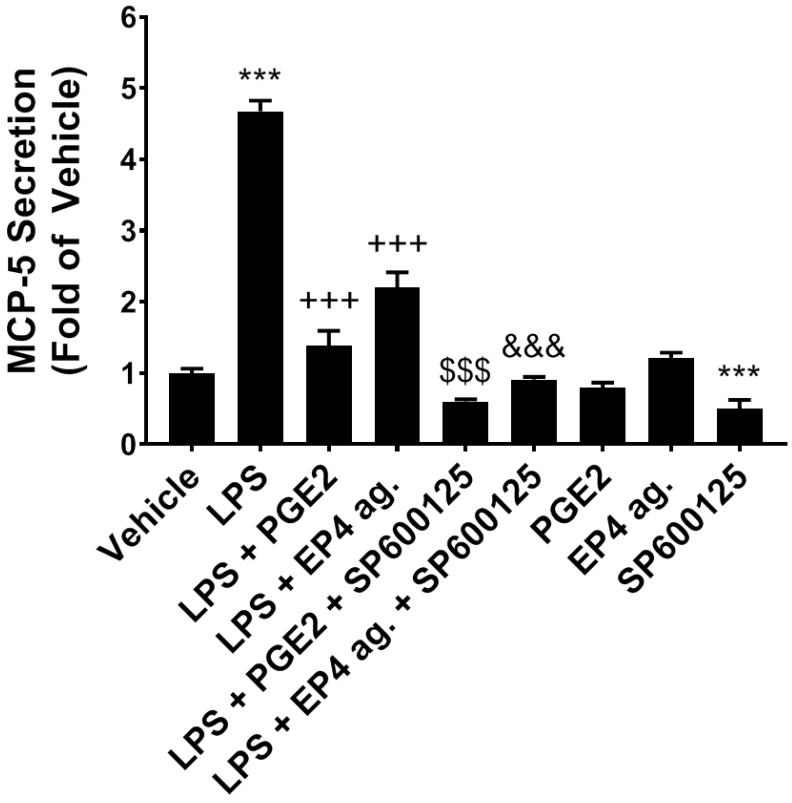

Figure 20 B: MCP-5 ELISA Analysis with JNK Inhibitor. AVF were pre-treated with the JNK inhibitor, SP600125 (10 µM), PGE_2 (1 µM), and/or the EP4 agonist (1 µM) for 1 hour, followed by treatment with LPS (10 µg/ml) for 24 hours. Data were obtained as pg/ml of MCP-5, corrected to the amount of protein in each sample and presented as fold of vehicle ± SEM. *** p<0.005 vs. vehicle. +++ p< 0.005 vs. LPS, $$$ p< 0.005 vs. LPS + PGE_2, &&& p< 0.005 vs. LPS + EP4 ag. B, N=4-6.

C

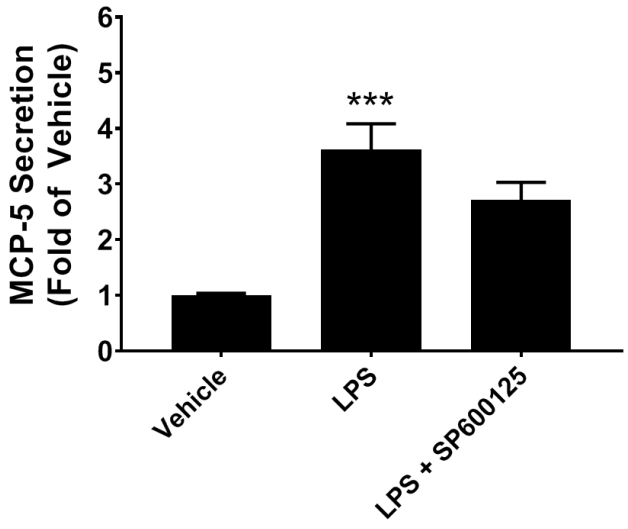

Figure 20 C: MCP-5 ELISA Analysis with JNK Inhibitor. AVF were pre-treated with the JNK inhibitor, SP600125 (10 µM) for 1 hour, followed by treatment with LPS (10 µg/ml) for 24 hours. Data were obtained as pg/ml of MCP-5, corrected to the amount of protein in each sample and presented as fold of vehicle ± SEM. *** $p<0.005$ vs. vehicle. N=12-14

D

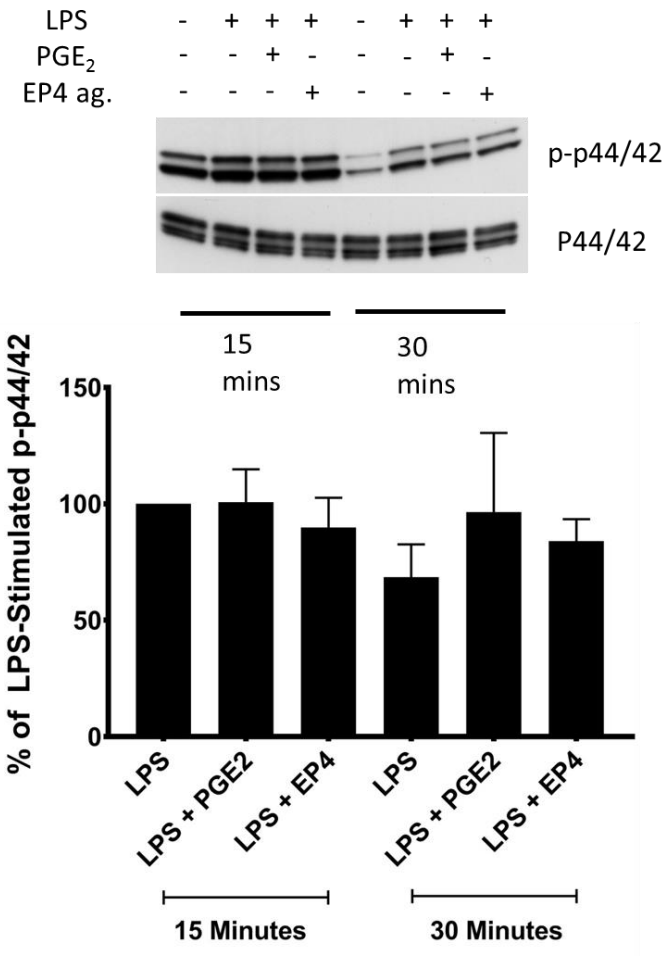

Figure 20 D: Representative p44/42 Western Blot Analysis. *Top panel.* Representative western blot analysis using antibodies against phosphorylated p44/42. AVF were pre-treated with PGE_2 (1 µM) and the EP4 agonist (1 µM) for 1 hour, followed by treatment with LPS (10 µg/ml) for 15 and 30 minutes. Data obtained were corrected to total p44/42. *bottom panel.* LPS stimulation at 15 mins was set to 100% and data were calculated as a percentage of the LPS stimulation. N=4.

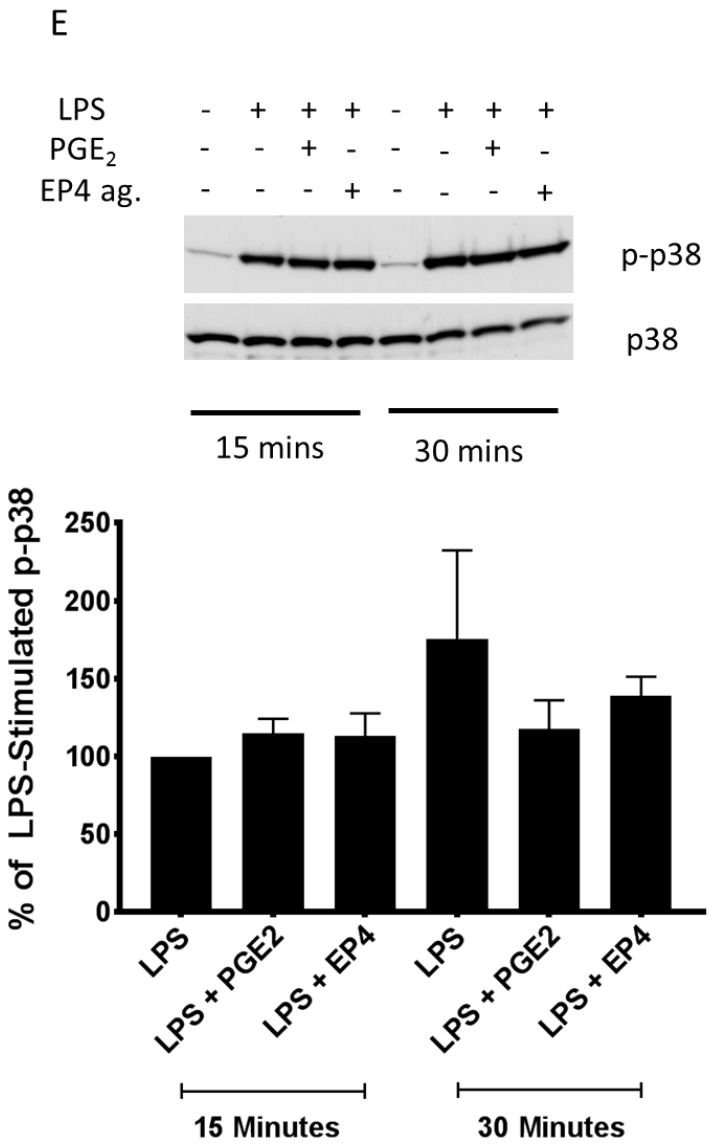

Figure 20 E: Representative p38 Western Blot Analysis. *Top panel.* Representative western blot analysis using antibodies against phosphorylated p38. AVF were pre-treated with PGE_2 (1 µM) and the EP4 agonist (1 µM) for 1 hour, followed by treatment with LPS (10 µg/ml) for 15 and 30 minutes. Data obtained were corrected to total p38. *Bottom panel.* LPS stimulation at 15 mins was set to 100% and data was calculated as a percentage of the LPS stimulation. N=4.

Inhibition of MCP-5 via PGE_2 and the EP4 Agonist is Independent of cAMP

One of the major downstream signaling pathways of the EP4 receptor is activation of adenylate cyclase and increased cAMP production. We sought to determine if PGE_2 or the EP4 agonist contributes to the reduction of LPS-induced MCP-5 production via this

pathway. Using ELISA, we found that LPS stimulation for 24 hours increased MCP-5 secretion (Figure 21 A). Importantly, when cells were pre-treated with dibutyryl cAMP (db cAMP), the cell permeable analogue of cAMP, there was no reduction of LPS-stimulated MCP-5 secretion (1.95 ± 0.17 in LPS + db cAMP vs. 2.29 ± 0.20 in LPS treated cells; p=0.190). Interestingly, db cAMP alone increased MCP-5 secretion (2.55 ± 0.35 vs. 1.00 ± 0.0 in vehicle treated cells; p=0.001). These data suggest that the inhibitory effect of the EP4 agonist is not occurring through cAMP production. Activation of the EP2 receptor is also linked to cAMP [408]. However, Figure 21 B shows that when we treated AVF with the EP2 agonist butaprost (500 nM), we observed no change in LPS-stimulated MCP-5 (2.89 ± 0.43 in LPS treated cells vs. 2.04 ± 0.18 in LPS + butaprost treated cells; ns). This data suggests that the inhibitory effect of PGE_2 is independent of EP2 signaling.

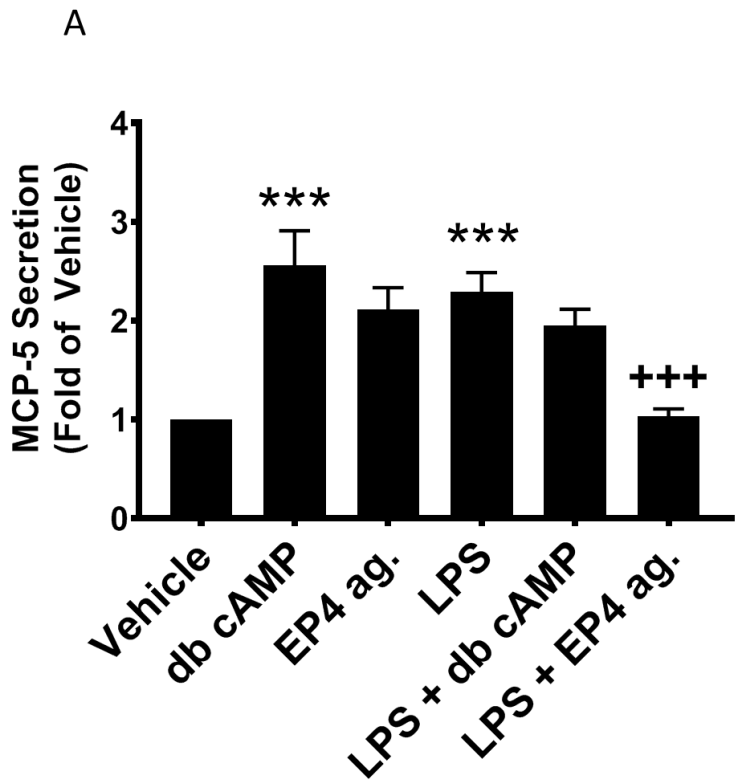

Figure 21 A: MCP-5 ELISA Analysis with Dibutyryl cAMP. AVF were pre-treated for 1 hour with the EP4 agonist (1 µM), or dibutyryl cAMP (db CAMP; 100 µM) followed by treatment with LPS (10 µg/ml) for 24 hours. All results were obtained as pg/ml and corrected for the amount of protein in each well. Data is presented as fold of vehicle treatment ± SEM. *** p<0.005 vs. vehicle. +++ p< 0.005 vs. LPS. N=10.

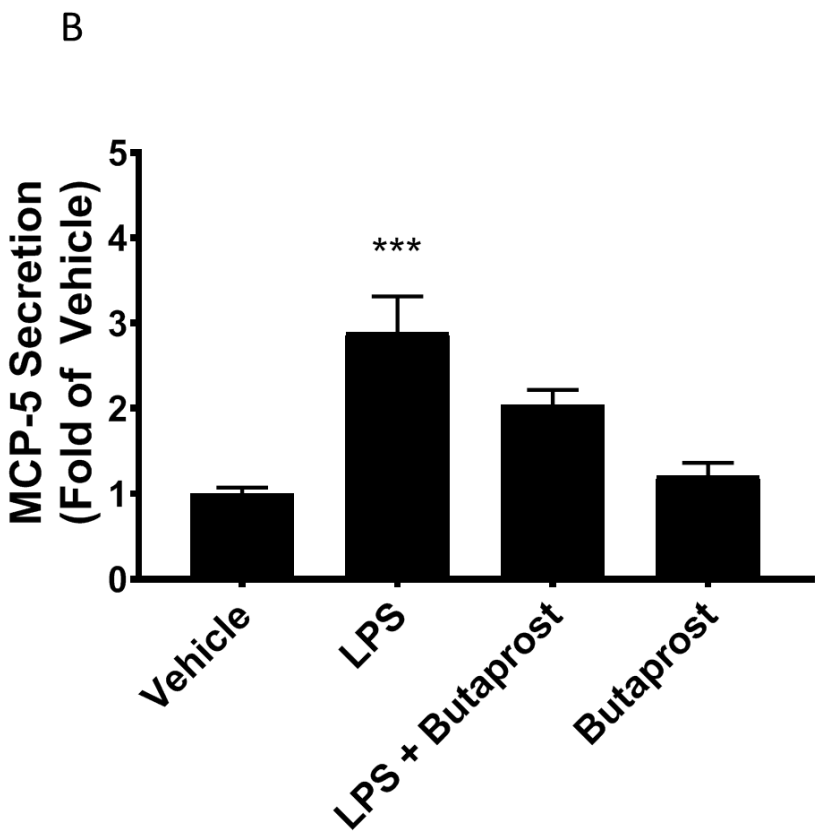

Figure 21 B: MCP-5 ELISA Analysis with Butaprost. AVF were pre-treated for 1 hour with the EP2 agonist butaprost (0.5 µM) followed by treatment with LPS (10 µg/ml) for 24 hours. All results were obtained as pg/ml and corrected for the amount of protein in each well. Data is presented as fold of vehicle treatment ± SEM. *** $p<0.005$ vs. vehicle. N=6-8.

Inhibition of MCP-5 via PGE_2 and an EP4 Agonist is Partly Dependent on the PI3K Pathway

PGE_2 via EP4 signaling can also activate the PI3K-Akt pathway [254]. We therefore investigated the effects of the PI3K inhibitor wortmannin on LPS-stimulated MCP-5 production. As expected, LPS increased MCP-5 secretion after 24 hours (Figure 22 A; 4.04 ± 0.98 in LPS treated cells vs. 1.00 ± 0.0 in vehicle treated cells; $p=0.037$), but pretreatment with wortmannin did not affect the ability of either PGE_2 or the EP4 agonist to reduce the LPS-stimulation of MCP-5 (0.96 ± 0.22 in LPS + PGE_2 + wortmannin vs. 4.04 ± 0.98 in LPS treated cells; $p=0.050$ and 1.74 ± 0.51 in LPS + EP4+ wortmannin vs.

4.04 ± 0.98 in LPS treated cells; p=0.019). In a separate experiment (Figure 22 B), we show that under basal conditions wortmannin had significant effect on MCP-5 secretion itself (0.60 ± 0.17 in wortmannin vs. 1.00 ± 0.0 in vehicle treated cells; p=0.043). Furthermore, the treatment with wortmannin significantly reduced MCP-5 secretion after LPS stimulation suggesting that the PI3K-Akt pathway itself plays a role in the inflammatory response to LPS (1.45 ± 0.19 in LPS + Wortmannin vs. 2.44 ± 0.44 in LPS treated cells; p=0.012).

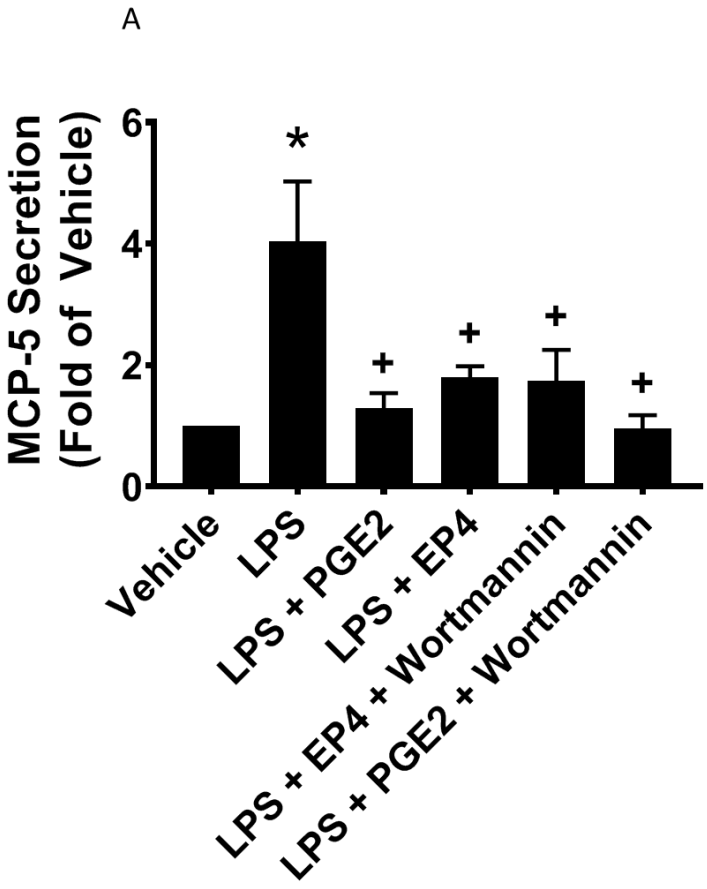

Figure 22 A: MCP-5 ELISA Analysis with Wortmannin. AVF were pre-treated for 1 hour with PGE_2 (1 µM), the EP4 agonist (1 µM), or the PI3K inhibitor, wortmannin (1 µM) followed by treatment with LPS (10 µg/ml) for 24 hours. All results were obtained as pg/ml and corrected for the amount of protein in each well. Data is presented as fold of vehicle treatment ± SEM. *p<0.05, *** p<0.005 vs. vehicle. + p<0.05, ++ p<0.01, +++ p< 0.005 vs. LPS. N=3.

B

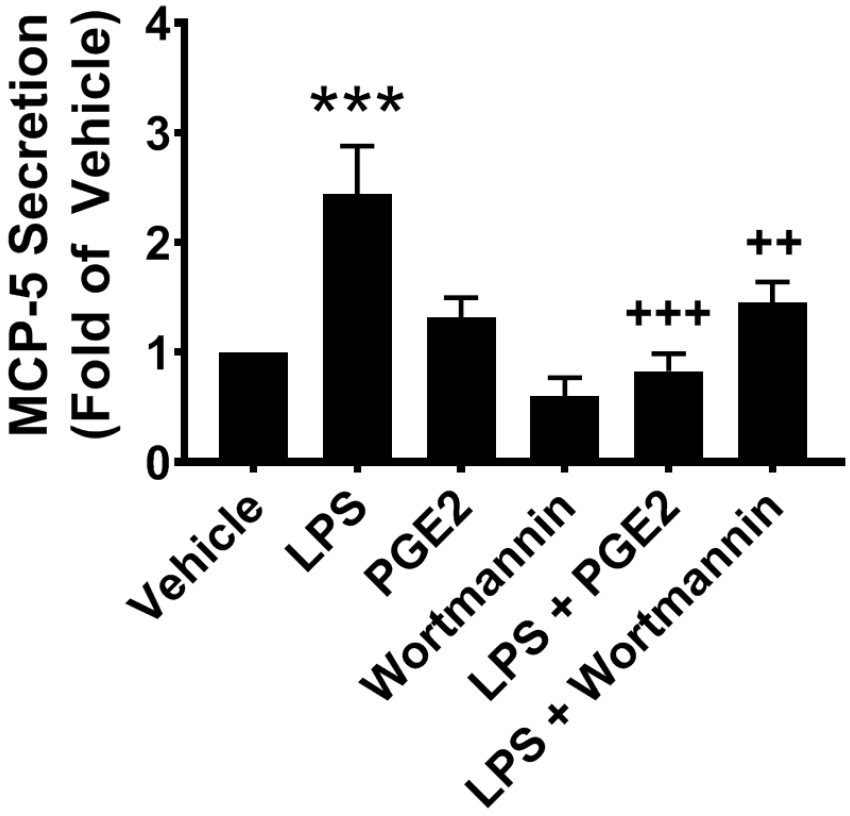

Figure 22 B: MCP-5 ELISA Analysis with wortmannin. AVF were pre-treated for 1 hour with PGE_2 (1 µM) or the PI3K inhibitor, wortmannin (1 µM) followed by treatment with LPS (10 µg/ml) for 24 hours. All results were obtained as pg/ml and corrected for the amount of protein in each well. Data are presented as fold of vehicle treatment ± SEM. *** $p<0.005$ vs. vehicle. ++ $p<0.01$, +++ $p< 0.005$ vs. LPS. N=6.

To confirm our findings, we repeated this experiment using a separate PI3K inhibitor, LY290042 (10 µM). Figure 22 C shows pre-treatment with LY290042 did not affect the ability of PGE_2 or the EP4 agonist to reduce LPS-stimulated MCP-5 (0.53 ± 0.09 in PGE_2 treated vs. 2.33 ± 0.24 in LPS treated cells; $p<0.005$ and 0.59 ± 0.13 in EP4 agonist treated vs. 2.33 ± 0.24 in LPS treated cells; $p<0.005$). However, LY290042 pre-treatment significantly reduced LPS-stimulated MCP-5 on its own (0.68 ± 0.13 vs. 2.33 ± 0.24 in LPS treated cells; $p<0.005$). To determine if PGE_2 and/or the EP4 agonist is acting

through the Akt pathway, we performed Western blot analysis of p-Akt. Figure 22 D shows that treatment with PGE_2 and the EP4 agonist had a significant reduction on LPS stimulation of p-Akt after 15 mins (36.80 ± 4.5 % in PGE_2 treated vs. 100 ± 0.0 % in LPS treated cells; $p<0.005$ and 47.40 ± 6.5 in EP4 agonist treated vs. 100 ± 0.0 % in LPS treated cells; $p< 0.005$). These data suggest that inhibition of the Akt pathway by PGE_2-EP4 signaling is at least partly responsible for the reduction in LPS-stimulated MCP-5.

C

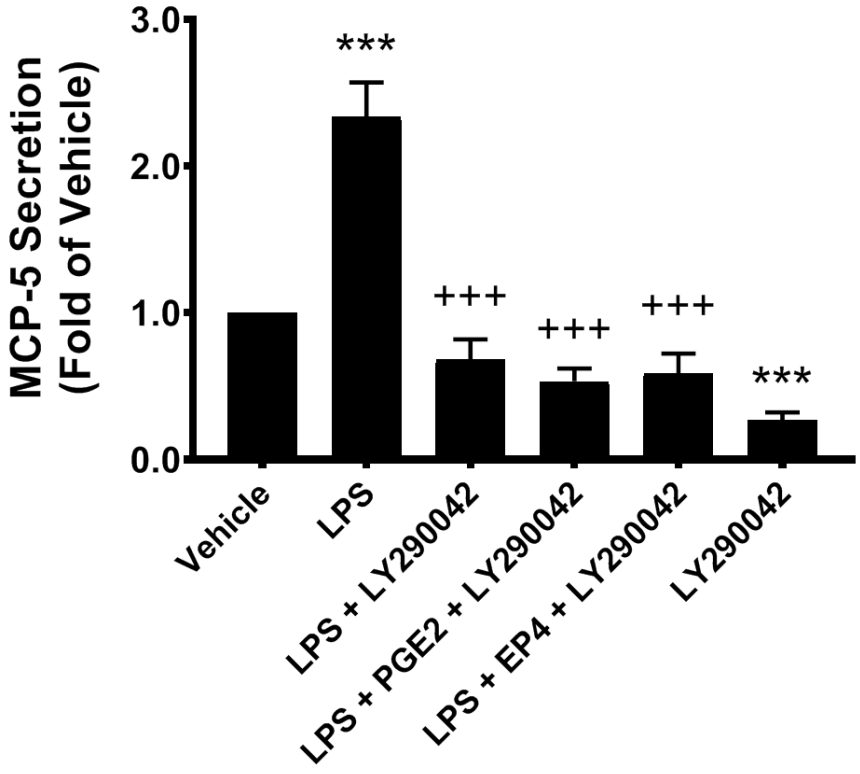

Figure 22 C: MCP-5 ELISA Analysis with LY290042. AVF were pre-treated for 1 hour with PGE_2 (1 µM), the EP4 agonist (1 µM), or the PI3K inhibitor, LY290042 (10 µM) followed by treatment with LPS (10 µg/ml) for 24 hours. All results were obtained as pg/ml and corrected for the amount of protein in each well. Data are presented as fold of vehicle treatment ± SEM. *** $p<0.005$ vs. vehicle, +++ $p< 0.005$ vs. LPS. N=3.

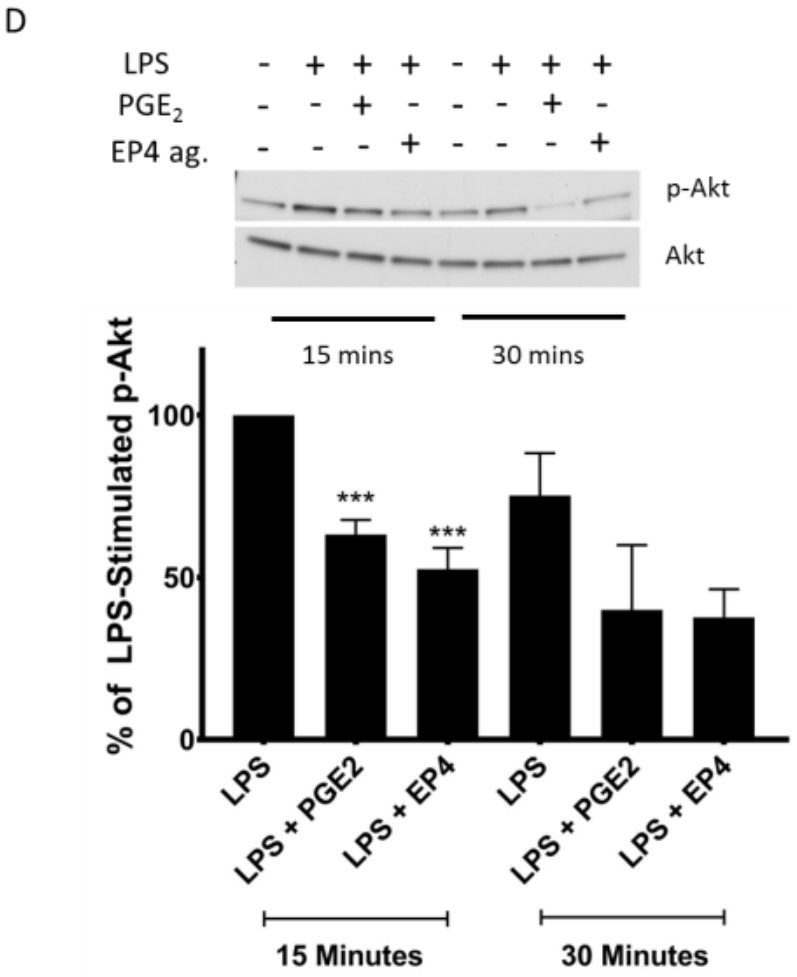

Figure 22 D: Representative AKT Western Blot Analysis. *Top panel.* Representative western blot analysis using antibodies against phosphorylated Akt. AVF were pre-treated with PGE_2 (1 µM) and the EP4 agonist (1 µM) for 1 hour, followed by treatment with LPS (10 µg/ml) for 15 and 30 minutes. Data obtained were corrected to total Akt. *Bottom panel.* LPS stimulation at 15 mins was set to 100% and data was calculated as a percentage of the LPS stimulation. ***p<0.005 vs. vehicle. N=3.

Discussion

The results of this study show, for the first time, that MCP-5 secretion induced by treatment with LPS, can be inhibited by PGE_2 and an EP4 receptor agonist in isolated adult mouse cardiac fibroblasts. We have recently published that overexpression of the EP4 receptor in the cardiomyocytes was protective in a model of myocardial infarction [10]. In addition to the direct protective effects on cardiac function, we observed reduced inflammation in the whole heart. We speculated that overexpression of EP4 in the

cardiomyocytes may have paracrine effects mediated by the cardiac fibroblasts. Our lab has data that show that the cardiac fibroblasts produce a much larger quantity of chemokines than the cardiomyocytes (unpublished data). Therefore, this study may provide some understanding of the anti-inflammatory effects we observed in the previous publication. In the present study, we hypothesized that PGE_2 inhibits LPS-induced MCP-5 secretion in adult mouse cardiac fibroblasts via its EP4 receptor (summarized in proposed scheme, Figure 23).

The results from our current study support our hypothesis, with significant reductions in LPS-stimulated MCP-5 secretion after treatment with either PGE_2 or an EP4 agonist. Treatment with an EP1, EP2 or an EP3 antagonist did not reverse the effect of PGE_2, suggesting that these receptors do not play a role in this process. Surprisingly, treatment with the EP4 antagonist, GW627368X also did not fully reverse the effects of PGE_2, suggesting another mechanism may be involved. These unexpected data cannot be due to sub-maximal blockade of EP4 as the EP4 antagonist reversed the effect of the EP4 agonist and further studies are necessary to elucidate how PGE_2 is acting, upstream of p-Akt and NF-κB. Nevertheless, the fact that both PGE_2 and an EP4 agonist reduce LPS-stimulation of MCP-5 suggests some involvement of this receptor. PGE_2 has been shown to have anti-inflammatory effects in cell types other than in the heart [11-15, 31] and it was shown in mouse macrophages to be exclusively via EP4 signaling [32]. Ngoc et al. examined PGE_2-EP4 signaling in a rat model of experimental autoimmune myocarditis (EAM) using an EP4 receptor agonist (EP4RAG). *In vivo* the authors determined that treatment with the EP4RAG significantly reduced infiltration of CD4+, but not CD8+ T cells in the left ventricle. Interestingly, the authors did not find a reduction in cytokine mRNA expression in the left ventricles of EAM rats treated with the EP4RAG.

They show however that *in vitro*, spleen cells treated with myosin to induce EAM exhibit higher levels of MCP-1 in the supernatant, which is reduced with EP4RAG treatment [12]. Our study also supports an anti-inflammatory role for the EP4 receptor, in cardiac fibroblasts, a novel finding. We also show that the transcription factor NF-κB plays an important role in regulating MCP-5, at least in response to LPS in cardiac fibroblasts. Furthermore, the inhibitory effect of both PGE_2 and the EP4 receptor appears to be through reduction of Akt signaling and inhibition of NF-κB translocation, determined by reduced phosphorylation of IκBα.

The p38 and p44/42 MAPKs have been shown previously to become activated by a wide variety of inflammatory signals [33]. Furthermore, it has been demonstrated that LPS induces the phosphorylation of p38 in monocytes and macrophages [34, 35]. We have been able to demonstrate in the current study that the endpoint of this signaling cascade, NF-κB activation, is reduced with exogenous PGE_2 and EP4 agonist treatment by using two separate and specific inhibitors of NF-κB activation (cardamonin, and IKK inhibitor III). However, we find no evidence to support a role for either p38 or p44/42 phosphorylation in the inhibitory effects of PGE_2 and the EP4 agonist on LPS-induced MCP-5 secretion.

Evidence in the literature suggests that some chemokines and cytokines are rapidly released upon stimulation from intracellular secretory compartments. Oynebraten and colleagues showed that several chemokines, including MCP-1, were secreted in this manner in human endothelial cells [36]. Additionally, Catalfamo et al. reported that the chemokine RANTES is stored in intracellular vesicles and secreted rapidly from human CD8+ T-cells [37]. To our knowledge, there has been no report of this mechanism in cardiac fibroblasts. Furthermore, our data in this study would disagree with their findings.

LPS stimulation only resulted in a significant increase in MCP-5 after 4 hours of treatment. Moreover, we observed changes in MCP-5 mRNA after 1 hr. of LPS stimulation, suggesting transcription is necessary. Evidence also suggests several cytokines are regulated at the post transcriptional level [38, 39]. However, we have shown in this study that the stability of the MCP-5 mRNA is not altered with exogenous PGE_2 treatment combined with LPS treatment. Together, these data would suggest that it is not a rapid release of MCP-5 via secretory vesicles. Instead, the data suggest that transcription of MCP-5 needs to take place.

cAMP is a well-known second messenger in the EP2 and EP4 signaling cascade [29]. Largo et al. showed that in human synovial fibroblasts, PGE_2 reduces MCP-1 production after IL-1β stimulation via its EP4 receptor [15]. Importantly, they show that this was due to production of cAMP, since the inhibitory effect on MCP-1 was reversed using a cAMP inhibitor. This is in contrast to our current data, which show that treatment with dibutyryl cAMP alone actually stimulated the production of MCP-5 significantly. Also, pre-treatment of the AVF with butaprost, the EP2 agonist, had no effect on LPS-stimulated MCP-5. Furthermore, the combination of LPS and dibutyryl cAMP had no inhibitory effect on MCP-5 production. Another study conducted by Takayama et al. utilized human macrophages and they showed that PGE2 inhibited the production of chemokines via the EP4 receptor after LPS stimulation [14]. Furthermore, in agreement with our data, they showed that this was independent of cAMP-PKA signaling, although the exact mechanism was unclear. Therefore, our current study may shed light on the mechanism by showing the involvement of reduced NF-κB activation. Minami and colleagues [40] showed that in LPS stimulated RAW264.7 cells, forced expression of an EP4 receptor-associated protein mitigated the pro-inflammatory response. Specifically,

they showed that the EP4 receptor-associated protein resulted in reduced NF-κB activation by directly interacting with the p105 subunit. This study differs from ours in that we show treatment with exogenous PGE_2 or EP4 agonist, reduces phosphorylated Akt and IκBα.

Studies in tissues other than the heart have also implicated the PI3K-Akt signaling pathway in playing an important role in regulating LPS-induced inflammation [41, 42]. Our data agrees with the literature in that treatment with the PI3K inhibitors, wortmannin or LY290042, reduced LPS-stimulated MCP-5. Furthermore, inhibition of the PI3K pathway did not affect the ability of PGE_2 or the EP4 agonist to reduce LPS-stimulated MCP-5, nor was there an additional inhibitory effect, suggesting they are signaling through the same pathway. Western blot analysis of p-Akt revealed that PGE2 and the EP4 agonist had a significant reduction of LPS-stimulated p-Akt after 15 mins. In contrast, treatment with the JNK inhibitor, SP600125, in combination with both PGE_2 and the EP4 agonist resulted in a further reduction in LPS-stimulated MCP-5. These data suggest that the JNK signaling pathway plays some role in regulating MCP-5 production. However, the inhibitory effect of PGE_2 and the EP4 agonist is occurring via a different pathway, presumably through Akt signaling.

Clinically, the use of an EP4 receptor agonist in the treatment of heart failure has merit as being a potential therapy. The use of an EP4 agonist has been tested clinically in healthy dogs [43, 44] and in humans [45] and was determined safe to use. However, the use of an EP4 agonist in humans under heart failure conditions has not yet been examined. We speculate that the use of an EP4 agonist in heart failure conditions may prove beneficial due to its anti-inflammatory properties and ability to reduce cytokines/chemokine production, potentially reducing chronic cardiac remodeling via

effects on fibroblasts. The process of cardiac remodeling post MI is of critical importance to the survival of patients clinically [46]. Cytokines and chemokines are produced rapidly following myocardial ischemia [47, 48] and not only have direct effects on cardiac contractility [49], but also have major effects chronically on extracellular matrix remodeling [50], integrin expression [51], and angiogenesis [52]. Since cardiac fibroblasts are the most abundant non-cardiomyocyte population in the heart, they contribute substantially to the activation of the inflammation cascade following MI [53]. Evidence from clinical studies suggest that patients with chronically elevated serum inflammatory biomarkers, like MCP-1, have increased mortality even without new coronary events [54]. Therefore, our study may help shed light on the mechanism of regulating chemokine production in the cardiac fibroblasts via PGE_2-EP4 signaling to mitigate adverse cardiac remodeling in clinical situations.

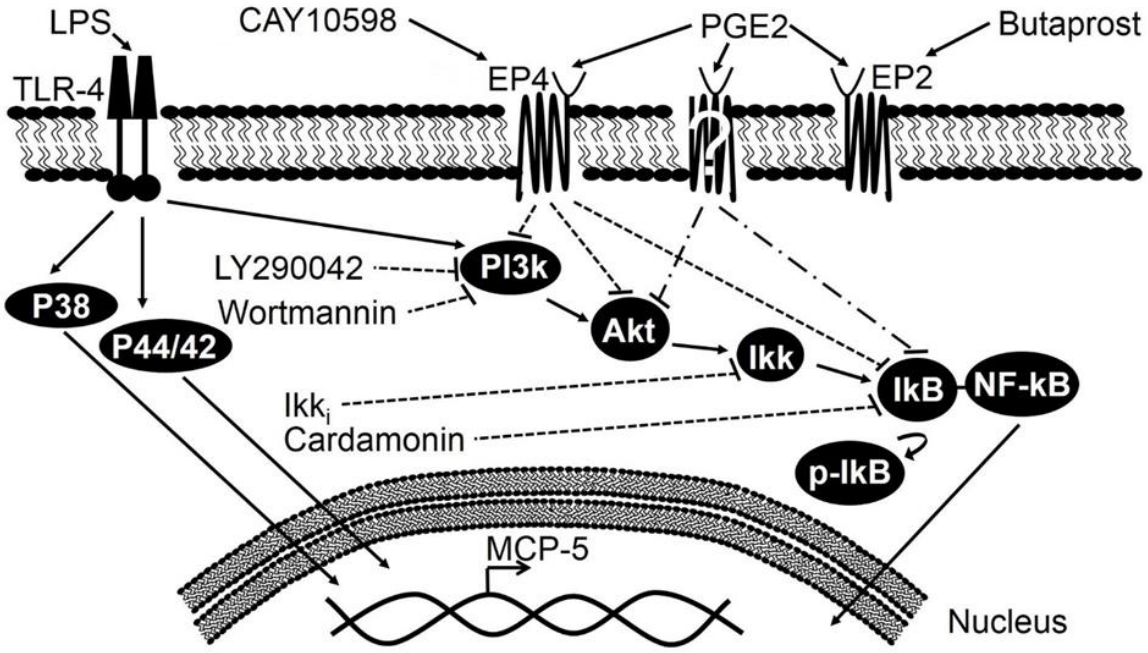

Figure 23: Scheme Depicting the Proposed Pathway of PGE_2 and EP4 Inhibition on LPS-induced MCP-5. Also shown are the various agonists and antagonists used in the study. Filled lines indicated activation, dashed lines indicate inhibition, dashed/dotted lines indicate inhibition via an unknown pathway.

CHAPTER 4 – CONDITIONED MEDIA FROM DAMAGED CARDIOMYOCYTES PROMOTES MCP-5-DEPENDENT MACROPHAGE MIGRATION

Introduction

Our lab has previously published that mice lacking the EP4 receptor in the cardiomyocytes (CM-EP4 KO) develop heart failure with a phenotype of dilated cardiomyopathy, reduced cardiac function after MI, and increased cellular infiltrate. We also reported that these mice have increased levels of cytokines/chemokines in their left ventricles, including MCP-5 [73]. MCP-5 is a potent chemoattractor for monocytes and macrophages. Although the increased cellular infiltrate in the CM-EP4 KO is of unknown origin, we hypothesize that the increased MCP-5 among other cytokines and chemokines, is responsible for this increase. In this chapter, we tested the hypothesis that MCP-5 is responsible for increased macrophage migration in the CM-EP4 KO heart. This hypothesis was tested *in vitro* using the Boyden migration assay.

Methods

Animal Use

Male C57BL/6, CM-EP4 KO, and EP4 WT mouse cardiomyocytes were isolated as previously described [73]. All studies involving the use of animals were approved by the animal care and use committee (IACUC) at Henry Ford Hospital, in accordance with Federal Guidelines.

Cardiomyocyte Treatment

To generate conditioned media from the CM-EP4 KO mice, cardiomyocytes were isolated from 31-36 wk. old mice, plated for 1 hour in MEM containing serum (10 % FBS) and then starved in serum free media (MEM) for an additional hour. As a control, cardiomyocytes from age-matched EP4 WT littermates were plated and incubated for the

same amount of time. For all plates, media were collected after 1 hour of serum starvation, snap frozen in liquid nitrogen, and stored at -80^{o}C until future macrophage migration assay analysis. In another set of treatments, cardiomyocytes were isolated from CM-EP4 KO and EP4 WT littermate mice and were then treated with or without 100 µM H_2O_2 for 90 minutes. The media were collected from all plates, snap frozen in liquid nitrogen, and stored at -80^{o}C until future macrophage migration assay analysis.

In a third set of experiments, cardiomyocytes were isolated from CM-EP4 KO mice and plated for 1 hour in MEM containing serum, prior to being serum starved for 1 hour. After 1 hour of serum starvation, media were collected and snap frozen in liquid nitrogen and stored at -80^{o}C. The media were thawed and incubated with either an IgG control, or a neutralizing antibody to MCP-5 (R&D Systems, Cat No. MAB428) at a concentration of 17.5 ng/ml. This concentration is 25 times more concentrated than what is needed to specifically neutralize MCP-5 at the amount secreted by cardiomyocytes. Anti MCP-5 or the IgG control was incubated for 30 minutes at 37^{o}C with the media samples. The media were then used in a macrophage migration assay.

In a fourth set of experiments to address the effect of H_2O_2 alone, cardiomyocytes were isolated from 10-12 wk. old C57BL/6 mice, plated for 1 hour, then serum starved for an additional hour. As a control, media were placed in dishes in the absence of cells. Next, all dishes were treated with or without 100 µM H_2O_2. After 90 minutes, media were collected and snap frozen in liquid nitrogen and stored at -80^{o}C until macrophage migration assay was performed.

Macrophage Migration Assay

For macrophage migration experiments, the porous membrane of a Boyden migration chamber (Figure 24) was first coated with 0.5 % BSA in PBS overnight. On the

day of the experiment, BSA was removed and RAW 264.7 macrophages (0.3-0.6 x 10^6 cells) were plated on the membranes of a 24-well Boyden chamber plate. Next, either conditioned or non-conditioned media were plated in the bottom of each well and the macrophages were allowed to migrate for 4 hours at 37^{o}C, 5 % CO_2, before being stained and imaged. Membranes were stained by first rinsing the wells with cold PBS and using a sterile cotton tip to remove any non-migrating cells from the top of the membrane. Next, the cells were fixed by adding methanol to the top and bottom chambers and incubating at room temperature for 10 minutes. Membranes were then rinsed with water and stained with hematoxylin for 6 minutes at room temperature. Membranes were once again rinsed with water and then the chambers were filled with water and visualized on an inverted light microscope under the 20X objective. The number of migrating macrophages from four different fields per membrane was counted by an observer who was blind to the treatment protocol.

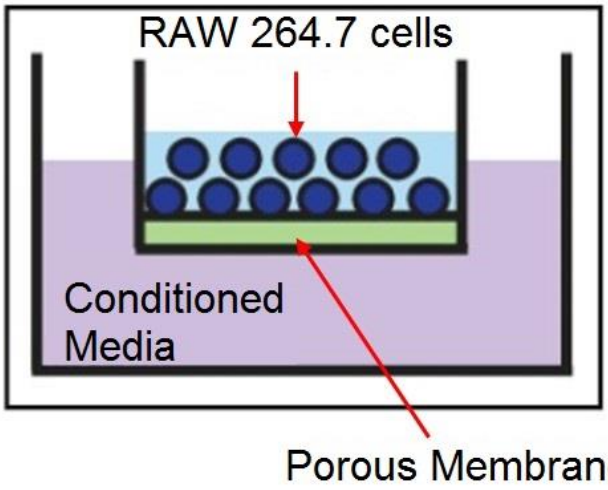

Figure 24: Scheme Depicting the Boyden Macrophage Migration Plate Setup. The Boyden chamber is inserted inside a well filled with conditioned or non-conditioned media. RAW 264.7 macrophages are plated on top of the porous membrane containing 0.5 µm pores and allowed to migrate for 4 hours. After, the membrane is rinsed, removed, and stained with hematoxylin to visualize the migrating macrophages. Image adapted from CliniSciences website [409].

Results

Damaged Cardiomyocytes Promote Macrophage Migration

Since the CM-EP4 KO mice have increased cytokines/chemokines, like MCP-5, in their left ventricles, we investigated the effect of media taken from these cardiomyocytes under basal and damaged conditions on macrophage migration using the Boyden migration assay. Figure 25 shows a representative image of the stained porous membrane. Arrows indicate examples of cells that were migrating and included in

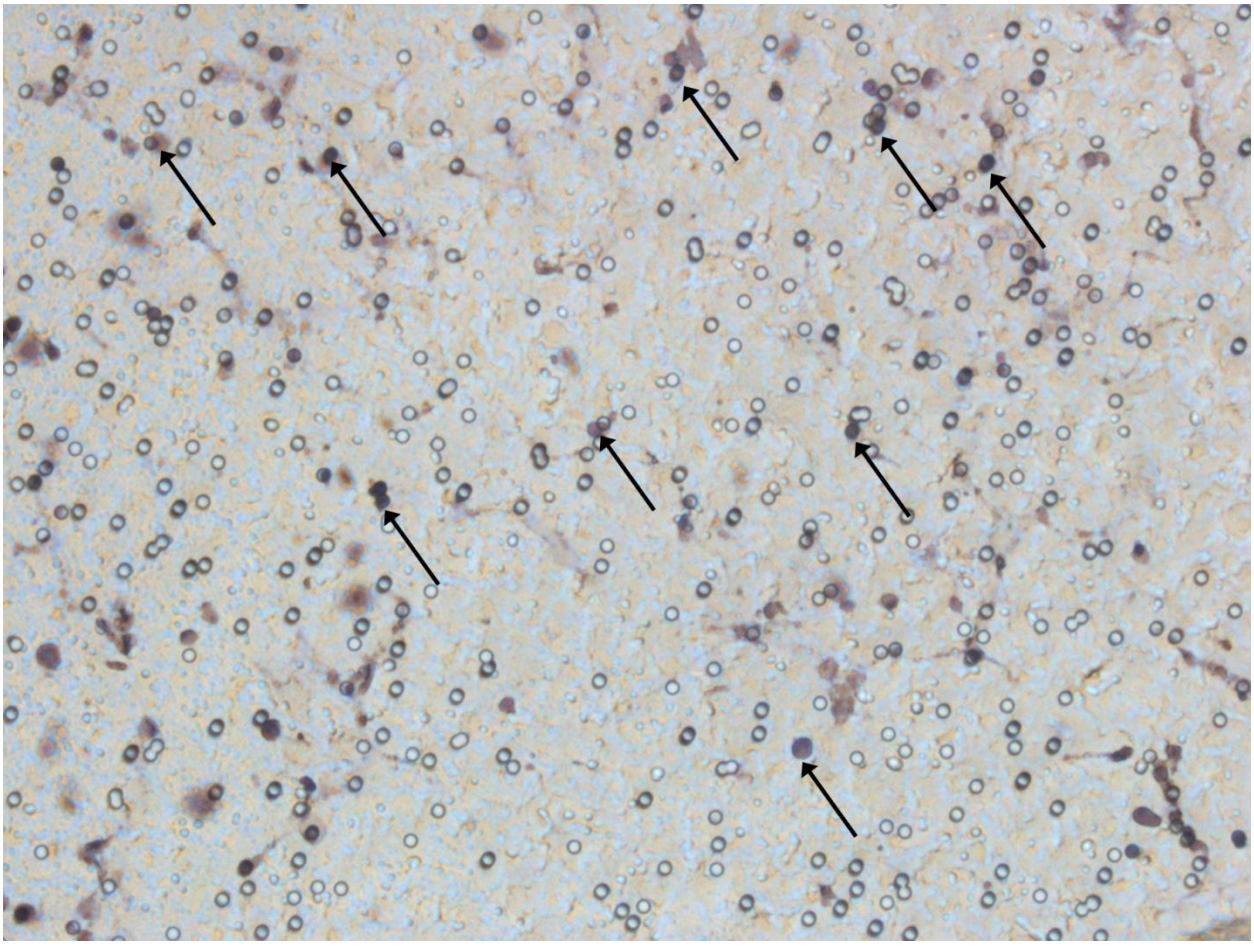

Figure 25: Representative Image of Migrated Macrophages. 20X image of a Boyden migration membrane. Empty white circles are the 0.5 µm pores within the membrane. The black arrows are a representation of some of the pores positive with hematoxylin stain where macrophages are migrating through. The number of migrating macrophages were counted by a blinded observer from four different fields per membrane and averaged.

analysis. Figure 26 shows that the conditioned media taken from EP4 WT cardiomyocytes treated with H_2O_2 resulted in a significant increase in the number of macrophages that migrated (162.7 ± 14.1 in EP4 WT vs. 240.2 ± 21.9 in EP4 WT + H_2O_2; $p<0.01$). Conditioned media taken from the CM-EP4 KO cardiomyocytes significantly increased macrophage migration under baseline conditions suggesting that these cardiomyocytes are already damaged/injured and releasing some factor(s) that promote the migration of macrophages (162.7 ± 14.1 in EP4 WT vs. 204.8 ± 9.2 in CM-EP4 KO; $p<0.05$). Interestingly, when these cells were treated with H_2O_2, the increase in macrophage migration did not exceed that of the wild type mice (240.2 ± 21.9 in EP4 WT + H_2O_2 vs. 204.8 ± 9.2 in CM-EP4 KO; p=ns).

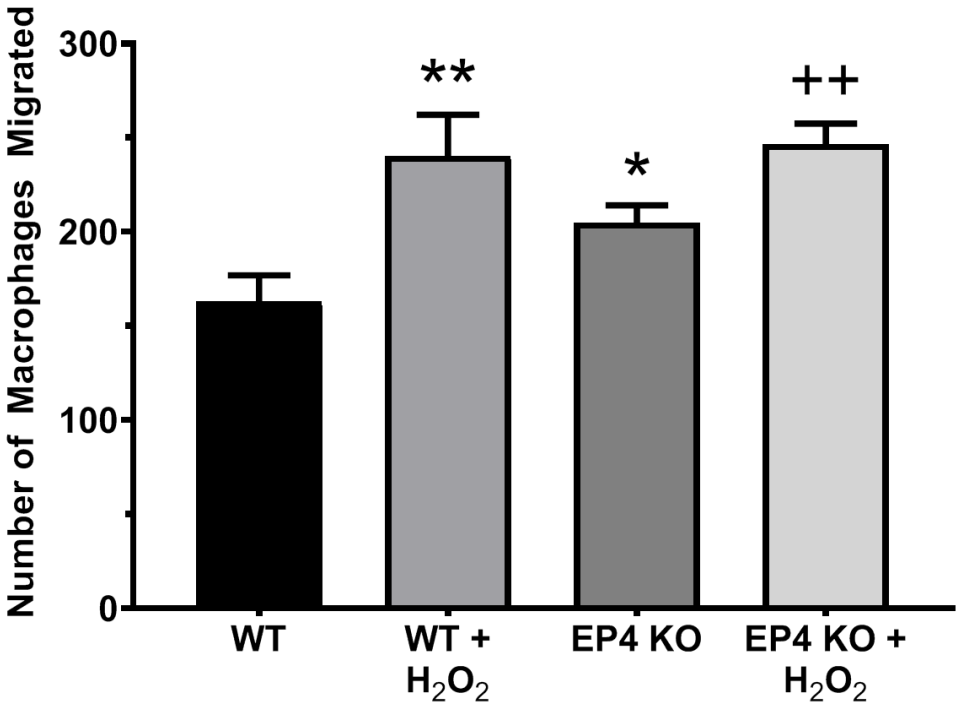

Figure 26: Macrophage Migration with CM-EP4 KO Cardiomyocytes. Macrophages were plated on a Boyden migration chamber and allowed to migrate for 4 hours through the porous membrane with either conditioned (media from H_2O_2 cells) or non-conditioned media plated in the bottom of the chamber. The number of macrophages that migrated were counted using a 20X objective on an inverted light microscope. * $p<0.05$, ** $p<0.01$ vs. EP4 WT. ++ $p<0.01$ vs. EP4 KO. N=4.

Macrophage Migration Due to Damaged Cardiomyocytes Appears to Be MCP-5 Dependent

MCP-5 is a potent chemoattractor for monocytes and macrophages. Since MCP-5 was significantly upregulated in the CM-EP4 KO mouse hearts, we investigated if MCP-5 was responsible for the increase in macrophage migration that was observed under basal conditions using CM-EP4 KO conditioned media. To test this, conditioned media from CM-EP4 KO cardiomyocytes were incubated in the presence or absence of a neutralizing antibody to MCP-5. These media were then used in a macrophage migration experiment. Figure 27 shows that there was a substantial reduction in the number of macrophages migrated when the media were treated with the neutralizing antibody (313.3 ± 72.1 in IgG treated media vs. 187.2 ± 46.7 in anti MCP-5 treated media; $p<0.05$). These data indicate that MCP-5 is an important factor released from the CM-EP4 KO cardiomyocytes to promote macrophage migration.

Figure 27: Macrophage Migration with MCP-5 Neutralizing Antibody. Conditioned media were obtained from CM-EP4 KO mice and incubated with either IgG control or 17.5 ng/ml of a neutralizing antibody to MCP-5 (anti MCP-5). Macrophages were allowed to migrate for 4 hours. The number of macrophages that migrated were counted using a 20X objective on an inverted light microscope. * $p<0.05$ vs. IgG control. N=5.

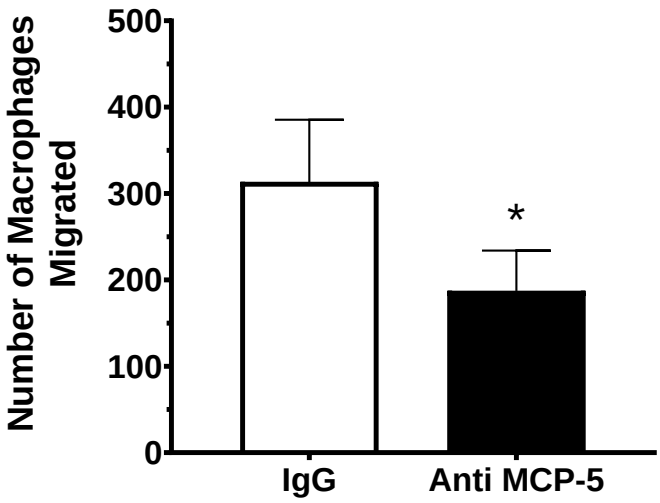

H_2O_2 Alone Significantly Stimulates Macrophage Migration

As a control experiment, we investigated the chemoattractant effect of H_2O_2 alone on macrophage migration. To test this, cardiomyocytes from C57BL/6 mice were treated with or without H_2O_2 as already described (conditioned). As a control, cell culture dishes

lacking any plated cells were treated with or without H_2O_2 (non-conditioned). The media were then collected and used in a macrophage migration assay. Figure 28 shows that in the non-conditioned media, treatment with H_2O_2 significantly increased macrophage migration in the absence of any cellular stimuli (186.6 ± 11.8 in vehicle vs. 265.9 ± 4.0 in H_2O_2 treated; $p<0.005$). However, this increase was less than the increase observed in the conditioned media group, confirming a role for released cellular factors, like MCP-5 (322.3 ± 7.1 in vehicle vs. 415.9 ± 4.9 in H_2O_2 treated).

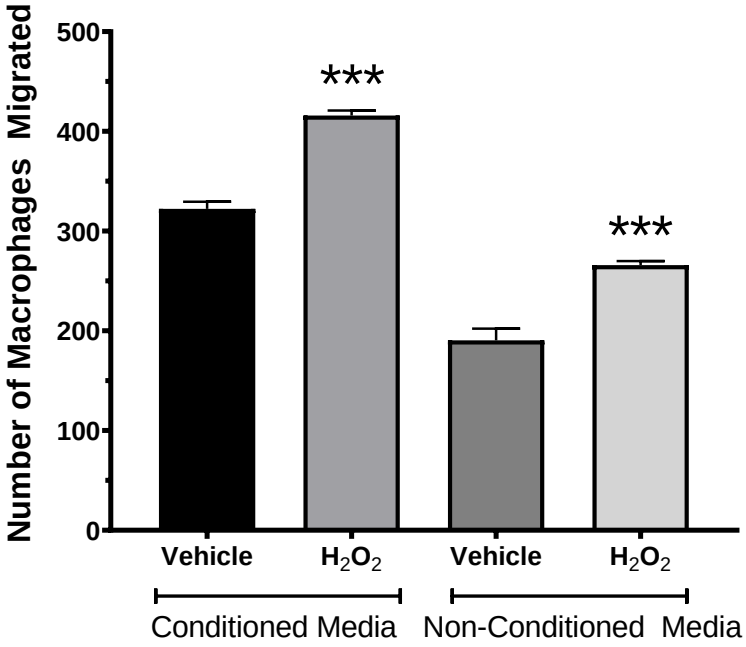

Figure 28: Macrophage migration with H_2O_2 Treatment. Media taken from cardiomyocytes treated with or without H_2O_2 (conditioned media), or media taken from media alone treated with or without H_2O_2 were used in a macrophage migration assay. Macrophages were allowed to migrate for 4 hours. The number of macrophages that migrated was counted using a 20X objective on an inverted light microscope. *** $p<0.005$ vs. respective vehicle control. N=3.

Discussion

MCP-1 has been shown to play a major role in inflammation in cardiovascular diseases, by increasing in the myocardium during the early phase of MI for example [410, 411]. MCP-1 deletion or inhibition of MCP-1 prevents adverse post-MI remodeling [390] and MCP-1 levels are increased in patients with HF [412].

The presence of oxidative stress in all phases of heart failure has been shown in animals and humans [413-415]. Reactive oxygen species (ROS) like H_2O_2 can be produced in the heart by several different sources: NADPH oxidases, xanthine oxidase,

lipoxygenases, cyclooxygenases, peroxidase, mitochondrial respiration, cytochrome P-450, nitric oxide synthase. ROS is detrimental by acting directly with lipids within membranes, proteins, and nucleic acids, resulting in death via apoptosis and necrosis. Additionally, ROS can trigger inflammation by acting as a signaling molecule.

MCP-5, the murine analogue of human MCP-1 is a potent chemoattractant for monocytes and macrophages. We hypothesized that the increased expression of MCP-5 in the CM-EP4 KO mouse heart was responsible for the increased interstitial cellular infiltrate. Although the work in this chapter is *in vitro*, it highlights the importance of MCP-5 as a chemoattractant molecule. Treatment with a neutralizing antibody to MCP-5 reduced macrophage migration by 40 % in CM-EP4 KO cells under baseline conditions. This result was surprising, although reproducible. It was not expected that a neutralizing antibody against one chemokine would have such a large effect. Nonetheless, the CM-EP4 KO cardiomyocytes appear to be releasing a factor(s) that increase macrophage migration even under basal conditions. Furthermore, treatment with H_2O_2 on these cells only increased macrophage migration to the same magnitude as wild type, suggesting the CM-EP4 KO cells are already damaged, potentially caused by oxidative stress.

CHAPTER 5 – THE DELETERIOUS ROLE OF THE PROSTAGLANDIN E2 EP3 RECEPTOR IN ANG II HYPERTENSION

Introduction

Angiotensin II

Angiotensin II (Ang II) is the major effector peptide of the renin-angiotensin system (RAS) [416]. Ang II plays an important role in both blood pressure regulation and inflammation, along with other functions (i.e., regulating cell growth and apoptosis, extracellular matrix deposition, cell migration, vascular motor tone.). As shown in Figures 3 and 4, Ang II is released from circulating hepatic-derived angiotensinogen via the actions of renal-derived renin and ACE [38-40]. Ang II is a potent vasoconstrictor, causing an increase in blood pressure, and vasculature remodeling in chronic hypertension (HTN) [417]. Ang II also promotes increased vascular permeability leading to increased inflammatory processes [305, 418, 419]. The various actions of Ang II are mediated by specific intracellular signaling pathways downstream of Ang II binding to its surface receptors. In mammals, Ang II binds to two G protein-coupled receptors; AT_1 and AT_2 [420, 421]. The AT_1 receptor typically activates phospholipase C through the Gq protein. AT_1 is highly expressed in smooth muscle cells, while AT_2 receptors are present in the kidneys, pancreas, heart, adrenals, brain, and vasculature [62, 63, 422]. Both receptors signal via complex intracellular signaling cascades, although, it is the consensus that AT_2 antagonizes the effects of AT_1 [55, 423].

Angiotensin II in Cardiovascular Disease

Ang II plays a critical role in cardiovascular disease [48]. It has been shown that Ang II promotes pathological cardiac hypertrophy in both neonatal rat cardiomyocytes [151, 424-426] and in adult cardiomyocytes [50, 427, 428]. Cardiomyocytes express both

AT_1 and AT_2 receptors, although there is an abundance of evidence to support that Ang II primarily signals through AT_1 in the cardiomyocytes [429, 430]. Ang II can also act on cardiac fibroblasts in the heart, increasing extracellular matrix proteins and collagen deposition; an important factor in pathological left ventricle remodeling. This effect of Ang II is also driven by activation of AT_1 receptors, as AT_2 receptors are undetectable in both neonatal and adult rat cardiac fibroblasts [431, 432].

Inflammation and Oxidative Stress in ANG II HTN

In recent years, links between the immune system and hypertension have been described [433, 434]. In various cell types and tissues, Ang II can directly activate immune cells (i.e., chemotaxis and differentiation) [435], promote the transcription of pro-inflammatory mediators (i.e. chemokines and cytokines) [312, 418], and activate pro-inflammatory signaling pathways (i.e. NF-κB and MAPK) [321, 322]. It has been reported that Ang II promotes the production of ROS through stimulation of NADPH oxidase, via signaling through the AT_1 receptor [436, 437]. This increase in oxidative stress promotes further endothelial dysfunction and vascular inflammation and contributes to increased activity of transcription factors like NF-κB combined with increases in chemokines, cytokines, and adhesion molecules [52, 438].

Prostaglandin E_2

Prostaglandin E2 (PGE_2) is produced by three known prostaglandin E synthase isoforms; a cytosolic form (cPGES) and two microsomal forms (mPGES-1 and mPGES-2), which are membrane bound. PGE_2 signals through 4 distinct G-protein coupled receptor sub-types (EP1, EP2, EP3 and EP4) to produce a variety of physiological and pathological effects. EP2 and EP4 increase cAMP levels in the cell via activation of adenylate cyclase, whereas EP3 inhibits cAMP production, and EP1 increases

Ca^{2+} levels in the cell. However, the cardiac effects of these receptors have not been fully elucidated. We have previously published that mPGES-1 null mice were more susceptible to the deleterious effects of chronic Ang II infusion on the heart [218], suggesting a cardioprotective role for PGE_2. Also, we previously published that PGE_2 via its EP3 receptor could reduce contractility of isolated myocytes and in the whole heart by mechanisms that appeared to involve decreased phospholamban phosphorylation [217]. Thus, we hypothesize that the relative abundance of EP3 and EP4 receptors is a crucial determinant of end organ damage in the diseased heart. Furthermore, we hypothesize that overexpression of EP3 is detrimental to cardiac function and promotes inflammation, while inhibition of the EP3 receptor is protective in an Ang II HTN model.

Methods

Animal Use

For experimental protocols 1 and 3 (experimental protocol section below), male 10-12 wks. old C57Bl/6 mice were purchased from Jackson labs. For protocol 2, male EP3 transgenic (Tg) and EP3 WT mice were kindly provided to the Harding Lab from Dr. Hohlfield at the University of Dusseldorf in Germany. All animal experiments were approved by the Henry Ford Health System Institutional Animal Care and Use Committee in accordance with federal guidelines.

Experimental Protocol

1. *Effect of an EP3 agonist on Ang II HTN:* Male 10-12 weeks old C57BL/6 were treated with either vehicle (0.01 M acetic acid in 0.9 % NaCl) or Ang II (1.4 mg x kg^{-1} x day^{-1}) for a period of 2 weeks. Additionally, mice were treated with either vehicle (ethanol diluted in 0.9 % NaCl) or an EP3 agonist (sulprostone; 80 µg/kg/day i.p.) daily. The dose of sulprostone was chosen based on Ki = 0.35 nM

for human recombinant EP3.

2. *Effect of EP3 overexpression on Ang II HTN:* Male 10-12 weeks old EP3 Tg mice overexpressing EP3 in the cardiomyocytes and their wild type littermates (EP3 WT) were treated with either vehicle (0.01 M acetic acid in 0.9 % NaCl) or Ang II (1.4 mg x kg^{-1} x day^{-1}) for a period of 2 weeks.
3. *Effect of an EP3 antagonist on Ang II HTN and Isoproterenol model:* Male 10-12 weeks old C57BL/6 mice were treated with either vehicle or Ang II (1.4 mg x kg^{-1} x day^{-1}) for a period of 2 weeks. Additionally, mice were treated with either vehicle (ethanol diluted in 0.9 % NaCl) or an EP3 antagonist (L798, 106; 40 µg/kg/day i.p.) daily. The dose of L798, 106 was chosen based on Ki = 0.3 nM for EP3 and 916 nM for EP4. In separate experiments mice received 10 days of isoproterenol infusion (30 mg x kg^{-1} x day^{-1}) or vehicle (0.9 % NaCl). Mice were also treated with either vehicle or an EP3 antagonist (L798, 106; 40 µg/kg/day i.p.) daily or the EP3 antagonist (L798, 106; 40 µg/kg/day).

For all experiments, echocardiography was performed on conscious animals before surgery and at the end of the study. Blood pressure was monitored on a weekly basis to ensure that all animals receiving Ang II exhibited the expected increase in systolic blood pressure. At the end of the study, animals were anesthetized with pentobarbital sodium (100 mg/kg i.p.), and the heart was injected with 15% potassium chloride, causing arrest in diastole. The heart was excised and washed thoroughly in ice-cold Hanks Buffered Salt Solution, followed by dissection of the atria and right ventricle. If hearts were used for RNA isolation and PCR, they were stored in Trireagent (Molecular Research Center, Cincinnati, OH) at −80°C. For histological analysis, hearts were frozen in OCT media prechilled in isopentane and stored at −80°C. For protein extraction, pieces of heart

were snap-frozen in liquid N_2 and stored at −80°C.

Blood Pressure Measurements

Systolic blood pressure was measured on a weekly basis using the tail cuff method. Pressure was obtained using a MC 4000 blood pressure analysis system for mice (Hatteras Instruments, Cary, NC). Briefly, mice were trained for at least 1 week before analysis. They were maintained at 38–40°C and subjected to 10 cycles of blood pressure analysis. At least seven good readings in a cycle of 10 measurements were needed to accept the measurements. In addition, a minimum systolic value of >75 mmHg was implemented as an exclusion criterion.

Echocardiography

Echocardiography was performed on conscious animals before surgery and at 2 weeks post-infusion. The cardiac function of all mice was assessed by echocardiography using an Acuson 256 system (Mountain View, CA) with a 15-MHz linear transducer, as reported previously [219, 267]. All echocardiography assessment was performed on conscious mice. Diastolic measurements were made at the maximum left ventricle cavity dimension, whereas systolic parameters were measured during maximum anterior motion of the posterior wall. All echocardiography was performed by the same investigator who was blinded to the genotype. Additionally, all mice were trained for 2-3 days prior to assessment.

Implantation of Osmotic Mini Pumps

Osmotic mini pumps contained Ang II, isoproterenol, or vehicle solution. Ang II was dissolved in 0.01 M acetic acid diluted in 0.9 % NaCl saline and given at a dose of 1.4 mg x kg^{-1} x day^{-1} s.c. [218]. Control mice for these experiments received vehicle (0.01 M acetic acid diluted in physiological 0.9 % saline). Isoproterenol was dissolved in 0.9 %

NaCl and administered at a dose of 30 mg x kg^{-1} x day^{-1} s.c. Control mice for the isoproterenol experiments received 0.9 % NaCl. Mice at 10–12 weeks of age were anesthetized with sodium pentobarbital (10 mg/kg), and osmotic minipumps were implanted under the skin. Mice were allowed to recover on a heated pad followed by administration of buprenorphine as an analgesic (0.05 mg/kg).

Histology

Mouse hearts were harvested and sectioned transversely into three slices from apex to base (sections A–C). The sections were frozen in pre-chilled isopentane and stored at −80°C for determination of interstitial collagen fraction and myocyte cross-sectional area (MCSA). For MCSA, sections of the heart were double-stained with fluorescein-labeled peanut agglutinin to delineate the myocytes and rhodamine-labeled Griffonia simplicifolia lectin I to outline the capillaries. Four radially oriented microscope fields were selected from each section and photographed under the 20 × objective. MCSA was measured by computer-based planimetry (NIH Image J) and averaged across all four fields of the sections. Photographs of five randomly chosen fields per section were taken under the ×20 objective, and the percentage of collagen staining per field was measured using Image J software. The mean percentage was then calculated for each animal. All assessments were performed by observers that were blinded to animal identification and treatment groups.

Myocyte Cross Sectional Area (MCSA)

This methodology is described in detail on pg. 38 of this dissertation. Briefly, frozen left ventricle sections were stained with fluorescein-labeled peanut agglutinin to delineate the myocytes. Four radially orientated microscopic fields were obtained under 20X objective. The size of the myocytes was averaged across fields. All image analysis was

performed by a blinded observer.

Immunohistochemistry of Macrophages and T Cells

The number of macrophages and T cells were assessed using $CD68^+$ staining (rat anti-$CD68^+$ antibody, BioRad) and $CD3^+$ staining (rabbit-anti $CD3^+$ antibody, Abcam) respectively, on frozen heart sections as we previously described [216]. Briefly, frozen sections were fixed in acetone for 10 min, followed by incubation with fresh 0.3% hydrogen peroxide for 30 min. Sections were then blocked in 5% centrifuged milk in TBS and incubated with either anti-$CD68^+$ or anti-$CD3^+$ overnight at 4 °C. Biotinylated secondary antibodies were placed onto sections for 1 h at room temperature. Sections were then incubated with horseradish peroxidase reagent for 40 min at room temperature and then visualized by AEC single solution (Vector laboratories; Burlingame, CA). Slides were rinsed in tap water and then counterstained with Harris' hematoxylin solution for 1 min, then rinsed again in tap water and mounted onto slides using Aquamount (Lerner laboratories). Negative controls consisted of sections incubated in the absence of primary antibody. Photographs of four randomly-chosen fields per section were taken under the multiple objectives and the number of positively-stained cells were counted by a blinded observer. The number of cells per mm^2 was measured by a blinded observer using Image J software

Real time RT-PCR

Measurement of MCP-5 mRNA expression was performed by real-time RT-PCR using a SYBR green method as follows. 2 µg of DNase I-treated RNA sample was reverse transcribed using random primers and Omniscript reverse transcriptase kit (Qiagen). 2 µL of the reverse transcription reaction was amplified in a Roche version 2.0 light cycler PCR machine (Roche; Indianapolis, IN) using SYBR green dye and specific primers against

MCP-5, IL-1β, TNF-α, IL-10, and Arg-1 were used. Primer sequences are in Table 4.

Table 4: Primer Sequences

Gene	Sense	Anti-Sense
MCP-5	5'-caagagratcaccagcagcagg-3'	5'- tgcttgaggtggttgtggaa-3'
GAPDH	5'-caaggtcatcccagagctg-3'	5'-tgtcatcatacttggcaggtt-3'
IL-1β	Qiagen, NM_008361	
TNF-α	Qiagen, NM_013693.3	
IL-10	5'-gctgcctgctcttactgact-3'	5'-ctgggaagtgggtgcagtta-3'
Arg-1	5'-gaacacggcagtggctttaac-3'	5'-tgcttagctctgtctgctttgc-3'

Primers from Qiagen are proprietary and only the Refseq number is provided.

Western Blot Analysis

RhoA (1:1000), RhoB (1:1000), Nox2 (1:1000), and GAPDH (1:2000) were measured by western blot using a method previously described by us [217]. All results were corrected to GAPDH and expressed as fold of vehicle or EP3 WT. All antibodies were from Cell Signaling (Danvers, MA).

Chemicals

EP3 agonist (Sulprostone) and prostaglandin E_2 were from Cayman Chemical (Ann Arbor, MI). EP3 antagonist (L798, 106) was from Tocris Bioscience (Minneapolis, MN). Angiotensin II was from Bachem (Torrance, CA). Tri-reagent was from Molecular Research Center. All other compounds were obtained from Sigma Aldrich.

Statistical Analysis

Statistical analysis was performed by a statistician in the Department of Public Health Sciences of Henry Ford Hospital using the statistical package SAS Version 9.4. For all tests, a two-sample Wilcoxon test with the Fligner-Policello correction for unequal variances was used. We also used a Hochberg's method for multiple testing. A p-value <0.05 was considered as evidence of a statistically significant difference for experimental data with the p values being two-sided.

Results

Expression of the EP3 Receptor Increases after Ang II Infusion

We have previously shown that mRNA expression of the EP3 receptor increases in the infarcted heart [217] and leads to reduced cardiac function. To determine expression levels of the EP4 and EP3 receptors in the left ventricle and to examine whether EP3 receptor expression increases in the Ang II HTN model, we implanted osmotic mini-pumps containing either vehicle or Ang II for 2 weeks. Figure 29 shows the expression of both receptors for both time points. Figure 29 shows that after 2 weeks, the expression of EP3 increased 2.5-fold compared to vehicle infused animals (1.02 ± 0.13 in vehicle treated vs. 2.59 ± 0.63 in Ang II treated mice; $p<0.05$), while expression of the EP4 receptor was unchanged (1.01 ± 0.10 in vehicle treated vs. 0.96 ± 0.11 in Ang II infused mice; ns). In additional studies, we sought to examine whether the changes in EP3 expression were occurring in cardiomyocytes or fibroblasts, the two major cell types of the heart. We infused Ang II or vehicle control for 2 weeks and then isolated cardiomyocytes (AVM) and fibroblasts (AVF) from each animal simultaneously. Real time RT-PCR was used to determine EP3 and EP4 mRNA expression. Figure 29 shows that EP3 mRNA expression increases approximately 5-fold in the AVM (5.14 ± 1.52 in Ang II vs. 1.20 ± 0.46 in vehicle treated; $p<0.05$) while it increases only 25 % in the fibroblasts (1.25 ± 0.05 in Ang II vs. 1.00 ± 0.07; $p<0.05$). There was no significant increase in EP4 in the AVM (2.08 ± 0.92 in Ang II vs. 1.08 ± 0.28 in vehicle treated; ns), however EP4 significantly increased in the fibroblasts in response to Ang II (1.80 ± 0.05 in Ang II vs. 1.01 ± 0.09 in vehicle; $p<0.005$).

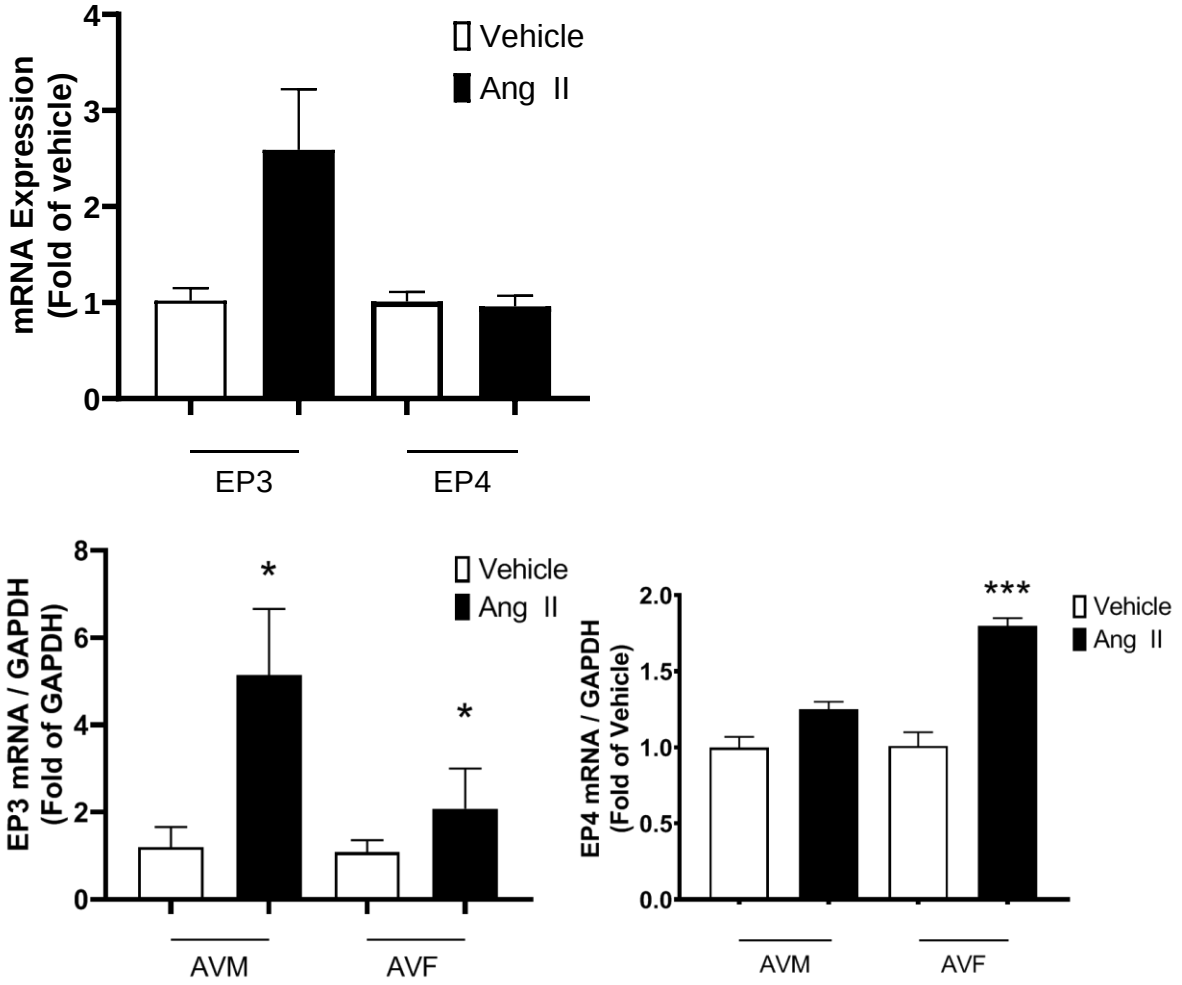

Figure 29: EP3 and EP4 Expression in AVM and AVF. *Top:* Real time RT-PCR analysis of EP3 and EP4 mRNA expression in left ventricles after 2 weeks of vehicle (black bars) or Ang II (blue bars) infusion (1.4 mg x kg^{-1} x day^{-1}) via osmotic mini pumps. *p<0.05 vs. Vehicle infused mice. N=3/group. *Bottom:* Real time RT-PCR analysis of EP3 (left) and EP4 (right) mRNA expression in adult cardiomyocytes (AVM) or adult cardiac fibroblasts (AVF) after 2 weeks of vehicle (white bars) or Ang II (black bars) infusion (1.4 mg x kg^{-1} x day^{-1}).

EP3 Agonist Sulprostone Exacerbates Cardiac Dysfunction in Ang II Hypertension

Since EP3 receptor mRNA is increased in the left ventricle of mice with hypertension, we hypothesized that treatment with the EP3 agonist sulprostone would reduce cardiac function after Ang II infusion. The results in Figure 30 show that there were significant differences in cardiac function measured by echocardiography in the conscious mice after treatment with Ang II. There was no significant difference between

vehicle

treated and Ang II treated mice on shortening fraction, a measure of contractility (56.54 ± 0.82 % in vehicle vs. 61.28 ± 1.82 % in Ang II infused mice; ns). However, there was a reduction in shortening fraction when the mice received daily injections of sulprostone in combination with Ang II infusion (56.71 ± 0.90 % in Ang II + sulprostone vs. 61.28 ± 1.82 % in Ang II infused mice; $p<0.05$). There was a trend for a reduction in ejection fraction,

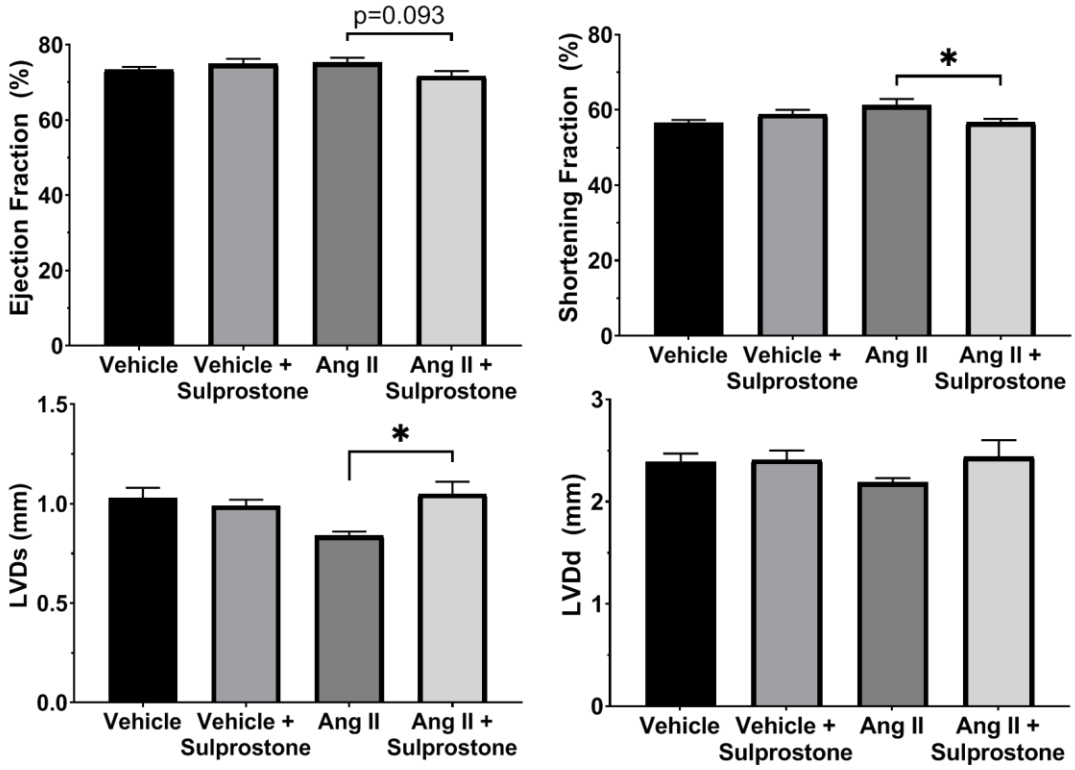

Figure 30: Echocardiography with Sulprostone Treatment. Cardiac function assessed by echocardiography in conscious mice 2 weeks after vehicle or Ang II (1.4 mg x kg^{-1} x day^{-1}) ± daily injections of Sulprostone (40 µg x kg^{-1} x day^{-1}) or diluted ethanol vehicle. *$p<0.05$ vs. Ang II. N=4-5. *LVDs* - Left ventricular dimension at systole, *LVDd*-Left ventricular dimension at diastole.

although this failed to reach statistical significance (71.75 ± 1.25 % in Ang II + sulprostone vs. 75.27 ± 1.28 % in Ang II; $p=0.093$). Additionally, we observed an increase in left ventricle dimension in systole with sulprostone treatment (1.05 ± 0.06 mm in Ang II +

sulprostone vs. 0.84 ± 0.03 mm in Ang II infused mice; p<0.05). There was a tendency for an increase in the left ventricle dimension in diastole, although this failed to reach statistical significance (2.44 ±0.16 mm in Ang II + sulprostone vs. 2.19 ± 0.05 mm in Ang II; ns). These data suggest that the addition of the EP3 agonist to Ang II hypertension prompts a decline in cardiac function and increases left ventricle chamber dilatation. Blood pressure was monitored throughout the study and Figure 31 shows that after 1 week of Ang II blood pressure was significantly increased (156 ± 15.4 in Ang II group vs. 111 ± 1.9 in vehicle; p<0.05). There was no difference between the group that received Ang II + sulprostone treatment versus those that received Ang II alone (151 ± 17.6 in Ang II + sulprostone vs. 156 ± 15.4 in Ang II group; p=ns). Similarly, after 2 weeks of Ang II, there was no significant difference in the level of systolic blood pressure achieved in the mice that received Ang II + sulprostone versus those that received Ang II alone (172 ±12.1 mmHg in the Ang II group vs. 153 ± 11.4 mmHg in the Ang II + sulprostone group; p=ns).

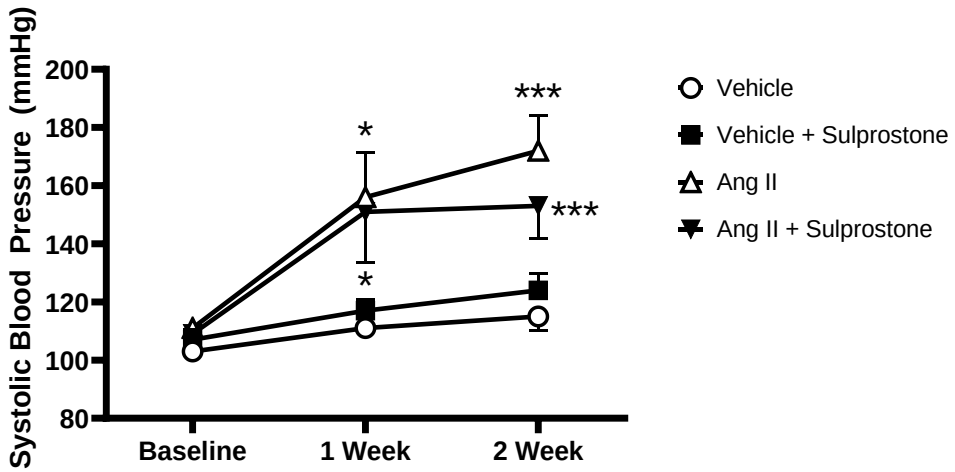

Figure 31: Systolic Blood Pressure with sulprostone Treatment. Systolic blood pressure measured by tail cuff plethysmography in conscious mice at baseline, 1 week, and 2 weeks after vehicle or Ang II (1.4 mg x kg^{-1} x day^{-1}) ± daily injections of sulprostone (40 µg x kg^{-1} x day^{-1}) or diluted ethanol vehicle. *p<0.05, *******p<0.005 vs. vehicle**.** N=4-5/group.

EP3 Antagonist L798, 106 Improves Cardiac Function and Hypertrophy in Ang II Hypertension

Since the addition of the EP3 agonist sulprostone worsened cardiac function in Ang II hypertension, we hypothesized that antagonism of the EP3 receptor would reverse the decline in cardiac function. Figure 32 shows that there was a modest, but significant reduction in ejection fraction after 2 weeks of Ang II and this was attenuated when animals were treated with an EP3 antagonist (77.26 ± 0.47 % in vehicle treated vs. 69.82 ± 1.01 % in Ang II treated, $p<0.005$; and 72.61 ± 0.51 % in Ang II + L798, 106 treated; $p<0.05$ vs. Ang II). Similarly, shortening fraction was reduced with Ang II and improved with L798, 106 treatment (51.61 ± 1.71 % in Ang II treated vs. 56.97 ± 1.01 % in Ang II + L798, 106 treated; $p<0.05$ vs. Ang II). Additionally, there were significant increases in posterior wall thickness at systole after Ang II infusion, which was attenuated with an EP3 antagonist (1.19 ± 0.02 mm in vehicle treated vs. 1.42 ± 0.02 mm in Ang II treated, $p<0.01$; and 1.30 ± 0.03 mm in Ang II + L798, 106 treated; $p<0.05$ vs. Ang II). We did not observe any change in cardiac output between the groups (14.43 ± 1.33 ml/min/10g in vehicle treated vs. 12.38 ± 0.98 ml/min/10g in Ang II treated, p=ns; and 13.12 ± 1.10 ml/min/10g in Ang II + L798, 106 treated; p=ns). These results suggest that the effect of L798, 106 on blood pressure is not occurring via alterations in cardiac function.

Ang II infusion is known to produce cardiac hypertrophy [218]. We observed an increase in heart weight to body ratio (Figure 33) with Ang II infusion (39.86 ± 1.08 in vehicle treated vs. 45.31 ± 1.68 in Ang II treated; $p<0.05$). This increase was prevented when animals were treated with L798, 106 (36.92 ± 1.74 in vehicle treated vs. 41.08 ±

1.31 in Ang II + L798, 106; p=ns).

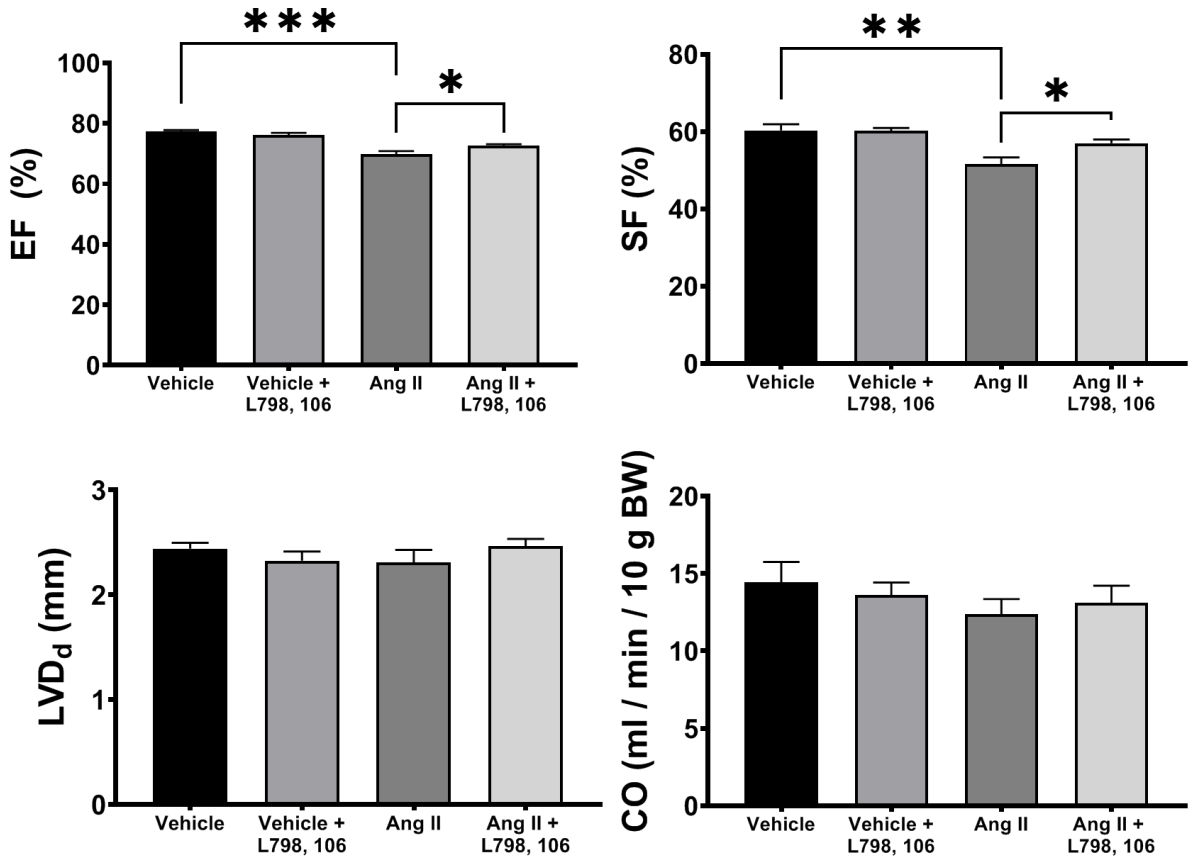

Figure 32: Echocardiography with L798, 106 Treatment. Cardiac function assessed by echocardiography in conscious mice 2 weeks after vehicle or Ang II (1.4 mg x kg^{-1} x day^{-1}) ± daily injections of L798, 106 (40 µg x kg^{-1} x day^{-1}) or diluted ethanol vehicle. ** p<0.05, *** p<0.005 vs. Vehicle. + p<0.05, ++ p<0.01 vs. Ang II. N=11-13. *LVDd*-Left ventricular dimension at diastole, *PWTs*-Posterior wall thickness at systole.

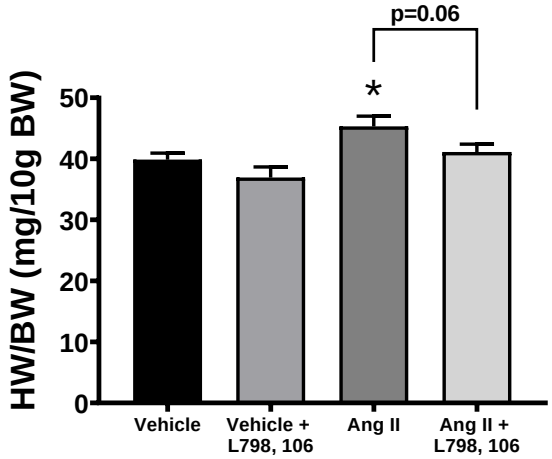

Figure 33: Heart Weight (HW) to Body Weight (BW) Ratio. Mice were anesthetized, hearts were removed and weighed. Values shown are means ± SEM in mg/10g BW. *p<0.05 vs. vehicle.

Treatment with L798, 106 Significantly Diminishes Pressor Response of Ang II

It has been shown in isolated mesenteric arteries lacking the EP3 receptor, that the vasoconstrictive action of Ang II is ameliorated, suggesting an important role for EP3 in the control of blood pressure via the resistance vessels [439]. Indeed, daily administration of the EP3 antagonist L798, 106 substantially reduced the hypertensive effect of chronic Ang II treatment (Figure 34; 168 ± 5.0 mmHg in Ang II to 136 ± 9.7 in Ang II + L798, 106; $p<0.05$).

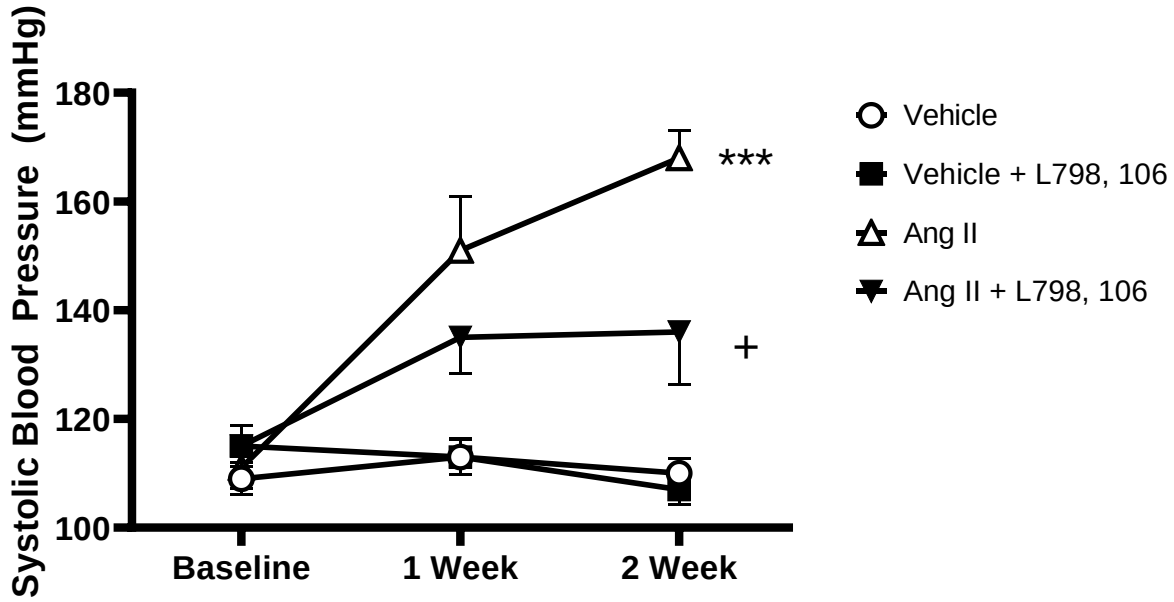

Figure 34: Systolic Blood Pressure with L798, 106 Treatment. Systolic blood pressure measured by tail cuff plethysmography in conscious mice at baseline, 1 week, or 2 weeks after vehicle or Ang II (1.4 mg x kg^{-1} x day^{-1}) ± daily injections of L798, 106 (80 µg x kg^{-1} x day^{-1}) or diluted ethanol vehicle for 2 weeks. *******$p<0.005$ vs. Vehicle, + $p<0.05$ vs. Ang II**.** N=11-13/group.

L798, 106 Treatment Has No Effect on AT_1 mRNA Expression

It is known that upregulation of the AT_1 receptor plays an important role in mediating the pathophysiology of increased blood pressure [440]. Therefore, we examined if L798, 106 administrations is affecting mRNA levels of the Ang II AT_1 receptor in the left ventricles. Figure 35 shows that after Ang II infusion there was no change in

AT_1 mRNA levels (1.02 ± 0.09 in vehicle treated vs. 1.16 ± 0.13 in Ang II treated; p=ns). Similarly, there was no significant change between mice that received Ang II infusion with vehicle injection and those that received Ang II infusion with L798, 106 treatment (1.16 ± 0.13 in Ang II treated vs. 0.86 ± 0.10 in Ang II + L798, 106 treated; p=ns).

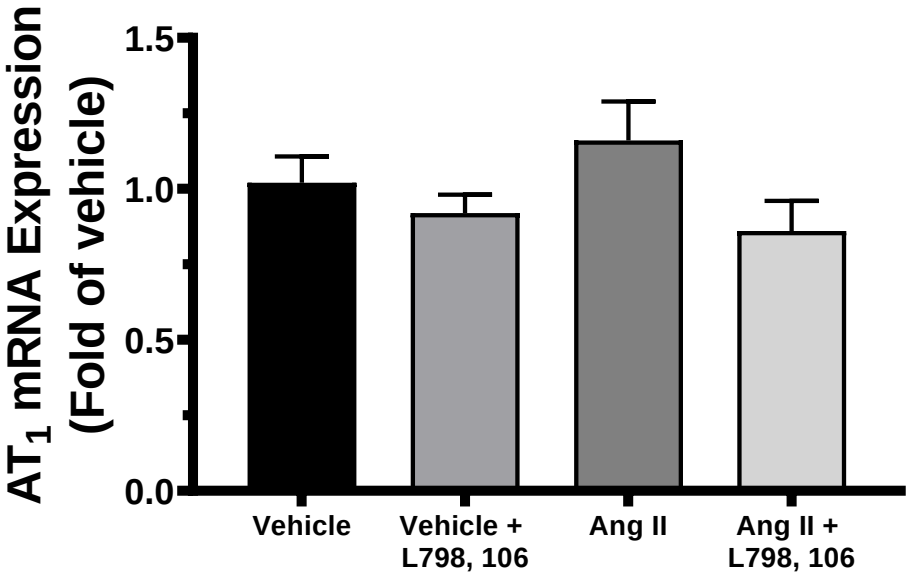

Figure 35: AT1 mRNA Expression with L798, 106 Treatment. AT_1 mRNA expression in left ventricle samples after 2 weeks of Ang II infusion ± L798, 106 (40 µg x kg^{-1} x day^{-1}, i.p.). Data presented are means ± SEM. N=6

Treatment with L798, 106 Significantly Prevents Ang II-Induced RhoB Expression in Mesenteric Arteries

Changes in Rho-kinase signaling have been shown to contribute to increases in total peripheral resistance in hypertension. This has been demonstrated in resistance vessels such as the mesenteric arteries [441-443]. Western blot analysis using mesenteric arteries from the mice revealed a significant increase in RhoB protein expression after 2 weeks of Ang II infusion (Figure 36; 1.00 ± 0.14 in vehicle treated vs. 3.84 ± 1.39 in Ang II treated, p<0.005). This was dramatically attenuated when mice were treated with L798, 106 (0.94 ± 0.32 in Ang II + L798, 106 vs. 3.84 ± 1.39 in Ang II treated, p<0.005). These results suggest that Ang II increases RhoB expression, potentially

increasing contraction in the vasculature. RhoB expression is reduced by L798, 106 treatment, possibly serving as a mechanism for the reduction in blood pressure we observed. RhoB expression was undetectable in left ventricle homogenates 2 weeks after Ang II infusion.

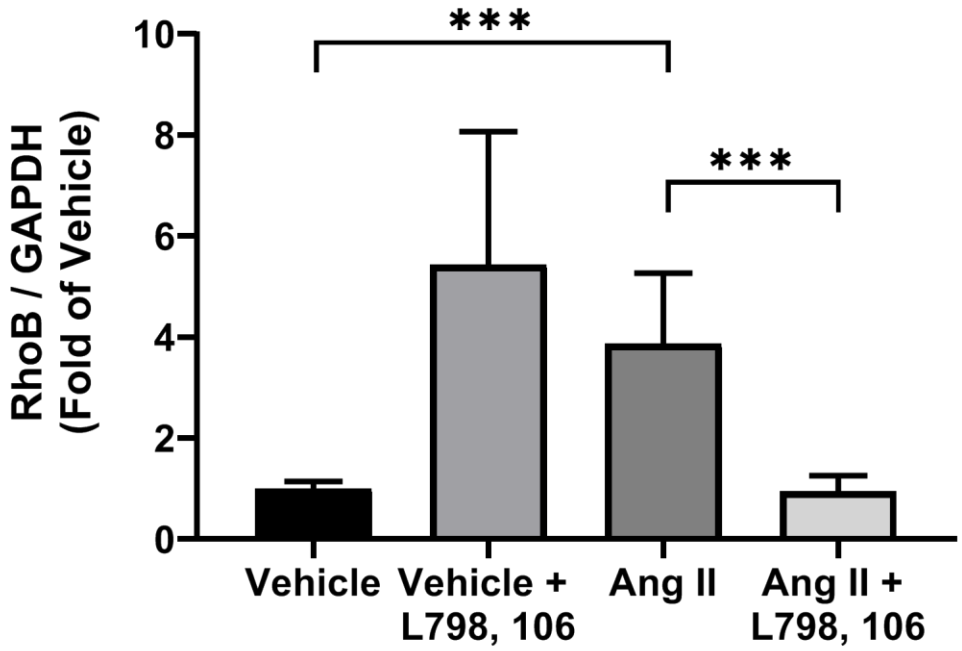

Figure 36: Quantification of RhoB Expression. Western Blot analysis for RhoB expression in mouse mesenteric arteries with 2 weeks of vehicle or Ang II (1.4 mg/kg/day) ± L798, 106 (40 µg/kg/day). *** p<0.005, N=3-5/group.

Figure 37 shows that in contrast to RhoB, RhoA expression was unchanged in the mesenteric arteries with infusion of Ang II (1.00 ± 0.20 in vehicle vs. 1.08 ± 0.40 in Ang II; p=ns). Although expression of RhoB was undetectable in the LV, RhoA expression was detectable in the LV homogenates. Interestingly, there was a small but significant decrease in RhoA expression with Ang II infusion and this was unchanged with L798, 106 treatment. (Figure 37; 1.00 ± 0.03 in vehicle vs. 0.82 ± 0.04 in Ang II; p<0.05) and (0.82 ± 0.04 in Ang II vs. 0.91 ± 0.14 in Ang II + L798, 106; p=ns).

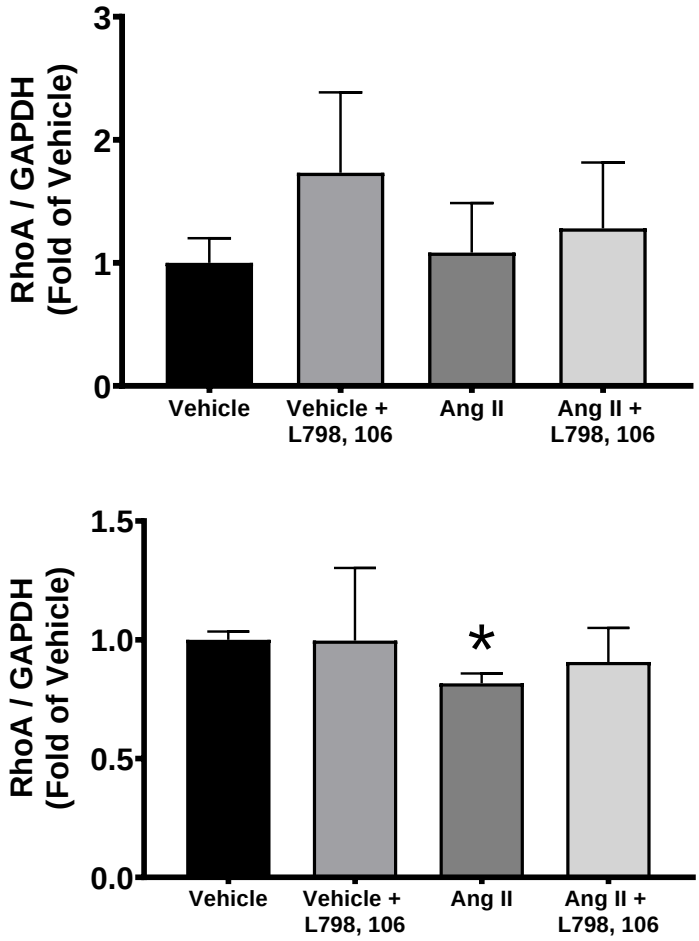

Figure 37: Quantification of RhoB Expression. Western Blot analysis for RhoA expression in mouse mesenteric artery (top panel) and left ventricle (bottom panel) homogenates with 2 weeks of vehicle or Ang II (1.4 mg^{-1} x kg^{-1} x day^{-1}) ± L798, 106 (40 μg^{-1} x kg^{-1} x day^{-1}). * $p<0.05$ vs. vehicle group, N=3/group.

EP3 Transgenic Mice Overexpressing EP3 Have Normal Blood Pressure but Reduced Cardiac Function

Since the increase in the EP3 receptor is occurring mainly in the cardiomyocytes, we obtained mice that overexpress the porcine analogue of human EP3 in the cardiomyocytes (EP3 Tg) and their wild type littermates (EP3 WT). To assess the effect of EP3 overexpression in the cardiomyocytes on blood pressure, we measured systolic blood pressure in EP3 Tg and their WT littermates under baseline conditions and after infusion of Ang II for 2 weeks. Figure 38 shows that under baseline conditions, the EP3

Tg mice have normal systolic blood pressure as measured by tail cuff and this increases significantly after Ang II infusion, albeit to a similar extent to that observed in C57BL/6 mice (106 ± 2.01 mmHg at baseline vs. 152 ± 3.13 after Ang II infusion; $p<0.05$). These data suggest that overexpression of EP3 in the cardiomyocytes has no direct effect on blood pressure.

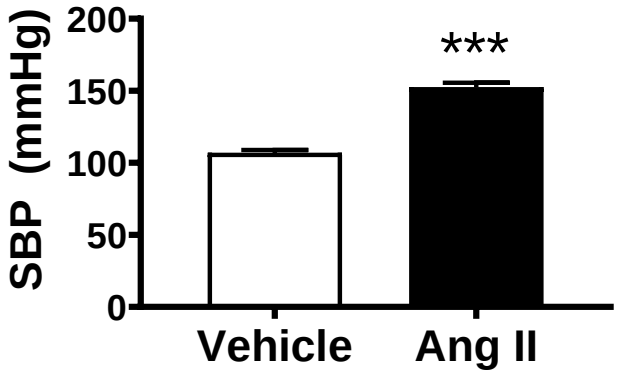

Figure 38: Systolic Blood Pressure in EP3 Tg. Systolic blood pressure measured by tail cuff plethysmography in conscious EP3 Tg mice 2 weeks after vehicle or Ang II (1.4 mg x kg^{-1} x day^{-1}). ******* $p<0.005$ vs. vehicle**.** N=4-5/group

Figure 39 shows that as early as 10-12 weeks of age, EP3 Tg mice have reduced ejection fraction (56.93 ± 4.94 % in EP3 Tg vs. 76.18 ± 1.25 % in EP3 WT; $p<0.05$) and reduced shortening fraction at baseline (38.49 ± 3.46 % in EP3 Tg vs. 61.69 ± 2.93 % in

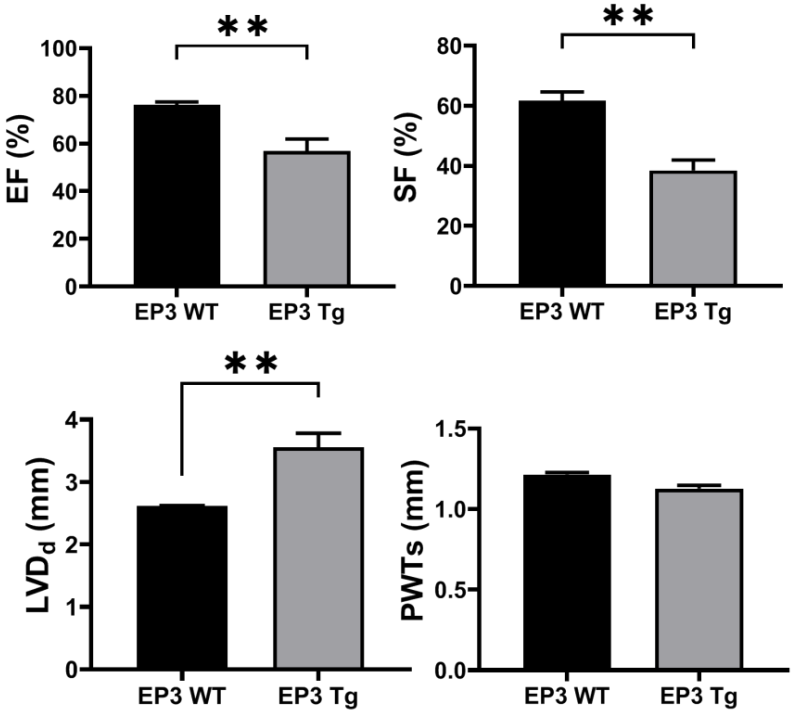

Figure 39: Baseline Echocardiography in EP3 WT and EP3 Tg. Cardiac function assessed by echocardiography in conscious male EP3 Tg or EP3 WT mice at 10-12 weeks of age under baseline conditions. *LVDd* - Left ventricular dimension at diastole, *PWTs*-Posterior wall thickness at systole. **$p<0.01$, vs. EP3 WT. N=3 EP3 WT and N=5 EP3 Tg.

EP3 WT; p<0.01). Additionally, the hearts display robust dilatation as shown by the left ventricular dimensions in diastole (3.55 ± 0.23 mm in EP3 Tg vs. 2.62 ± 0.01 mm in EP3 WT; p<0.01). The posterior wall thickness is unchanged between EP3 Tg and EP3 WT, thus the data suggest that the hearts display a phenotype of eccentric hypertrophy (1.13 ± 0.02 mm in EP3 Tg vs. 1.21 ± 0.01 in EP3 WT; ns).

To measure the hypertrophy of the EP3 Tg hearts at baseline, we performed myocyte cross sectional area staining on frozen sections of LV at baseline. Figure 40 shows that the average myocyte area is increased in EP3 Tg compared to the WT littermates (191.4 ± 2.6 in EP3 WT vs. 218.9 ± 2.8 in EP3 Tg;p<0.005). These data suggest that the EP3 Tg hearts are hypertrophied under baseline conditions and confirm the echocardiography data showing ventricle dilatation.

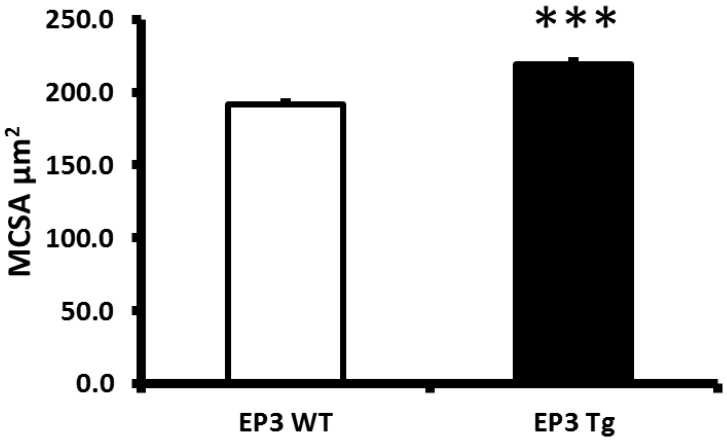

Figure 40: Myocyte Cross Sectional Area Analysis EP3 WT vs. EP3 Tg. Myocyte cross sectional area (MCSA) analysis using NIH Image J software. Values shown are means ± SEM. *** p<0.005. N=5

We hypothesized that the decline in cardiac function is exacerbated in Ang II hypertension. Figure 41 shows that in response to Ang II, the hearts of EP3 WT mice are well compensated and maintain ejection fraction (76.49 ± 0.70 % in vehicle vs. 75.30 ± 0.80 % in Ang II; ns) and shortening fraction (63.19 ± 0.98 % in vehicle vs. 63.21 ± 1.37 % in Ang II; ns). In contrast, the transgenic mice have reduced ejection fraction and

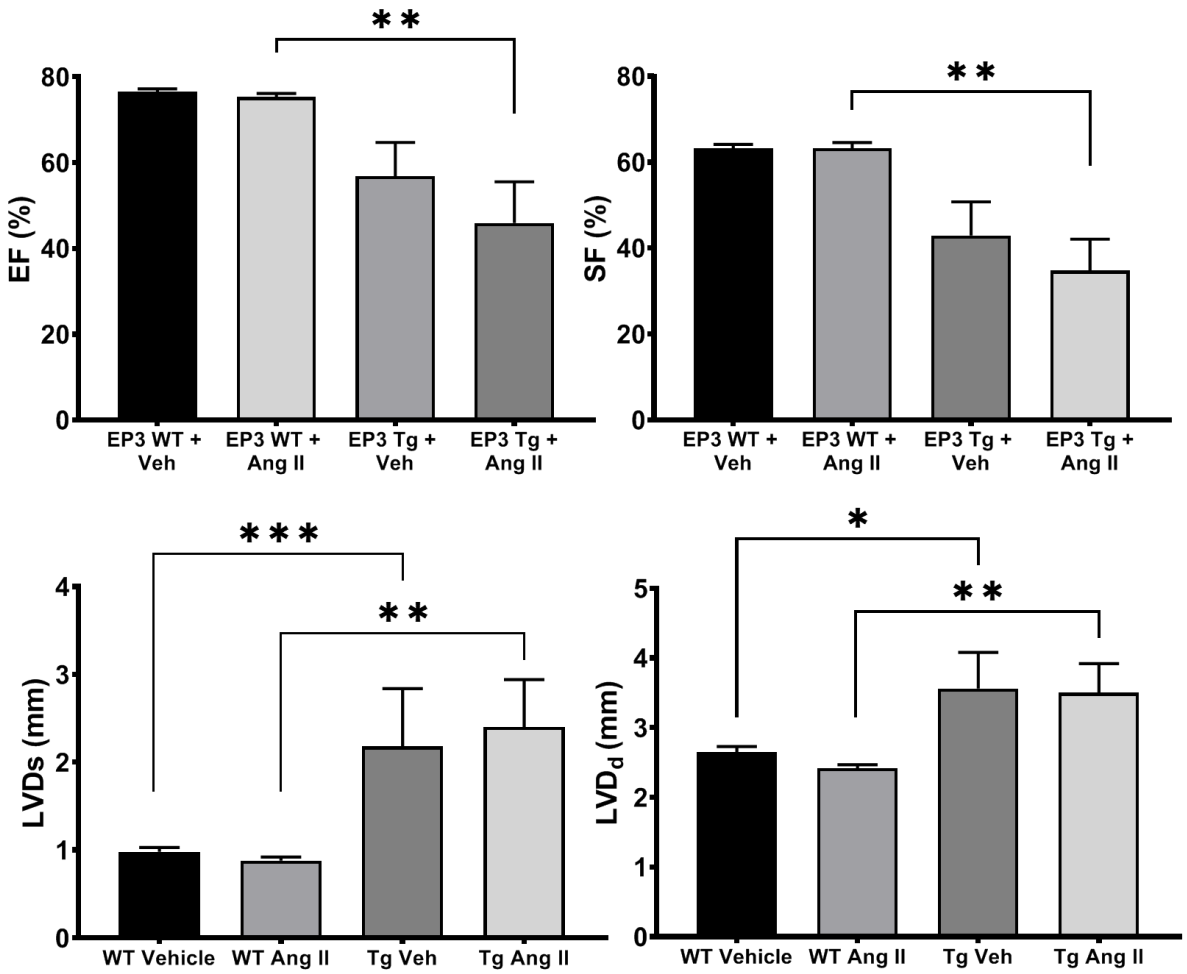

Figure 41: Echocardiography in EP3 WT and EP3 Tg After 2 Wks. Ang II. Cardiac function assessed by echocardiography in conscious male EP3 Tg or EP3 WT mice at 10-12 weeks of age after 2 weeks of vehicle or Ang II infusion (1.4 mg x kg^{-1} x day^{-1}). N=3 EP3 WT and N=5 EP3 Tg. *EF* – Ejection fraction, *SF*-Shortening fraction, *LVDs* – Left ventricular dimension in systole, *LVDd* – Left ventricle dimension in diastole. *p<0.05, **p<0.01, ***p<0.005. N=3-5.

shortening fraction at baseline and there is a greater response to Ang II (ejection fraction: 75.30 ± 0.83 % in WT + Ang II vs. 45.92 ± 9.63 % in EP3 Tg + Ang II; p<0.01) and (Shortening fraction: 63.21 ± 1.37 % in WT + Ang II vs. 34.77 ± 7.33 % in Tg + Ang II). Similarly, there was an exacerbated increase in left ventricle dimensions at systole and diastole (0.88 ± 0.04 in WT + Ang II vs. 2.40 ± 0.54 in Tg + Ang II; p<0.005) and (2.42 ± 0.05 in WT + Ang II vs. 3.50 ± 0.42 in Tg + Ang II; p<0.005) respectively.

EP3 Tg Mice Have Increased Markers of Inflammation in their Left Ventricle

We hypothesized that the depressed cardiac function observed in EP3 Tg mice correlates with an increase in inflammation. We performed real time RT-PCR for several pro-inflammatory cytokines and chemokines using left ventricles from EP3 Tg and their WT littermates under baseline conditions. Figure 42 shows that there was a significant increase in TNF-α mRNA levels in EP3 Tg mice, (1.01 ± 0.08 in EP3 WT vs. 1.45 ± 0.22 in EP3 Tg; $p<0.05$). Additionally, we observed an increase in IL-1β (1.04 ± 0.21 in EP3 WT vs. 1.87 ± 0.46 in EP3 Tg; $p<0.05$). Interestingly, the mRNA levels of the chemokine

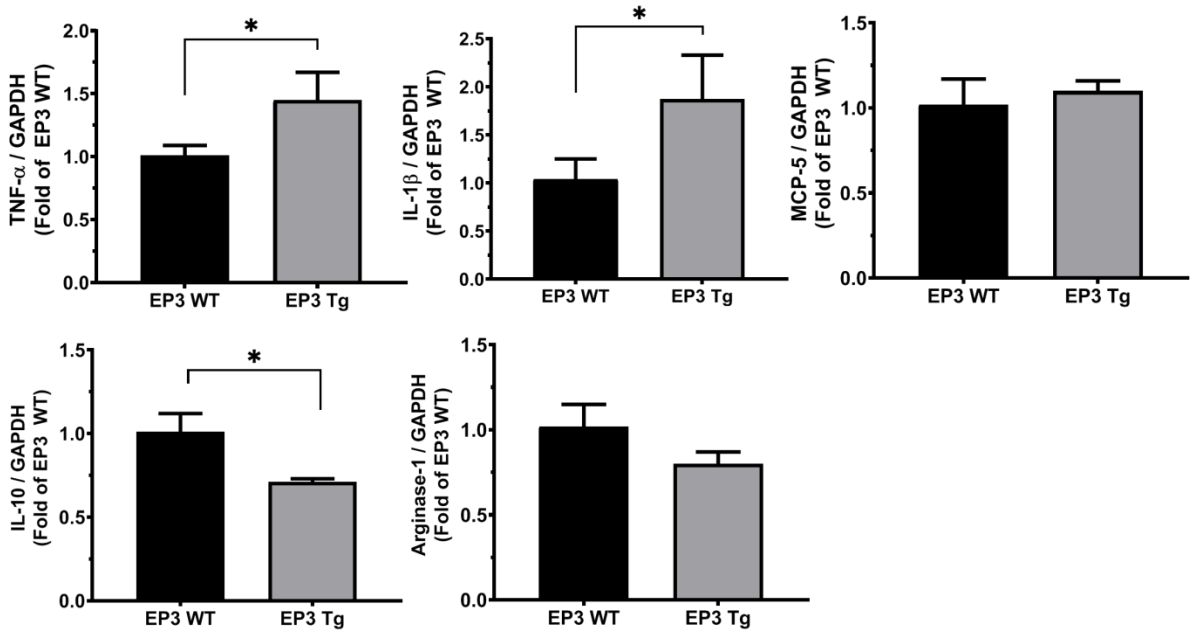

Figure 42: Real Time RT-PCR of Cytokines. Real time RT-PCR analysis of several cytokines in the left ventricles of EP3 WT and EP3 Tg mice under baseline conditions. * $p<0.05$ vs. EP3 WT. N=3/group.

MCP-5 were unchanged between the two groups (1.02 ± 0.15 in EP3 WT vs. 1.10 ± 0.06 in EP3 Tg). We also observed a significant reduction in the anti-inflammatory cytokine IL-10 and a reduction in the anti-inflammatory M2 macrophage marker arginase-1, although this failed to reach statistical significance (IL-10: 1.01 ± 0.11 in EP3 WT vs. 0.71 ± 0.02

in EP3 Tg; $p<0.05$. Arginase-1: 1.02 ± 0.13 in EP3 WT vs. 0.80 ± 0.07 in EP3 Tg; $p=0.26$). Together these data suggest that the EP3 Tg mice have increased pro-inflammatory signaling in their left ventricles by upregulating pro-inflammatory genes and down regulating anti-inflammatory genes. To confirm our PCR results, we examined the protein expression of several cytokines and chemokines using a multiplex ELISA array. Figure 43 shows that there was a reduction in IL-10, confirming our real time RT-PCR results (0.04 ± 0.01 A.U. in EP3 WT vs. 0.02 ± 0.01 A.U. in EP3 Tg; $p<0.05$). There was also a significant reduction in IL-4 in the EP3 Tg mice (0.03 ± 0.01 A.U. in EP3 WT vs. 0.02 ± 0.0 A.U. in EP3 Tg; $p<0.005$). Unfortunately, levels of other cytokines were below the kit's limit of detection.

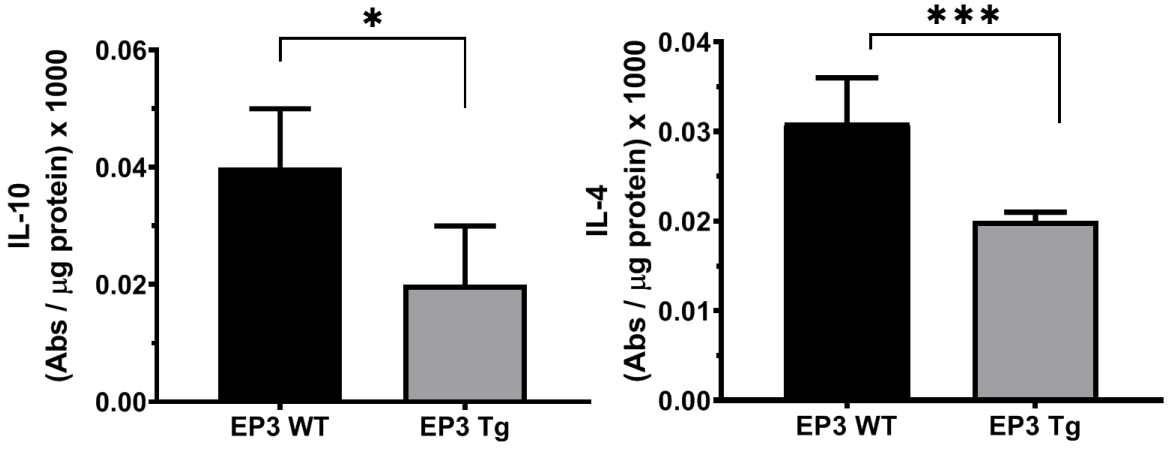

Figure 43: Multiplex ELISA Analysis. Multiplex ELISA array analysis of cytokines in the left ventricles of EP3 WT and EP3 Tg mice under baseline conditions. Absorbance was obtained at 570 nm, corrected for the absorbance at 450 nm and then corrected for the total µg of protein per well. * $p<0.05$, *** $p<0.005$ vs. EP3 WT. N=3/group.

EP3 Tg Mice Have Increased T Cells but Not Macrophages in their Left Ventricle

Since the EP3 Tg mice have increased markers of inflammation with a reduction in anti-inflammatory markers, we hypothesized that they would have increased infiltration of immune cells. In this study, we investigated the presence of $CD68^{+}$ macrophages and

$CD3^+$ T cells in the left ventricles of EP3 WT and EP3 Tg mice under baseline conditions by immunohistochemistry. Figure 44 shows that there was no change in the number of

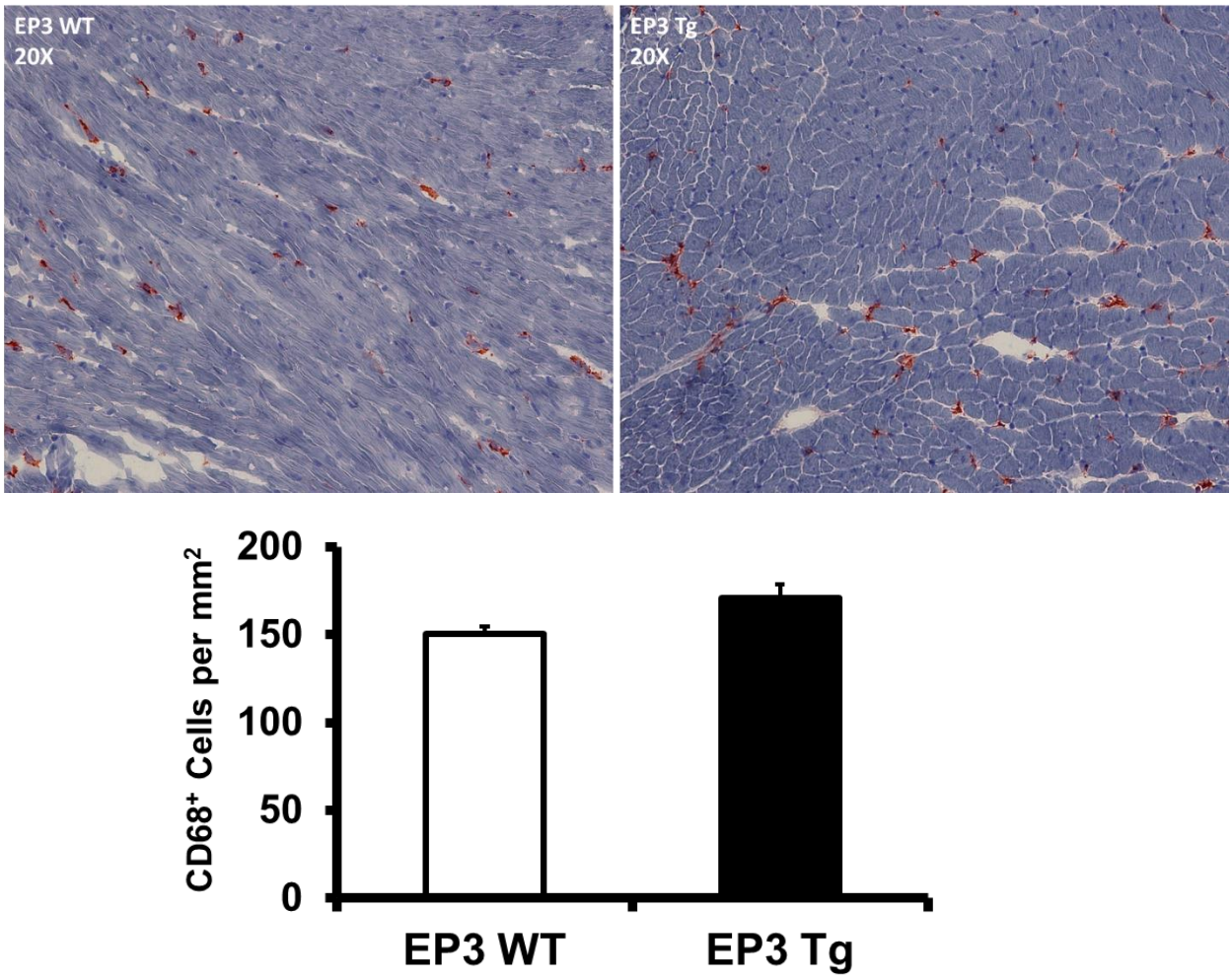

Figure 44: CD68+ Staining. *Top.* Representative immunohistochemistry for macrophages ($CD68^+$). *Bottom.* Quantitative $CD68^+$ analysis. Images were taken under 20X objective and analyzed using Image J software. The number of positive cells were counted by a blinded observer and corrected to mm^2 of tissue. Data are presented as means ± SEM. N=5 in EP3 WT, N=10 in EP3 Tg.

macrophages in the left ventricle of EP3 Tg mice compared to EP3 WT littermates (170.8 ± 7.6 cells/mm^2 in EP3 WT vs. 150.4 ± 4.5 cells/mm^2 in EP3 Tg; p=ns). However, Figure 45 shows that when we analyzed T cells, there was a significantly higher number of $CD3^+$ cells in EP3 Tg left ventricles (32.3 ± 2.4 cells/mm^2 in EP3 WT vs. 62.9 ± 5.6 cells/mm^2 in EP3 Tg; $p<0.005$). These data confirm our findings with the cytokines/chemokine

mRNA levels as a lack of chemokines specific for macrophages like MCP-5, correlates with a lack of increased macrophages. Similarly, the increase in IL-1β could attribute to the increase in T cells.

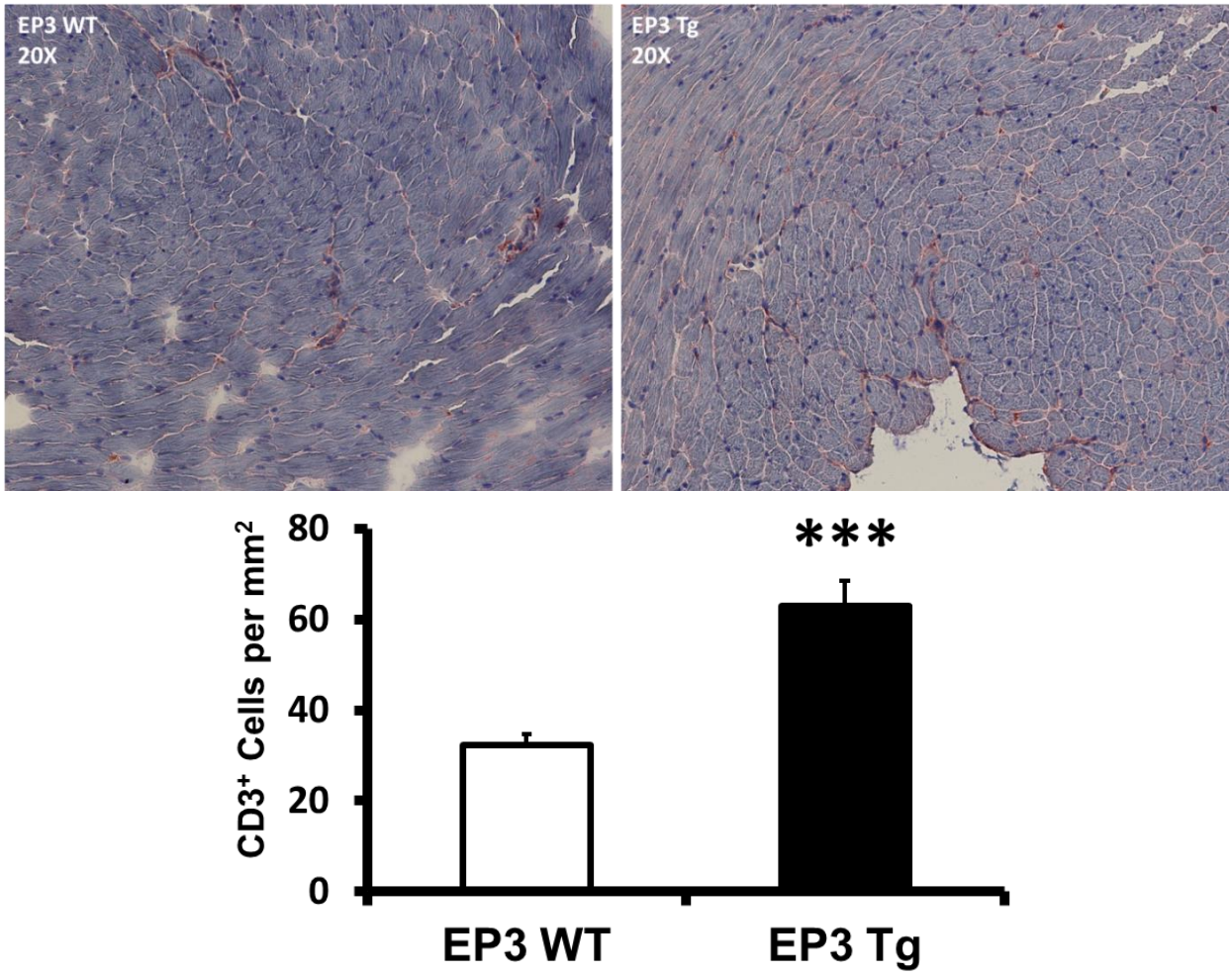

Figure 45: CD3+ Staining. *Top.* Representative immunohistochemistry for T cells ($CD3^+$). *Bottom.* Quantitative $CD3^+$ analysis. Images were taken under 20X objective and analyzed using Image J software. The number of positive cells were counted by a blinded observer and corrected to mm^2 of tissue. Data are presented as means ± SEM. ***p<0.005 vs. EP3 WT. N=5 in EP3 WT, N=10 in EP3 Tg.

EP3 Tg Mice Have Increased Expression of the Reactive Oxygen Species Generator NADPH Oxidase 2 (Nox2)

Left ventricle hypertrophy and heart failure have been associated with increased reactive oxygen species (ROS) in various models [444, 445]. To determine if the EP3 Tg mice have increased ROS in their left ventricles, we performed western blot for Nox2, a

major enzyme responsible for ROS production. Figure 46 shows that compared to EP3 WT, EP3 Tg mice have a 2-fold increase in Nox2 expression in their left ventricles (1.00 ± 0.19 in EP3 WT vs. 2.02 ± 0.42 in EP3 Tg; $p<0.05$). Although ROS generation was not measured per se, increased Nox2 expression suggests there is increased oxidative stress in the EP3 Tg mice.

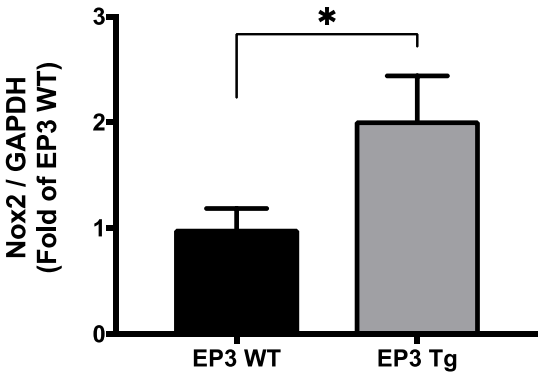

Figure 46: Western Blot Analysis of Nox2 Expression. Western blot analysis for Nox2 in left ventricles of EP3 WT and EP3 Tg mice. Nox2 was corrected for protein loading by GAPDH and the results are presented as means ± SEM, fold of EP3 WT. * $p<0.05$. N=3.

The Effects of L798, 106 on Blood Pressure and Cardiac Function are Unique to the Ang II Model

Infusion of the β-adrenergic receptor agonist, isoproterenol, is another non-ischemic model that has been used to induce heart failure in rodents [446-449]. Figure 47 shows that when mice received isoproterenol infusion for 10 days, there was a

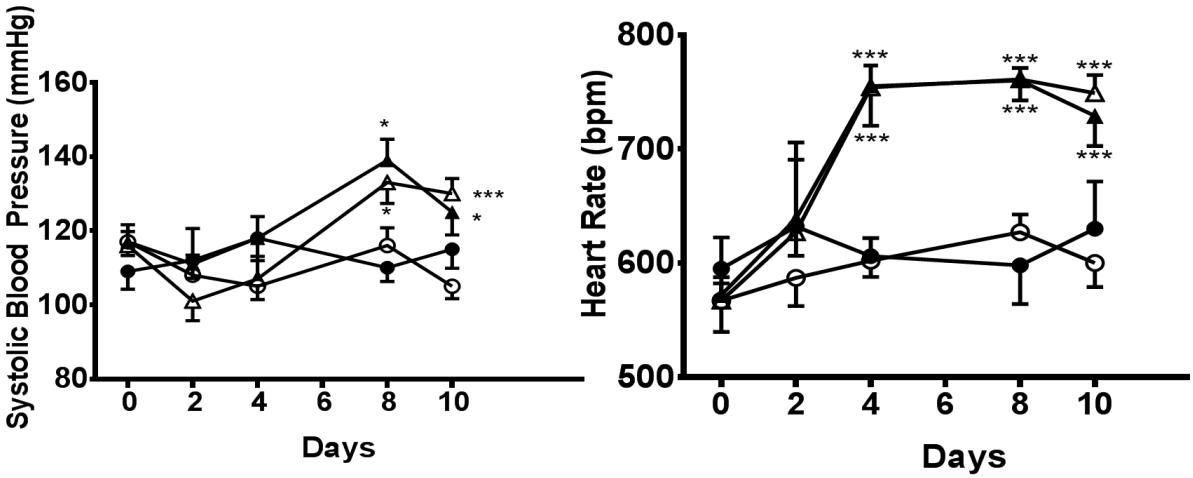

Figure 47: Systolic Blood Pressure and Heart Rate in Isoproterenol Infusion. Systolic blood pressure (left panel) or heart rate (right panel) measured by tail cuff plethysmography in conscious mice throughout the infusion protocol of vehicle or isoproterenol (30 mg x kg^{-1} x day^{-1}) ± daily injections of L798, 106 (80 µg x kg^{-1} x day^{-1}) or diluted ethanol vehicle. * $p<0.05$, ******* $p<0.005$ vs. Vehicle**.** N=4-6/group.

significant increase in heart rate, as expected (594 ± 24.0 bpm in vehicle treated vs. 739 ± 33.6 bpm in isoproterenol treated; p<0.005). This was evident as early as 4 days after treatment. Treatment with an EP3 antagonist had no effect on this increase (670 ± 37.5 bpm in isoproterenol + L798, 106 group vs. 739 ± 33.6 bpm in isoproterenol group; ns). Isoproterenol infusion also resulted in a significant, but modest increase in systolic blood pressure compared with vehicle infused mice (122 ± 2.8 mmHg in isoproterenol vs. 108 ± 4.4 mmHg in vehicle; p<0.05). EP3 antagonist treatment did not reduce this increase in blood pressure (114 ± 7.3 mmHg in isoproterenol + L798, 106 vs. 122 ± 2.8 mmHg in isoproterenol; ns). Cardiac function was assessed in these mice by echocardiography. Figure 48 shows that there was a modest but significant reduction in shortening fraction

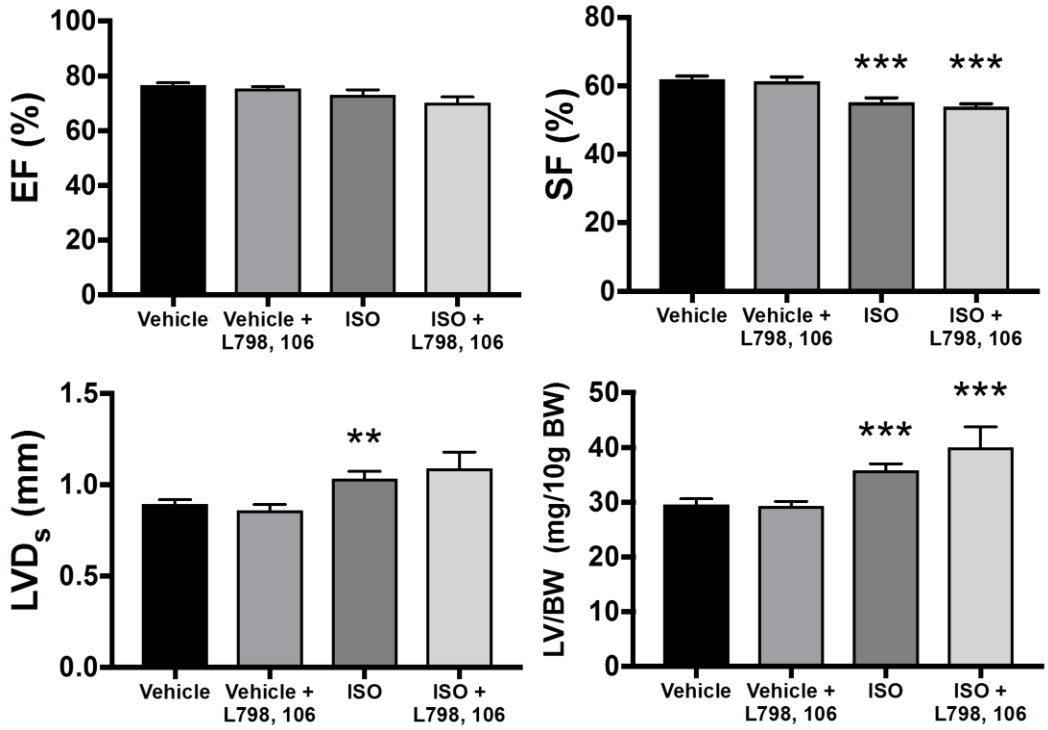

Figure 48: Echocardiography after Isoproterenol Infusion. Cardiac function assessed by echocardiography in conscious mice at 10-12 weeks of age 10 days after vehicle or isoproterenol (ISO) infusion (30 mg x kg^{-1} x day^{-1}). Ejection fraction (top left), shortening fraction (top right), and left ventricle diameter in systole (LVDs; bottom left). The left ventricle to body weight ratio (bottom right) was obtained using weights at sacrifice. Data presented as means ± SEM. ** p < 0.01, *** p< 0.005 vs. vehicle. N=7-8.

(55.16 ± 1.3 % in isoproterenol vs. 61.81 ± 1.0 % in vehicle; $p<0.005$). However, this reduction was not altered when mice were treated with L798, 106 (53.87 ± 1.2 % in isoproterenol + L798, 106 vs. 55.16 ± 1.3 % in isoproterenol; ns). Figure 48 also shows a significant increase in left ventricular dimension at systole, and a corresponding increase in left ventricle mass as measured by echocardiography. Neither of these parameters of hypertrophy were attenuated when mice received L798, 106 treatment. Altogether, these data suggest the protective effects of EP3 antagonism are selective to the Ang II model and are not promiscuous for other non-ischemic models of heart failure.

Discussion

The results of this study show, for the first time, that administration of an EP3 agonist, sulprostone, reduces cardiac function after 2 weeks of Ang II infusion, although it has no effect on systolic blood pressure. In contrast, administration of an EP3 antagonist, L798, 106 prevented a reduction in cardiac function with Ang II infusion and substantially attenuates the increase in blood pressure. Furthermore, we report that mice overexpressing EP3 in the cardiomyocytes have reduced cardiac function at baseline, an exacerbated decline in cardiac function in response to Ang II and increased inflammatory cytokines/chemokines in their left ventricles.

Previous studies have documented the role of the EP3 receptor in hypertension by performing studies on vascular reactivity [439]. Using global EP3 knockout mice, Chen et al. showed that the mice display reduced systolic blood pressure at baseline and a reduced pressor response to Ang II [439]. Our current study is novel in that utilizes systemic administration of the EP3 agonist and antagonist and employs the cardiomyocyte-specific EP3 overexpressing mice. Our data suggests that the EP3 receptor may act synergistically with Ang II to increase blood pressure.

The Rho/Rho-kinase cascade has been shown to play an important role in regulating cardiovascular function [251, 281, 282, 284, 450, 451]. For example, Guan et al. have shown in rats with transverse aortic constriction pressure overload, cardiac function was improved when the rats were treated with the Rho-kinase inhibitor fasudil [452]. Moreover, they showed this was due to a reduction in reactive oxygen species. Similar cardioprotective effects were observed in a mouse model of autoimmune myocarditis when mice were treated with fasudil [453]. Interestingly, in the aforementioned study, Dai et al. found a shift in the cardiac T cell population from Th17 to Treg, suggesting Rho-kinase may directly affect the T cell population and IL-17 production. In our current study, we observed an increase in RhoB expression in the mesenteric arteries in response to Ang II, and this was reduced with L798, 106 treatment. There was no change in RhoA expression in the mesenteric arteries. We speculate that because RhoA is the constitutively expressed isoform, it would be necessary to measure RhoA activity rather than the expression. These experiments were not performed in this study. In the left ventricle, RhoB expression was completely undetectable, while RhoA was robustly detected. This agrees with the literature showing only the RhoA isoform is expressed in cardiomyocytes [454]. Interestingly, when animals received Ang II infusion for 2 weeks, there was a significant decrease in RhoA expression in the LV. It is possible that 2 weeks of Ang II infusion may cause a down-regulation of RhoA, as RhoA is typically shown to be fast-acting in response to Ang II, however this is purely speculation. Furthermore, the RhoA/Rho kinase signaling cascade in response to Ang II treatment has been studied in depth [278-282, 454, 455]. However, little is known about the role of RhoB in Ang II HTN, therefore making our results a novel finding. RhoB could play a role in promoting inflammation in Ang II HTN as it has been shown that RhoB, but not RhoA, is

a mediator of Rho-Kinase-induced NF-κB activation [456]. Inflammation in the mesenteric arteries in response to increased RhoB expression was not studied in this dissertation.

Although the response to L798, 106 in Ang II hypertension in the kidneys and/or central nervous system was not studied in this dissertation, It is known that renal AT1 receptors play a role in Ang II hypertension [457]. It was also shown that EP3 receptor activation in the rostral ventrolateral medulla mediates the pressor effects of PGE_2 [458]. Surprisingly, the EP3 agonist sulprostone had no effect on blood pressure in the Ang II hypertension model. It was previously reported that sulprostone invokes contraction of guinea-pig aorta and induces Ca^{2+} influx [459]. Other studies have confirmed the ability of EP3 receptor activation to mobilize Ca^{2+} [460-462]. Unlike these studies performed *in vitro* or on isolated artery preparations, our current study utilized systemic injections of the EP3 agonist. The calcium dynamics of EP3 antagonism was not studied in this dissertation, however, and this could serve as a future project.

We repeated the L798, 106 experiment using isoproterenol infusion, another model of non-ischemic heart failure. We observed a robust increase in heart rate, as expected with β-adrenergic stimulation, and a modest, but significant increase in systolic blood pressure after 10 days of isoproterenol infusion. However, there was no effect of L798, 106 on heart rate, blood pressure, or cardiac function. These data suggest that the effects of EP3 receptor antagonism are unique to the Ang II signaling pathway.

To study the effects of EP3 in the heart specifically, we obtained transgenic mice that overexpress EP3 in the cardiomyocytes. The EP3 Tg mice were a gift from the University of Dusseldorf. They previously reported that the hearts of these mice are markedly hypertrophied, which is obvious as early as 5-6 weeks of age and that they have reduced ejection fraction at baseline [463]. They also reported that overexpression of EP3

is protective in a mouse ischemia-reperfusion model due to the reduced contractility of the left ventricle, which would normally result in depletion of ATP [268, 463]. However, we are the first to show that these mice have an exacerbated response to Ang II infusion as well as increased inflammation in their left ventricles as evidenced by increased TNF-α and IL-1β, two cytokines associated with heart failure [384, 464, 465]. There was also reduction of anti-inflammatory cytokines IL-10 and IL-4. Interestingly, it was also observed that mRNA levels of the chemokine MCP-5 were unchanged between EP3 WT and EP3 Tg mice. MCP-5 is a potent chemoattractant molecule for monocytes and macrophages and we speculate that this could account for the lack of increased macrophages in the EP3 Tg heart, as determined by immunohistochemistry. However, the EP3 Tg mouse hearts did show a significant increase in the number of infiltrating T cells.

The work in this chapter has resulted in a manuscript that is in preparation. The results showing the importance of the EP3 in hypertension could lead to the development of new drugs targeting both the Angiotensin II receptors as well as EP3 for example. Furthermore, it is important to understand the deleterious effects of EP3 in the heart during hypertension as well as the detrimental effects of EP3 independent of blood pressure.

CHAPTER 6 – DEVELOPMENTAL METHODOLOGY

Importance of a Cardiomyocyte Specific EP3 KO Mouse

We published that treatment of adult mouse cardiomyocytes with the EP1/EP3 agonist sulprostone and/or PGE_2 resulted in reduced departure velocity, a measure of contractility. We verified this using a Langendorff preparation and *in vivo* using pressure-volume loops and showed reduced +dp/dt and –dp/dt. PGE_2 and sulprostone both decreased +dp/dt, while the EP4 agonist increased +dp/dt [217]. Therefore, we concluded that the deleterious effects of PGE_2 are likely mediated via the EP3 receptor. Furthermore, we have reported that expression of the EP3 receptor increases in the mouse heart in response to injury (MI and/or Ang II infusion). Therefore, we overexpressed EP4 in the cardiomyocytes (Chapter 2) and observed significant improvements in parameters of cardiac function, a reduction in infiltrating macrophages and T cells, reduced MMP expression and fibrosis, and a reduction of the pro-inflammatory chemokine MCP-1 [216]. We concluded that overexpression of EP4 helps tip the balance towards activation of the EP4 receptor. Based on these previous studies, we sought to generate the cardiomyocyte specific EP3 knockout and hypothesized that lack of EP3 in the cardiomyocyte would improve cardiac function after injury.

Generation of a Conditional Cardiomyocyte Specific EP3 Knockout Mouse

The use of recombinases such as Cre recombinase to generate tissue specific knockouts has become a very common research tool. In general, the gene of interest to be knocked out is flanked by loxP sites. If two loxP sites are placed in the same orientation in sequence, the floxed gene will be excised by the activity of Cre [466].

Our cardiomyocyte specific EP3 knockout mouse (EP3 KO) utilizes this technology to generate a conditional knockout model. The model is conditional since the EP3 gene

is only knocked out once the mice are treated with tamoxifen. Once tamoxifen is administered, a conformation change in the ER ligand-binding domain induces nuclear translocation and activation of the Cre recombinase. This results in excision of the loxP-flanked gene sequence [467]. Verification of our mouse genotype is performed by a company called Transnetyx®. This company is a non-biased automated genotyping service. Ear biopsies of the mice are sent to their lab and they detect the presence or absence of MerCreMer (indicated by a + or – symbol) and the presence or absence of the EP3 floxed gene (Figure 49). We have confirmed the presence of MerCreMer in the heart by western blot analysis (Figure 50).

Conditional EP3 KO	Esr-Cre TG	Ptger3-4 FL	Ptger3-4 WT
Wellplate: T672395			
A1 34945	-	+	-
B1 34946	+	+	-
C1 34947	-	+	-
D1 34948	-	+	-
E1 34949	+	+	-
F1 34950	-	+	-

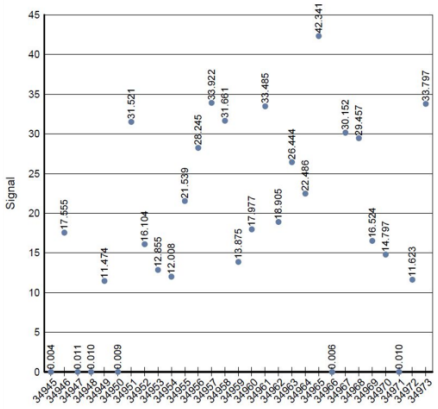

Figure 49: Representative Transnetyx® Genotyping Results. *Left*: Representative genotyping results from Transnetyx® (not all results are shown). 3 probes are used to genotype the mice. Esr-Cre detects the presence of the MerCreMer, Ptger3-4 FL detects the presence of EP3 floxed by LoxP sites in exon 1, while Ptger3-4 WT detects the presence of unfloxed, wild type EP3. The results indicate that all mice are positive for floxed EP3 and negative for wild type. *Right*: Representative 'raw data' file from Transnetyx® demonstrating the results for MerCreMer. Note the very low signals for 34945, 34947, 34948, and 34950, all of which were negative (-) for MerCreMer expression. Also note there is varying signal strength for MerCreMer positive (+) mice, most likely a difference between heterozygote and homozygote mice.

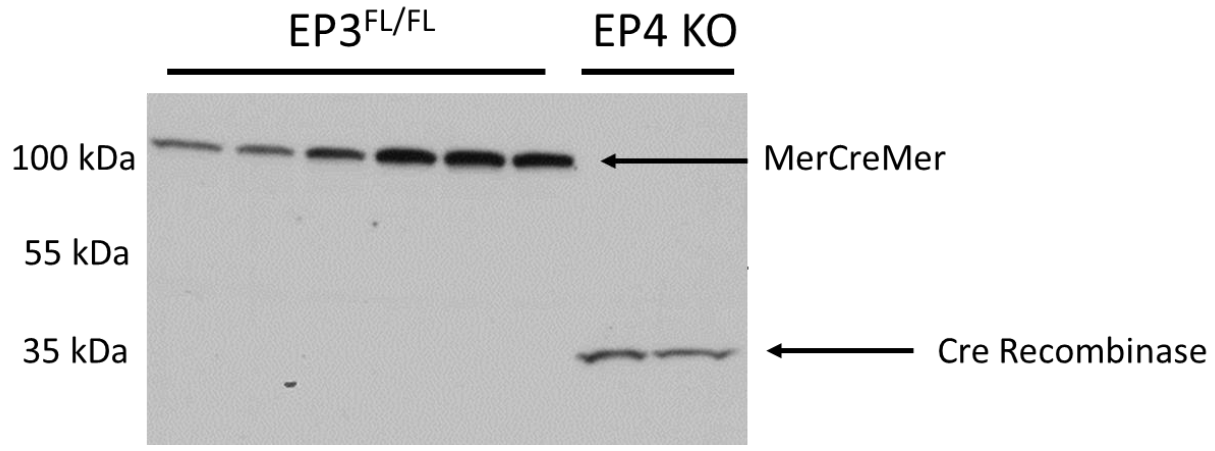

Figure 50: Western Blot Analysis of MerCreMer and Cre Recombinase. Representative western blot from left ventricle tissue of EP3 floxed (EP3 $^{FL/FL}$) mice showing constitutive expression of the MerCreMer protein. As a control, we loaded equal amounts of two EP4 KO left ventricle samples which express the Cre recombinase protein. Thus, our EP3 KO mice express only MerCreMer.

The EP3 floxed mice were acquired from cryopreservation from Jackson Laboratories. To generate the EP3 floxed mice, a vector containing the *Ptger3* (EP3) sequence and neomycin/kanamycin resistance genes was used. 70 bp upstream of the start codon for exon 1, a loxP site was inserted. Another loxP site was inserted 408 bp downstream of exon 1. This construct was electroporated into 129S4/SVJ derived J1 embryonic stem cells. Correct embryonic stem cells were then transfected with a plasmid to remove the marker cassette. The cells that now only retained the loxP-flanked exon 1 were injected into C57BL/6 blastocysts resulting in chimeric male animals. These mice were then back crossed to 129X1/SVJ mice (Stock No. 000691). The resulting mice were crossed to generate homozygotes and then back crossed one time to C57 BL/6J mice. Once we obtained the EP3 floxed mice from Jackson Labs, we began establishing breeder pairs to maintain the EP3 floxed gene. At the same time, we established breeding with another line of mouse, the αMHC-MerCreMer mouse.

The αMHC-MerCreMer mouse line expresses Cre recombinase fused to mutated

estrogen receptor (ER) ligand-binding domains (MerCreMer) only in the cardiomyocytes. This MerCreMer protein is under control of the alpha myosin heavy chain promoter (αMHC). There are two myosin heavy chain genes that are expressed in the mammalian heart; αMHC and βMHC [468]. The alpha myosin heavy chain gene encodes a cardiac-specific protein involved in muscle force generation and has been widely used in transgenic models to drive the expression of proteins of interest in the cardiac muscle specifically. Therefore, the αMHC drives the expression of Cre specifically in the cardiomyocytes. The Cre-ER proteins are sensitive to tamoxifen but insensitive to estrogen. Also, the fusion proteins are sequestered in the cytoplasm in an inactive state in the absence of a ligand (tamoxifen).

Treatment with tamoxifen has well known cardiac toxicity in the mouse model, although the mechanism is unknown [469-472]. Consistent with published data, injection of tamoxifen in our mice resulted in substantial left ventricle dilatation and reduction of cardiac function. This condition improved however after allowing the mice to rest for at least 1 week following tamoxifen treatment. In fact, ventricle size and function is completely back to normal by 2 weeks (Table 5). We determined that the optimal time and dose of tamoxifen was daily intraperitoneal injections of 30 μg x g^{-1} x day^{-1} for 7 days followed by at least 7 days of rest. This resulted in approximately 80 % knockdown of EP3 using real time RT-PCR primers targeting only exon 1.

Table 5: **Echocardiography Data of EP3 KO Mice**

7 days Tamoxifen - No Rest	Treatment Group		
Cardiac Parameter	**Vehicle (Corn oil)**	**30 μg x g^{-1} x day^{-1}**	**60 μg x g^{-1} x day^{-1}**
Ejection Fraction (%)	73.88 ± 0.39	69.91 ± 5.56	67.37 ± 3.13
Shortening Fraction (%)	61.03 ± 1.52	56.87 ± 2.73	54.81 ± 3.56
Left Ventricle Dimension in Systole (mm)	1.00 ± 0.07	1.18 ± 0.14	1.33 ± 0.16
Left Ventricle Dimension in Diastole (mm)	2.58 ± 0.16	2.70 ± 0.13	2.92 ± 0.16
Posterior Wall Thickness in Systole (mm)	1.28 ± 0.01	1.23 ± 0.02	1.25 ± 0.01
Area in Systole (mm^2)	0.97 ± 0.18	1.39 ± 0.56	1.59 ± 0.39
Area in Diastole (mm^2)	3.68 ± 0.62	3.70 ± 0.70	4.64 ± 0.67
Sample Number (N)	4	6	5

7 days Tamoxifen - 2 Weeks Rest	Treatment Group		
Cardiac Parameter	**Vehicle (Corn oil)**	**30 μg x g^{-1} x day^{-1}**	**60 μg x g^{-1} x day^{-1}**
Ejection Fraction (%)	73.88 ± 1.18	72.15 ± 0.64	70.34 ± 0.45
Shortening Fraction (%)	64.35 ± 0.97	59.38 ± 0.53	64.04 ± 1.60
Left Ventricle Dimension in Systole (mm)	0.91 ± 0.04	1.04 ± 0.05	0.94 ± 0.06
Left Ventricle Dimension in Diastole (mm)	2.57 ± 0.09	2.58 ± 0.10	2.63 ± 0.13
Posterior Wall Thickness in Systole (mm)	1.28 ± 0.04	1.25 ± 0.01	1.26 ± 0.05
Area in Systole (mm^2)	0.88 ± 0.15	0.83 ± 0.04	0.88 ± 0.06
Area in Diastole (mm^2)	3.23 ± 0.42	2.98 ± 0.10	2.98 ± 0.15
Sample Number (N)	4	6	5

Cardiac parameters assessed in conscious mice by echocardiography immediately following tamoxifen injections (top-no rest) or 2 weeks after tamoxifen (bottom-2 weeks rest). Mice received either corn oil vehicle or tamoxifen at 30 μg x g^{-1} x day^{-1} or 60 μg x g^{-1} x day^{-1} for 7 days.

Troubleshooting the Generation of the EP3 KO Mouse

Initial tests of the mice resulted in zero knockdown of EP3 with the treatment of tamoxifen. We used various different doses of tamoxifen and different rest times. All initial attempts resulted in inconsistent results, although no consistent knockdown of EP3. The first attempts utilized intraperitoneal injections of tamoxifen at 40 μg x g^{-1} x day^{-1} or corn oil vehicle for 6 days followed by 2 weeks recovery time. Using real time RT-PCR and EP3 primers designed by Qiagen (Cat No. 330001 PPM04249A) we did not generate any knockdown of EP3 (Figure 51). Next, it was investigated if the length of time for tamoxifen administration was the limiting factor. We administered tamoxifen for 2 weeks at 30 μg x g^{-1} x day^{-1} I.P. Again, there was no reduction of EP3 mRNA expression with tamoxifen treatment (Figure 52).

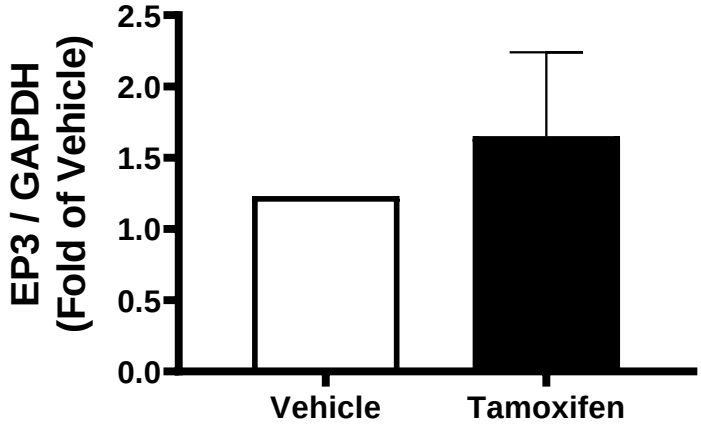

Figure 51: EP3 mRNA Expression to Test Knockdown. Real time RT-PCR analysis of EP3 using primers from Qiagen that recognize exon 2 of the EP3 transcript and detect all three splice variants of EP3. N=2 in vehicle group and N=3 in tamoxifen group.

Figure 52: EP3 mRNA Expression to Test Knockdown. Real time RT-PCR analysis of EP3 mRNA using primers that recognize exon 2 of the EP3 transcript and detect all three splice variants of EP3. Mice received tamoxifen at 30 µg x g^{-1} x day^{-1} for 2 weeks. N=4 in vehicle group and N=6 in tamoxifen group.

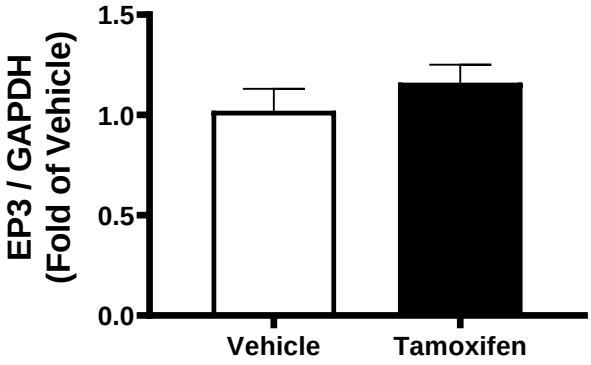

After several months of administering different doses, for various lengths of time, and varying the recovery time, it was decided to re-analyze the detection method for EP3 mRNA knockdown. The primers being used detected exon 2 of the EP3 gene. Since exon 1 is the floxed region in the EP3 KO model, we requested that the company TIB MolBiol design three different sets of primers that are only in exon 1 (Figure 53). We then repeated the tamoxifen protocol, administering 30 µg x g^{-1} x day^{-1} or 60 µg x g^{-1} x day^{-1} for 7 days followed by rest. After 2 weeks, there was knockdown of EP3 mRNA with both doses (Figure 54). Since cardiac function was worse with the higher 60 µg x g^{-1} x day^{-1} dose, it was determined that 30 µg x g^{-1} x day^{-1} is the optimal dose.

920899	Mus musculus prostaglandin E receptor 3 (subtype EP3) (Ptger3), transcript variant 1, mRNA		NM_001359745	Tm
Ptger3 F1	CACCTTCTTCgggCTAACCA	S	520-539	59.0 °C
Ptger3 R1	ggTTgCAggCAAAggTCAC	A	878-860	58.7 °C
Ptger3 F2	CTTAgTggggCAgCTCCTgA	S	427-446	59.3 °C
Ptger3 R2	ggCCACTgCACgCTgTA	A	741-725	57.7 °C
Ptger3 F3	CTgCTATCCCgCAgCTgAg	S	137-155	58.4 °C
Ptger3 R3	TgCACAgCAggAAAgACTTCTT	A	404-383	58.1 °C

Figure 53: Exon 1 Primer Design. (Primer design from TIB MolBiol). Top panel shows the different sequences, ascension number used for sequence identification, and the melting temperature (Tm) for each primer. Bottom scheme shows the location of each primer set within exon 1 of the EP3 gene.

Lastly, tamoxifen was administered daily to mice in their chow. We purchased food containing 40 µg x g^{-1} x day^{-1} tamoxifen (Teklad, Cat no. 130856). This dose assumes that the mice are consuming three-four grams of chow daily. Food consumption was simply monitored by weighing the food daily to be sure that the mice were consuming the chow. It took at least one week for the mice to acclimate to the new chow and begin consuming the recommended amount to achieve the advertised dose. We then left the

mice on this diet for 6 weeks. There was an approximate 57 % decrease in EP3 mRNA compared with mice that received normal chow, unfortunately these data did not reach statistical significance (1.09 ± 0.20 in normal chow vs. 0.43 ± 0.15 in tamoxifen chow mice; p = 0.146, N=6). We concluded that administering tamoxifen via the diet would not be a practical method to obtain EP3 knockdown as it took 6 weeks to achieve only 57 % knockdown.

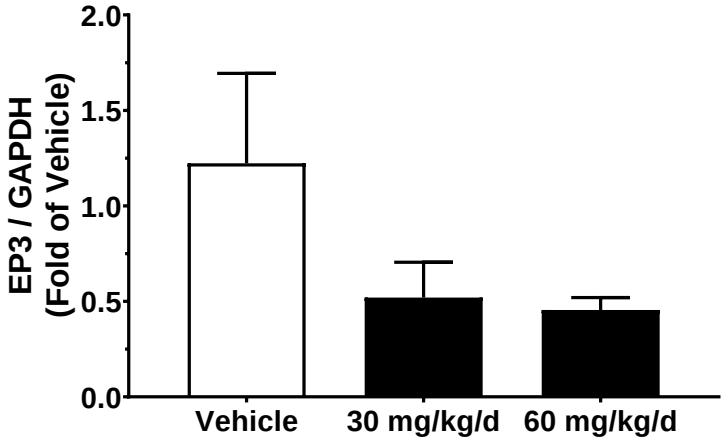

Figure 54: EP3 mRNA Expression to Test Knockdown. Real time RT-PCR analysis of EP3 using primers from TIB MolBiol that recognize exon 1 of EP3 (primer design pair F3/R3). Mice received tamoxifen at 30 µg x g^{-1} x day^{-1} or 60 µg x g^{-1} x day^{-1} for 7 days, followed by 2 weeks rest. N=3

Flow Cytometry for the Characterization of the EP3 Transgenic Mouse

In order to confirm our immunohistochemistry results showing increased T cell infiltration in the EP3 Tg mouse heart under basal conditions, we sought to perform flow cytometry analysis from EP3 WT and EP3 Tg mouse hearts for F4/80+ macrophages and CD3+ T cells. Flow cytometry is a sensitive and quantitative method to rapidly count cells in any tissue of interest on a much larger scale than possible by normal immunohistochemistry or immunofluorescence.

Flow Cytometry Methods

Hearts were excised from 10-12 wk. old C57Bl/6 mice and immediately immersed in ice-cold HBSS to wash out red blood cells. Washes were repeated until buffer was clear. The hearts were then transferred to a beaker containing ice-cold HBSS and

mechanically minced using scissors. Hearts were then allowed to pellet via gravity on ice. The HBSS was then aspirated off and the minced pellet was resuspended in 2.5 ml of digestion buffer (200 U/ml collagenase + 100 µg/ml DNase II). This solution was then stirred on low power at room temperature until the hearts were fully digested. After digestion, the solution was pipetted twice through an 80 µm sieve to remove undigested tissue and cardiomyocytes. This was followed by a wash with Dulbecco's PBS (dPBS) by centrifuging at 1500 rpm for 10 minutes. This was repeated once more. On the last wash, the supernatant was aspirated and the pellet resuspended in 1 % paraformaldehyde solution and fixed overnight at 4^{o}C. The following day, samples were washed with wash buffer (2% heat-inactivated FBS in dPBS) and then each heart was sub divided into aliquots for staining. Nonspecific reactivity was blocked for 1 hour at room temperature with 2 % heat-inactivated FBS as a blocking buffer. Fluorochrome-conjugated antibodies against the T cell surface marker CD3 (anti-CD3 PE, BD Biosciences), anti-F4/80 FITC (BD Biosciences) for detection of the macrophage marker F4/80, and anti-CD45 (CD45-PerCP, BD Biosciences) were added in a 1:10 dilution to the staining aliquots. Fluorochrome-matched isotype controls were used in each assay to adjust for nonspecific staining. Cells were stained for 30 minutes at room temperature, followed by a wash step. Samples were stored at 4^{o}C and flow cytometry was performed within 1-2 hours of staining. Flow cytometry analysis was performed using a LSR II flow cytometer (BD Biosciences) and the data was analyzed using BD FACSDiva^{TM} v8.0.1 software. Cells were gated based on forward and side scatter and a minimum of 20,000 gated events were acquired.

In one experiment, spleens were removed to serve as a control to test specificity of the antibodies. Spleens were handled and stained in the same manner as described

above for the hearts.

Flow Cytometry Troubleshooting

The first attempt at performing flow cytometry and optimizing the protocol to detect macrophages and T cells was with using the left ventricle from an EP3 WT mouse. Working with an expert immunologist in the flow cytometry core at Henry Ford Hospital, we obtained protocols to begin a trial experiment. This initial attempt involved an additional step in the methods using a Ficoll-paque gradient centrifugation to concentrate the leukocytes from the heart digest. The major issue that occurred was the small number of cells that we obtained. Figure 55 shows a representative forward/side scatter plot from an unstained control sample with the gating set to obtain live cell events and a chart displaying the total number of events. The resulting number of events was small (1,254 events). It was later determined that the Ficoll-paque reagent used would not work for mouse samples, as mouse leukocytes have a higher density than human leukocytes. In subsequent experiments, hearts were digested, washed, and fixed without the Ficoll-paque centrifugation step.

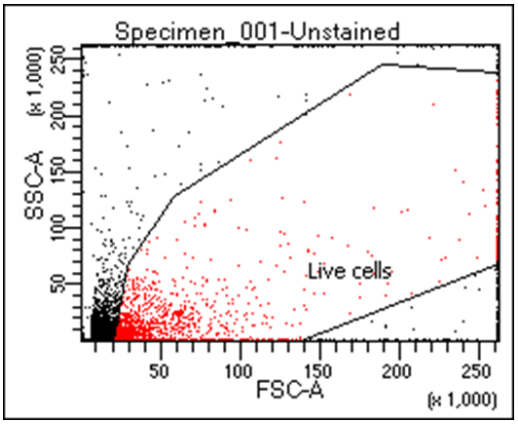

Tube Name:	Unstained			
Record Date:	Oct 26, 2018 3:18:02 PM			
Population	#Events	%Parent	FITC-A Geo Mean	PE-A Geo Mean
All Events	5,546	####	####	####
Live cells	1,254	22.6	####	####
488	15	1.2	9,721	####
PE	84	6.7	####	3,781

Figure 55: Flow Cytometry Side/Forward Scatter Plot. The plot on the left shows the forward and side scatter from an unstained control sample to demonstrate the gating technique used to obtain live cell events. The table on the right shows the quantified number of live events.

In the next experiment, the number of gated live cells improved dramatically by skipping the Ficoll-paque protocol. However, there was an issue of antibody signal acquisition as the F4/80-FITC signal was weaker than its isotype control (Figure 56) making it difficult to determine if the F4/80-FITC signal was truly macrophage specific (4.2 % in the FITC isotype vs. 2.0 % in F4/80-FITC). Likewise, Figure 57 shows the background isotype signal for the CD3-PE antibody signal was just as strong as the CD3-PE signal itself (5.0 % in the PE isotype vs. 5.3 % in CD3-PE). As a positive control for the antibody specificity, the spleen was collected since it is known to contain a large amount of leukocytes. Figure 59 shows that the antibody signal / isotype signal for the CD3 T cells was much higher than in the heart, suggesting the antibody used is in fact specific (0.7 % in the PE isotype vs. 28.0 % in CD3-PE). For the F4/80 macrophages however, the F4/80-FITC signal was identical to the FITC isotype (Figure 58; 2.5 % in FITC isotype vs. 2.6 % in F4/80-FITC). Thus, the antibody signal / isotype signal improved, although it is still not optimal.

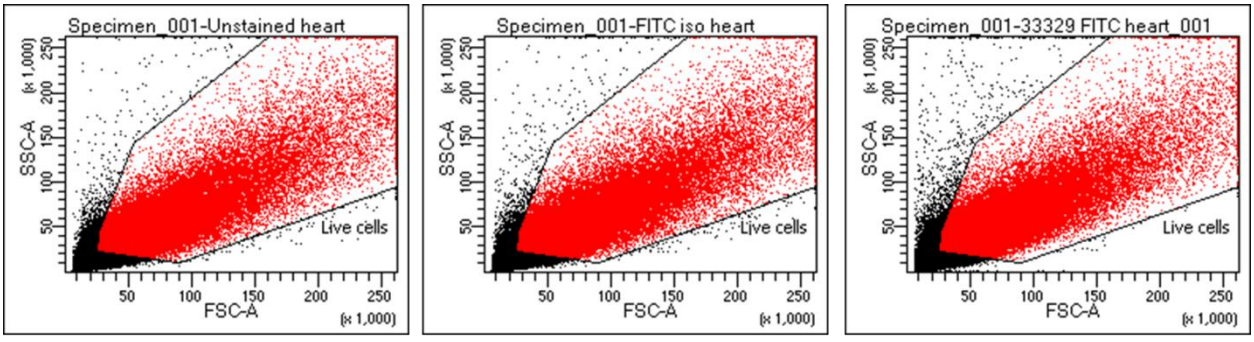

Tube Name: Unstained heart
Record Date: Dec 27, 2018 2:14:18 PM

Population	#Events	%Parent	FITC-A Geo Mean	PE-A Geo Mean
All Events	302,669	####	####	####
Live cells	48,975	16.2	####	####
F4/80	527	1.1	4,174	4,671
CD3	21	0.0	12,553	13,775

Tube: FITC iso heart

Population	#Events	%Parent	%Total
All Events	282,073	####	100.0
Live cells	58,730	20.8	20.8
F4/80	2,455	4.2	0.9
CD3	21	0.0	0.0

Tube: 33329 FITC heart_001

Population	#Events	%Parent	%Total
All Events	254,919	####	100.0
Live cells	54,483	21.4	21.4
F4/80	1,110	2.0	0.4
CD3	10	0.0	0.0

Figure 56: Flow Cytometry F4/80-FITC Results in LV. Left panel shows the unstained portion of the heart as a control to set the live cell gating. The middle panel represents the portion of the heart that was stained with the isotype-FITC control antibody. Note the % parent = 4.2 % for the control antibody. The right panel represents the portion of the heart that was stained with F4/80-FITC. Note the % parent is less than the isotype control = 2.0 %. N=1 mouse heart.

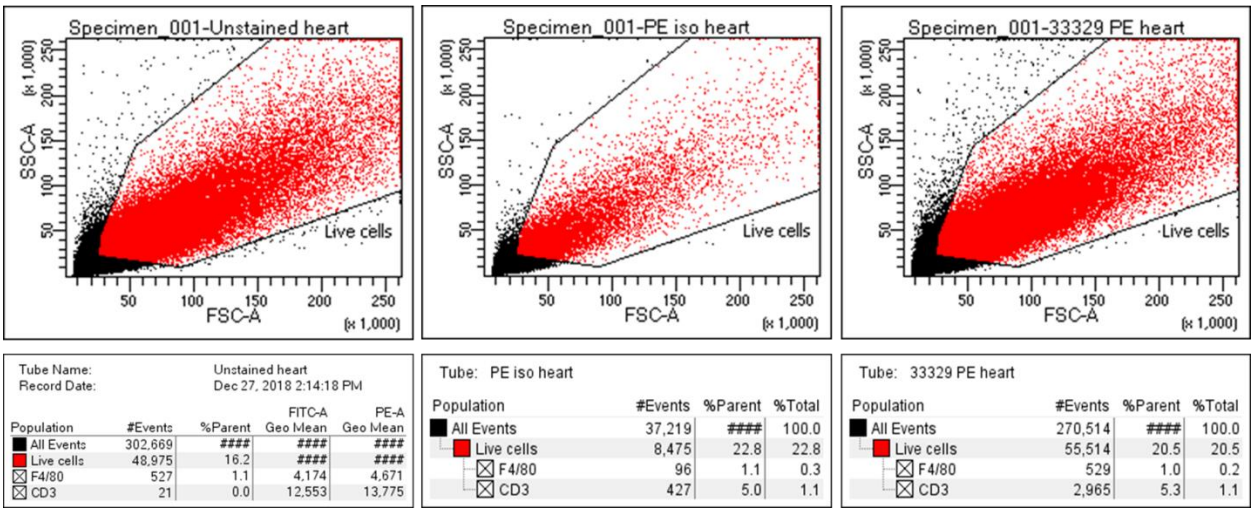

Figure 57: Flow Cytometry CD3-PE Results in LV. Left panel shows the unstained portion of the heart as a control to set the live cell gating. The middle panel represents the portion of the heart that was stained with the isotype-PE control antibody. Note the % parent = 5.0 % for the control antibody. The right panel represents the portion of the heart that was stained with CD3-PE. Note the % parent is only 5.3 % compared to the control. N=1 mouse heart.

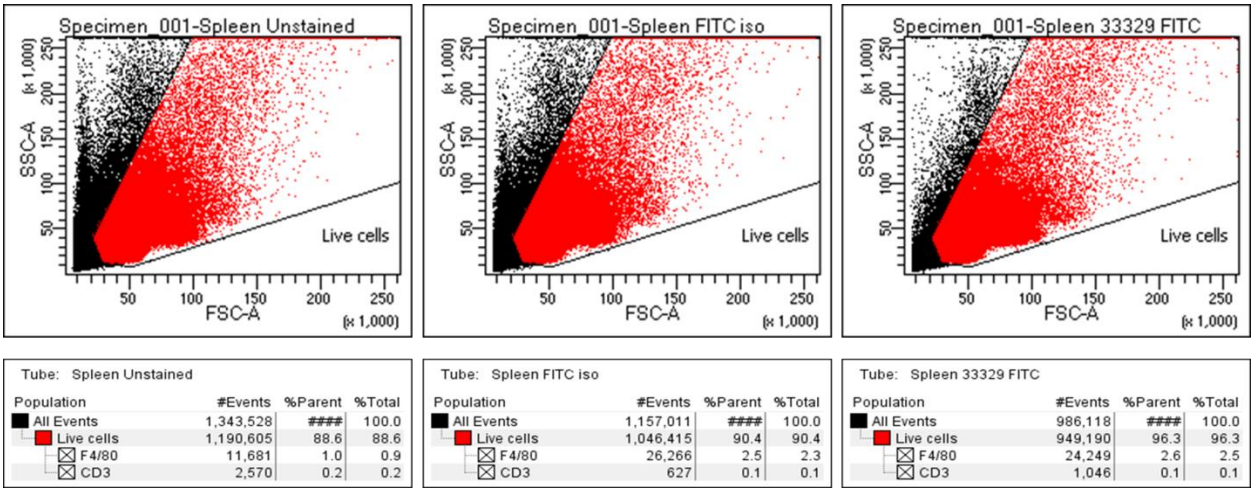

Figure 58: Flow Cytometry F4/80-FITC Results in Spleen. Left panel shows the unstained portion of the spleen as a control to set the live cell gating. The middle panel represents the portion of the spleen that was stained with the isotype-FITC control antibody. Note the % parent = 2.5 % for the control antibody. The right panel represents the portion of the spleen that was stained with F4/80-FITC. Note the % parent is 2.6 % compared to the control. N=1 mouse spleen.

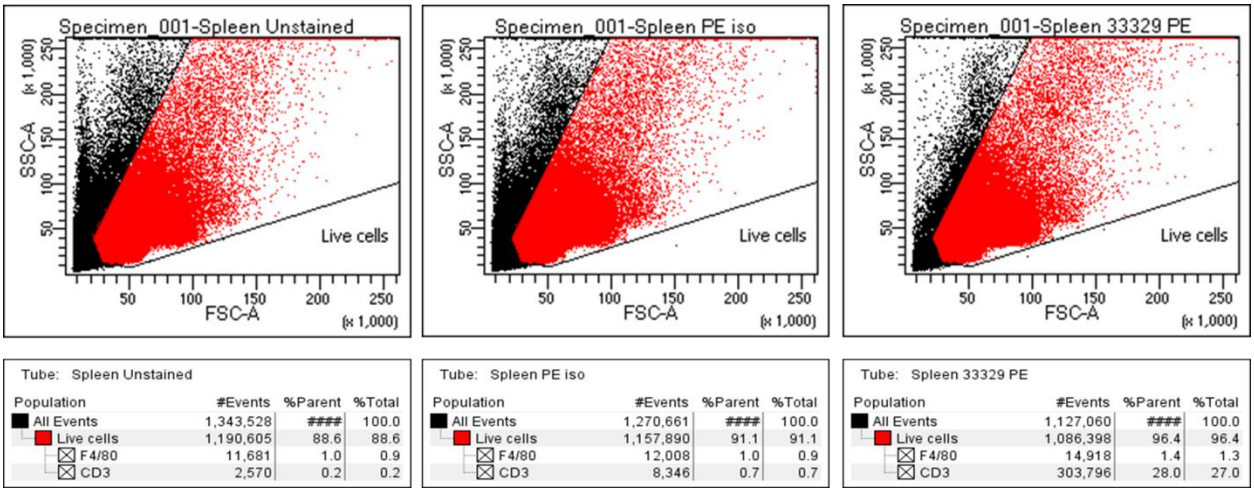

Figure 59: Flow Cytometry CD3-PE Results in Spleen. Left panel shows the unstained portion of the spleen as a control to set the live cell gating. The middle panel represents the portion of the spleen that was stained with the isotype-PE control antibody. Note the % parent = 0.7 % for the control antibody. The right panel represents the portion of the spleen that was stained with CD3-PE. Note the % parent is 28.0 % compared to the control. N=1 mouse spleen.

Since all cells of hematopoietic origin express the surface marker CD45+, we have also tried to first gate the cells based on CD45+ expression and then acquire the subsequent CD3+ and F4/80+ cells. Figure 60 demonstrates our ability to gate the cells based on CD45+ cells. The cells in this population were $CD3^-$ and $F4/80^-$, as expected when the gate was specific for CD45+ cells. Surprisingly, when the cells were stained for CD3+ and F4/80+, there was no F4/80+ cells within the CD45+ population. CD3+ cells comprised 24.0 % of that same CD45+ population (Figure 61).

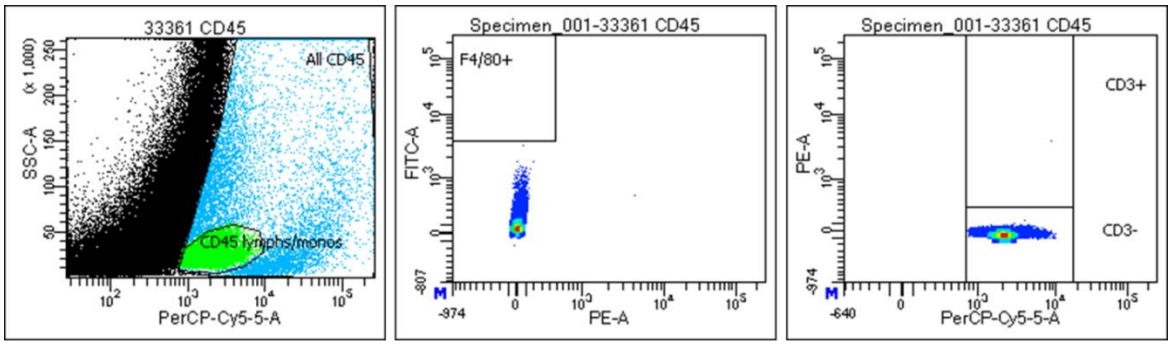

Tube: 33361 CD45

Population	#Events	%Parent	%Total
All Events	222,686	####	100.0
CD45 lymphs/monos	18,497	8.3	8.3
CD3-	18,495	100.0	8.3
F4/80+	0	0.0	0.0
CD3+	1	0.0	0.0
All CD45	31,221	14.0	14.0

Figure 60: Flow Cytometry CD45 Gating Strategy (Control). Top left panel shows the portion of the heart used as a control to set the live cell gating based on the CD45-PerCP+ population. Note the gate is much smaller than in previous figures, and only surrounds the lymphocyte/monocyte population. The top middle panel represents the portion of the heart that was F4/80-FITC positive (0.0 %). The top right panel represents the portion of the heart that was CD3-PE+ (0.0 %). N=1 mouse heart.

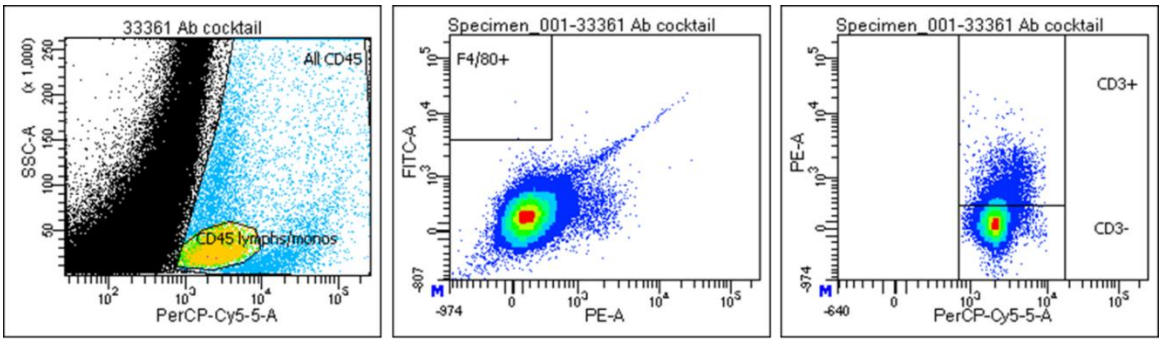

Tube: 33361 Ab cocktail

Population	#Events	%Parent	%Total
All Events	307,349	####	100.0
CD45 lymphs/monos	17,589	5.7	5.7
CD3-	13,605	77.3	4.4
F4/80+	6	0.0	0.0
CD3+	4,227	24.0	1.4
All CD45	27,266	8.9	8.9

Figure 61: Flow Cytometry CD45 Gating Strategy (F4/80+ and CD3+ Cocktail). Top left panel shows the live cell gating based on the CD45-PerCP+ population. The top middle panel represents the portion of the heart that was F4/80-FITC positive (0.0 %). The top right panel represents the portion of the heart that was CD3-PE+ (24.0 %). N=1 mouse heart.

Flow Cytometry Conclusion

Further optimization of the protocol is necessary in order to accurately determine the number of macrophages and T cells present in the heart. Once the ideal protocol is determined, flow cytometry will be a very useful tool for the lab to analyze any cell type of interest in the heart at baseline or in the disease state (Ang II hypertension, MI, etc.). One potential issue with the current protocol could be the isotype controls being used. Consistently we obtain higher signal with the isotype control, although the isotype is the same IgG and of the same host species as the primary antibody. One possible solution is to try isotypes from alternative companies. Additionally, to circumvent the low number of macrophages at baseline, we could first use a model like MI, whereby there is a known increase in macrophages and T cells. This would confirm that the antibodies are specific and that the dilutions of antibody are appropriately titrated. Lastly, we think the initial gate on CD45+ cells (Figures 60 and 61) is ideal to obtain the highest yield of macrophages and T cells.

CHAPTER 7 – OVERALL DISCUSSION

In this thesis, we sought to determine the role of PGE_2 in heart failure and cardiac remodeling in MI and the Ang II hypertension models. Building on our previously published work, we hypothesized in the initial study that overexpression of the EP4 receptor is cardioprotective in a mouse model of MI by antagonizing the deleterious effects of EP3. Our results support our hypothesis and show, for the first time, that delivery of the EP4 receptor via an AAV9 viral package is sufficient to improve cardiac function in mice with MI. After administration of AAV9-EP4 there were significant improvements in ejection fraction, shortening fraction, and left ventricular dimensions. There was also reduced fibrosis determined by picrosirius red staining and reduced hypertrophy, determined by real time RT-PCR for BNP and β-MHC as well as myocyte cross sectional area analysis. With regard to inflammation, administration of AAV9-EP4 prevented an increase in TNF-α mRNA after MI, reduced MCP-1 protein levels, and increased levels of IL-10, thus promoting an anti-inflammatory environment. The mechanism of how EP4 overexpression affects production of these chemokines/cytokines is unclear and was not addressed in the present study but lays a solid foundation for future projects. However, we speculate that due to the close proximity of cardiomyocytes and cardiac fibroblasts and/or their direct interactions within the heart, perhaps there are paracrine effects resulting in altered fibroblast/myofibroblast activity. It is also possible that the reduced macrophage and T cell infiltration that occurred with EP4 overexpression is responsible for the reduced pro-inflammatory signaling. Characterizing the cell infiltrate post-MI with EP4 overexpression using flow cytometry would be a useful and novel project for future studies with important therapeutic implications. Additionally, we showed reduced expression of iNOS, a M1 macrophage marker, in the left ventricles of these mice,

although we never delineated which cell type this was occurring in. Furthermore, additional markers of the M1 phenotype would be needed to draw this conclusion. Future studies could use the flow cytometry to analyze the M1/M2 macrophage populations in the heart.

In the course of these studies, I also gained invaluable experience in generating a novel mouse strain. This dissertation has led to the generation of a conditional cardiomyocyte-specific EP3 knockout mice in which EP3 is deleted in the cardiomyocyte upon administration of Tamoxifen (see Chapter 6). Preliminary data indicate that these mice have normal cardiac function at baseline, but we hypothesize will be protected from the deleterious effects of MI and Ang II hypertension and that these effects will be similar to those observed after EP4 overexpression. These hypotheses will be tested in future work.

To investigate how EP4 receptor signaling affects chemokine production (MCP-5 specifically) within the cardiac fibroblasts, we performed *in-vitro* experiments that are presented in this dissertation (chapter 3). The cardiac fibroblasts are known to express both TLR-2 and TLR-4 and thus respond to stimuli such as lipopolysaccharide. We therefore utilized LPS treatment to induce production of the pro-inflammatory chemokine MCP-5 and investigate the role of PGE_2 and its EP4 receptor on MCP-5 regulation. Little is known about the regulation of MCP-5 but we showed that a neutralizing antibody to MCP-5 prevents macrophage migration *in vitro* after mouse cardiomyocytes are damaged with hydrogen peroxide. Therefore, MCP-5 seems to be a key chemoattractant in mice for monocytes/macrophages. We hypothesized that PGE_2 inhibits LPS-induced MCP-5 secretion in mouse cardiac fibroblasts via its EP4 receptor. Our results show that both PGE_2 and an EP4 receptor agonist (CAY10598) reduce LPS-stimulated MCP-5 secretion.

This was shown to be due to reduced AKT phosphorylation and subsequent NF-κB activation. It remains to be determined however, whether MCP-5 has NF-κB binding domains in its promoter region, as review of the literature and promoter analysis software show little evidence for that fact. However, our data strongly suggests a role for NF-κB in the regulation of MCP-5 under LPS-stimulated conditions. Also, it has been shown that the close human analogue to MCP-5, MCP-1, does have NF-κB binding domains in its promoter and is largely regulated by NF-κB [473], thus supporting our results. Surprisingly, blockade of the EP4 receptor using a specific antagonist did not reverse the effects of PGE_2 suggesting another mechanism is involved. However, the fact that both PGE_2 and its EP4 receptor agonist both antagonize LPS-stimulated MCP-5 production, suggest some involvement of this receptor. Although these *in vitro* studies with cardiac fibroblasts do not represent the full complexity of the *in vivo* situation, they are useful to discern signaling pathways utilized by activation of the EP4 receptor. Indeed, the inhibition of MCP-5 production by an EP4 agonist in cultured cardiac fibroblasts is in complete agreement with a reduction in cytokine production *in vivo* after overexpression of the EP4 receptor.

Similar to the MI model, we have shown here that Ang II hypertension results in an increase in EP3 expression in the heart, particularly in the cardiomyocytes. Systemic administration of an EP3 agonist, sulprostone, had no effect on blood pressure neither under baseline conditions nor after 2 weeks of Ang II infusion. The combination of sulprostone and Ang II did have deleterious effects on cardiac function by significantly reducing ejection fraction and shortening fraction, although these reductions were modest and still within normal physiological limits. Future studies with the transgenic EP3 mice that overexpress EP3 only in the cardiomyocytes, and the cardiomyocyte specific

conditional EP3 KO mice would be able to compare and contrast systemic EP3 activation versus the specific effects of EP3 in the heart. Surprisingly, antagonism of the EP3 receptor using L798, 106 substantially attenuated the increase in blood pressure with Ang II infusion by approximately 30 mmHg. We speculate that the Ang II receptor (AT_1) and the EP3 receptor may share common downstream signaling. sulprostone treatment in combination with Ang II did not exacerbate the increase in systolic blood pressure but antagonism of the EP3 receptor reduced blood pressure, suggesting commonality between these two pathways and that the EP3 receptor may be necessary for the effects of Ang II. It also cannot be ruled out that there is a dimerization events between EP3 and AT_1, or other G-protein coupled receptors, as this is not known and should be investigated in future studies. Ang II infusion along with L798, 106 administration did not affect cardiac output, measured by echocardiography, thus the effects on blood pressure are likely not occurring at the level of the heart. Interestingly, we found that RhoB, but not RhoA, expression increased significantly in the mesenteric artery, a resistance vessel. This increase in RhoB was significantly attenuated with L798, 106 treatment. RhoA expression decreased in the left ventricle in response to Ang II, however, we speculate that this small, but significant effect is not physiologically relevant. Activity assays for RhoA would need to be performed to truly determine if RhoA signaling was reduced in response to Ang II. Nonetheless, our data with RhoB suggests the effects on blood pressure with L798, 106 are occurring at the level of the vasculature and via changes in total peripheral resistance. Little is known about RhoB and its role in hypertension, therefore these data is novel in suggesting that EP3 signaling may modulate its expression. However, we cannot exclude the possibility that EP3 antagonism in the kidneys or the central nervous system may play a key role in regulating blood pressure and those studies were beyond the scope of this

research. In contrast to sulprostone, L798, 106 treatment prevented a decline in cardiac function after 2 weeks of Ang II; specifically, by improving ejection fraction, shortening fraction, and posterior wall thickness. One limitation of these studies is that both sulprostone and L798, 106 were administered via systemic injection and the concentration of compound reaching the heart was not determined. Additionally, studying the effects of the compound on the heart specifically poses challenges.

To circumvent this, the EP3 Tg mouse model was used, whereby EP3 is overexpressed specifically in the cardiomyocytes. In chapter 4 of this dissertation, we confirm the previously published findings using echocardiography, showing the EP3 Tg mice have reduced cardiac function at baseline [268, 463]. Importantly, we are the first to show that the left ventricles of these mice have increased expression of TNF-α and IL-1β mRNA, with reductions in IL-10 and the M2 macrophage marker, arginase-1. We also show that the protein levels of IL-10 and IL-4 are reduced by ELISA. The cytokine levels were coupled with an increase in $CD3^+$ T cells in the left ventricle of EP3 Tg hearts. The inflammatory profile of these mice has not been previously determined and therefore provides important insight into the deleterious effects of EP3 activation independent of changes in blood pressure. Since cardiac function is already reduced at baseline, we hypothesized this decline would be exacerbated in hypertension. There was a propensity for a further reduction in ejection fraction and shortening fraction with Ang II infusion, although more mice are needed to confirm this hypothesis in future studies.

There is increasing evidence for the beneficial effects of EP4 receptor activation in various models [244, 257-259, 372, 393, 394, 474]. Very recently, it was reported that mPGES-1 reduces ischemia/reperfusion injury via activation of endothelial EP4 and improvements in microcirculation [475]. An EP4 receptor agonist has also been tested

clinically, with positive potential, although it has not been tested in heart failure conditions as of yet [476]. Altogether, the results of this dissertation support a role for the use of an EP4 receptor agonist in human heart failure conditions, both ischemic and non-ischemic, to offset the deleterious actions of the EP3 receptor by improving cardiac function and reducing persistent myocardial inflammation. Finally, it is expected that future studies derived from the results of these studies will indicate whether use of EP3 antagonists have a role in the treatment of heart failure.

APPENDIX A

IACUC PROTOCOL APPROVAL LETTERS

WAYNE STATE UNIVERSITY

Institutional Animal Care
And Use Committee
87 East Canfield, Second Floor
Detroit, Michigan 48201
Phone: (313) 577-1629

ANIMAL WELFARE ASSURANCE # A3310-01

TO: Timothy Bryson
Physiology

FROM: Institutional Animal Care and Use Committee

DATE: March 31, 2017

SUBJECT: Approval of Protocol 17-01-191

TITLE: The Balance Between Prostaglandin E2 EP3 and EP4 Receptors Determines Severity of Cardiac Damage in an Angiotensin II- Induced Model of Hypertension

Protocol Effective Period: March 31, 2017 - March 30, 2020

Your animal research protocol has been approved by the Wayne State University Institutional Animal Care and Use Committee (IACUC).

Be advised that this protocol must be reviewed by the IACUC on an annual basis to remain active. Any changes (e.g. procedures, lab personnel, strains, additional numbers of animals) must be submitted as amendments and require prior approval by the IACUC. Any animal work on this research protocol beyond the expiration date will require the submission of a new IACUC protocol application for committee review and approval.

The *Guide for the Care and Use of Laboratory Animals* (the Guide, NRC 2011) is the primary reference used for standards of animal care at Wayne State University. The University has submitted an appropriate assurance statement to the Office for Laboratory Animal Welfare (OLAW) of the National Institutes of Health. The animal care program at Wayne State University is accredited by the Association for Assessment and Accreditation of Laboratory Animal Care International (AAALAC).

Research Administration
One Ford Place, 2F
Detroit, MI 48202
(313) 874-4360 Office

September 12, 2017

To: Pamela Harding

Fm: Pamela Harding, Ph.D., Chair
Carol Vich., Vice Chair
Institutional Animal Care and Use Committee

Re: **"DELETERIOUS ROLE OF THE EP3 RECEPTOR IN HEART FAILURE "**
(IACUC No. 1579)

Period of IACUC Approval: **Sept. 08, 2017 through Sept. 07, 2020**

Number of Animals Approved: 3, 263 mice/rats

Species:	Ordering Information					Housing Information		Animal Numbers			Total
Experimental Group	Strain	Age	Sex	Weight	Vendor/ Source	Duration of Stay	Type of Housing	Category of Discomfort (see Note 3)			
								C	D	E	
Mouse	C57Bl/6	10-12 wk	M/F		Jackson Labs	3-10 weeks	MI-N/MI/S	155	588		743
Mouse	EP3 KO	10-12 wk	M/F		BC	3-10 weeks	MI-N/MI/S	62	792		854
Mouse	EP3 Tg	10-12 wk	M/F		BC	3-10 weeks	MI-N/MI/S	59	396		455
Mouse	EP3 WT	10-12 wk	M/F		BC	3-10 weeks	MI-N/MI/S	59	396		455
	EP4 KO	10-12 wk	M		BC	3-10 weeks	MI-N/MI/S	0	48		48
	EP4 WT	10-12 wk	M		BC	3-10 weeks	MI-N/MI/S		48		48
Rats	Sprague Dawley Mother Rats with Pups	1-2 day old pups			Charles River	Overnight	Mothers with pups stay in crates overnight and are used the next day.	50			50
Early Mortality								43	567		610
										Total:	3263

Dear Dr. Harding:

Thank you for submitting an application for review by the Institutional Animal Care and Use Committee. The application was presented at a convened meeting on September 08, 2017. A revised application responding to IACUC concerns was reviewed and all concerns were adequately addressed.

The expiration date for this study is September 07, 2020. In order to remain compliant with federal regulations, a new protocol application must be submitted to the IACUC office prior to expiration if you

APPENDIX B

LICENSING AGREEMENT

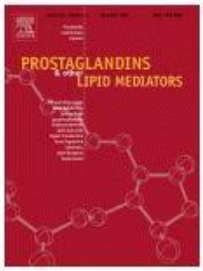

Title: Prostaglandin E2 and an EP4 receptor agonist inhibit LPS-Induced monocyte chemotactic protein 5 production and secretion in mouse cardiac fibroblasts via Akt and NF-κB signaling

Author: Timothy D. Bryson,Jacob Ross,Edward Peterson,Pamela Harding

Publication: Prostaglandins and Other Lipid Mediators

Publisher: Elsevier

Date: October 2019

REFERENCES

1. Touyz, R.M. and E.L. Schiffrin, *Signal transduction mechanisms mediating the physiological and pathophysiological actions of angiotensin II in vascular smooth muscle cells.* Pharmacol Rev, 2000. **52**(4): p. 639-72.
2. von Euler, U.S., *On the specific vaso-dilating and plain muscle stimulating substances from accessory genital glands in man and certain animals (prostaglandin and vesiglandin).* J Physiol, 1936. **88**(2): p. 213-34.
3. Goldblatt, M.W., *Properties of human seminal plasma.* J Physiol, 1935. **84**(2): p. 208-18.
4. Ricciotti, E. and G.A. FitzGerald, *Prostaglandins and inflammation.* Arterioscler Thromb Vasc Biol, 2011. **31**(5): p. 986-1000.
5. Smith, W.L., D.L. DeWitt, and R.M. Garavito, *Cyclooxygenases: structural, cellular, and molecular biology.* Annu Rev Biochem, 2000. **69**: p. 145-82.
6. Shinohara, H., et al., *Regulation of delayed prostaglandin production in activated P388D1 macrophages by group IV cytosolic and group V secretory phospholipase A2s.* J Biol Chem, 1999. **274**(18): p. 12263-8.
7. Murakami, M., et al., *Functional coupling between various phospholipase A2s and cyclooxygenases in immediate and delayed prostanoid biosynthetic pathways.* J Biol Chem, 1999. **274**(5): p. 3103-15.
8. Ueno, N., et al., *Coupling between cyclooxygenases and terminal prostanoid synthases.* Biochem Biophys Res Commun, 2005. **338**(1): p. 70-6.
9. Caughey, G.E., et al., *Roles of cyclooxygenase (COX)-1 and COX-2 in prostanoid production by human endothelial cells: selective up-regulation of prostacyclin synthesis by COX-2.* J Immunol, 2001. **167**(5): p. 2831-8.

10. Wang, L.H. and R.J. Kulmacz, *Thromboxane synthase: structure and function of protein and gene.* Prostaglandins Other Lipid Mediat, 2002. **68-69**: p. 409-22.

11. Yamada, M., et al., *Prostacyclin synthase gene transfer modulates cyclooxygenase-2-derived prostanoid synthesis and inhibits neointimal formation in rat balloon-injured arteries.* Arterioscler Thromb Vasc Biol, 2002. **22**(2):256-62.

12. Kanaoka, Y. and Y. Urade, *Hematopoietic prostaglandin D synthase.* Prostaglandins Leukot Essent Fatty Acids, 2003. **69**(2-3): p. 163-7.

13. Samuelsson, B., et al., *Prostaglandins and thromboxanes.* Annu Rev Biochem, 1978. **47**: p. 997-1029.

14. Yang, G. and L. Chen, *An Update of Microsomal Prostaglandin E Synthase-1 and PGE2 Receptors in Cardiovascular Health and Diseases.* Oxid Med Cell Longev, 2016. **2016**: p. 5249086.

15. Ellis, E.F., et al., *Effect of oral aspirin dose on platelet aggregation and vascular prostacyclin (PGI2) synthesis in humans and rabbits.* J Cardiovasc Pharmacol, 1980. **2**(4): p. 387-97.

16. Harker, L.A. and C.A. Finch, *Thrombokinetics in man.* J Clin Invest, 1969. **48**(6): p. 963-74.

17. Zarghi, A. and S. Arfaei, *Selective COX-2 Inhibitors: A Review of Their Structure-Activity Relationships.* Iran J Pharm Res, 2011. **10**(4): p. 655-83.

18. Essex, M.N., et al., *Safety of celecoxib compared with placebo and non-selective NSAIDs: cumulative meta-analysis of 89 randomized controlled trials.* Expert Opin Drug Saf, 2013. **12**(4): p. 465-77.

19. Whelton, A., *Nephrotoxicity of nonsteroidal anti-inflammatory drugs: physiologic foundations and clinical implications.* Am J Med, 1999. **106**(5b): p. 13s-24s.

20. Brater, D.C., *Effects of nonsteroidal anti-inflammatory drugs on renal function: focus on cyclooxygenase-2-selective inhibition.* Am J Med, 1999. **107**(6a): p. 65S-70S; discussion 70S-71S.

21. Bombardier, C., et al., *Comparison of upper gastrointestinal toxicity of rofecoxib and naproxen in patients with rheumatoid arthritis. VIGOR Study Group.* N Engl J Med, 2000. **343**(21): p. 1520-8, 2 p following 1528.

22. Mukherjee, D., S.E. Nissen, and E.J. Topol, *Risk of cardiovascular events associated with selective COX-2 inhibitors.* Jama, 2001. **286**(8): p. 954-9.

23. Iniguez, M.A., et al., *Prostanoid function and cardiovascular disease.* Arch Physiol Biochem, 2008. **114**(3): p. 201-9.

24. Narumiya, S. and G.A. FitzGerald, *Genetic and pharmacological analysis of prostanoid receptor function.* J Clin Invest, 2001. **108**(1): p. 25-30.

25. Chen, L., G. Yang, and T. Grosser, *Prostanoids and inflammatory pain.* Prostaglandins Other Lipid Mediat, 2013. **104-105**: p. 58-66.

26. Beloeil, H., et al., *The effect of a peripheral block on inflammation-induced prostaglandin E2 and cyclooxygenase expression in rats.* Anesth Analg, 2009. **109**(3): p. 943-50.

27. Hay, C. and J. de Belleroche, *Carrageenan-induced hyperalgesia is associated with increased cyclo-oxygenase-2 expression in spinal cord.* Neuroreport, 1997. **8**(5): p. 1249-51.

28. Hay, C.H. and J.S. de Belleroche, *Dexamethasone prevents the induction of COX-2 mRNA and prostaglandins in the lumbar spinal cord following intraplantar FCA in parallel with inhibition of oedema.* Neuropharmacology, 1998. **37**(6): p. 739-44.

29. Maihofner, C., et al., *Localization and regulation of cyclo-oxygenase-1 and -2 and neuronal nitric oxide synthase in mouse spinal cord.* Neuroscience, 2000. **101**(4): p. 1093-108.

30. Samad, T.A., et al., *Interleukin-1beta-mediated induction of Cox-2 in the CNS contributes to inflammatory pain hypersensitivity.* Nature, 2001. **410**(6827):471-5.

31. Funk, C.D., *Prostaglandins and leukotrienes: advances in eicosanoid biology.* Science, 2001. **294**(5548): p. 1871-5.

32. Curry, F.R. and R.H. Adamson, *Vascular permeability modulation at the cell, microvessel, or whole organ level: towards closing gaps in our knowledge.* Cardiovasc Res, 2010. **87**(2): p. 218-29.

33. Feletou, M., E. Bonnardel, and E. Canet, *Bradykinin and changes in microvascular permeability in the hamster cheek pouch: role of nitric oxide.* Br J Pharmacol, 1996. **118**(6): p. 1371-6.

34. Nathan, R.A., *The pathophysiology, clinical impact, and management of nasal congestion in allergic rhinitis.* Clin Ther, 2008. **30**(4): p. 573-86.

35. Omori, K., et al., *Multiple roles of the PGE2 -EP receptor signal in vascular permeability.* Br J Pharmacol, 2014. **171**(21): p. 4879-89.

36. Kamei, D., et al., *Reduced pain hypersensitivity and inflammation in mice lacking microsomal prostaglandin e synthase-1.* J Biol Chem, 2004. **279**(32): p. 33684-95.

37. Trebino, C.E., et al., *Impaired inflammatory and pain responses in mice lacking an inducible prostaglandin E synthase.* Proc Natl Acad Sci U S A, 2003. **100**(15): p. 9044-9.

38. Skeggs, L.T., et al., *Biochemistry and kinetics of the renin-angiotensin system.* Fed Proc, 1967. **26**(1): p. 42-7.

39. Dorer, F.E., et al., *Purification and properties of angiotensin-converting enzyme from hog lung.* Circ Res, 1972. **31**(3): p. 356-66.

40. Phillips, M.I., E.A. Speakman, and B. Kimura, *Levels of angiotensin and molecular biology of the tissue renin angiotensin systems.* Regul Pept, 1993. **43**(1-2):1-20.

41. Yugandhar, V.G. and M.A. Clark, *Angiotensin III: a physiological relevant peptide of the renin angiotensin system.* Peptides, 2013. **46**: p. 26-32.

42. Haulica, I., W. Bild, and D.N. Serban, *Angiotensin peptides and their pleiotropic actions.* J Renin Angiotensin Aldosterone Syst, 2005. **6**(3): p. 121-31.

43. Ferrario, C.M., *New physiological concepts of the renin-angiotensin system from the investigation of precursors and products of angiotensin I metabolism.* Hypertension, 2010. **55**(2): p. 445-52.

44. Ferreira, A.J., et al., *Therapeutic implications of the vasoprotective axis of the renin-angiotensin system in cardiovascular diseases.* Hypertension, 2010. **55**(2): p. 207-13.

45. Coble, J.P., et al., *Mechanisms of brain renin angiotensin system-induced drinking and blood pressure: importance of the subfornical organ.* Am J Physiol Regul Integr Comp Physiol, 2015. **308**(4): p. R238-49.

46. Lavoie, J.L. and C.D. Sigmund, *Minireview: overview of the renin-angiotensin system--an endocrine and paracrine system.* Endocrinology, 2003. **144**(6): p. 2179-83.

47. Satou, R., W. Shao, and L.G. Navar, *Role of stimulated intrarenal angiotensinogen in hypertension.* Ther Adv Cardiovasc Dis, 2015. **9**(4): p. 181-90.

48. Kim, S. and H. Iwao, *Molecular and cellular mechanisms of angiotensin II-mediated cardiovascular and renal diseases.* Pharmacol Rev, 2000. **52**(1):11-34.

49. Kurdi, M. and G.W. Booz, *New take on the role of angiotensin II in cardiac hypertrophy and fibrosis.* Hypertension, 2011. **57**(6): p. 1034-8.

50. Liu, Y., et al., *Angiotensin II stimulation in vitro induces hypertrophy of normal and postinfarcted ventricular myocytes.* Circ Res, 1998. **82**(11): p. 1145-59.

51. Nicoletti, A. and J.B. Michel, *Cardiac fibrosis and inflammation: interaction with hemodynamic and hormonal factors.* Cardiovasc Res, 1999. **41**(3): p. 532-43.

52. Sriramula, S., et al., *Involvement of tumor necrosis factor-alpha in angiotensin II-mediated effects on salt appetite, hypertension, and cardiac hypertrophy.* Hypertension, 2008. **51**(5): p. 1345-51.

53. Williams, B., et al., *Angiotensin II increases vascular permeability factor gene expression by human vascular smooth muscle cells.* Hypertension, 1995. **25**(5): p. 913-7.

54. Wu, R., M.A. Laplante, and J. de Champlain, *Cyclooxygenase-2 inhibitors attenuate angiotensin II-induced oxidative stress, hypertension, and cardiac hypertrophy in rats.* Hypertension, 2005. **45**(6): p. 1139-44.

55. Yamada, T., et al., *Angiotensin II type 2 receptor mediates vascular smooth muscle cell apoptosis and antagonizes angiotensin II type 1 receptor action: an in vitro gene transfer study.* Life Sci, 1998. **63**(19): p. Pl289-95.

56. Forrester, S.J., et al., *Angiotensin II Signal Transduction: An Update on Mechanisms of Physiology and Pathophysiology.* Physiol Rev, 2018. **98**(3): p. 1627-1738.

57. de Gasparo, M., et al., *Proposed update of angiotensin receptor nomenclature.* Hypertension, 1995. **25**(5): p. 924-7.

58. Inagami, T., *Recent progress in molecular and cell biological studies of angiotensin receptors.* Curr Opin Nephrol Hypertens, 1995. **4**(1): p. 47-54.

59. Sadoshima, J., *Versatility of the angiotensin II type 1 receptor.* Circ Res, 1998. **82**(12): p. 1352-5.

60. Allen, A.M., J. Zhuo, and F.A. Mendelsohn, *Localization and function of angiotensin AT1 receptors.* Am J Hypertens, 2000. **13**(1 Pt 2): p. 31S-38S.

61. Zhuo, J., et al., *Mapping tissue angiotensin-converting enzyme and angiotensin AT1, AT2 and AT4 receptors.* J Hypertens, 1998. **16**(12 Pt 2): p. 2027-37.

62. Viswanathan, M., A. Seltzer, and J.M. Saavedra, *Heterogeneous expression of angiotensin II AT1 receptors in neointima of rat carotid artery and aorta after balloon catheter injury.* Peptides, 1994. **15**(7): p. 1205-12.

63. Touyz, R.M. and E.L. Schiffrin, *Activation of the Na(+)-H+ exchanger modulates angiotensin II-stimulated Na(+)-dependent Mg2+ transport in vascular smooth muscle cells in genetic hypertension.* Hypertension, 1999. **34**(3): p. 442-9.

64. Romero-Nava, R., et al., *Changes in protein and gene expression of angiotensin II receptors (AT1 and AT2) in aorta of diabetic and hypertensive rats.* Clin Exp Hypertens, 2016. **38**(1): p. 56-62.

65. Frangogiannis, N.G., *Chemokines in ischemia and reperfusion.* Thromb Haemost, 2007. **97**(5): p. 738-47.

66. Frangogiannis, N.G., *Regulation of the inflammatory response in cardiac repair.* Circ Res, 2012. **110**(1): p. 159-73.

67. Frangogiannis, N.G., *The inflammatory response in myocardial injury, repair, and remodelling.* Nat Rev Cardiol, 2014. **11**(5): p. 255-65.

68. Detmers, P.A., et al., *Neutrophil-activating protein 1/interleukin 8 stimulates the binding activity of the leukocyte adhesion receptor CD11b/CD18 on human neutrophils.* J Exp Med, 1990. **171**(4): p. 1155-62.

69. Herter, J. and A. Zarbock, *Integrin Regulation during Leukocyte Recruitment.* J Immunol, 2013. **190**(9): p. 4451-7.

70. Dewald, O., et al., *CCL2/Monocyte Chemoattractant Protein-1 regulates inflammatory responses critical to healing myocardial infarcts.* Circ Res, 2005. **96**(8): p. 881-9.

71. Legler, D.F. and M. Thelen, *Chemokines: Chemistry, Biochemistry and Biological Function.* Chimia (Aarau), 2016. **70**(12): p. 856-859.

72. Sarafi, M.N., et al., *Murine monocyte chemoattractant protein (MCP)-5: a novel CC chemokine that is a structural and functional homologue of human MCP-1.* J Exp Med, 1997. **185**(1): p. 99-109.

73. Harding, P., et al., *Gene expression profiling of dilated cardiomyopathy in older male EP4 knockout mice.* Am J Physiol Heart Circ Physiol, 2010. **298**(2):H623-32.

74. Luster, A.D., *Chemokines--chemotactic cytokines that mediate inflammation.* N Engl J Med, 1998. **338**(7): p. 436-45.

75. Dewald, O., et al., *Of mice and dogs: species-specific differences in the inflammatory response following myocardial infarction.* Am J Pathol, 2004. **164**(2): p. 665-77.

76. Herskowitz, A., et al., *Cytokine mRNA expression in postischemic/reperfused myocardium.* Am J Pathol, 1995. **146**(2): p. 419-28.

77. Mann, D.L., *Stress-activated cytokines and the heart: from adaptation to maladaptation.* Annu Rev Physiol, 2003. **65**: p. 81-101.

78. Deten, A., et al., *Cardiac cytokine expression is upregulated in the acute phase after myocardial infarction. Experimental studies in rats.* Cardiovasc Res, 2002. **55**(2): p. 329-40.

79. Irwin, M.W., et al., *Tissue expression and immunolocalization of tumor necrosis factor-alpha in postinfarction dysfunctional myocardium.* Circulation, 1999. **99**(11): p. 1492-8.

80. Ono, K., et al., *Cytokine gene expression after myocardial infarction in rat hearts: possible implication in left ventricular remodeling.* Circulation, 1998. **98**(2):149-56.

81. Nian, M., et al., *Inflammatory cytokines and postmyocardial infarction remodeling.* Circ Res, 2004. **94**(12): p. 1543-53.

82. Palojoki, E., et al., *Cardiomyocyte apoptosis and ventricular remodeling after myocardial infarction in rats.* Am J Physiol Heart Circ Physiol, 2001. **280**(6): p. H2726-31.

83. Krown, K.A., et al., *Tumor necrosis factor alpha-induced apoptosis in cardiac myocytes. Involvement of the sphingolipid signaling cascade in cardiac cell death.* J Clin Invest, 1996. **98**(12): p. 2854-65.

84. Yokoyama, T., et al., *Tumor necrosis factor-alpha provokes a hypertrophic growth response in adult cardiac myocytes.* Circulation, 1997. **95**(5): p. 1247-52.

85. Kubota, T., et al., *Dilated cardiomyopathy in transgenic mice with cardiac-specific overexpression of tumor necrosis factor-alpha.* Circ Res, 1997. **81**(4): p. 627-35.

86. Furukawa, Y., et al., *Cytokine gene expression during the development of graft coronary artery disease in mice.* Jpn Circ J, 1999. **63**(10): p. 775-82.

87. Beg, A.A. and D. Baltimore, *An essential role for NF-kappaB in preventing TNF-alpha-induced cell death.* Science, 1996. **274**(5288): p. 782-4.

88. Chen, B. and N.G. Frangogiannis, *Immune cells in repair of the infarcted myocardium.* Microcirculation, 2017. **24**(1).

89. Frangogiannis, N.G., et al., *Histochemical and morphological characteristics of canine cardiac mast cells.* Histochem J, 1999. **31**(4): p. 221-9.

90. Mylonas, K.J., et al., *The adult murine heart has a sparse, phagocytically active macrophage population that expands through monocyte recruitment and adopts an 'M2' phenotype in response to Th2 immunologic challenge.* Immunobiology, 2015. **220**(7): p. 924-33.

91. Pinto, A.R., et al., *Revisiting Cardiac Cellular Composition.* Circ Res, 2016. **118**(3): p. 400-9.

92. Frangogiannis, N.G., *The immune system and the remodeling infarcted heart: cell biological insights and therapeutic opportunities.* J Cardiovasc Pharmacol, 2014. **63**(3): p. 185-95.

93. Mann, D.L., *The emerging role of innate immunity in the heart and vascular system: for whom the cell tolls.* Circ Res, 2011. **108**(9): p. 1133-45.

94. Chen, C., et al., *Role of extracellular RNA and TLR3-Trif signaling in myocardial ischemia-reperfusion injury.* J Am Heart Assoc, 2014. **3**(1): p. e000683.

95. Oka, T., et al., *Mitochondrial DNA that escapes from autophagy causes inflammation and heart failure.* Nature, 2012. **485**(7397): p. 251-5.

96. Bliksoen, M., et al., *Increased circulating mitochondrial DNA after myocardial infarction.* Int J Cardiol, 2012. **158**(1): p. 132-4.

97. Dobaczewski, M., et al., *Extracellular matrix remodeling in canine and mouse myocardial infarcts.* Cell Tissue Res, 2006. **324**(3): p. 475-88.

98. Huebener, P., et al., *CD44 is critically involved in infarct healing by regulating the inflammatory and fibrotic response.* J Immunol, 2008. **180**(4): p. 2625-33.

99. Waldenstrom, A., et al., *Accumulation of hyaluronan and tissue edema in experimental myocardial infarction.* J Clin Invest, 1991. **88**(5): p. 1622-8.

100. Li, Y., et al., *Myocardial ischemia activates an injurious innate immune signaling via cardiac heat shock protein 60 and Toll-like receptor 4.* J Biol Chem, 2011. **286**(36): p. 31308-19.

101. Lin, L., et al., *HSP60 in heart failure: abnormal distribution and role in cardiac myocyte apoptosis.* Am J Physiol Heart Circ Physiol, 2007. **293**(4): p. H2238-47.

102. Lugrin, J., et al., *Cutting edge: IL-1alpha is a crucial danger signal triggering acute myocardial inflammation during myocardial infarction.* J Immunol, 2015. **194**(2): p. 499-503.

103. Frangogiannis, N.G., L.H. Michael, and M.L. Entman, *Myofibroblasts in reperfused myocardial infarcts express the embryonic form of smooth muscle myosin heavy chain (SMemb).* Cardiovasc Res, 2000. **48**(1): p. 89-100.

104. Virag, J.I. and C.E. Murry, *Myofibroblast and endothelial cell proliferation during murine myocardial infarct repair.* Am J Pathol, 2003. **163**(6): p. 2433-40.

105. Cleutjens, J.P., et al., *Collagen remodeling after myocardial infarction in the rat heart.* Am J Pathol, 1995. **147**(2): p. 325-38.

106. Shinde, A.V. and N.G. Frangogiannis, *Fibroblasts in myocardial infarction: a role in inflammation and repair.* J Mol Cell Cardiol, 2014. **70**: p. 74-82.

107. Heim, A., et al., *Transient induction of cytokine production in human myocardial fibroblasts by coxsackievirus B3.* Circ Res, 2000. **86**(7): p. 753-9.

108. Lafontant, P.J., et al., *Oncostatin M differentially regulates CXC chemokines in mouse cardiac fibroblasts.* Am J Physiol Cell Physiol, 2006. **291**(1): p. C18-26.

109. Zymek, P., et al., *Interleukin-10 is not a critical regulator of infarct healing and left ventricular remodeling.* Cardiovasc Res, 2007. **74**(2): p. 313-22.

110. Frangogiannis, N.G., et al., *Resident cardiac mast cells degranulate and release preformed TNF-alpha, initiating the cytokine cascade in experimental canine myocardial ischemia/reperfusion.* Circulation, 1998. **98**(7): p. 699-710.

111. Frangogiannis, N.G., et al., *Cytokines and the microcirculation in ischemia and reperfusion.* J Mol Cell Cardiol, 1998. **30**(12): p. 2567-76.

112. Kong, P., et al., *Lack of specificity of fibroblast-specific protein 1 in cardiac remodeling and fibrosis.* Am J Physiol Heart Circ Physiol, 2013. **305**(9):H1363-72.

113. Frangogiannis, N.G., *The mechanistic basis of infarct healing.* Antioxid Redox Signal, 2006. **8**(11-12): p. 1907-39.

114. Cleutjens, J.P., et al., *The infarcted myocardium: simply dead tissue, or a lively target for therapeutic interventions.* Cardiovasc Res, 1999. **44**(2): p. 232-41.

115. Richardson, W.J., et al., *Physiological Implications of Myocardial Scar Structure.* Compr Physiol, 2015. **5**(4): p. 1877-909.

116. Nahrendorf, M., M.J. Pittet, and F.K. Swirski, *Monocytes: protagonists of infarct inflammation and repair after myocardial infarction.* Circulation, 2010. **121**(22): p. 2437-45.

117. Opie, L.H., et al., *Controversies in ventricular remodelling.* Lancet, 2006. **367**(9507): p. 356-67.

118. Sun, Y., et al., *Infarct scar as living tissue.* Basic Res Cardiol, 2002. **97**(5):343-7.

119. DeLeon-Pennell, K.Y., et al., *Matrix Metalloproteinases in Myocardial Infarction and Heart Failure.* Prog Mol Biol Transl Sci, 2017. **147**: p. 75-100.

120. Lindsey, M.L., et al., *Matrix metalloproteinases as input and output signals for post-myocardial infarction remodeling.* J Mol Cell Cardiol, 2016. **91**: p. 134-40.

121. Wilson, E.M., et al., *Plasma matrix metalloproteinase and inhibitor profiles in patients with heart failure.* J Card Fail, 2002. **8**(6): p. 390-8.

122. Spinale, F.G., et al., *Matrix metalloproteinase inhibition during the development of congestive heart failure : effects on left ventricular dimensions and function.* Circ Res, 1999. **85**(4): p. 364-76.

123. Iyer, R.P., M. Jung, and M.L. Lindsey, *Using the laws of thermodynamics to understand how matrix metalloproteinases coordinate the myocardial response to injury.* Metalloproteinases Med, 2015. **2**: p. 75-82.

124. Pfeffer, M.A., *ACE inhibitors in acute myocardial infarction: patient selection and timing.* Circulation, 1998. **97**(22): p. 2192-4.

125. Zhang, P., et al., *[Comparison of doxycycline, losartan, and their combination on the expression of matrix metalloproteinase, tissue inhibitor of matrix metalloproteinase, and collagen remodeling in the noninfarcted myocardium after acute myocardial infarction in rats].* Zhongguo Yi Xue Ke Xue Yuan Xue Bao, 2005. **27**(1): p. 53-61.

126. Harada, K., et al., *Angiotensin II type 1A receptor knockout mice display less left ventricular remodeling and improved survival after myocardial infarction.* Circulation, 1999. **100**(20): p. 2093-9.

127. Katz, A.M., *The cardiomyopathy of overload: an unnatural growth response.* Eur Heart J, 1995. **16 Suppl O**: p. 110-4.

128. Stone, G.W., et al., *Predictors of infarct size after primary coronary angioplasty in acute myocardial infarction from pooled analysis from four contemporary trials.* Am J Cardiol, 2007. **100**(9): p. 1370-5.

129. Weisman, H.F., et al., *Cellular mechanisms of myocardial infarct expansion.* Circulation, 1988. **78**(1): p. 186-201.

130. Gaasch, W.H., *Diagnosis and treatment of heart failure based on left ventricular systolic or diastolic dysfunction.* JAMA, 1994. **271**(16): p. 1276-80.

131. Lawes, C.M., S. Vander Hoorn, and A. Rodgers, *Global burden of blood-pressure-related disease, 2001.* Lancet, 2008. **371**(9623): p. 1513-8.

132. Gradman, A.H. and F. Alfayoumi, *From left ventricular hypertrophy to congestive heart failure: management of hypertensive heart disease.* Prog Cardiovasc Dis, 2006. **48**(5): p. 326-41.

133. Zile, M.R. and D.L. Brutsaert, *New concepts in diastolic dysfunction and diastolic heart failure: Part II: causal mechanisms and treatment.* Circulation, 2002. **105**(12): p. 1503-8.

134. Zile, M.R. and D.L. Brutsaert, *New concepts in diastolic dysfunction and diastolic heart failure: Part I: diagnosis, prognosis, and measurements of diastolic function.* Circulation, 2002. **105**(11): p. 1387-93.

135. Berk, B.C., K. Fujiwara, and S. Lehoux, *ECM remodeling in hypertensive heart disease.* J Clin Invest, 2007. **117**(3): p. 568-75.

136. Levy, D., et al., *Echocardiographically detected left ventricular hypertrophy: prevalence and risk factors. The Framingham Heart Study.* Ann Intern Med, 1988. **108**(1): p. 7-13.

137. Verdecchia, P., et al., *Left ventricular mass and cardiovascular morbidity in essential hypertension: the MAVI study.* J Am Coll Cardiol, 2001. **38**(7):1829-35.

138. Verdecchia, P., et al., *Left ventricular hypertrophy as an independent predictor of acute cerebrovascular events in essential hypertension.* Circulation, 2001. **104**(17): p. 2039-44.

139. Gardin, J.M., et al., *M-mode echocardiographic predictors of six- to seven-year incidence of coronary heart disease, stroke, congestive heart failure, and mortality in an elderly cohort (the Cardiovascular Health Study).* Am J Cardiol, 2001. **87**(9): p. 1051-7.

140. Cipriano, C., et al., *Prognostic value of left ventricular mass and its evolution during treatment in the Bordeaux cohort of hypertensive patients.* Am J Hypertens, 2001. **14**(6 Pt 1): p. 524-9.

141. Diez, J., et al., *Clinical aspects of hypertensive myocardial fibrosis.* Curr Opin Cardiol, 2001. **16**(6): p. 328-35.

142. Rowlands, D.B., et al., *The relationship between ambulatory blood pressure and echocardiographically assessed left ventricular hypertrophy.* Clin Sci (Lond), 1981. **61 Suppl 7**: p. 101s-103s.

143. Devereux, R.B., et al., *Left ventricular hypertrophy in patients with hypertension: importance of blood pressure response to regularly recurring stress.* Circulation, 1983. **68**(3): p. 470-6.

144. White, W.B., H.M. Dey, and P. Schulman, *Assessment of the daily blood pressure load as a determinant of cardiac function in patients with mild-to-moderate hypertension.* Am Heart J, 1989. **118**(4): p. 782-95.

145. Verdecchia, P., et al., *Circadian blood pressure changes and left ventricular hypertrophy in essential hypertension.* Circulation, 1990. **81**(2): p. 528-36.

146. Mancia, G., et al., *Ambulatory blood pressure is superior to clinic blood pressure in predicting treatment-induced regression of left ventricular hypertrophy. SAMPLE Study Group. Study on Ambulatory Monitoring of Blood Pressure and Lisinopril Evaluation.* Circulation, 1997. **95**(6): p. 1464-70.

147. Gosse, P., et al., *Ambulatory blood pressure and left ventricular hypertrophy.* Blood Press Monit, 1997. **2**(2): p. 70-74.

148. Drazner, M.H., et al., *Left ventricular hypertrophy is more prevalent in blacks than whites in the general population: the Dallas Heart Study.* Hypertension, 2005. **46**(1): p. 124-9.

149. Lauer, M.S., K.M. Anderson, and D. Levy, *Separate and joint influences of obesity and mild hypertension on left ventricular mass and geometry: the Framingham Heart Study.* J Am Coll Cardiol, 1992. **19**(1): p. 130-4.

150. Diez, J., et al., *Losartan-dependent regression of myocardial fibrosis is associated with reduction of left ventricular chamber stiffness in hypertensive patients.* Circulation, 2002. **105**(21): p. 2512-7.

151. Sadoshima, J. and S. Izumo, *Molecular characterization of angiotensin II--induced hypertrophy of cardiac myocytes and hyperplasia of cardiac fibroblasts. Critical role of the AT1 receptor subtype.* Circ Res, 1993. **73**(3): p. 413-23.

152. Janicki, J.S. and G.L. Brower, *The role of myocardial fibrillar collagen in ventricular remodeling and function.* J Card Fail, 2002. **8**(6 Suppl): p. S319-25.

153. Shirwany, A. and K.T. Weber, *Extracellular matrix remodeling in hypertensive heart disease.* J Am Coll Cardiol, 2006. **48**(1): p. 97-8.

154. Iwanaga, Y., et al., *Excessive activation of matrix metalloproteinases coincides with left ventricular remodeling during transition from hypertrophy to heart failure in hypertensive rats.* J Am Coll Cardiol, 2002. **39**(8): p. 1384-91.

155. Mujumdar, V.S., L.M. Smiley, and S.C. Tyagi, *Activation of matrix metalloproteinase dilates and decreases cardiac tensile strength.* Int J Cardiol, 2001. **79**(2-3): p. 277-86.

156. Laviades, C., et al., *Abnormalities of the extracellular degradation of collagen type I in essential hypertension.* Circulation, 1998. **98**(6): p. 535-40.

157. Ahmed, S.H., et al., *Matrix metalloproteinases/tissue inhibitors of metalloproteinases: relationship between changes in proteolytic determinants of matrix composition and structural, functional, and clinical manifestations of hypertensive heart disease.* Circulation, 2006. **113**(17): p. 2089-96.

158. Sporn, M.B. and A.B. Roberts, *Transforming growth factor-beta: recent progress and new challenges.* J Cell Biol, 1992. **119**(5): p. 1017-21.

159. Frossard, P.M., et al., *A study of five human cytokine genes in human essential hypertension.* Mol Immunol, 2002. **38**(12-13): p. 969-76.

160. Cambien, F., et al., *Polymorphisms of the transforming growth factor-beta 1 gene in relation to myocardial infarction and blood pressure. The Etude Cas-Temoin de l'Infarctus du Myocarde (ECTIM) Study.* Hypertension, 1996. **28**(5): p. 881-7.

161. Guzik, T.J., et al., *Role of the T cell in the genesis of angiotensin II induced hypertension and vascular dysfunction.* J Exp Med, 2007. **204**(10): p. 2449-60.

162. Marvar, P.J., et al., *Central and peripheral mechanisms of T-lymphocyte activation and vascular inflammation produced by angiotensin II-induced hypertension.* Circ Res, 2010. **107**(2): p. 263-70.

163. Marvar, P.J., et al., *T lymphocytes and vascular inflammation contribute to stress-dependent hypertension.* Biol Psychiatry, 2012. **71**(9): p. 774-82.

164. Mattson, D.L., et al., *Immune suppression attenuates hypertension and renal disease in the Dahl salt-sensitive rat.* Hypertension, 2006. **48**(1): p. 149-56.

165. Epelman, S., K.J. Lavine, and G.J. Randolph, *Origin and functions of tissue macrophages.* Immunity, 2014. **41**(1): p. 21-35.

166. Ma, Y., A.J. Mouton, and M.L. Lindsey, *Cardiac macrophage biology in the steady-state heart, the aging heart, and following myocardial infarction.* Transl Res, 2018. **191**: p. 15-28.

167. Nguyen, K.D., et al., *Alternatively activated macrophages produce catecholamines to sustain adaptive thermogenesis.* Nature, 2011. **480**(7375): p. 104-8.

168. Okabe, Y. and R. Medzhitov, *Tissue-specific signals control reversible program of localization and functional polarization of macrophages.* Cell, 2014. **157**(4):832-44.

169. Swirski, F.K., C.S. Robbins, and M. Nahrendorf, *Development and Function of Arterial and Cardiac Macrophages.* Trends Immunol, 2016. **37**(1): p. 32-40.

170. Frantz, S., et al., *Monocytes/macrophages prevent healing defects and left ventricular thrombus formation after myocardial infarction.* Faseb j, 2013. **27**(3): p. 871-81.

171. Ben-Mordechai, T., et al., *Macrophage subpopulations are essential for infarct repair with and without stem cell therapy.* J Am Coll Cardiol, 2013. **62**(20): p. 1890-901.

172. Heidt, T., et al., *Differential contribution of monocytes to heart macrophages in steady-state and after myocardial infarction.* Circ Res, 2014. **115**(2): p. 284-95.

173. Nahrendorf, M. and F.K. Swirski, *Monocyte and macrophage heterogeneity in the heart.* Circ Res, 2013. **112**(12): p. 1624-33.

174. Swirski, F.K. and M. Nahrendorf, *Macrophage-stem cell crosstalk after myocardial infarction.* J Am Coll Cardiol, 2013. **62**(20): p. 1902-4.

175. Gombozhapova, A., et al., *Macrophage activation and polarization in post-infarction cardiac remodeling.* J Biomed Sci, 2017. **24**(1): p. 13.

176. ter Horst, E.N., et al., *Modulators of Macrophage Polarization Influence Healing of the Infarcted Myocardium.* Int J Mol Sci, 2015. **16**(12): p. 29583-91.

177. Pinto, A.R., et al., *An abundant tissue macrophage population in the adult murine heart with a distinct alternatively-activated macrophage profile.* PLoS One, 2012. **7**(5): p. e36814.

178. Chistiakov, D.A., et al., *CD68/macrosialin: not just a histochemical marker.* Lab Invest, 2017. **97**(1): p. 4-13.

179. Epelman, S., et al., *Embryonic and adult-derived resident cardiac macrophages are maintained through distinct mechanisms at steady state and during inflammation.* Immunity, 2014. **40**(1): p. 91-104.

180. Tsou, C.L., et al., *Critical roles for CCR2 and MCP-3 in monocyte mobilization from bone marrow and recruitment to inflammatory sites.* J Clin Invest, 2007. **117**(4): p. 902-9.

181. Todd, R.F., 3rd, *The continuing saga of complement receptor type 3 (CR3).* J Clin Invest, 1996. **98**(1): p. 1-2.

182. Zhou, H., et al., *CD11b/CD18 (Mac-1) is a novel surface receptor for extracellular double-stranded RNA to mediate cellular inflammatory responses.* J Immunol, 2013. **190**(1): p. 115-25.

183. Etzerodt, A. and S.K. Moestrup, *CD163 and inflammation: biological, diagnostic, and therapeutic aspects.* Antioxid Redox Signal, 2013. **18**(17): p. 2352-63.

184. Rafatian, N., et al., *Cardiac macrophages and apoptosis after myocardial infarction: effects of central MR blockade.* Am J Physiol Regul Integr Comp Physiol, 2014. **307**(7): p. R879-87.

185. Lin, H.H., et al., *The macrophage F4/80 receptor is required for the induction of antigen-specific efferent regulatory T cells in peripheral tolerance.* J Exp Med, 2005. **201**(10): p. 1615-25.

186. Ting, J.P. and J. Trowsdale, *Genetic control of MHC class II expression.* Cell, 2002. **109 Suppl**: p. S21-33.

187. Ben-Mordechai, T., et al., *Targeting macrophage subsets for infarct repair.* J Cardiovasc Pharmacol Ther, 2015. **20**(1): p. 36-51.

188. Cohen, H.B. and D.M. Mosser, *Cardiac macrophages: how to mend a broken heart.* Immunity, 2014. **40**(1): p. 3-5.

189. Yan, X., et al., *Temporal dynamics of cardiac immune cell accumulation following acute myocardial infarction.* J Mol Cell Cardiol, 2013. **62**: p. 24-35.

190. Harel-Adar, T., et al., *Modulation of cardiac macrophages by phosphatidylserine-presenting liposomes improves infarct repair.* Proc Natl Acad Sci U S A, 2011. **108**(5): p. 1827-32.

191. Courties, G., et al., *In vivo silencing of the transcription factor IRF5 reprograms the macrophage phenotype and improves infarct healing.* J Am Coll Cardiol, 2014. **63**(15): p. 1556-66.

192. Zhou, L.S., et al., *Silencing collapsin response mediator protein-2 reprograms macrophage phenotype and improves infarct healing in experimental myocardial infarction model.* J Inflamm (Lond), 2015. **12**: p. 11.

193. Weirather, J., et al., *Foxp3+ CD4+ T cells improve healing after myocardial infarction by modulating monocyte/macrophage differentiation.* Circ Res, 2014. **115**(1): p. 55-67.

194. Ma, Y., et al., *Matrix metalloproteinase-28 deletion exacerbates cardiac dysfunction and rupture after myocardial infarction in mice by inhibiting M2 macrophage activation.* Circ Res, 2013. **112**(4): p. 675-88.

195. Jung, M., et al., *IL-10 improves cardiac remodeling after myocardial infarction by stimulating M2 macrophage polarization and fibroblast activation.* Basic Res Cardiol, 2017. **112**(3): p. 33.

196. Yabluchanskiy, A., et al., *Myocardial Infarction Superimposed on Aging: MMP-9 Deletion Promotes M2 Macrophage Polarization.* J Gerontol A Biol Sci Med Sci, 2016. **71**(4): p. 475-83.

197. Nahrendorf, M., et al., *The healing myocardium sequentially mobilizes two monocyte subsets with divergent and complementary functions.* J Exp Med, 2007. **204**(12): p. 3037-47.

198. Dutta, P. and M. Nahrendorf, *Monocytes in myocardial infarction.* Arterioscler Thromb Vasc Biol, 2015. **35**(5): p. 1066-70.

199. Hilgendorf, I., et al., *Ly-6Chigh monocytes depend on Nr4a1 to balance both inflammatory and reparative phases in the infarcted myocardium.* Circ Res, 2014. **114**(10): p. 1611-22.

200. Luan, B., et al., *CREB pathway links PGE2 signaling with macrophage polarization.* Proc Natl Acad Sci U S A, 2015. **112**(51): p. 15642-7.

201. Franco, F., M. Wenes, and P.C. Ho, *Sparks Fly in PGE2-Modulated Macrophage Polarization.* Immunity, 2018. **49**(6): p. 987-989.

202. Montero, J., et al., *Prostaglandin E2 promotes M2 polarization of macrophages via a cAMP/CREB signaling pathway and deactivates granulocytes in teleost fish.* Fish Shellfish Immunol, 2016. **55**: p. 632-41.

203. Liberale, L., A. Bonaventura, and F. Montecucco, *T-cells in myocardial infarction: Culprit instigators or mere effectors?* World J Cardiol, 2018. **10**(10): p. 123-126.

204. Hofmann, U. and S. Frantz, *Role of T-cells in myocardial infarction.* Eur Heart J, 2016. **37**(11): p. 873-9.

205. Rochman, Y., R. Spolski, and W.J. Leonard, *New insights into the regulation of T cells by gamma(c) family cytokines.* Nat Rev Immunol, 2009. **9**(7): p. 480-90.

206. Kuniyasu, Y., et al., *Naturally anergic and suppressive CD25(+)CD4(+) T cells as a functionally and phenotypically distinct immunoregulatory T cell subpopulation.* Int Immunol, 2000. **12**(8): p. 1145-55.

207. Hofmann, U. and S. Frantz, *Role of lymphocytes in myocardial injury, healing, and remodeling after myocardial infarction.* Circ Res, 2015. **116**(2): p. 354-67.

208. Hofmann, U., et al., *Activation of CD4+ T lymphocytes improves wound healing and survival after experimental myocardial infarction in mice.* Circulation, 2012. **125**(13): p. 1652-63.

209. Itani, H.A., et al., *Activation of Human T Cells in Hypertension: Studies of Humanized Mice and Hypertensive Humans.* Hypertension, 2016. **68**(1):123-32.

210. Ren, J. and S.D. Crowley, *Role of T-cell Activation in Salt-sensitive Hypertension.* Am J Physiol Heart Circ Physiol, 2019.

211. Williams, R.J., J.P. Spencer, and C. Rice-Evans, *Flavonoids: antioxidants or signalling molecules?* Free Radic Biol Med, 2004. **36**(7): p. 838-49.

212. Mendez, M. and M.C. LaPointe, *Trophic effects of the cyclooxygenase-2 product prostaglandin E(2) in cardiac myocytes.* Hypertension, 2002. **39**(2 Pt 2): p. 382-8.

213. Anderson, R.J., et al., *Prostaglandins: effects on blood pressure, renal blood flow, sodium and water excretion.* Kidney Int, 1976. **10**(3): p. 205-15.

214. Daniels, E.G., et al., *Identification of prostaglandin E2 as the principal vasodepressor lipid of rabbit renal medulla.* Nature, 1967. **215**(5107): p. 1298-9.

215. Kida, T., et al., *Diverse effects of prostaglandin E(2) on vascular contractility.* Heart Vessels, 2014. **29**(3): p. 390-5.

216. Bryson, T.D., et al., *Overexpression of prostaglandin E2 EP4 receptor improves cardiac function after myocardial infarction.* J Mol Cell Cardiol, 2018.

217. Gu, X., et al., *Prostaglandin E2 Reduces Cardiac Contractility via EP3 Receptor.* Circ Heart Fail, 2016. **9**(8).

218. Harding, P., et al., *Lack of microsomal prostaglandin E synthase-1 reduces cardiac function following angiotensin II infusion.* Am J Physiol Heart Circ Physiol, 2011. **300**(3): p. H1053-61.

219. LaPointe, M.C., et al., *Inhibition of cyclooxygenase-2 improves cardiac function after myocardial infarction in the mouse.* Am J Physiol Heart Circ Physiol, 2004. **286**(4): p. H1416-24.

220. Nicola, C., P.K. Lala, and C. Chakraborty, *Prostaglandin E2-mediated migration of human trophoblast requires RAC1 and CDC42.* Biol Reprod, 2008. **78**(6):976-82.

221. Tang, E.H., et al., *Lack of EP4 receptors on bone marrow-derived cells enhances inflammation in atherosclerotic lesions.* Cardiovasc Res, 2011. **89**(1): p. 234-43.

222. Sugimoto, Y., et al., *Distinct cellular localization of mRNAs for three subtypes of prostaglandin E receptor in kidney.* Am J Physiol, 1994. **266**(5 Pt 2): p. F823-8.

223. Ishibashi, R., et al., *Roles of prostaglandin E receptors in mesangial cells under high-glucose conditions.* Kidney Int, 1999. **56**(2): p. 589-600.

224. Qian, Q., et al., *PGE2 causes mesangial cell hypertrophy and decreases expression of cyclin D3.* Nephron Physiol, 2009. **113**(2): p. p7-p14.

225. Bek, M., et al., *Characterization of prostanoid receptors in podocytes.* J Am Soc Nephrol, 1999. **10**(10): p. 2084-93.

226. Srivastava, T., et al., *Fluid flow shear stress upregulates prostanoid receptor EP2 but not EP4 in murine podocytes.* Prostaglandins Other Lipid Mediat, 2013. **104-105**: p. 49-57.

227. Guan, Y., et al., *Antihypertensive effects of selective prostaglandin E2 receptor subtype 1 targeting.* J Clin Invest, 2007. **117**(9): p. 2496-505.

228. Mechiche, H., et al., *Prostanoid receptors involved in regulation of the beating rate of neonatal rat cardiomyocytes.* PLoS One, 2012. **7**(9): p. e45273.

229. Harding, P. and M.C. LaPointe, *Prostaglandin E2 increases cardiac fibroblast proliferation and increases cyclin D expression via EP1 receptor.* Prostaglandins Leukot Essent Fatty Acids, 2011. **84**(5-6): p. 147-52.

230. Woodward, D.F., R.L. Jones, and S. Narumiya, *International Union of Basic and Clinical Pharmacology. LXXXIII: classification of prostanoid receptors, updating 15 years of progress.* Pharmacol Rev, 2011. **63**(3): p. 471-538.

231. Nasrallah, R., R. Hassouneh, and R.L. Hebert, *Chronic kidney disease: targeting prostaglandin E2 receptors.* Am J Physiol Renal Physiol, 2014. **307**(3):F243-50.

232. Regan, J.W., *EP2 and EP4 prostanoid receptor signaling.* Life Sci, 2003. **74**(2-3): p. 143-53.

233. Gu, G., et al., *Immunolocalization of adipocytes and prostaglandin E2 and its four receptor proteins EP1, EP2, EP3, and EP4 in the caprine cervix during spontaneous term labor.* Biol Reprod, 2012. **86**(5): p. 159, 1-10.

234. Suzuki, J., et al., *Roles of prostaglandin E2 in cardiovascular diseases.* Int Heart J, 2011. **52**(5): p. 266-9.

235. Namba, T., et al., *Alternative splicing of C-terminal tail of prostaglandin E receptor subtype EP3 determines G-protein specificity.* Nature, 1993. **365**(6442):166-70.

236. Negishi, M., et al., *Two isoforms of prostaglandin E receptor EP3 subtype. Different COOH-terminal domains determine sensitivity to agonist-induced desensitization.* J Biol Chem, 1993. **268**(13): p. 9517-21.

237. Hasegawa, H., et al., *Different membrane targeting of prostaglandin EP3 receptor isoforms dependent on their carboxy-terminal tail structures.* FEBS Lett, 2000. **473**(1): p. 76-80.

238. Bilson, H.A., D.L. Mitchell, and B. Ashby, *Human prostaglandin EP3 receptor isoforms show different agonist-induced internalization patterns.* FEBS Lett, 2004. **572**(1-3): p. 271-5.

239. Macias-Perez, I.M., et al., *Mouse EP3 alpha, beta, and gamma receptor variants reduce tumor cell proliferation and tumorigenesis in vivo.* J Biol Chem, 2008. **283**(18): p. 12538-45.

240. Jia, Z., et al., *mPGES-1-derived PGE2 mediates dehydration natriuresis.* Am J Physiol Renal Physiol, 2013. **304**(2): p. F214-21.

241. Coleman, R.A., et al., *A novel inhibitory prostanoid receptor in piglet saphenous vein.* Prostaglandins, 1994. **47**(2): p. 151-68.

242. Davis, R.J., et al., *EP4 prostanoid receptor-mediated vasodilatation of human middle cerebral arteries.* Br J Pharmacol, 2004. **141**(4): p. 580-5.

243. Foudi, N., et al., *Vasorelaxation induced by prostaglandin E2 in human pulmonary vein: role of the EP4 receptor subtype.* Br J Pharmacol, 2008. **154**(8): p. 1631-9.

244. Hristovska, A.M., et al., *Prostaglandin E2 induces vascular relaxation by E-prostanoid 4 receptor-mediated activation of endothelial nitric oxide synthase.* Hypertension, 2007. **50**(3): p. 525-30.

245. Lawrence, R.A. and R.L. Jones, *Investigation of the prostaglandin E (EP-) receptor subtype mediating relaxation of the rabbit jugular vein.* Br J Pharmacol, 1992. **105**(4): p. 817-24.

246. Lydford, S.J., K.C. McKechnie, and I.G. Dougall, *Pharmacological studies on prostanoid receptors in the rabbit isolated saphenous vein: a comparison with the rabbit isolated ear artery.* Br J Pharmacol, 1996. **117**(1): p. 13-20.

247. Yang, T. and Y. Du, *Distinct roles of central and peripheral prostaglandin E2 and EP subtypes in blood pressure regulation.* Am J Hypertens, 2012. **25**(10):1042-9.

248. Francois, H., et al., *Role of microsomal prostaglandin E synthase 1 in the kidney.* J Am Soc Nephrol, 2007. **18**(5): p. 1466-75.

249. Matsuda, H., et al., *Distinct modulation of superficial and juxtamedullary arterioles by prostaglandin in vivo.* Hypertens Res, 2002. **25**(6): p. 901-10.

250. Foudi, N., et al., *Differential reactivity of human mammary artery and saphenous vein to prostaglandin E(2) : implication for cardiovascular grafts.* Br J Pharmacol, 2011. **163**(4): p. 826-34.

251. Kobayashi, K., et al., *Prostaglandin E2-prostanoid EP3 signal induces vascular contraction via nPKC and ROCK activation in rat mesenteric artery.* Eur J Pharmacol, 2011. **660**(2-3): p. 375-80.

252. Jia, Z., et al., *Microsomal prostaglandin synthase-1-derived prostaglandin E2 protects against angiotensin II-induced hypertension via inhibition of oxidative stress.* Hypertension, 2008. **52**(5): p. 952-9.

253. Barnthaler, T., et al., *Imatinib stimulates PGE2 and attenuates cytokine release via EP4 receptor activation.* J Allergy Clin Immunol, 2018.

254. George, R.J., et al., *EP4 mediates PGE2 dependent cell survival through the PI3 kinase/AKT pathway.* Prostaglandins Other Lipid Mediat, 2007. **83**(1-2): p. 112-20.

255. Sokolowska, M., et al., *Prostaglandin E2 Inhibits NLRP3 Inflammasome Activation through EP4 Receptor and Intracellular Cyclic AMP in Human Macrophages.* J Immunol, 2015. **194**(11): p. 5472-87.

256. Takayama, K., et al., *Prostaglandin E2 suppresses chemokine production in human macrophages through the EP4 receptor.* J Biol Chem, 2002. **277**(46): p. 44147-54.

257. Tang, E.H., et al., *Activation of prostaglandin E2-EP4 signaling reduces chemokine production in adipose tissue.* J Lipid Res, 2015. **56**(2): p. 358-68.

258. Tang, E.H., et al., *Anti-inflammation therapy by activation of prostaglandin EP4 receptor in cardiovascular and other inflammatory diseases.* J Cardiovasc Pharmacol, 2012. **59**(2): p. 116-23.

259. Ngoc, P.B., et al., *The anti-inflammatory mechanism of prostaglandin e2 receptor 4 activation in rat experimental autoimmune myocarditis.* J Cardiovasc Pharmacol, 2011. **57**(3): p. 365-72.

260. Tilley, S.L., T.M. Coffman, and B.H. Koller, *Mixed messages: modulation of inflammation and immune responses by prostaglandins and thromboxanes.* J Clin Invest, 2001. **108**(1): p. 15-23.

261. Harris, S.G., et al., *Prostaglandins as modulators of immunity.* Trends Immunol, 2002. **23**(3): p. 144-50.

262. Nataraj, C., et al., *Receptors for prostaglandin E(2) that regulate cellular immune responses in the mouse.* J Clin Invest, 2001. **108**(8): p. 1229-35.

263. Morichika, T., et al., *Effect of prostaglandin E2 on intercellular adhesion molecule-1 and B7 expression in mixed lymphocyte reaction.* Transplantation, 2003. **75**(12): p. 2100-5.

264. Sanin, D.E., et al., *Mitochondrial Membrane Potential Regulates Nuclear Gene Expression in Macrophages Exposed to Prostaglandin E2.* Immunity, 2018. **49**(6): p. 1021-1033 e6.

265. Tang, J., et al., *Activation of E-prostanoid 3 receptor in macrophages facilitates cardiac healing after myocardial infarction.* Nat Commun, 2017. **8**: p. 14656.

266. Hishikari, K., et al., *Pharmacological activation of the prostaglandin E2 receptor EP4 improves cardiac function after myocardial ischaemia/reperfusion injury.* Cardiovasc Res, 2009. **81**(1): p. 123-32.

267. Qian, J.Y., et al., *Reduced cardiac remodeling and function in cardiac-specific EP4 receptor knockout mice with myocardial infarction.* Hypertension, 2008. **51**(2): p. 560-6.

268. Martin, M., et al., *Cardiospecific overexpression of the prostaglandin EP3 receptor attenuates ischemia-induced myocardial injury.* Circulation, 2005. **112**(3):400-6.

269. Hohlfeld, T., et al., *Reduction of infarct size by selective stimulation of prostaglandin EP(3)receptors in the reperfused ischemic pig heart.* J Mol Cell Cardiol, 2000. **32**(2): p. 285-96.

270. Thiemermann, C. and K. Zacharowski, *Selective activation of E-type prostanoid(3)-receptors reduces myocardial infarct size. A novel insight into the cardioprotective effects of prostaglandins.* Pharmacol Ther, 2000. **87**(1): p. 61-7.

271. Zacharowski, K., et al., *Selective activation of the prostanoid EP(3) receptor reduces myocardial infarct size in rodents.* Arterioscler Thromb Vasc Biol, 1999. **19**(9): p. 2141-7.

272. Alexander, R.W., et al., *Angiotensin increases inositol trisphosphate and calcium in vascular smooth muscle.* Hypertension, 1985. **7**(3 Pt 1): p. 447-51.

273. Berk, B.C., et al., *Angiotensin II-stimulated Na+/H+ exchange in cultured vascular smooth muscle cells. Evidence for protein kinase C-dependent and -independent pathways.* J Biol Chem, 1987. **262**(11): p. 5057-64.

274. Griendling, K.K., et al., *Sustained diacylglycerol formation from inositol phospholipids in angiotensin II-stimulated vascular smooth muscle cells.* J Biol Chem, 1986. **261**(13): p. 5901-6.

275. Griendling, K.K., et al., *Angiotensin II stimulation of vascular smooth muscle.* J Cardiovasc Pharmacol, 1989. **14 Suppl 6**: p. S27-33.

276. Robinson, M.J. and M.H. Cobb, *Mitogen-activated protein kinase pathways.* Curr Opin Cell Biol, 1997. **9**(2): p. 180-6.

277. Nguyen Dinh Cat, A., et al., *Angiotensin II, NADPH oxidase, and redox signaling in the vasculature.* Antioxid Redox Signal, 2013. **19**(10): p. 1110-20.

278. Loirand, G. and P. Pacaud, *The role of Rho protein signaling in hypertension.* Nat Rev Cardiol, 2010. **7**(11): p. 637-47.

279. Nguyen Dinh Cat, A. and R.M. Touyz, *Cell signaling of angiotensin II on vascular tone: novel mechanisms.* Curr Hypertens Rep, 2011. **13**(2): p. 122-8.

280. Jin, L., et al., *Increased RhoA/Rho-kinase signaling mediates spontaneous tone in aorta from angiotensin II-induced hypertensive rats.* J Pharmacol Exp Ther, 2006. **318**(1): p. 288-95.

281. Yamakawa, T., et al., *Involvement of Rho-kinase in angiotensin II-induced hypertrophy of rat vascular smooth muscle cells.* Hypertension, 2000. **35**(1 Pt 2): p. 313-8.

282. Seko, T., et al., *Activation of RhoA and inhibition of myosin phosphatase as important components in hypertension in vascular smooth muscle.* Circ Res, 2003. **92**(4): p. 411-8.

283. Kroon, J., et al., *The small GTPase RhoB regulates TNFalpha signaling in endothelial cells.* PLoS One, 2013. **8**(9): p. e75031.

284. Reinhard, N.R., et al., *Spatiotemporal analysis of RhoA/B/C activation in primary human endothelial cells.* Sci Rep, 2016. **6**: p. 25502.

285. Bonventre, J.V., *Phospholipase A2 and signal transduction.* J Am Soc Nephrol, 1992. **3**(2): p. 128-50.

286. Rao, G.N., et al., *Angiotensin II stimulates phosphorylation of high-molecular-mass cytosolic phospholipase A2 in vascular smooth-muscle cells.* Biochem J, 1994. **299 (Pt 1)**: p. 197-201.

287. Griendling, K.K., et al., *Angiotensin II stimulates NADH and NADPH oxidase activity in cultured vascular smooth muscle cells.* Circ Res, 1994. **74**(6):1141-8.

288. Jaimes, E.A., J.M. Galceran, and L. Raij, *Angiotensin II induces superoxide anion production by mesangial cells.* Kidney Int, 1998. **54**(3): p. 775-84.

289. Pagano, P.J., et al., *Angiotensin II induces p67phox mRNA expression and NADPH oxidase superoxide generation in rabbit aortic adventitial fibroblasts.* Hypertension, 1998. **32**(2): p. 331-7.

290. Touyz, R.M. and E.L. Schiffrin, *Ang II-stimulated superoxide production is mediated via phospholipase D in human vascular smooth muscle cells.* Hypertension, 1999. **34**(4 Pt 2): p. 976-82.

291. Ushio-Fukai, M., et al., *p38 Mitogen-activated protein kinase is a critical component of the redox-sensitive signaling pathways activated by angiotensin II. Role in vascular smooth muscle cell hypertrophy.* J Biol Chem, 1998. **273**(24): p. 15022-9.

292. Ushio-Fukai, M., et al., *Reactive oxygen species mediate the activation of Akt/protein kinase B by angiotensin II in vascular smooth muscle cells.* J Biol Chem, 1999. **274**(32): p. 22699-704.

293. Group, C.T.S., *Effects of enalapril on mortality in severe congestive heart failure. Results of the Cooperative North Scandinavian Enalapril Survival Study (CONSENSUS).* N Engl J Med, 1987. **316**(23): p. 1429-35.

294. Dusing, R., *Mega clinical trials which have shaped the RAS intervention clinical practice.* Ther Adv Cardiovasc Dis, 2016. **10**(3): p. 133-50.

295. Kim, S., et al., *Cardiovascular effects of combination of perindopril, candesartan, and amlodipine in hypertensive rats.* Hypertension, 2000. **35**(3): p. 769-74.

296. Li, J.S., A.M. Sharifi, and E.L. Schiffrin, *Effect of AT1 angiotensin-receptor blockade on structure and function of small arteries in SHR.* J Cardiovasc Pharmacol, 1997. **30**(1): p. 75-83.

297. Schiffrin, E.L., *Correction of remodeling and function of small arteries in human hypertension by cilazapril, an angiotensin I-converting enzyme inhibitor.* J Cardiovasc Pharmacol, 1996. **27 Suppl 2**: p. S13-8.

298. Schiffrin, E.L. and L.Y. Deng, *Comparison of effects of angiotensin I-converting enzyme inhibition and beta-blockade for 2 years on function of small arteries from hypertensive patients.* Hypertension, 1995. **25**(4 Pt 2): p. 699-703.

299. Schiffrin, E.L., L.Y. Deng, and P. Larochelle, *Effects of a beta-blocker or a converting enzyme inhibitor on resistance arteries in essential hypertension.* Hypertension, 1994. **23**(1): p. 83-91.

300. Schiffrin, E.L., et al., *Correction of arterial structure and endothelial dysfunction in human essential hypertension by the angiotensin receptor antagonist losartan.* Circulation, 2000. **101**(14): p. 1653-9.

301. Touyz, R.M. and E.L. Schiffrin, *The effect of angiotensin II on platelet intracellular free magnesium and calcium ionic concentrations in essential hypertension.* J Hypertens, 1993. **11**(5): p. 551-8.

302. Coffman, T.M., *The inextricable role of the kidney in hypertension.* J Clin Invest, 2014. **124**(6): p. 2341-7.

303. Mennuni, S., et al., *Hypertension and kidneys: unraveling complex molecular mechanisms underlying hypertensive renal damage.* J Hum Hypertens, 2014. **28**(2): p. 74-9.

304. Gurley, S.B., et al., *AT1A angiotensin receptors in the renal proximal tubule regulate blood pressure.* Cell Metab, 2011. **13**(4): p. 469-475.

305. Beilin, L.J., F.S. Goldby, and J. Mohring, *High arterial pressure versus humoral factors in the pathogenesis of the vascular lesions of malignant hypertension.* Clin Sci Mol Med, 1977. **52**(2): p. 111-7.

306. Goldby, F.S. and L.J. Beilin, *How an acute rise in arterial pressure damages arterioles. Electron microscopic changes during angiotensin infusion.* Cardiovasc Res, 1972. **6**(5): p. 569-84.

307. Goldby, F.S. and L.J. Beilin, *Relationship between arterial pressure and the permeability of arterioles to carbon particles in acute hypertension in the rat.* Cardiovasc Res, 1972. **6**(4): p. 384-90.

308. Valentin, J.P., et al., *Losartan prevents thromboxane A2/prostanoid (TP) receptor mediated increase in microvascular permeability in the rat.* Am J Hypertens, 1997. **10**(9 Pt 1): p. 1058-63.

309. Linz, W., et al., *Contribution of kinins to the cardiovascular actions of angiotensin-converting enzyme inhibitors.* Pharmacol Rev, 1995. **47**(1): p. 25-49.

310. Swartz, S.L. and G.H. Williams, *Angiotensin-converting enzyme inhibition and prostaglandins.* Am J Cardiol, 1982. **49**(6): p. 1405-9.

311. Hulsmans, M., F. Sam, and M. Nahrendorf, *Monocyte and macrophage contributions to cardiac remodeling.* J Mol Cell Cardiol, 2016. **93**: p. 149-55.

312. Rahman, S.T., et al., *Effects of eprosartan versus hydrochlorothiazide on markers of vascular oxidation and inflammation and blood pressure (renin-angiotensin system antagonists, oxidation, and inflammation).* Am J Cardiol, 2002. **89**(6): p. 686-90.

313. Soejima, H., et al., *Angiotensin-converting enzyme inhibition reduces monocyte chemoattractant protein-1 and tissue factor levels in patients with myocardial infarction.* J Am Coll Cardiol, 1999. **34**(4): p. 983-8.

314. Gomez, R.A., et al., *Leukocytes synthesize angiotensinogen.* Hypertension, 1993. **21**(4): p. 470-5.

315. Klickstein, L.B., C.E. Kaempfer, and B.U. Wintroub, *The granulocyte-angiotensin system. Angiotensin I-converting activity of cathepsin G.* J Biol Chem, 1982. **257**(24): p. 15042-6.

316. Owen, C.A. and E.J. Campbell, *Angiotensin II generation at the cell surface of activated neutrophils: novel cathepsin G-mediated catalytic activity that is resistant to inhibition.* J Immunol, 1998. **160**(3): p. 1436-43.

317. Reilly, C.F., et al., *Rapid conversion of angiotensin I to angiotensin II by neutrophil and mast cell proteinases.* J Biol Chem, 1982. **257**(15): p. 8619-22.

318. Tonnesen, M.G., et al., *Identification of a human neutrophil angiotension II-generating protease as cathepsin G.* J Clin Invest, 1982. **69**(1): p. 25-30.

319. Mattana, J., R.T. Sankaran, and P.C. Singhal, *Repetitive mechanical strain suppresses macrophage uptake of immunoglobulin G complexes and enhances cyclic adenosine monophosphate synthesis.* Am J Pathol, 1995. **147**(2):529-40.

320. Mattana, J. and P.C. Singhal, *Effects of atrial natriuretic peptide and cGMP on uptake of IgG complexes by macrophages.* Am J Physiol, 1993. **265**(1 Pt 1): p. C92-8.

321. Barnes, P.J. and M. Karin, *Nuclear factor-kappaB: a pivotal transcription factor in chronic inflammatory diseases.* N Engl J Med, 1997. **336**(15): p. 1066-71.

322. Guijarro, C. and J. Egido, *Transcription factor-kappa B (NF-kappa B) and renal disease.* Kidney Int, 2001. **59**(2): p. 415-24.

323. Morrissey, J.J. and S. Klahr, *Differential effects of ACE and AT1 receptor inhibition on chemoattractant and adhesion molecule synthesis.* Am J Physiol, 1998. **274**(3 Pt 2): p. F580-6.

324. Ruiz-Ortega, M., et al., *Angiotensin II participates in mononuclear cell recruitment in experimental immune complex nephritis through nuclear factor-kappa B activation and monocyte chemoattractant protein-1 synthesis.* J Immunol, 1998. **161**(1): p. 430-9.

325. Matsui, Y., et al., *Role of osteopontin in cardiac fibrosis and remodeling in angiotensin II-induced cardiac hypertrophy.* Hypertension, 2004. **43**(6): 1195-201.

326. Han, J., et al., *MD2 mediates angiotensin II-induced cardiac inflammation and remodeling via directly binding to Ang II and activating TLR4/NF-kappaB signaling pathway.* Basic Res Cardiol, 2017. **112**(1): p. 9.

327. Ferrario, C.M., *Cardiac remodelling and RAS inhibition.* Ther Adv Cardiovasc Dis, 2016. **10**(3): p. 162-71.

328. Altara, R. and G.W. Booz, *Deleting Vascular ADAM17 Sheds New Light on Hypertensive Cardiac Hypertrophy.* Hypertension, 2016. **68**(4): p. 849-50.

329. Peng, J., et al., *Tumor necrosis factor-alpha-induced AT1 receptor upregulation enhances angiotensin II-mediated cardiac fibroblast responses that favor fibrosis.* Circ Res, 2002. **91**(12): p. 1119-26.

330. Xu, J., et al., *Local angiotensin II aggravates cardiac remodeling in hypertension.* Am J Physiol Heart Circ Physiol, 2010. **299**(5): p. H1328-38.

331. Li, Y.S., et al., *Angiotensin II facilitates fibrogenic effect of TGF-beta1 through enhancing the down-regulation of BAMBI caused by LPS: a new pro-fibrotic mechanism of angiotensin II.* PLoS One, 2013. **8**(10): p. e76289.

332. Sadoshima, J., et al., *Autocrine release of angiotensin II mediates stretch-induced hypertrophy of cardiac myocytes in vitro.* Cell, 1993. **75**(5): p. 977-84.

333. De Mello, W.C. and A.H. Danser, *Angiotensin II and the heart : on the intracrine renin-angiotensin system.* Hypertension, 2000. **35**(6): p. 1183-8.

334. Reudelhuber, T.L., K.E. Bernstein, and P. Delafontaine, *Is angiotensin II a direct mediator of left ventricular hypertrophy? Time for another look.* Hypertension, 2007. **49**(6): p. 1196-201.

335. Shimizu, T., et al., *Fibroblast deletion of ROCK2 attenuates cardiac hypertrophy, fibrosis, and diastolic dysfunction.* JCI Insight, 2017. **2**(13).

336. Tham, Y.K., et al., *Pathophysiology of cardiac hypertrophy and heart failure: signaling pathways and novel therapeutic targets.* Arch Toxicol, 2015. **89**(9): p. 1401-38.

337. Frieler, R.A. and R.M. Mortensen, *Immune cell and other noncardiomyocyte regulation of cardiac hypertrophy and remodeling.* Circulation, 2015. **131**(11): p. 1019-30.

338. Marko, L., et al., *Bcl10 mediates angiotensin II-induced cardiac damage and electrical remodeling.* Hypertension, 2014. **64**(5): p. 1032-9.

339. Singh, M.V., et al., *Dual Activation of TRIF and MyD88 Adaptor Proteins by Angiotensin II Evokes Opposing Effects on Pressure, Cardiac Hypertrophy, and Inflammatory Gene Expression.* Hypertension, 2015. **66**(3): p. 647-56.

340. Valente, A.J., et al., *CIKS (Act1 or TRAF3IP2) mediates Angiotensin-II-induced Interleukin-18 expression, and Nox2-dependent cardiomyocyte hypertrophy.* J Mol Cell Cardiol, 2012. **53**(1): p. 113-24.

341. Kossmann, S., et al., *Inflammatory monocytes determine endothelial nitric-oxide synthase uncoupling and nitro-oxidative stress induced by angiotensin II.* J Biol Chem, 2014. **289**(40): p. 27540-50.

342. Timmers, L., et al., *Toll-like receptor 4 mediates maladaptive left ventricular remodeling and impairs cardiac function after myocardial infarction.* Circ Res, 2008. **102**(2): p. 257-64.

343. Ji, Y., et al., *PPARgamma agonist, rosiglitazone, regulates angiotensin II-induced vascular inflammation through the TLR4-dependent signaling pathway.* Lab Invest, 2009. **89**(8): p. 887-902.

344. Matsuda, S., et al., *Angiotensin Activates MCP-1 and Induces Cardiac Hypertrophy and Dysfunction via Toll-like Receptor 4.* J Atheroscler Thromb, 2015. **22**(8): p. 833-44.

345. Falkenham, A., et al., *Nonclassical resident macrophages are important determinants in the development of myocardial fibrosis.* Am J Pathol, 2015. **185**(4): p. 927-42.

346. Gomolak, J.R. and S.P. Didion, *Angiotensin II-induced endothelial dysfunction is temporally linked with increases in interleukin-6 and vascular macrophage accumulation.* Front Physiol, 2014. **5**: p. 396.

347. Ma, F., et al., *The requirement of CD8+ T cells to initiate and augment acute cardiac inflammatory response to high blood pressure.* J Immunol, 2014. **192**(7): p. 3365-73.

348. Thygesen, K., et al., *Fourth Universal Definition of Myocardial Infarction (2018).* Circulation, 2018. **138**(20): p. e618-e651.

349. Zamilpa, R., et al., *Cardiac wound healing post-myocardial infarction: a novel method to target extracellular matrix remodeling in the left ventricle.* Methods Mol Biol, 2013. **1037**: p. 313-24.

350. Bacmeister, L., et al., *Inflammation and fibrosis in murine models of heart failure.* Basic Res Cardiol, 2019. **114**(3): p. 19.

351. Cohen, M., C. Boiangiu, and M. Abidi, *Therapy for ST-segment elevation myocardial infarction patients who present late or are ineligible for reperfusion therapy.* J Am Coll Cardiol, 2010. **55**(18): p. 1895-906.

352. Lutgens, E., et al., *Chronic myocardial infarction in the mouse: cardiac structural and functional changes.* Cardiovasc Res, 1999. **41**(3): p. 586-93.

353. Iyer, R.P., et al., *Defining the sham environment for post-myocardial infarction studies in mice.* Am J Physiol Heart Circ Physiol, 2016. **311**(3): p. H822-36.

354. Mouton, A.J., et al., *Mapping macrophage polarization over the myocardial infarction time continuum.* Basic Res Cardiol, 2018. **113**(4): p. 26.

355. Hinrichs, S., et al., *Precursor proadrenomedullin influences cardiomyocyte survival and local inflammation related to myocardial infarction.* Proc Natl Acad Sci U S A, 2018. **115**(37): p. E8727-e8736.

356. Paul, M., A. Poyan Mehr, and R. Kreutz, *Physiology of local renin-angiotensin systems.* Physiol Rev, 2006. **86**(3): p. 747-803.

357. Westermann, D., et al., *Selective PDE5A inhibition with sildenafil rescues left ventricular dysfunction, inflammatory immune response and cardiac remodeling in angiotensin II-induced heart failure in vivo.* Basic Res Cardiol, 2012. **107**(6): 308.

358. Regan, J.A., et al., *A mouse model of heart failure with preserved ejection fraction due to chronic infusion of a low subpressor dose of angiotensin II.* Am J Physiol Heart Circ Physiol, 2015. **309**(5): p. H771-8.

359. Gonzalez, G.E., et al., *Cardiac-deleterious role of galectin-3 in chronic angiotensin II-induced hypertension.* Am J Physiol Heart Circ Physiol, 2016. **311**(5): p. H1287-h1296.

360. Lindner, D., et al., *Cardiac fibroblasts support cardiac inflammation in heart failure.* Basic Res Cardiol, 2014. **109**(5): p. 428.

361. Redgrave, R.E., et al., *Using MRI to predict future adverse cardiac remodelling in a male mouse model of myocardial infarction.* Int J Cardiol Heart Vasc, 2016. **11**: p. 29-34.

362. Gu, X., et al., *Fractalkine neutralization improves cardiac function after myocardial infarction.* Exp Physiol, 2015. **100**(7): p. 805-17.

363. Takagawa, J., et al., *Myocardial infarct size measurement in the mouse chronic infarction model: comparison of area- and length-based approaches.* J Appl Physiol (1985), 2007. **102**(6): p. 2104-11.

364. Sharma, U., et al., *Novel anti-inflammatory mechanisms of N-Acetyl-Ser-Asp-Lys-Pro in hypertension-induced target organ damage.* Am J Physiol Heart Circ Physiol, 2008. **294**(3): p. H1226-H1232.

365. Tsujita, K., et al., *Targeted deletion of class A macrophage scavenger receptor increases the risk of cardiac rupture after experimental myocardial infarction.* Circulation, 2007. **115**(14): p. 1904-1911.

366. Winer, J., et al., *Development and validation of real-time quantitative reverse transcriptase-polymerase chain reaction for monitoring gene expression in cardiac myocytes in vitro.* Anal Biochem, 1999. **270**(1): p. 41-9.

367. Sternlicht, M.D. and Z. Werb, *How matrix metalloproteinases regulate cell behavior.* Annu Rev Cell Dev Biol, 2001. **17**: p. 463-516.

368. Creemers, E.E., et al., *Matrix metalloproteinase inhibition after myocardial infarction: a new approach to prevent heart failure?* Circ Res, 2001. **89**(3):201-10.

369. Matsumura, S., et al., *Targeted deletion or pharmacological inhibition of MMP-2 prevents cardiac rupture after myocardial infarction in mice.* J Clin Invest, 2005. **115**(3): p. 599-609.

370. Spinale, F.G., et al., *Time-dependent changes in matrix metalloproteinase activity and expression during the progression of congestive heart failure: relation to ventricular and myocyte function.* Circ Res, 1998. **82**(4): p. 482-95.

371. Xiao, C.Y., et al., *Prostaglandin E2 protects the heart from ischemia-reperfusion injury via its receptor subtype EP4.* Circulation, 2004. **109**(20): p. 2462-2468.

372. Wang, Q., et al., *An EP4 Receptor Agonist Inhibits Cardiac Fibrosis Through Activation of PKA Signaling in Hypertrophied Heart.* Int Heart J, 2016.

373. Haywood, G.A., et al., *Expression of inducible nitric oxide synthase in human heart failure.* Circulation, 1996. **93**(6): p. 1087-94.

374. Kim, S.H., et al., *Distinct protein kinase A anchoring proteins direct prostaglandin E2 modulation of Toll-like receptor signaling in alveolar macrophages.* J Biol Chem, 2011. **286**(11): p. 8875-83.

375. Morato-Marques, M., et al., *Leukotrienes target F-actin/cofilin-1 to enhance alveolar macrophage anti-fungal activity.* J Biol Chem, 2011. **286**(33):28902-13.

376. Domingo-Gonzalez, R., et al., *Prostaglandin E2-induced changes in alveolar macrophage scavenger receptor profiles differentially alter phagocytosis of Pseudomonas aeruginosa and Staphylococcus aureus post-bone marrow transplant.* J Immunol, 2013. **190**(11): p. 5809-17.

377. Hayashidani, S., et al., *Targeted deletion of MMP-2 attenuates early LV rupture and late remodeling after experimental myocardial infarction.* Am J Physiol Heart Circ Physiol, 2003. **285**(3): p. H1229-35.

378. Heymans, S., et al., *Inhibition of plasminogen activators or matrix metalloproteinases prevents cardiac rupture but impairs therapeutic angiogenesis and causes cardiac failure.* Nat Med, 1999. **5**(10): p. 1135-42.

379. Lindsey, M.L., et al., *Selective matrix metalloproteinase inhibition reduces left ventricular remodeling but does not inhibit angiogenesis after myocardial infarction.* Circulation, 2002. **105**(6): p. 753-8.

380. Mukherjee, R., et al., *Myocardial infarct expansion and matrix metalloproteinase inhibition.* Circulation, 2003. **107**(4): p. 618-25.

381. Schellings, M.W., et al., *Absence of SPARC results in increased cardiac rupture and dysfunction after acute myocardial infarction.* J Exp Med, 2009. **206**(1):113-23.

382. Barrans, J.D., D. Stamatiou, and C. Liew, *Construction of a human cardiovascular cDNA microarray: portrait of the failing heart.* Biochem Biophys Res Commun, 2001. **280**(4): p. 964-969.

383. Harris, B.S., et al., *SPARC regulates collagen interaction with cardiac fibroblast cell surfaces.* Am J Physiol Heart Circ Physiol, 2011. **301**(3): p. H841-7.

384. Feldman, A.M., et al., *The role of tumor necrosis factor in the pathophysiology of heart failure.* J Am Coll Cardiol, 2000. **35**(3): p. 537-44.

385. Khanna, D., M. McMahon, and D.E. Furst, *Anti-tumor necrosis factor alpha therapy and heart failure: what have we learned and where do we go from here?* Arthritis Rheum, 2004. **50**(4): p. 1040-50.

386. Zlotnik, A. and O. Yoshie, *Chemokines: a new classification system and their role in immunity.* Immunity, 2000. **12**(2): p. 121-7.

387. Blanchet, X., et al., *Touch of chemokines.* Front Immunol, 2012. **3**: p. 175.

388. Rollins, B.J., *Monocyte chemoattractant protein 1: a potential regulator of monocyte recruitment in inflammatory disease.* Mol Med Today, 1996. **2**(5): p. 198-204.

389. Gullestad, L., et al., *Effect of high- versus low-dose angiotensin converting enzyme inhibition on cytokine levels in chronic heart failure.* J Am Coll Cardiol, 1999. **34**(7): p. 2061-7.

390. Hayashidani, S., et al., *Anti-monocyte chemoattractant protein-1 gene therapy attenuates left ventricular remodeling and failure after experimental myocardial infarction.* Circulation, 2003. **108**(17): p. 2134-40.

391. Rundhaug, J.E., et al., *The role of the EP receptors for prostaglandin E2 in skin and skin cancer.* Cancer Metastasis Rev, 2011. **30**(3-4): p. 465-80.

392. Sugimoto, Y. and S. Narumiya, *Prostaglandin E receptors.* J Biol Chem, 2007. **282**(16): p. 11613-7.

393. Liang, X., et al., *Signaling via the prostaglandin E(2) receptor EP4 exerts neuronal and vascular protection in a mouse model of cerebral ischemia.* J Clin Invest, 2011. **121**(11): p. 4362-71.

394. Xiao, C.Y., et al., *Prostaglandin E2 protects the heart from ischemia-reperfusion injury via its receptor subtype EP4.* Circulation, 2004. **109**(20): p. 2462-8.

395. Largo, R., et al., *EP2/EP4 signalling inhibits monocyte chemoattractant protein-1 production induced by interleukin 1beta in synovial fibroblasts.* Ann Rheum Dis, 2004. **63**(10): p. 1197-204.

396. Shen, Y., et al., *PGE2 downregulates LPS-induced inflammatory responses via the TLR4-NF-kappaB signaling pathway in bovine endometrial epithelial cells.* Prostaglandins Leukot Essent Fatty Acids, 2018. **129**: p. 25-31.

397. Mesquita, R.F., et al., *Protein kinase Cepsilon-calcineurin cosignaling downstream of toll-like receptor 4 downregulates fibrosis and induces wound healing gene expression in cardiac myofibroblasts.* Mol Cell Biol, 2014. **34**(4): p. 574-94.

398. Frantz, S., G. Ertl, and J. Bauersachs, *Mechanisms of disease: Toll-like receptors in cardiovascular disease.* Nat Clin Pract Cardiovasc Med, 2007. **4**(8): p. 444-54.

399. Chen, W. and N.G. Frangogiannis, *Fibroblasts in post-infarction inflammation and cardiac repair.* Biochim Biophys Acta, 2013. **1833**(4): p. 945-53.

400. Cinar, M.U., et al., *Evaluation of suitable reference genes for gene expression studies in porcine PBMCs in response to LPS and LTA.* BMC Res Notes, 2013. **6**: p. 56.

401. Dean, J.L., et al., *p38 mitogen-activated protein kinase regulates cyclooxygenase-2 mRNA stability and transcription in lipopolysaccharide-treated human monocytes.* J Biol Chem, 1999. **274**(1): p. 264-9.

402. Biswas, R., et al., *Regulation of chemokine mRNA stability by lipopolysaccharide and IL-10.* J Immunol, 2003. **170**(12): p. 6202-8.

403. Neininger, A., et al., *MK2 targets AU-rich elements and regulates biosynthesis of tumor necrosis factor and interleukin-6 independently at different post-transcriptional levels.* J Biol Chem, 2002. **277**(5): p. 3065-8.

404. Blackwell, T.S. and J.W. Christman, *The role of nuclear factor-kappa B in cytokine gene regulation.* Am J Respir Cell Mol Biol, 1997. **17**(1): p. 3-9.

405. Lawrence, T., *The nuclear factor NF-kappaB pathway in inflammation.* Cold Spring Harb Perspect Biol, 2009. **1**(6): p. a001651.

406. Liu, T., et al., *NF-κB signaling in inflammation.* Signal Transduction And Targeted Therapy, 2017. **2**: p. 17023.

407. Guha, M. and N. Mackman, *LPS induction of gene expression in human monocytes.* Cell Signal, 2001. **13**(2): p. 85-94.

408. Sagana, R.L., et al., *Phosphatase and tensin homologue on chromosome 10 (PTEN) directs prostaglandin E2-mediated fibroblast responses via regulation of E prostanoid 2 receptor expression.* J Biol Chem, 2009. **284**(47): p. 32264-71.

409. CliniSciences, *Boyden Chamber Assays.* 2019.

410. Maekawa, Y., et al., *Effect of granulocyte-macrophage colony-stimulating factor inducer on left ventricular remodeling after acute myocardial infarction.* J Am Coll Cardiol, 2004. **44**(7): p. 1510-20.

411. Hayasaki, T., et al., *CC chemokine receptor-2 deficiency attenuates oxidative stress and infarct size caused by myocardial ischemia-reperfusion in mice.* Circ J, 2006. **70**(3): p. 342-51.

412. Kohno, T., et al., *Angiotensin-receptor blockade reduces border zone myocardial monocyte chemoattractant protein-1 expression and macrophage infiltration in post-infarction ventricular remodeling.* Circ J, 2008. **72**(10): p. 1685-92.

413. LeLeiko, R.M., et al., *Usefulness of elevations in serum choline and free F2)-isoprostane to predict 30-day cardiovascular outcomes in patients with acute coronary syndrome.* Am J Cardiol, 2009. **104**(5): p. 638-43.

414. Polidori, M.C., et al., *Increased F2 isoprostane plasma levels in patients with congestive heart failure are correlated with antioxidant status and disease severity.* J Card Fail, 2004. **10**(4): p. 334-8.

415. Hokamaki, J., et al., *Urinary biopyrrins levels are elevated in relation to severity of heart failure.* J Am Coll Cardiol, 2004. **43**(10): p. 1880-5.

416. Swales, J.D., *Renin-angiotensin system in hypertension.* Pharmacol Ther, 1979. **7**(1): p. 173-201.

417. Griffin, S.A., et al., *Angiotensin II causes vascular hypertrophy in part by a non-pressor mechanism.* Hypertension, 1991. **17**(5): p. 626-35.

418. Suzuki, Y., et al., *Inflammation and angiotensin II.* Int J Biochem Cell Biol, 2003. **35**(6): p. 881-900.

419. Baylis, C. and B.M. Brenner, *Modulation by prostaglandin synthesis inhibitors of the action of exogenous angiotensin II on glomerular ultrafiltration in the rat.* Circ Res, 1978. **43**(6): p. 889-98.

420. Murphy, T.J., et al., *Isolation of a cDNA encoding the vascular type-1 angiotensin II receptor.* Nature, 1991. **351**(6323): p. 233-6.

421. Sasaki, K., et al., *Cloning and expression of a complementary DNA encoding a bovine adrenal angiotensin II type-1 receptor.* Nature, 1991. **351**(6323): p. 230-3.

422. Viswanathan, M., et al., *Expression of a novel non-angiotensin II [125I]CGP 42112 binding site in healing wounds of the rat brain.* Brain Res, 1994. **658**(1-2):265-70.

423. Ciuffo, G.M., et al., *Heterogeneity of rat angiotensin II AT2 receptor.* Adv Exp Med Biol, 1996. **396**: p. 189-97.

424. Baker, K.M. and J.F. Aceto, *Angiotensin II stimulation of protein synthesis and cell growth in chick heart cells.* Am J Physiol, 1990. **259**(2 Pt 2): p. H610-8.

425. Baker, K.M., G.W. Booz, and D.E. Dostal, *Cardiac actions of angiotensin II: Role of an intracardiac renin-angiotensin system.* Annu Rev Physiol, 1992. **54**:227-41.

426. Sadoshima, J. and S. Izumo, *The cellular and molecular response of cardiac myocytes to mechanical stress.* Annu Rev Physiol, 1997. **59**: p. 551-71.

427. Wada, H., et al., *Comparative effects of contraction and angiotensin II on growth of adult feline cardiocytes in primary culture.* Am J Physiol, 1996. **271**(1 Pt 2): p. H29-37.

428. Ritchie, R.H., et al., *Angiotensin II-induced hypertrophy of adult rat cardiomyocytes is blocked by nitric oxide.* Am J Physiol, 1998. **275**(4 Pt 2): p. H1370-4.

429. Booz, G.W. and K.M. Baker, *Role of type 1 and type 2 angiotensin receptors in angiotensin II-induced cardiomyocyte hypertrophy.* Hypertension, 1996. **28**(4): p. 635-40.

430. Booz, G.W. and K.M. Baker, *The role of the renin-angiotensin system in the pathophysiology of cardiac remodeling.* Blood Press Suppl, 1996. **2**: p. 10-8.

431. Villarreal, F.J., et al., *Identification of functional angiotensin II receptors on rat cardiac fibroblasts.* Circulation, 1993. **88**(6): p. 2849-61.

432. Crabos, M., et al., *Characterization of angiotensin II receptors in cultured adult rat cardiac fibroblasts. Coupling to signaling systems and gene expression.* J Clin Invest, 1994. **93**(6): p. 2372-8.

433. Rodriguez-Iturbe, B., H. Pons, and R.J. Johnson, *Role of the Immune System in Hypertension.* Physiol Rev, 2017. **97**(3): p. 1127-1164.

434. Harrison, D.G., et al., *Inflammation, immunity, and hypertension.* Hypertension, 2011. **57**(2): p. 132-40.

435. Kim, J.A., J.A. Berliner, and J.L. Nadler, *Angiotensin II increases monocyte binding to endothelial cells.* Biochem Biophys Res Commun, 1996. **226**(3): p. 862-8.

436. Griendling, K.K., et al., *Modulation of protein kinase activity and gene expression by reactive oxygen species and their role in vascular physiology and pathophysiology.* Arterioscler Thromb Vasc Biol, 2000. **20**(10): p. 2175-83.

437. Griendling, K.K., D. Sorescu, and M. Ushio-Fukai, *NAD(P)H oxidase: role in cardiovascular biology and disease.* Circ Res, 2000. **86**(5): p. 494-501.

438. Papaharalambus, C.A. and K.K. Griendling, *Basic mechanisms of oxidative stress and reactive oxygen species in cardiovascular injury.* Trends Cardiovasc Med, 2007. **17**(2): p. 48-54.

439. Chen, L., et al., *Inactivation of the E-prostanoid 3 receptor attenuates the angiotensin II pressor response via decreasing arterial contractility.* Arterioscler Thromb Vasc Biol, 2012. **32**(12): p. 3024-32.

440. Mitra, A.K., L. Gao, and I.H. Zucker, *Angiotensin II-induced upregulation of AT(1) receptor expression: sequential activation of NF-kappaB and Elk-1 in neurons.* Am J Physiol Cell Physiol, 2010. **299**(3): p. C561-9.

441. Uehata, M., et al., *Calcium sensitization of smooth muscle mediated by a Rho-associated protein kinase in hypertension.* Nature, 1997. **389**(6654): p. 990-4.

442. Weber, D.S. and R.C. Webb, *Enhanced relaxation to the rho-kinase inhibitor Y-27632 in mesenteric arteries from mineralocorticoid hypertensive rats.* Pharmacology, 2001. **63**(3): p. 129-33.

443. Asano, M. and Y. Nomura, *Comparison of inhibitory effects of Y-27632, a Rho kinase inhibitor, in strips of small and large mesenteric arteries from spontaneously hypertensive and normotensive Wistar-Kyoto rats.* Hypertens Res, 2003. **26**(1): p. 97-106.

444. Riba, A., et al., *Cardioprotective Effect of Resveratrol in a Postinfarction Heart Failure Model.* Oxid Med Cell Longev, 2017. **2017**: p. 6819281.

445. Munzel, T., et al., *Pathophysiological role of oxidative stress in systolic and diastolic heart failure and its therapeutic implications.* Eur Heart J, 2015. **36**(38): p. 2555-64.

446. Tang, Y., et al., *Oltipraz attenuates the progression of heart failure in rats through inhibiting oxidative stress and inflammatory response.* Eur Rev Med Pharmacol Sci, 2018. **22**(24): p. 8918-8923.

447. Wang, Q.W., et al., *Ginsenoside Re Improves Isoproterenol-Induced Myocardial Fibrosis and Heart Failure in Rats.* Evid Based Complement Alternat Med, 2019. **2019**: p. 3714508.

448. Zhang, X.J., et al., *Growth differentiation factor 11 is involved in isoproterenolinduced heart failure.* Mol Med Rep, 2019. **19**(5): p. 4109-4118.

449. Aluja, D., et al., *Calpains mediate isoproterenol-induced hypertrophy through modulation of GRK2.* Basic Res Cardiol, 2019. **114**(3): p. 21.

450. Funakoshi, Y., et al., *Rho-kinase mediates angiotensin II-induced monocyte chemoattractant protein-1 expression in rat vascular smooth muscle cells.* Hypertension, 2001. **38**(1): p. 100-4.

451. Hartmann, S., A.J. Ridley, and S. Lutz, *The Function of Rho-Associated Kinases ROCK1 and ROCK2 in the Pathogenesis of Cardiovascular Disease.* Frontiers in Pharmacology, 2015. **6**: p. 276.

452. Guan, P., Y. Liang, and N. Wang, *Fasudil alleviates pressure overload-induced heart failure by activating Nrf2-mediated antioxidant responses.* J Cell Biochem, 2018. **119**(8): p. 6452-6460.

453. Dai, K., et al., *Fasudil exerts a cardio-protective effect on mice with coxsackievirus B3-induced acute viral myocarditis.* Cardiovasc Ther, 2018. **36**(6): p. e12477.

454. Aoki, H., S. Izumo, and J. Sadoshima, *Angiotensin II activates RhoA in cardiac myocytes: a critical role of RhoA in angiotensin II-induced premyofibril formation.* Circ Res, 1998. **82**(6): p. 666-76.

455. Zafirovic, S., et al., *Involvement of PI3K, Akt and RhoA in Oestradiol Regulation of Cardiac iNOS Expression.* Curr Vasc Pharmacol, 2019. **17**(3): p. 307-318.

456. Rodriguez, P.L., et al., *ROCK I-mediated activation of NF-kappaB by RhoB.* Cell Signal, 2007. **19**(11): p. 2361-9.

457. Crowley, S.D., et al., *Distinct roles for the kidney and systemic tissues in blood pressure regulation by the renin-angiotensin system.* J Clin Invest, 2005. **115**(4): p. 1092-9.

458. Rezq, S. and A.A. Abdel-Rahman, *Rostral Ventrolateral Medulla EP3 Receptor Mediates the Sympathoexcitatory and Pressor Effects of Prostaglandin E2 in Conscious Rats.* J Pharmacol Exp Ther, 2016. **359**(2): p. 290-299.

459. Shum, W.W., et al., *Involvement of Rho-kinase in contraction of guinea-pig aorta induced by prostanoid EP3 receptor agonists.* Br J Pharmacol, 2003. **139**(8): p. 1449-61.

460. Hatae, N., Y. Sugimoto, and A. Ichikawa, *Prostaglandin receptors: advances in the study of EP3 receptor signaling.* J Biochem, 2002. **131**(6): p. 781-4.

461. An, S., et al., *Isoforms of the EP3 subtype of human prostaglandin E2 receptor transduce both intracellular calcium and cAMP signals.* Biochemistry, 1994. **33**(48): p. 14496-502.

462. Irie, A., et al., *Mouse prostaglandin E receptor EP3 subtype mediates calcium signals via Gi in cDNA-transfected Chinese hamster ovary cells.* Biochem Biophys Res Commun, 1994. **204**(1): p. 303-9.

463. Meyer-Kirchrath, J., et al., *Overexpression of prostaglandin EP3 receptors activates calcineurin and promotes hypertrophy in the murine heart.* Cardiovasc Res, 2009. **81**(2): p. 310-8.

464. Toldo, S., B.W. Van Tassell, and A. Abbate, *Interleukin-1 Blockade in Acute Myocardial Infarction and Heart Failure: Getting Closer and Closer.* JACC Basic Transl Sci, 2017. **2**(4): p. 431-433.

465. Van Tassell, B.W., et al., *Targeting interleukin-1 in heart disease.* Circulation, 2013. **128**(17): p. 1910-23.

466. Araki, K., M. Araki, and K. Yamamura, *Targeted integration of DNA using mutant lox sites in embryonic stem cells.* Nucleic Acids Res, 1997. **25**(4): p. 868-72.

467. Andersson, K.B., et al., *Tamoxifen administration routes and dosage for inducible Cre-mediated gene disruption in mouse hearts.* Transgenic Res, 2010. **19**(4): p. 715-25.

468. Molkentin, J.D., S.M. Jobe, and B.E. Markham, *Alpha-myosin heavy chain gene regulation: delineation and characterization of the cardiac muscle-specific enhancer and muscle-specific promoter.* J Mol Cell Cardiol, 1996. **28**(6):1211-25.

469. Bersell, K., et al., *Moderate and high amounts of tamoxifen in alphaMHC-MerCreMer mice induce a DNA damage response, leading to heart failure and death.* Dis Model Mech, 2013. **6**(6): p. 1459-69.

470. Buerger, A., et al., *Dilated cardiomyopathy resulting from high-level myocardial expression of Cre-recombinase.* J Card Fail, 2006. **12**(5): p. 392-8.

471. Hall, M.E., et al., *Systolic dysfunction in cardiac-specific ligand-inducible MerCreMer transgenic mice.* Am J Physiol Heart Circ Physiol, 2011. **301**(1): p. H253-60.

472. Hougen, K., et al., *Cre-loxP DNA recombination is possible with only minimal unspecific transcriptional changes and without cardiomyopathy in Tg(alphaMHC-MerCreMer) mice.* Am J Physiol Heart Circ Physiol, 2010. **299**(5): p. H1671-8.

473. Roebuck, K.A., et al., *Stimulus-specific regulation of chemokine expression involves differential activation of the redox-responsive transcription factors AP-1 and NF-kappaB.* J Leukoc Biol, 1999. **65**(3): p. 291-8.

474. Pang, L., et al., *Prostaglandin E Receptor Subtype 4 Signaling in the Heart: Role in Ischemia/Reperfusion Injury and Cardiac Hypertrophy.* J Diabetes Res, 2016. **2016**: p. 1324347.

475. Cheng, J., et al., *miRNA-451a Targets IFN Regulatory Factor 8 for the Progression of Systemic Lupus Erythematosus.* Inflammation, 2017. **40**(2): p. 676-687.

476. Honda, A., et al., *Effects of a prostagrandin EP4-receptor agonist ONO-AE1-329 on the left ventricular pressure-volume relationship in the halothane-anesthetized dogs.* Eur J Pharmacol, 2016. **775**: p. 130-7.

THE BALANCE BETWEEN PROSTAGLANDIN E2 EP3 AND EP4 RECEPTORS DETERMINES SEVERITY OF CARDIAC DAMAGE IN MYOCARDIAL INFARCTION AND AN ANGIOTENSIN II-INDUCED MODEL OF HYPERTENSION

by

TIMOTHY DEAN BRYSON

August 2019

Advisor: Dr. Pamela Harding

Major: Physiology

Degree: Doctor of Philosophy

According to the center for disease control about 610,000 people die every year in the United States from heart disease, of which, coronary heart disease is the most common form. One major risk factor for heart attack is hypertension, which affects nearly half of all Americans [472, 473]. PGE_2 plays an important role in regulating cardiovascular function and mediating inflammation, both of which contribute to the development of hypertension and/or heart disease. Prostaglandin E_2 can act as a vasodilator or vasoconstrictor depending on which of its receptor subtypes are activated.

In general, activation of the EP1 and EP3 receptors is vasoconstrictive while EP2/EP4 activation promotes vasodilation [13]. Treatment with an EP4 agonist has been shown to protect the heart during reperfusion after ischemia, while antagonizing EP4 reduced cardiac function and exacerbated cardiac remodeling [267, 394]. We have published that mice lacking the EP4 receptor in cardiomyocytes develop heart failure and have worsened cardiac function after MI [73, 268]. With regard to the EP3 receptor, we have published that its activation reduces contractility in isolated cardiomyocyte preparations and in the ex-vivo Langedorff system [219].

In this dissertation, we have been the first to show in both the MI and the Ang II

hypertension model, that EP3 expression increases significantly, whereby the expression of EP4 does not change or increases slightly. Thus, we hypothesize that the deleterious effects of PGE_2 are via the EP3 receptor. Furthermore, we have presented here that overexpression of the EP4 receptor in the cardiomyocytes is protective in a mouse model of MI by improving cardiac function, and reducing fibrosis and inflammation [218]. We postulated that the mechanism of reduced inflammation may be mediated by the cardiac fibroblasts. We therefore show in isolated adult mouse cardiac fibroblasts, that PGE_2 and an EP4 receptor agonist reduce LPS-stimulated MCP-5 production. Lastly, we report that activation of the EP3 receptor is deleterious in Ang II hypertension and that systemic administration of an EP3 antagonist can reduce blood pressure after Ang II infusion.

AUTOBIOGRAPHICAL STATEMENT

TIMOTHY DEAN BRYSON

EDUCATION

Ph.D. Candidate in Physiology (Minor: Molecular Biology), Wayne State University (WSU) School of Medicine (SoM).
Bachelor of Science in Biological Sciences, Wayne State University, 2013

FELLOWSHIPS AND SCHOLARSHIPS

NIH T32 Cardiovascular Training Grant, 2017-2019, WSU SoM
Departmental Discretionary Fellowship, 2015-2017, WSU SoM
Thomas C. Rumble Recruitment Fellowship, 2014-2015, WSU SoM

HONORS AND AWARDS

Awarded 1st place in "Inflammation and Pathophysiology" poster competition at 16th annual Research symposium – Henry Ford Health System (HFHS), 2019
Awarded Oral presentation – Lipids at Wayne, WSU, 2019
GALL Excellence in Cardiovascular Research Travel Award – ASIP, 2019
Marion I. Barnhart Graduate Student Award – Department of Physiology, WSU SoM, 2018
Awarded Oral presentation 14th Annual Research Symposium – HFHS, 2017

SCIENTIFIC MEETINGS (SELECTED)

April 2019: Experimental Biology, Orlando FL. Oral presentation (GALL travel award; ASIP).
July 2018: AHA Basic Cardiovascular Sciences, San Antonio, TX. Poster.
April 2018: Experimental Biology, San Diego, CA. Poster.
September 2017: AHA Council on Hypertension, San Francisco, CA. Poster.
June 2017: Michigan Physiological Society, Alma, MI. Oral presentation.
May 2017: Henry Ford Health System Research Symposium, Detroit, MI. Oral presentation.
April 2017: Experimental Biology, Chicago, IL. Oral presentation.
April 2016: Experimental Biology, San Diego, CA. Oral presentation.

PUBLICATIONS

1. **Bryson TD,** Pandrangi T, Peterson E, Harding P. The Deleterious Role of the Prostaglandin E2 EP3 Receptor in Ang II Hypertension. (Manuscript in preparation).
2. **Bryson TD,** Ross J, Peterson E, Harding P. Prostaglandin E2 and an EP4 Receptor Agonist Inhibit LPS-Induced Monocyte Chemotactic Protein 5 Production and Secretion in Mouse Cardiac Fibroblasts via Akt and NF-κB Signaling. Prostaglandins Other Lipid Mediat. 2019 Jun 20:106349. [Epub ahead of print]. Impact factor: 2.25
3. **Bryson TD**, Gu X, Khalil RM, Khan S, Zhu L, Xu J, Peterson E, Yang XP and Harding P. Overexpression of prostaglandin E2 EP4 receptor improves cardiac function after myocardial infarction. J Mol Cell Cardiol. 2018 Mar 06. doi:10.1016/j.yjmcc.2018.03.005. [epub ahead of print]. Impact factor: 5.68 (2016)
4. Xiaosong Gu, Jiang Xu, Liping Zhu, **Timothy Bryson**, Xiao-Ping Yang, Edward Peterson and Pamela Harding. Prostaglandin E2 reduces cardiac contractility via EP3 receptor. Circ Heart Fail. 2016 Aug; 9(8). pii: e003291. Impact factor: 18.88 (2017)
5. Jingye Fang, Ming Liu, Xuebao Zhang, Takeshi Sakamoto, Douglas J. Taatjes, Bhanu P. Jena, Fei Sun, James Woods, **Tim Bryson**, Anjaneyulu Kowluru, Kezhong Zhang, and Xuequn Chen. COP II Dependent ER Export: a Critical Component of Insulin Biogenesis and Beta Cell ER Homeostasis. Mol Endocrinol. 2015 June 07. PMID: 26083833 (Impact factor: 4.022).